N° d'ordre 2013-ISAL-0163   Année 2013

Thèse

Fundamental Studies of Interfacial Rheology at Multilayered Model Polymers for Coextrusion Process

(Rhéologie interfaciale de matériaux multicouches modèles: Etudes fondamentales et application au procédé de la coextrusion)

présentée devant

l'Institut National des Sciences Appliquées de Lyon

pour obtenir

Le grade de docteur

École Doctorale : Matériaux de Lyon
Spécialité : Matériaux Polymères et Composites

Par

Huagui ZHANG

Soutenue le 19 Décembre 2013 devant la Commission d'Examen :

JURY

Reviewer *(Rapporteur)*	MAIA João M.	Associate Professor *(Case Western Reserve University CWRU, USA)*
Reviewer *(Rapporteur)*	HU Guo-Hua	Professeur *(Université de Nancy-Membre de l'Institut Universitaire de France)*
Examiner *(Examinateur)*	CASSAGNAU Philippe	Professeur *(Université de Lyon 1)*
Examiner *(Examinateur)*	BOUSMINA Mosto	Professeur *(Président de l'université Euro-méditerranéenne de Fès (UEMF)- Chancelier de l'académie Hassan 2 des Sciences et Techniques)*
Supervisor *(Directeur de thèse)*	MAAZOUZ Abderrahim	Professeur *(INSA de Lyon)*
Co-Supervisor *(Co-encadrant de thèse)*	LAMNAWAR Khalid	Maître de Conférences *(INSA de Lyon)*

INSA de Lyon-Université de Lyon

Acknowledgements

In this moment, I would like to express my sincere appreciations to numerous people who have given me helps and supports throughout my study during the past three years.

First of all, my most sincere and deep gratitude is for my supervisors, Prof. Abderrahim MAAZOUZ and Dr. Khalid LAMNAWAR, without whose constant guidance and assistances this thesis would not be possible. I feel that I am lucky enough to be a member in their research group. Prof. A. Maazouz, who cannot be more kind, offered me all the possible opportunities to learn and expand my knowledge. Discussions with him always gave me some inspirations to move forth. Dr. K. Lamnawar, an associate professor with fruitful knowledge, generously accompanied me from the outdoor into the profound and fascinating halls of rheology field. He was always ready for me to listen patiently, to discuss and analyze in-depth till finally solve any problems I had met in scientific researches and academic communications. Both of them taught me a great deal, which will be values for my whole life. They also gave many cares to my life in a foreign land and provided me valuable advices on my further career. Their endless patience and kindness deserve greatest thanks.

Besides, I would like to sincerely acknowledge Prof. MAIA João M., Prof. HU Guo-Hua, Prof. CASSAGNAU Philippe and Prof. BOUSMINA Mosto for their kindness to become my thesis reviewers and examiners and their time on constructive and meticulous assessment of this thesis work.

I am indebted to many members who gave kind assistances in this study. Mr. Pierre ALCOUFFE is greatly appreciated for his kind contributions with the SEM-EDX and TEM characterizations. Mr. Stephane RAYNAUD is appreciated for his kind help with some calculations in mechanics; Mme. Jocelyne GALY is also appreciated for her help on SEC. Besides, I am grateful for technicians of Mr. Murat ARLI, Mr. Jean BALCAEN and Mme. Hayet LAKDAR at Bellignat as well as Mme. Marion COLLELLA, Mr. Guilhem QUINTARD at Lyon for their kind assistances. Helpful provision of polymer samples from ARKEMA Company made this dissertation work become real.

I want to thank all the members I have met both from IMP@INSA at Lyon and from Site de La Plasturgie at Bellignat. The office members including Dr. Racha Al-itry, Nora Dergham, Arnaud Bondon, Mohamed Dkier, Ludovic Sallet, Molka Louizi, Julien L'Intermy, Dr. Skander Mani, etc. for their kind help, constructive discussions and also the enjoyable time they have brought to me. Particularly the friendship from my Chinese fellows including Dr. Senbin Chen, Dr. Zhen Peng, Dr.

Ying Zhu, Dr. Jing Chen,Dr. Yuanming Deng, Xibo Yan, Wenyong Zhang, Biao Zhang, Jing Yang, Qing Liu and Hang Shen, etc. for their kindness and generosity as supports and help have always been available when needed. Thanks also go to others like Georgiy, Benoit, Claire, Isabelle, and certainly those not mentioned here for their kind helps and interesting discussions during my stay in the lab. More importantly, all the professors, staffs and graduate students at Site de La Plasturgie for providing me a very friendly and comfortable ambiance to work are deeply appreciated. Thanks a lot for all the favors you have done for me!!

Je retiendrai un bon souvenir du temps passé parmi vous!!

Special acknowledges go to Prof. Yongshen Xu at Tianjin University, China, for his generous helps, constant encouragements and valuable advices for my career.

Besides, I would like to thank all my friends for sharing their enjoyable time with me during my stay in Lyon!

Certainly, all my family members deserve the most important appreciations for their endless loves, their understandings and supports over all the past years of my study till completing my Ph.D. I also thank my relatives for their warm supports in need.

Finally, China Scholarship Council (CSC) for providing the scholarship is gratefully acknowledged.

Encore, Je vous remercie sincèrement pour tout !!

Amicalement,

Huagui ZHANG

Fundamental Studies of Interfacial Rheology at Multilayered Model Polymers for Coextrusion Process

Abstract

Fundamental studies have been devoted in this work to probe and modelize the interfacial phenomena at multilayered polymer systems based on two model compatible polymers of poly(vinylidene fluoride)(PVDF) and poly(methyl methacrylate)(PMMA) with varying molar masses. Linear and nonlinear rheology have been demonstrated to be sensitive to the presence of diffuse interphase triggered from interdiffusion at polymer/polymer interface. Firstly, the interdiffusion kinetics as well as the development of the interphase decoupled to flow as generated at a symmetrical (self diffusion) and an asymmetrical (mutual diffusion) bilayer have been investigated using small-amplitude oscillatory shear measurements. Results were analyzed according to Doi-Edwards theory (tube model) and the effects of annealing factors as well as structural properties on the diffusion kinetics have been studied. The PMMA/PVDF mixtures have been examined to be a couple of weak thermorheological complexity, owning close monomeric friction coefficients of each species in the present experimental conditions. Based on this physics, a new rheological model was developed to quantify the interdiffusion coefficients by taking into account the component dynamics in mixed state and the concept of interfacial rheology. Rheological and geometrical properties of the interphase have been able to be quantified through this model, as validated by scanning electron microscopy coupled with energy dispersive X-ray analysis (SEM-EDX) and transmission electron microscopy (TEM).

Secondly, experiments of step strain, startup in simple shear and in uni-axial extension have been carried out on the PMMA/PVDF multilayer structures to investigate the sensitivity of nonlinear rheology to the well-defined diffuse interphase. An original model was proposed to fit the stress relaxation behavior of multilayer structures and to estimate the relaxation behavior of the interphase. Lack of entanglement at the interface and weak entanglement intensity at the diffuse interphase make them to be subsequently readily to suffer from interfacial yielding even interfacial failure during and after continuous large deformations in simple shear and un-axial extension. Presence of interphase delays the interfacial yielding to a larger external deformation or a higher deformation rate. Besides, elongational properties of the multilayer structures have been shown to be a function of composition as controlled by layer number(interfacial area) and interphase properties (rheology related to entanglement intensity). Finally, the diffuse interphase development coupled to flow in practical coextrusion process has been considered. The compromising result between negative effect of chain orientation and favorable effect of flow on diffusion kinetics gives rise to a broadening interphase after coextrusion. An experimental strategy was formulated to optimize the coextrusion processing by considering the classical factors based on a flow stability chart. Presence of the diffuse interphase was demonstrated to significantly weaken (or even eliminate) the viscous and elastic instabilities despite of the high rheological contrast between PMMA and PVDF melts especially at low temperatures. Hence, this work gives guidelines on the key role of the interphase plays in structure-property-processing relationships.

Keywords: Linear and Nonlinear Rheology; Shear and Elongation; Multilayer; Interphase; Interdiffusion Process; Coextrusion; Modeling

Rhéologie interfaciale de matériaux multicouches modèles:

Etudes fondamentales et application au procédé de la coextrusion

Résumé étendu :

Les travaux de cette thèse concernent des études fondamentales liées à la rhéologie interfaciale des systèmes polymères multicouches. Les matériaux choisis sont à base de deux polymères compatibles : le poly(fluorure de vinylidène) (PVDF) et le poly(méthacrylate de méthyle) (PMMA) de différentes masses molaires. Ces systèmes ont été étudiés sous sollicitations en cisaillement et en élongation suivant les deux régimes en viscoélasticité linéaire (VEL) et non-linéaire (VENL). Les études en VEL ont permis d'étudier la cinétique de développement de l'interphase. Quant aux études en VENL, elles ont permis d'étudier les propriétés intrinsèques de l'interphase aux temps courts et sous hautes déformations, simulant ainsi les conditions de mise en œuvre proches de celles des procédés usuels. On démontre ainsi que la rhéologie joue le rôle d'une sonde très fine pour explorer les propriétés aux interfaces des matériaux multicouches. Les propriétés rhéologiques de ces matériaux multicouches ont été analysées par diverses méthodes spectroscopiques. Des modélisations ont été établies en se basant sur les mécanismes physiques et physico-chimiques mis en jeu.

Dans un premier temps, le comportement rhéologique à l'état fondu des multicouches a été étudié par spectrométrie mécanique dynamique en viscoélasticité linéaire (VEL) en vue de découpler les phénomènes cinétiques et d'écoulement. Les cinétiques d'interdiffusion ainsi que le développement de l'interphase générée aux interfaces de systèmes bicouches symétriques et asymétriques ont été étudiés. L'influence des paramètres expérimentaux et des propriétés structurales des polymères sur les cinétiques de diffusion a été mise en évidence. Les résultats obtenus ont été analysés et modélisés en se basant sur les concepts de la dynamique moléculaire en l'occurrence le modèle de Doi et Edwards. De plus, un nouveau modèle rhéologique a été développé. Il a permis de quantifier les coefficients d'interdiffusion en tenant en compte de la dynamique des chaines de chaque couche. Les coefficients de friction des chaines et les propriétés rhéologiques de l'interphase ont été modélisés à leur tour. Aussi, une modélisation simple et réaliste des coefficients de diffusion mutuelle a été réalisée. Les résultats obtenus corroborent ceux de la littérature, obtenus par des méthodes spectroscopiques très lourdes et sophistiquées (Diffusion des neutrons, RMN…). Ce nouveau modèle a permis de quantifier les grandeurs viscoélastiques et l'épaisseur de l'interphase. Ces résultats ont été confortés par les analyses microscopiques (MEB-EDX, MET).

Dans un second temps, des expérimentations en viscoélasticité non linéaire ont été réalisées sur les structures multicouches. Celles-ci ont été menées selon deux modes de sollicitations en cisaillement et en élongation en régime transitoire: i) expérience de démarrage ou croissance de contrainte sous gradients de vitesse de déformation ii) expérience de relaxation après chaque créneau déformation. Un modèle original a été également proposé pour décrire le comportement relatif à la relaxation des structures multicouches et de l'interphase en particulier. De plus, la sensibilité de la densité d'enchevêtrement a été étudiée pendant et après sollicitations mécaniques. On démontre que sa présence retarde l'écoulement interfacial surtout sous hautes déformations et vitesses de déformation. En outre, les études des structures multicouches sous sollicitation élongationnelle ont montrées que les propriétés dépendent de leurs structures (rapport de viscosité des couches utilisées, de leur nombre (aire interfaciale) et les propriétés de l'interphase diffuse).

Enfin, l'effet de l'écoulement sur la diffusion moléculaire dans les conditions réelles du procédé de mise en forme a été examiné. Les phénomènes mis en jeu sont particulièrement complexes puisqu'ils impliquent de façon couplée des phénomènes hydrodynamiques via l'écoulement et la rhéologie des différentes couches, et physiques via la diffusion des chaines aux interfaces. Les travaux de cette thèse mettent en lumière la compétition entre l'effet négatif de l'orientation des chaînes et l'effet favorable de l'écoulement sur les cinétiques de la diffusion. Ce dernier permet la formation d'une interphase robuste lors de la mise en forme. Ensuite, des cartes de stabilités ont été établies en relation avec le rapport d'élasticité, de viscosité et d'épaisseur des différentes couches. L'étude expérimentale a été réalisée au moyen d'une micro-coextrudeuse sur des écoulements stratifiés à deux, trois ou cinq couches pour des configurations symétriques et asymétriques. La présence de l'interphase diffuse a contribué à une réduction significative (voire élimination) des instabilités d'écoulement purement visqueuses et élastiques. On montre ainsi qu'outre la cinématique de l'écoulement en cisaillement et en élongation, les propriétés de l'interphase ont un rôle important dans la stabilité des écoulements stratifiés.

***Mots clés:** Rhéologie Linéaire et Non-linéaire; Cisaillement ; Elongation; Multicouches; Interphase; Processus d'Interdiffusion; Coextrusion; Modélisation*.

Table of Contents

v

LIST OF FIGURES

General Introduction

In a multiphase polymer system (blend/multilayer), polymer/polymer interface is now attracting wide interests due to its key role in determining the final properties of the system. Main interfacial phenomena involved therein include interdiffusion, interfacial slippage and interfacial reaction, whereby an interphase (i.e., a 3D physicochemical affinity instead of plane interface) may be produced. Despite of its high significance, full understanding of the interfacial phenomena is still far lacking, partially due to its difficulty of being experimentally accessible. Meanwhile, simultaneously occurrence and competitions among the interdiffusion, interfacial slippage and interfacial reaction in some cases make the problem even more complicated. These motivated us to first treat the problem in the present study by focusing on the diffuse interphase generated only from interdiffusion process between compatible polymers before disclosing its relations to polymer processing. Therefore, the objectives of this study consist in: understandings of the interdiffusion kinetics and the diffuse interphase development occurs at multilayer structures; properties of the diffuse interphase decoupled and coupled to flow; interfacial rheology in linear and nonlinear regimes of shear as well elongation; and the importance of such diffuse interphase in multilayer coextrusion. All these issues have been systematically studied in this Ph.D. study. To achieve these objectives, two model polymers are chosen, that is, poly (vinylidene fluoride) (PVDF) and poly (methyl methacrylate)(PMMA) with varying molar masses which are completely compatible thanks to their strong enthalpic interaction.

In Chapter I, we will give an overview about the work achieved in the literature during the past decades in the field of interfacial phenomena in multiphase system as well the flow properties in coextrusion process. The interdiffusion either between same polymers or between dissimilar compatible polymers, as a fundamental problem involved in processing, has been widely studied for a long period via various sophisticated spectroscopic techniques and common tools. Despite of this, full comprehension of the diffusion kinetics as well the triggered diffuse interphase and modeling of the interfacial rheology have not yet achieved. An apparent interfacial slippage may emerge under high shear conditions especially in incompatible multiphase systems, on which a number of studies have been devoted by researchers. Interfacial reaction is one of the most common means used to suppress the interfacial slippage and enhance the interfacial adhesion. Literature work on the interfacial reaction kinetics and its compatibilization effects in the multiphase system are also to be given in the chapter. The structure, rheology and properties of the interphase triggered from the interdiffusion (diffuse interphase) and that from the interfacial reaction (reacted interphase) are of high interest due to their close relations to the final morphological, barrier and mechanical properties, etc. For clarity purpose, only the former case (i.e. diffuse interphase) will be discussed in this

thesis. Moreover, to the best of our knowledge, nonlinear rheology at the interface/interphase of multiphase systems is still scarce in the number of literatures. We will give some brief introductions about the past work obtained on this subject. On the other hand, role of this triggered interphase in the multilayer flow stability is to be discussed. In multilayer polymer coextrusion processing, the main challenge is that interfacial defects such as interfacial flow instabilities and encapsulations may appear if the polymers simultaneously processed are of great rheological contrast. So far, most of the theoretical and experimental studies are restricted to numercial and mechanical approaches, with very few dedicated to the possible connection between the interfacial defect origins and the interfacial phenomena at neighboring layers. This open question constitutes one of the subjects in the present study. Actually, main parts of this bibliographic review have been published as a book chapter in *Encyclopedia of Polymer Science and Technology (4th edition, John Wiley & Sons Inc, 2013), DOI: 10.1002/0471440264.pst584.*

Chapter II is dedicated to the interdiffusion process occurs at a symmetrical molten polymer/polymer interface based on PVDF/PVDF and PMMA/PMMA bilayers with vairous molar masses via a small-amplitude oscillatory shear measurement (SAOS) in which the diffusion is decoupled from flow. The interdiffusion kinetics was analyzed on basis of the tube model of Doi-Edwards theory. Transition from non-Fickian to normal Fickian region of the interdiffusion was identified and these two regions were separately focused. Rheological modeling was carried out to determine the self diffusion coefficient (D_s) of polymers, then the results were compared to literatures using other sophisticated techniques. Furthermore, effects of healing time, angular frequency (ω), temperature and molecular weight on the interdiffusion kinetics have been investigated. In addition, properties of the symmetrical diffuse interphase triggered between the neighboring layers were examined. Main results in this part of symmetrical bilayer have been published in *Rheologica Acta (2012, 51:691–711).*

In Chapter III, an asymmetrical molten polymer/polymer interface based on a PMMA/PVDF bilayer was employed to investigate mutual diffusion process and diffuse interphase development via SAOS measurements. As diffusion coefficient is greatly related to the monomeric friction coefficient of components (ζ_i) in mixed state, it was indispensable to examine first the component dynamics before carrying out quantitative rheological modeling of the mutual diffusion process. Hence, rheology method based on "double reptation" model, Lodge-McLeish model and test of the time-temperature superposition (tTS) principle were introduced to probe the thermorheological complexity of this compatible polymer couple as a first step. The monomeric friction coefficient of each species in the blend have been examined to vary with composition and temperature and to be close in the present experimental conditions and the failure of tTS principle was demonstrated to be subtle. Based on this physics, a new quantitative rheological model modified from a primitive Qiu–Bousmina's model that connected the mobility in mixed state to the properties

of matrix was proposed to determine the mutual diffusion coefficient (D_m). Our motivation was based on that the primitive model would have some defects on determining the mutual diffusion coefficient if components of the asymmetrical bilayer have pronounced difference in their monomeric friction coefficients. One more originality of the modified model is that the rheological behavior of the interphase was taken into account for the first time to determine the D_m. More importantly, on the basis of the modified model, viscoelastic properties and geometrical properties of the interphase are able to be quantified. The interphase that with local entanglements gradually formed via interchain penetration during the interdiffusion process possesses similar performance with its equivalent blend. Scanning electron microscopy coupled with energy dispersive X-ray analysis (SEM-EDX) and transmission electron microscopy (TEM) were also used to examine the interfacial structure and to confirm the rheological results. Main results in this part of asymmetrical bilayer have been published in ***Macromolecules (2013***, *46:276–299)*.

In Chapter IV, as a further step, nonlinear rheology of the PMMA/PVDF alternating multilayer structures in both transient shear and extensional flow has been examined to see whether or not it is sensitive to the presence of the generated diffuse interphase and to discover its properties upon large deformatins. Stress relaxation after step shear strain, fast startup in simple shear and in uni-axial extension were performed to the un-annealed multilayers without and the annealed multilayers with well-characterized diffuse interphase, respectively. Nonlinear rheology of the neat PVDF and PMMA melts were studied and discussed under tube model as well as some recent theoretical scenarios. An original model was proposed to fit the relaxation behavior of multilayer systems and to estimate the relaxation modulus $G(t,\gamma)$ of the interphase. By comparing the nonlinear rheological responses in both step strain and startup shear between the un-annealed and the annealed multilayers, presence of the interface or interphase could be identified due to their entanglement differences. In startup uni-axial extension, elongation viscosity of multilayer system was demonstrated to depend on the component viscosity difference and the component fractions. Layer number was increased to amplify the interphase fraction in the multilayer structure and elongation rheology of the equivalent blend was introduced to assess the interphase contribution to the total elongation viscosity. This Part is to be submitted to ***Journal of Rheology***.

In Chapter V, the objective is to investigate the development of a diffuse interphase generated in a practical flow field of processing and to highlight its importance on controlling the final properties of multilayer materials based on PMMA and PVDF model polymers. Competition between diffusion and flow effect was assessed by taking into consideration of two important factors, i.e. chain orientation along the flow direction and intermixing at vicinity of interface. In particular, intermixing effect was simulated by performing a pre-shear on the

multilayer structures coupled with SEM observation. SEM-EDX and TEM were used in order to disclose the interfacial structure and geometrical property of the diffuse interphase generated during processing. Concerning the interfacial flow instability and encapsulation in coextrusion processing, some key classical decisive parameters such as viscosity ratio, thickness ratio and elasticity ratio, etc. were studied based on a stability chart. Incompatible and compatible multilayer systems were compared, from which role of the diffuse interphase in eliminating viscous and elastic instabilities have been emphasized. This Part is to be submitted to *Polymer Engineering and Science*.

Chapter I: State of the Art

I.1 Introduction

This review chapter of theoretical and experimental achievement in literatures begins with interfacial phenomena of interdiffusion, interfacial slippage as well interfacial reaction, to nonlinear rheology of multilayer structures including stress relaxation after step strain and transient rheology in shear as well in uni-axial extension, before reviewing the interfacial defects in coextrusion processing, and especially its relations to the interphase. For clarity purpose, some aspects regarding theoretical and experimental studies of interfacial defects are placed in the Appendix I at the end of the manuscript. In addition, we mention here that more focuses of relevant literature work are emphasized in the introduction of each chapter.

Nowadays, polymer blends and polymeric multilayers account for a very large fraction in industry as high performance materials, due to their easy and cheap preparation methods(Hu, et al. 1998;Utracki 1995). Indeed, in such multiphase polymer systems (blend or multilayer structure), the interfacial phenomena such as interdiffusion, interfacial slippage and/or interfacial reactions taking place at the polymer-polymer interface are of high interest among the researchers in polymer science(Bousmina, et al. 1999;Macosko, et al. 2005;Zhao and Macosko 2002). For instance, the interdiffusion process that occurs at the vicinities between polymers plays a very important role in mixing and homogenizing composition gradients during a processing course. The interfacial slippage is a well-known phenomenon that may happen in the incompatible polymer systems, which has been suggested to interpret viscosity negative deviation of blends. Nevertheless, it is not desirable due to its unfavorable effect on the final properties of the products such as reducing adhesion between neighboring polymer layers in coextrusion. To improve the weak polymer-polymer adhesion in an incompatible system, a compatibilization effect is often introduced by adding premade copolymers as compatibilizers or locally carrying out chemical reactions at the polymer-polymer interface(Sun, et al. 1996). Hence, according to these interfacial phenomena, an interphase (a non-zero thickness 3D physicochemical zone as opposed to a purely geometrical plane interface) could be triggered either by interdiffusion or by chemical reaction at the polymer-polymer interfacial zone in a multiphase system. So far, rheology, physics, morphological and geometrical properties associated with such interphase as well its contribution to the multiphase systems of blend and multilayers persists as a hot issue among the polymer scientists and rheologists.

Besides the linear rheology, nonlinear rheology(high deformation flow) which is more closely related to the processing conditions has also been introduced to study the multiphase polymer systems(Iza and Bousmina 2000;Silva, et al. 2007). In nonlinear rheology that involves transient regime, the flows could be well-controlled in terms of fast startup deformation with a step rate or imposing a step strain in both kinematics of simple shear and extension. Hence, much attention has been paid by the researchers to the morphology evolution/flow relations of polymer blends in response to shear and extensional flows. However, due to the complexities on the non-obvious relations between flow and structural evolution, this field is still more or less a subject of much ongoing research which desires further understandings. Reports on the nonlinear rheology on multilayer polymer structures especially for the interface/interphase contribution are even scarcer despite of its high significance.

Coextrusion is an industrial process widely used to form multilayered sheets or films that are suitable for various products ranging from food packaging materials to reflective polarizers(Dooley 2002b;Han 1981;Lamnawar, et al. 2013). Besides, it is also a good tool for fundamental studies, especially for studying interfacial dynamics in polymer blending, since the morphology in coextruded multilayers is well defined by layer number and layer thickness which makes it a suitable model system for multiphase systems like blend(Mueller, et al. 1997;Zhao and Macosko 2002). When it comes to the processing problem of coextrusion, the subject is very vast. Many aspects have been dealt with by various researchers, ranging from equipment designs (Dooley 2002a;Dooley 2002b;Mitsoulis, et al. 1988), fluid mechanics and analysis of multilayer flow (Dooley 2002b;Han 1981;Hannachi and Mitsoulis 1993;Mitsoulis 2005;Valette, et al. 2004), to interfacial defects and optimization of processing conditions (Lamnawar and Maazouz 2009;Schrenk, et al. 1978;Wilson and Khomami 1993b), etc.. Some of the advances in the field of multilayer polymer coextrusion reported in literatures have been stated in our recent publication in Encyclopedia of polymer science and technology (Lamnawar, et al. 2013). We refer the readers interested in this part to this reference. Because of space limitation, this chapter deals only with some more relevant topics such as the interfacial defects occur during coextrusion processing. It is known that under certain operating conditions, interfacial defects can be observed inside the die, especially for the case of simultaneously processing polymers with rheological contrast. They can be divided into two common types consisting of a waviness and/or rugged shape appearing at polymer-polymer interface (interfacial flow instability) and a layer–to-layer thickness non-uniformity (i.e., encapsulation of the less viscous polymer over the more viscous one). Important theoretical and experimental advances with regard to such interfacial defects being achieved during the last decades are mainly limited to mechanical and numerical approaches.

Despite the interesting nature of this kind of research, it is of no help when it comes to understanding either the origin of the generation of interfacial defects or the

connection of the physicochemical affinity at the interface of neighboring layers and the final properties of multilayer polymers. It is not difficult to imagine that the interphase (i.e. physicochemical affinity) resulted from the interfacial phenomena may be somewhat related to the interfacial flow stability. In fact, the importance of such interphase in the multilayer flow was firstly realized by Wilson and Khomami(Wilson and Khomami 1993b), though no further details have been focused till recent work of our group(Lamnawar and Maazouz 2009).

I.2. Interfacial Phenomena at Polymer/ Polymer Interface

I.2.1 Interdiffusion process (self/mutual diffusion)

I.2.1.1 Theory

I.2.1.1.1 Self diffusion

The diffusion process of a polymer across an interface has been a hot issue during the past decades. This is due to its incomparable role in practical applications of polymer processing and its academic significance for understanding chains motions (Klein 1978;Klein and Briscoe 1979;Wu, et al. 2008). When two polymer surfaces are brought into contact at a temperature above their glass transition temperature, the chain conformations at the interface tend to relax toward those in the bulk because of Brownian motion. Thus, from a macroscopic viewpoint, the interface of the assembly gradually disappears and the mechanical strength develops as the void in the contact area heals. In particular, regarding to the healing process at the interface, Wool and O'Connor (Wool 1995;Wool and Oconnor 1981) suggested a five-stage model to explain the mechanism of adhesion in terms of surface rearrangement, surface approach, wetting, diffusion and randomization. By the end of the wetting stage, potential barriers associated with inhomogeneities in the interface disappear and chains are free to move across the interface in the subsequent stages of diffusion and randomization. These stages are the most important since they enable the characteristic strength of the polymer material to appear.

Generally, the diffusion between small molecules can be well understood by the classic Fickian law and the diffusion of small molecules in polymer networks can be explained by the Case II diffusion model which involves a modification of Fick's law by the introduction of additional stresses due to the penetration of the solvent (fast-moving component) that swells the polymer network and stretches the chain segments between entanglements. For diffusion between polymers, since both the diffusing agent and the medium are highly entangled polymeric chains, the mechanism becomes even more complicated. To date, most work on polymer diffusion is interpreted under the framework of the theory of polymer dynamics, which was first proposed by de Gennes (de Gennes 1971) and later developed by Doi-Edwards(Doi and Edwards 1986). This so-called reptation theory involves each polymer chain slithering like a snake, since its motion is constrained by the

topological entanglement structure formed by the surrounding chains. In this theory, the topological effect of the surrounding chains on the test chain was assumed as a tube with a definite tube diameter, whereby it is also called tube model (Figure I-1a). According to this theory, the general motion behavior of an entangled polymer chain can be time dependent, where several characteristic time regimes can be delimited. They are τ_e, known as the Rouse relaxation time between entanglements, above which the chain starts to feel the topological constraints of the tube; τ_R, the Rouse relaxation time of the whole chain, a time the chain begins to move along the tube; and τ_{rep} (or τ_d), i.e., the reptation relaxation time, above which the chain motion can renew the initial tube by a reptational dynamics. Different time dependences of the displacement ($\Phi_n(t)$) of Rouse segments of entangled polymers has been predicted in these different characteristic time regimes, which are expected to be non-Fickian kinetics before entering the as normal Fickian diffusion for $t > \tau_{rep}$.
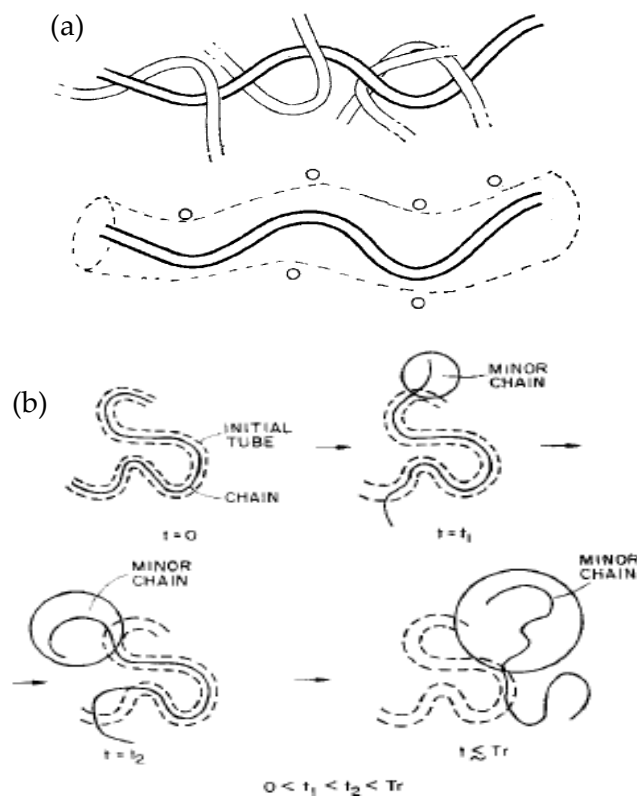
Figure I-1 (a)An illustration of a chain in an bulk entangled melt that may be regarded as within a virtual "tube" according to the reptation theory (from Klein 1978); (b) A schematic of disentangle dynamics of a chain from its initial tube according to the minor chain model (from Wool 1995).

Indeed, the diffusion at the interface is not exactly identical to the self diffusion mechanism in the bulk since it depends greatly on the configuration of chain ends (or minor chains) at the initial state of diffusion. Wool et al(1995) developed a minor chain model to interpret the diffusion dynamics at a polymer-polymer interface (Figure I-1b). They argued that a mixture and repartition of Rouse and reptation contributions should be considered due to the effect of the interface configuration.

The excess chain ends at the polymer surface may act as numerous minor chains at the initial period of interdiffusion process at the polymer-polymer interface.

I.2.1.1.2 Mutual diffusion

On the other hand, for an asymmetrical bilayer composed of different polymers, the interdiffusion process that occurs at the interface is a mutual diffusion between two different polymers, and the mechanisms can also be very different from that of identical polymers. First, in a mixed state of dissimilar polymer chains, the intrinsic mobilities of the chains, i.e., their monomeric friction coefficients, ζ, could be very different, with some case the ζ can differ by 2 orders of magnitude for different components. On the other hand, the mutual diffusion kinetics could be greatly affected by the miscibility of diffusing species (expressed by the Flory-Huggins interaction parameter,χ), which may accelerate or suppress the diffusion kinetics. Therefore, the problem of mutual diffusion between dissimilar polymer chains is far more complicated than self diffusion of same chains.

To date, the mechanism of mutual diffusion is described under the framework of the Flory-Huggins Lattice theory using the Onsager formalism. In fact, there are two divergent theories known as the slow-mode model(Brochard, et al. 1983) and the fast-mode model (Kramer, et al. 1984) appearing to deal with the mutual diffusion kinetics between dissimilar polymers. The slow-mode model argues that the mutual diffusion is dominated by a slower moving species, and the fast-mode model supports the opposite. The difference between these two theories lies in the treatment of the flux of vacancy J_v, the slow-mode theory assumed no vacancy flux and the fluxes of the two polymers are equal and opposite, which means that the interface remains symmetric as interdiffusion proceeds for symmetric boundary conditions. The fast-mode theory, on the other hand, assumes the existence of a vacancy flux, thus describing the interdiffusion with a moving interface by unequal fluxes of polymers that are balanced by a net flux of vacancies across the interface. It concludes a movement of the interface towards the faster-diffusion component and a broadening of the concentration profile on the slower-diffusion component side.

I.2.1.2 Experimental aspect

I.2.1.2.1 Techniques

Various sophisticated spectroscopic tools have been employed to study diffusion phenomena of polymers. Table I-1 summarizes the main techniques used in the literature. The tools range from sophisticated techniques like Secondary Ion Mass Spectroscopy and Neutron Reflection to commonly used techniques like FTIR and DSC. By virtue of some of these methods, concentration profiles can be directly obtained. Through fitting of a theoretical profile computed from Fick's equation (eq. I-1) to an experimentally achieved counterpart, one can receive a mutual diffusion coefficient D_m of the two species at a given time t and position z .

$$\frac{\partial \phi(z)}{\partial t} = \frac{\partial}{\partial z}\left[D(\phi)\frac{\partial \phi(z)}{\partial z} \right]$$ (I-1)

Table I-1 Techniques utilized for studying the polymer/polymer interdiffusion process

Technique	Depth resolution	Information content	References
Secondary Ion Mass Spectroscopy(SIMS)	-	Surface composition	(Wool 1995)
X-ray or Neutron Reflection(XR or NR)	1nm	Composition profile	(Kawaguchi, et al. 2011)
Forward Recoil Spectrometry(FRES)	80nm	Composition profile	(Kunz and Stamm 1996)
Rutherford Backscattering Spectrometry(RBS)	30nm	Composition profile of marker	(Kramer, et al. 1984)
Nuclear Reaction Analysis(NRA)	13nm	Composition profile	(Klein 1978)
Ellipsometry(ELLI)	1nm	Film thickness, refractive index profile	(Yukioka, et al. 1992)
Raman Microspectroscopy(RM)	~ μm	Composition profile	(Jonas, et al. 2010)
Energy-Fieald TEM	50nm	Composition profile	(Liao, et al. 2007)
Attenuated total reflection infrared spectroscopy (ATR-FTIR)	-	Relative IR intensity/Fraction volume	(High, et al. 1992)
Scanning electron microscope-energy dispersive x-ray analyzer(SEM-EDX)	10nm	Composition profile	(Gilmore, et al. 1980)
DSC	-	Melting endotherm/fraction volume	(Mueller, et al. 1997)

In fact, given that the interdiffusion process of a polymer is not absolutely Fickian, this is empirical. It is however worth meantioning that many sophisticated spectroscopic tools have a high spatial resolution, and thus need isotopic labeling or marked elements, which have been demonstrated to slow down mass transport.

I.2.1.2.2 Measurements by rheology

Nowadays, thanks to a highly developed knowledge, rheological methods have also been developed to investigate and quantify the interdiffusion processes at polymer-polymer interface. In particular, it can be carried out in rotational rheometers with parallel-plates geometry. The physics are based on tracking the rheological variations of a multilayer assembly structure annealed at a measured temperature in the oven of the rheometer. The sample setup for rheological measurements is depicted in Figure I-2, for example, with a polymer bilayer melted between parallel plates.
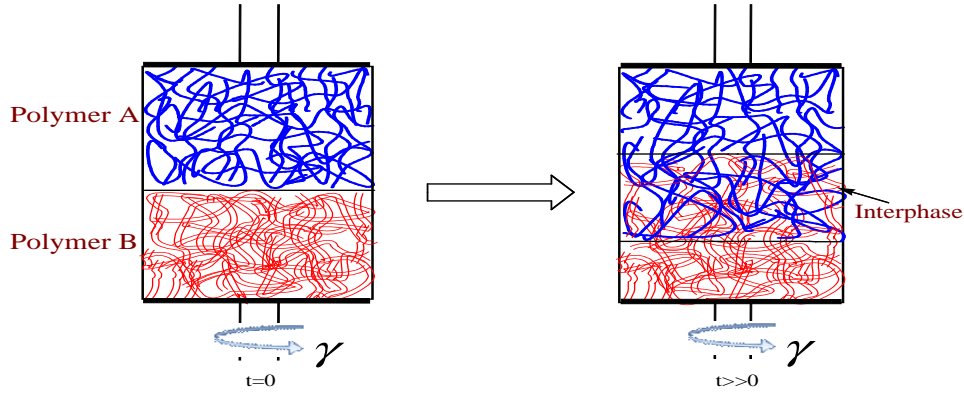
Figure I- 2 A schematic of a molten bilayer assembly used for rheological testing

A quantitative connection between the diffusion coefficient and the measured rheological variations has been derived by Qiu and Bousmina (1999) from Boltzmann's integral form

$$\tau(t) = \int_{-\infty}^{t} G(t - t')\dot{\gamma}(t')dt'$$

(I-2)

where the stress $\tau(t)$ measured at the time *t* is a function of the whole history of past deformation $\dot{\gamma}(t')$ at anterior times *t'*, and the shear relaxation modulus *G(t-t')*, which contains the whole past history of the deformation, can be related to the mass transport across the interface that occurred at previous times. Based on this principle, Qiu and Bousmina(1999) put forward a quantitative model for an apparent self diffusion coefficient between identical polymers in term of the storage modulus (G') measured for the bilayer assembly.

Likewise, the authors (Qiu and Bousmina 2000) also put forward a quantitative model for the mutual diffusion coefficient (Dm) between dissimilar polymers based on a PMMA/SAN bilayer system from the rheological variations of the bilayer assembly versus annealing time:

$$D_m = \frac{N_b^e N_b^3 b_b^4 K^{1/2}}{\pi^2 e_b^2}\left[\frac{(1-\varphi)}{N_A} + \frac{\varphi}{N_B}\right]\left[\frac{(1-\varphi)}{N_A} + \frac{\varphi}{N_B} - 2\chi\varphi(1-\varphi)\right]$$

(I-3)

$$\text{with} \quad K = \omega^2\left[\left(\frac{8 G_N^0}{\pi^2 G^*(\omega)}\right)^2 - 1\right]$$

(I-4)

where N_b^e, N_b, b_b, e_b and $G_{N,b}^0$ are the average number of repeat units between entanglements, the repeat unit numbers, the effective bond length, the step length of the virtual tube and the plateau modulus of the interphase (or equivalent blend), which is also a function of the composition.

As far as G*(ω) in eq.(I-4) is concerened, the time evolution of the complex

modulus ($G_s^*(t)$) of the overall sandwich was used by the authors to determine the D$_m$.

As a matter of fact, the only region where the mutual diffusion process occurs is restricted to the interfacial region (the interphase). This is particularly true for the bilayer system where the bulk phases of the constituents accounting for a great proportion should not be ignored. To some extent, the viscoelastic properties of the interphase do not straightforwardly equal the ones of the overall sandwich. Hence, questions remain that if one can determine the mutual diffusion coefficient based on the interfacial rheology, $G_I^*(t)$, of the real interphase instead of the overall sandwich structure.

Evidently, the calculation of the diffusion coefficient of polymers, whether the self diffusion coefficient or the mutual diffusion coefficient, is a gigantic task, especially considering that a large number of parameters are needed. It should also be mentioned that Zhao and Macosko(2007) proposed a different model from a phenomenological aspect for the mutual diffusion coefficient in their HDPE/LLDPE multilayer system by fitting the complex viscosity variation that theoretically calculated from Fick's law to the experimetal data. Besides, based on the rheological model of Zhao and Macosko, Wang and coworkers (Yang, et al. 2010) further investigated the effects of phase behavior on the mutual diffusion kinetics in an alternating multilayer system consisting of statistical copolymers of ethylene and 1-hexene (PEH) and of ethylene and 1-butene (PEB).

Even though a great number of interesting investigations have been carried out by Bousmina(Qiu and Bousmina 1999; 2000) and Macosko et al.(Zhao and Macosko 2007) on the quantification of the diffusion process by rheology, it is still far from enough with regard to some aspects. For instance, the rheological models proposed by Bousmina et al. have not been confirmed or extended to other polymer systems. The dependences of the interdiffusion coefficient on annealing factors like temperature, healing time as well structural properties such as molecular weight have not been detailed. Moreover, regarding the mutual diffusion, on the one hand, the intrinsic mobilities of the diffusing species, have not yet been focused, as mentioned before that the component dynamics in mixed state can be very different. On the other hand, the interfacial rheology of the interphase has not been considered for the diffusion coefficient determination.

I.2.1.2.3 Interdiffusion in coextrusion

To disclose the underlying mechanisms of the interphase on improving the interfacial defects, it is very important to first consider the interdiffusion in multilayer coextrusion. In a practical coextrusion process, the situation for interdiffusion is much more complicated than under static conditions. For example, the orientation of polymer chains in a shear flow field may influence the rate of interdiffusion. In the work of Kim and Han(1991), they first considered this problem by introducing an orientation factor concept. The authors argued that in static conditions (when there is

no flow and thus a random distribution), the polymer chains can be assumed to have an average orientation angle of 45 degrees while under a shear field the polymer chains will, in the respective phases, have average orientation angles that are greater than 45 degrees, as shown in Figure I-3.
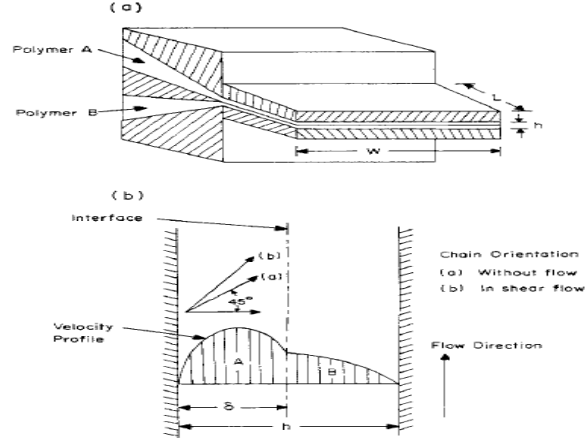
Figure I- 3 (a) A schematic of the flow of two polymer fluids; (b) A schematic of the velocity profile and average orientation angle. (from Kim and Han 1991)

To describe the diffusion process in this case, the authors proposed an apparent intrinsic diffusion coefficient, $\tilde{D}_i$, introducing an orientation factor α_i, defined by

$$\tilde{D}_i = \alpha_i D_i \qquad (i=A,B) \qquad (I\text{-}5)$$

where the intrinsic diffusion coefficient D_i is defined as (take D_A as an example):

$$D_A = N_A D_A^* \left[\frac{\varphi_B}{N_A} + \frac{\varphi_A}{N_B} - 2\varphi_A \varphi_B \chi \right] \qquad (I\text{-}6)$$

and the orientation factor is determined from the steady-state shear compliance $J_{eb,i}^0$ and the shear stress at the interface σ_{int} :

$$\alpha_i = \frac{\cos\left\{ (\pi/4) + \left[\tan^{-1}\left(J_{eb,i}^0 \sigma_{int} \right) \right] / 2 \right\}}{\cos(\pi/4)} \qquad (I\text{-}7)$$

Their observations suggested that the shear stress at the interface greatly influenced the interfacial position and thus the interfacial layer thickness. Due to the chain orientation in a shear flow field, the interface thickness, and hence the adhesive bond strength, will lower the interfacial layer thickness as the thickness ratio deviates from 1.

On the other hand, one should keep in mind that in the vicinity of the interface, a local pressure gradient may be developed due to the viscosity imbalance between upper and lower polymer layers in the presence of a steady shear flow field. It may thus lead to a formation of fractal branching structures, which greatly increase the

interfacial area for interdiffusion and promote the Intermixing at the interface. The greater the viscosity ratio, the more serious is the evolution of the interface disturbances. Consequently, the role of the interdiffusion, Intermixing and also the generated interphase in interfacial stability of coextrusion cannot be readily neglected.

I.2.2. Interfacial slippage at a polymer-polymer interface

One more interesting interfacial phenomenon described in the literature is the slippage that takes place at a polymer-polymer interface. The interfacial slippage was attributed to be the cause for the negative deviation from the log-additivity rule for immiscible blends, and it may also cause a reduction of the adhesion between neighboring polymer layers. It has been reported that the slip can be observed by microscopic tools and that the slip velocity can be quantified by rheology.

I.2.2.1 Experimental observations

In early years, anomalously low viscosities were observed for immiscible blends. In particular, the blend exhibits a negative deviation behavior from the log-additivity rule. To interpret the anomalously low viscosity behavior, a concept of interfacial slippage was first developed by Lin(1979) and it was considered in their developed model used to describe the rheological behavior of multilayer structures. This model was then extended by Bousmina, Utracki and Palierne (Bousmina, et al. 1999) to take into account the triggered interphase between the neighboring layers.

Zhao and Macosko (Zhao and Macosko 2002) and recently Lee et al. (2009) have investigated the interfacial slip using multilayers from coextrusion based on incompatible systems of PS/PP and LLDPE/fluoro-polymer pairs.The interfacial slip phenomenon can be detected in the steady shear measurements of the multilayer structures via the parallel-plate rotary rheometer, as evidenced by the reduced apparent viscosity that decreased with the number of layers (Figure I-4). Various types of rheometers ranging from a rotary rheometer with parallel-disks to an in-line slit-die rheometer and sliding-plate rheometer have been demonstrated to be able to detect the interfacial phenomena in incompatible polymer multilayers. In the method of the in-line slit rheometer for detecting the interfacial slip that occurs in multilayer structures, pressure drops are measured versus the volume flow rate and used to calculate the slip velocity. Increasing the number of layers yields a significant reduction of the pressure drop, pointing towards the presence of interfacial slip.

Independent of these studies, Lam et al.(2003) also demonstrated the existence of interfacial slip between polymer pairs. This was done experimentally by means of rheological measurements in PS/HDPE sheared between rotating parallel discs. A model based on the concept of energy was developed to describe and quantify the interfacial slip. The principle was based on the angular displacement that occurs between adjacent layers during the dynamic shearing measurements.
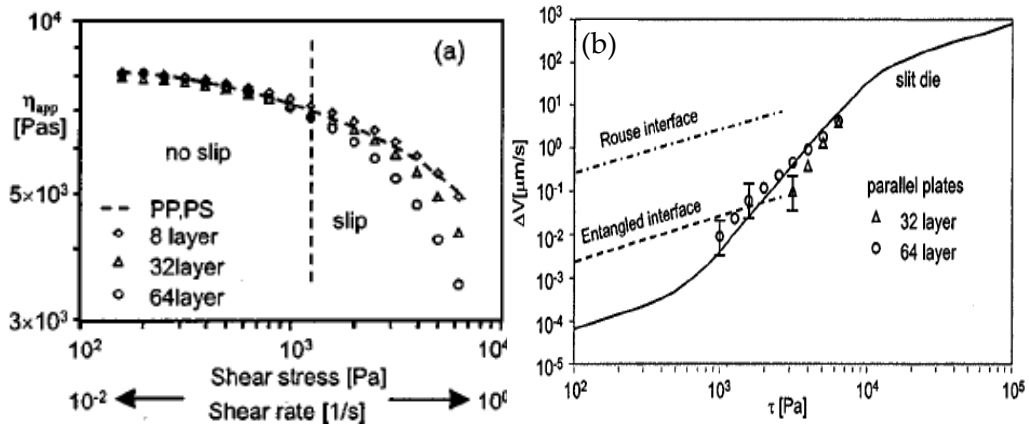
Figure I- 4 (a) Apparent viscosity of PP/PS multilayers measured in parallel plates of a rotary rheometer; (b) Interfacial slip velocity of a PP/PS system.(from Zhao and Macosko 2002)

In rheology measurements, the slip velocity (the velocity difference across the interface)can be calculated from the viscosity reduction (rotary plate rheometer), or from the stress reduction(sliding plate rheometer) as well as from the pressure drop in an in-line slit rheometer with the equations proposed by (Zhao and Macosko 2002);

$$V_{slip} = \frac{H\dot{\gamma}}{n-1}\left(1 - \frac{\eta_n}{\eta_{av,no-slip}}\right)$$ (I-8)

Here, H is the total thickness of the multilayer, n is the total number of layers, $\dot{\gamma}$ is the shear rate, and η_n and $\eta_{av,no-slip}$ are the measured nominal viscosity of multilayers and the harmonic average viscosity of the involved polymers with no slip, respectively. It can also be indirectly calculated from the dynamic shear measurement of a rotary plate rheometer by using a concept of the energy factor proposed by Lam and coworkers(2003). Figure I-4b depicts a typical result of the slip velocity of the PP/PS pair versus shear stress determined by Zhao and Macosko (2002), where a sigmoidal behavior is shown: a zone of very low slip at low shear stress, a strongly increasing zone above a critical stress followed by a linear zone. All together, the researchers observed that the slip velocity significantly depends on the shear stress, with a transition occurring above a critical stress. Moreover, the value is also greatly related to the thermodynamic interaction parameter.

In fact, in addition to the indirect measurement by rheological tools, the interfacial slip can be observed by direct visualization methods, with the aid of confocal microscopy(Lam, et al. 2003), digital photographs(Park, et al. 2010) or particle tracking velocimetry(Zartman and Wang 2011), etc.

I.2.2.2 Theoretical interpretations

On interpreting this interfacial slip phenomenon (velocity discontinuity across the interface), a convincing molecular mechanism based on polymer chain dynamics was firstly developed by Furukawa(1989), Brochard-Wyart and de Gennes(1993). They assume that polymers A and B are symmetric, with identical friction coefficient ξ, statistic segment length *b* and chain length *N*, and weakly incompatible, i.e., $1/N \ll \chi < 1$. There then exists an interfacial region consisting mainly of interpenetrating loops of chains A and B. The width h_I of the interfacial region was suggested to be:

$$h_I = 2b / \sqrt{6\chi} \tag{I-9}$$

Obviously, h_I is typically less than the radius of gyration $R_g \sim b/\sqrt{6/N}$. Thus, the number of chain entanglements in the interfacial region h_I/N_e is less than the entanglement density in the bulk phase R_g/N_e, where N_e is the length of one entanglement. Thus, there is a lower viscosity region near the interface. This low-viscosity region does not lead to a true interfacial slip, i.e., a velocity discontinuity, as observed at the interface between the polymer melts. Rather, as shown in Figure I-5, when a shear stress is applied parallel to the interface, the shear rate is discontinuous across the interfacial region. This lower viscosity of the interfacial region reduces the apparent blend viscosity.
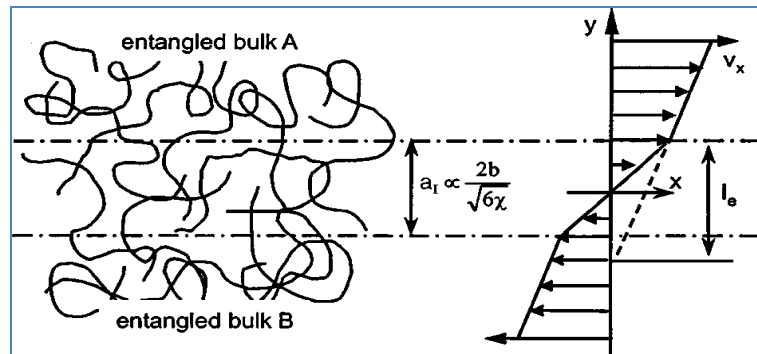
Figure I- 5 Interfacial zone between weakly incompatible polymers (from Zhao and Macosko 2002)

The authors used a concept of extrapolation of length l_e to measure the interfacial slip at the polymer–polymer interface. As shown in Figure I-5, l_e is defined as the distance to extrapolate the velocity at the interface back to zero, $l_e = (h_I / 2)\eta_{bulk} / \eta_I$, where η_{bulk} and η_I are the bulk and interfacial viscosities. Consequently, the deviation of the apparent viscosity of A/B bilayers, η_{app}, from the bulk viscosity, $\eta_{bulk,}$ is:

$$\frac{\eta_{bulk} - \eta_{app}}{\eta_{app}} = \frac{2 l_e}{L}\left(1 - \frac{\eta_I}{\eta_{bulk}}\right) \tag{I-10}$$

As demonstrated, the interfacial viscosity is always lower than the bulk viscosity for the system of incompatible polymers. Apparently, eq. (I-10) implies that the viscosity is reduced for the incompatible polymer blends (or multilayers) as opposed to their bulks. In a word, the origin of the interfacial slip is dedicated to the low viscosity and the lack of entanglements in the interfacial region, which cause the negative deviation of the viscosity.

I.2.2.3 Suppression or elimination of the interfacial slippage

The interfacial slippage is of practical importance due to its effect on the morphology and adhesion in multiphase systems such as blends or multilayer structures. For instance, Zhang et al.(2006b) demonstrated that above a critical value of shear stress, polymer chains at the interface are disentangled by the shear stress during coextrusion, resulting in slippage and reduced adhesion due to the rapid shear flow destroying interfacial entanglements. This raises a question of how the interfacial slippage can be suppressed. To the best of our knowledge, few studies have, with regard to fundamental and experimental aspects, been dedicated to the role of reactive compatibilization on the interfacial slip phenomenon. Researchers(Lamnawar, et al. 2013) have shown that the addition of block copolymers and in-situ formed graft copolymers at the interface is able to reduce the interfacial slip since such substances promote entanglements at the interface.
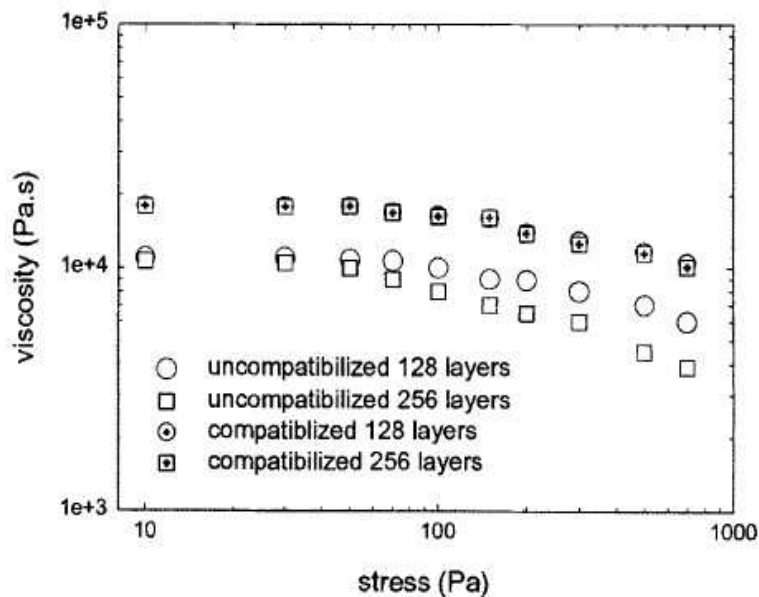
Figure I- 6 The viscosity of uncompatibilized (EPR/Nylon-6) and compatibilized (EPR/Nylon-6/ EPR-g-MA) multilayer samples (from Van Puyvelde et al. 2003)

Figure I-6 describes the results of Van Puyvelde et al.(2003) on the viscosity versus shear stress for multilayer structures of non-compatibilized (EPR/Nylon-6) and compatibilized (EPR/Nylon-6/ EPR-g-MA) systems. It is shown that the viscosity decreases with an increasing number of layers at the high shear stress for the non-compatiblilized systems whereas the viscosity of the compatilililized multilayers

is independent of their number, indicating that the interfacial slip occurring at non-compatililized multilayers can be suppressed by reactive compatibilization.

I.2.3 Interfacial reactions at polymer-polymer interfaces

One more important interfacial phenomenon that is widely described in the literature is the interfacial reaction that occurs especially between reactive incompatible polymer pairs. The main focus is on reaction kinetics (either reaction-controlled or diffusion-controlled), and the development of the interfacial morphology. The investigations of this phenomenon can be commonly divided into theoretical and experimental aspects.

From a theoretical aspect, O'Shaughnessy et al.(O'Shaughnessy and Vavylonis 1999;OShaughnessy and Sawhney 1996) and Fredrickson et al.(Fredrickson 1996;Fredrickson and Leibler 1996;Fredrickson and Milner 1996) dedicated much work to describing the reaction kinetics at an interface of two immiscible polymer melts. Meanwhile, some simulation studies, e.g., Monte Carlo simulations(Muller 1997), molecular dynamics simulations(Patashinski, et al. 2012), dissipative particle dynamics(Berezkin and Kudryavtsev 2013), etc. have also been attempted. These studies were mainly aimed at discerning the different regimes of time dependence of the reaction kinetics, taking into account the effects of several significant parameters like the local reactivity Q, reactive group densities n^∞, the interface width h, the molecular weight M, the diffusion coefficient D, and the reaction time t, etc. (see Figure I-7a). Such systematic theoretical work has presented some advances regarding the reactive coupling kinetics at polymer-polymer interfaces, with a typical prediction of three time regimes (see Figure I-7b):

i. The early stage (reaction-controlled regime): At times smaller than τ_ρ, a characteristic time for the density in the interfacial region, initially at ρ_0, to decay, the density of reactive chains at the interface remains close to its bulk value. In this stage, both depletion of reactants at the interface and copolymer saturation effects are negligible, the coverage grows linearly in time with a slope K_0, showing second-order kinetics as $\sigma(t) \approx K_0 n_A^\infty n_B^\infty t$. The time-independent quasi-local reaction rate coefficient, $K_0 = Qa^4$, where Q is the local reactivity and *a* is the reactive group size.

ii. The intermediate stage (diffusion-controlled regime): in this stage, copolymer saturation of the interface remains negligible, but a depletion hole of more dilute species builds up around the interface. The growth is dominated by the diffusion of the more dilute A reactive species to the interface and is independent of the reaction kinetics, i.e., K_0. The reaction shows first-order kinetics as

$\sigma(t) \approx (2/\pi^{1/2}) n_A^\infty (D_0 t)^{1/2}$, where $n^\infty{}_A$ is the reactive chain density of A and D_0

is the center-of-mass diffusion coefficient of a reactive chain.

iii. The late stage regime (saturation): for times exceeding the characteristic time

for the buildup of the copolymer layer,τ_σ, the copolymer coverage attains a critical level σ^*, a significant chemical potential barrier($>>k_BT$) is presented to reactive chains near the interface, the rate constant becomes exponentially small. The diffusion barrier presented by the growing copolymer layer suppresses the progress of reaction as $\sigma(t) \propto \sigma^* \ln^{1/2}[N^{1/2}t/(\tau_\sigma \ln N)]$.
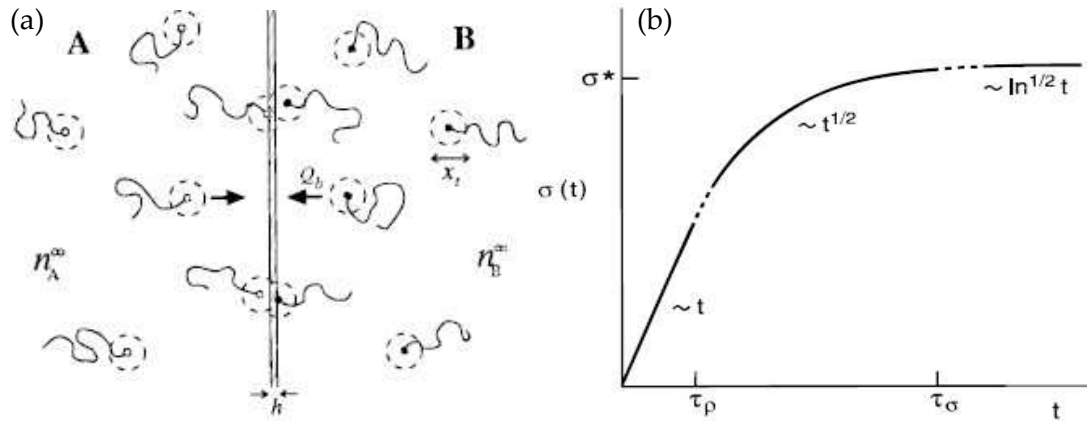
Figure I-7 (a) Interface width h between two reactive polymer couples (from O'Shaughnessy and Vavylonis 1999); (b) Predicted growth of copolymer coverage (number of diblocks per area of interface) $\sigma(t)$ versus time(from Fredrickson and Milner 1996)

In fact, interfacial kinetics is extremely complicated in realistic cases. In the simulation work, diffusion-controlled kinetics are well reproduced on the molecular level while the linear regime is distorted or not observed at all. These results are attributed to the unrealistically high reaction rates used in all simulations of end-coupling performed so far. Moreover, in principle, the most popular model utilized in theoretical studies is based on a flat interface between two polymer melts. This enables a saturation stage to be reached without the morphology development being considered. In fact, as demonstrated by experimental findings and computer simulations(Berezkin and Kudryavtsev 2011), the interface saturation at the late stage can give place to the possibility of accelerating the reaction kinetics, which is accompanied by an interfacial instability. This is because the flat interface becomes unstable when a large concentration of copolymer coverage causes the interfacial tension to vanish, thus inducing a roughening and emulsification morphology at the interface as reported in experimental studies.

Regarding the experimental aspect of interfacial reactions, the group of Macosko in University of Minnesota(Guegan, et al. 1994;Lyu, et al. 1999;Macosko, et al. 2005;Orr, et al. 2001;Schulze, et al. 2000;Schulze, et al. 2001;Scott and Macosko 1994;Zhang, et al. 2010) have performed much work on this subject from the end of the 1990s to date based on functional PS/functional PMMA as a model reaction system and with SEC,TEM,AFM,FRES (forward recoil electron spectrometry), etc. as characterization tools. Their wide interests range from reaction kinetics, interfacial

morphology changes to the effect of thermodynamic interactions, comparisons of reactivity order of different reactive functions, reactions in the shear field and the effect of flow, etc.

Table I-2. Comparison of the conversion at 2 min for different terminal reactive groups (from Macosko 2005)

Group1	Group2	Conversion at 2minutes at 180 ºC	K(kg/molmin)
Polystyrene			
Carboxylic acid	Aliphatic amine	0%	-
Aromatic amine	Aliphatic epoxy	0.6%	0.1
Aromatic amine	GMA epoxy	0.7%	0.15
Aliphatic amine	Aliphatic epoxy	1.1%	0.28
Aliphatic amine	GMA epoxy	1.8%	0.34
Carboxylic acid	Oxazoline	2.1%	0.92
Carboxylic acid	GMA epoxy	9.0%	2.1
Aromatic amine	Cyclic anhydride	12.5%	3.3
Aliphatic amine	Cyclic anhydride	99%	$\sim 10^3$
Aliphatic amine	Isocyanate	99%	$>10^5$(at 23ºC)
Poly(methyl methacrylate)			
Aromatic amine	Cyclic anhydride	5.2%	1.9
Aliphatic amine	Cyclic anhydride	99%	$\sim 10^3$

Other groups like the Kramer group at Cornell university(Jiao, et al. 1999;Kim, et al. 2005a), Harton et al.(2005), Oyama and Inoue (2001), etc. have also carried out numerous investigations on interfacial couplings via various spectroscopic tools such DSIMS (secondary ion mass spectroscopy), SFM (scanning force microscopy) and ellipsometry, XPS, etc. Among these, different reaction kinetics (either diffusion-controlled or reaction-controlled) was reported depending on the different experimental conditions. For example, Kramer's group(Jiao, et al. 1999;Kim, et al. 2005a), working with PS-NH2/PSMA and PS/P2VP, obtained reaction-controlled kinetics for their systems. They also demonstrated the idea that the interfacial roughening and emulsified droplets observed in their experiments were induced from the near-zero value of the interfacial tension resulting from the interfacial excess of generated copolymers. On the contrary, Harton et al.(2005) reported diffusion-controlled kinetics for their system of PS-OH/PMMA-MAA as determined by DSIMS. Nevertheless, using a PA/PSU system and ellipsometry and XPS techniques, Oyama and Inoue (2001) demonstrated pseudo-first-order (reaction-controlled) kinetics. Interestingly, the reactivity of different terminal functional groups attached to a polymer chain with their complementary functional

groups has been compared by Orr et al.(2001). As shown in Table I-2, the order of increasing reactivity for the functional group pairs are: acid/amine, hydroxyl/(anhydride or acid), aromatic amine/epoxy, aliphatic amine/epoxy, acid/oxazoline, acid/epoxy, aromatic amine/anhydride, and aliphaticamine/anhydride.

Furthermore, in a shear flow field, the flow affects the interfacial reaction tremendously, resulting in a rate constant that maybe 1000 times higher in heterogeneous melt blending than that in the static bilayer film(Jeon and Kim 2000). The interactions of the interfaces between the various layers can be affected by chemical reactions, the presence of a copolymer, and the involved stress-strain fields during the process(Guegan, et al. 1994;Zhang, et al. 2007). Another important feature of interfacial coupling is the morphology changes at the interface, with the appearance of an abrupt roughening and microemulsion (and micelles). This phenomenon was also observed in the experimental study of Kim et al.(Kim, et al. 2003;Kim, et al. 2005b) on PS-mCOOH/PMMA-GMA system, as shown in Figure I-8. The size of the roughening and microemulsion was reported to be on the order of one hundred nanometers. In their work, the authors employed rheology (SAOS) to probe the reaction kinetics at the interface by following the variations of the rheological functions and proposed three distinct stages for the change of complex viscosity (η^*) with time: (i) stage I, where η^*increased rapidly at short times and approached a steady value at later times; (ii) stage II, where η^*remained unchanged; and (iii) stage III, where η^* increased slowly again and reached a final value. The apparent reaction kinetics obtained from the results in stage I corresponded to a first-order reaction.
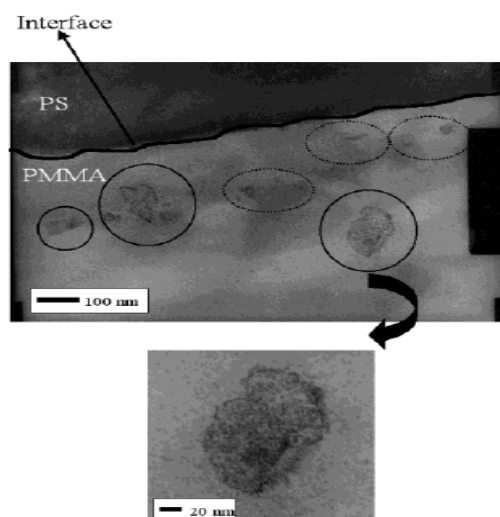
Figure I-8 Microemulsions and micelles observed from TEM images of PS-mCOOH/PMMA-GMA reacted at 180 °C for 17 h (scale: 100 nm in top, 20 nm in bottom). (From Kim et al 2003)

In addition, other rheological tools like extensional rheometry measured on

multilayered structures were shown to be sensitive to interfacial grafting or crosslinking reactions (Levitt, et al. 1997) and can be used to measure the interphase(Saito and Macosko 2002). Following these achievements, Lamnawar and Maazouz(Lamnawar, et al. 2010a;Lamnawar and Maazouz 2006; 2008) recently performed a great amount of work on the subject of interfacial reaction using a coextruded PE-GMA/PA6 multilayer system characterized with rheological tools. The authors focused on the competition of reaction/diffusion at the experimental conditions of 230 °C to 290 °C, and addressed 1) the effect of the temperature, the heating rate of the temperature, the angular frequency, the pre-shear exertion, the interfacial area etc.; 2) the determination of interfacial reaction kinetics in the investigated system; 3) the monitoring and quantification of the interphase generated from interfacial reactions, etc.

The significant increase in viscosity versus time for the reactive system of PE-GMA/PA6 in comparison with the invariable viscosity for the non-reactive system of PE/PA6 was evidence of the formation of a copolymer from the reaction of PE-GMA and the carboxylic and amine end functions of PA6 (Figure I-9a). Since a reactive polymer bilayer generates graft or block copolymers near the interface, each block (or graft) component can easily entangle (or stitch) with the corresponding homopolymer located near the interface. Thus, the interface should be strengthened compared with one without graft or block copolymers. This could increase the viscosity of the reactive polymer bilayer compared with a non-reactive one. When studying the reaction kinetics, the authors proposed the use of an expression of G' as a function of the welding time:

$$G'(t) = G o + k.(t)^c \qquad \text{(I-11)}$$

in which G_0 is the storage modulus at t=0; K is a constant and *c* is a time exponent. Eq. (I-11) was found to fit the experiment results well for both low and high temperatures. Interestingly, and as shown in Figure I-9b, the evolution of the time exponent (*c*) with temperature enabled to distinguish two ranges of temperature.
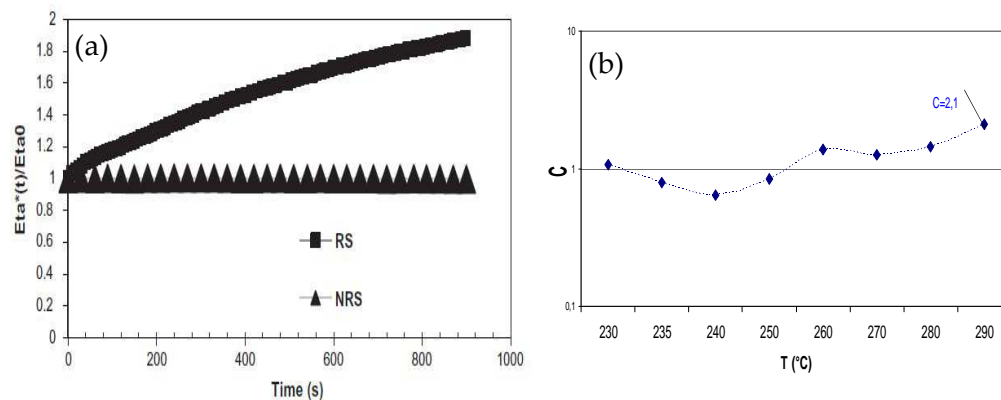
Figure I- 9 (a)Evolution comparison of Eta*/Eta0 vs. time at 240 °C of PE-GMA/PA6

bilayer system (RS) and non-reactive one based on PE/PA6 (NRS).(from Lamnawar et al. 2010a) (b)Evolution of the time exponent *c* with temperature obtained from the fitting data with Eq. (I-11) (from Lamnawar and Maazouz 2006)

The first one was below 240°C, for which C decreased to the lowest value (*c*=0.6 at 240°C), describing the mobility of chains at the interface governed by the Fickian diffusion accompanying the increase in reaction kinetics with temperature. Beyond 240°C, the time exponent(*c*) increased significantly and became very important at higher temperatures (*c*=2.1 at 290°C), confirming the remarkable incident of a secondary reaction (auto-cross-linking) in the evolution of the storage modulus. As a consequence, the variation in Eta* of the multilayer system reflected the occurrence of both diffusion and chemical reaction: because of the increase in the interfacial adhesion strength due to the coupling reactions between epoxy, carboxylic, and amino groups, interdiffusion phenomena were found to increase when the kinetics of the chemical reaction at the interfaces became improved.

I.2.4 Partial concluding remarks

A polymer interdiffusion process is usually described under the framework of the Doi-Edwards theory considering that the motion of a polymer chain is confined in a tube constructed by the topological entanglement structure of surrounding chains. For the interdiffusion between two compatible polymers, the thermodynamic interaction plays a significant role in the diffusion kinetics. Various techniques with different spatial resolutions and different principles have been developed to determine the interdiffusion kinetics and the diffusion coefficient. Rheology has been demonstrated to be a reliable tool when measuring the diffusion coefficients through some quantitative rheological models. Indeed, the interdiffusion process in coextrusion will be further affected by the polymer chain orientation in a shear flow field.

For an incompatible polymer multiphase system such as a blend or multilayer, the weak entanglement density and low viscosity at the polymer-polymer interface causes a discontinuity of the velocity across the interface (interfacial slip) when the system is subjected to a shear stress, especially above a critical stress value. This interfacial slip has been argued to be attributable to the abnormally low viscosity observed for an incompatible polymer blend or multilayer systems. The existence of interfacial slip has been demonstrated via microscopic tools and various rheometers, and the slip velocity has been quantified to be a function of shear stress. The interfacial slip is unfavorable for the adhesion between neighboring layers. The addition of block copolymers or in-situ formed graft copolymers at the interface was suggested to be able to suppress the interfacial slip to some extent.

In the vast theoretical and experimental studies of interfacial reactions at planar interfaces, the interfacial reaction kinetics were determined to be either reaction-controlled, diffusion-controlled or saturated, depending on a series of

parameters like the local reactivity, reactive group densities, the diffusion coefficient, reaction times, interface widths, molecular weights, etc. Besides, an interfacial reaction causes the interface to be unstable, which is accompanied by roughened and/or microemulsion morphology. This is due to the removal of the interfacial tension since enough copolymers are formed at the interface.

The phenomena of interdiffusion, interfacial slippage and interfacial reaction can have more or less favorable or unfavorable impacts on the adhesion, mixing, morphology development and properties, etc. at the interface of neighboring layers for a multilayer structure. Since this is the case, the importance of the interfacial physicochemical affinity cannot be neglected, especially in the study of the interfacial flow stabilities of coextrusion. In spite of the relevance of such research and the value it can have for practical applications, the contribution of the role of these physicochemical affinities in controlling the interfacial flow instabilities of coextrusion is still sparse.

I.3 Nonlinear Rheology of Multilayer Structures

In linear viscoelastic regime where the deformation is very small or very slow, rheological response of polymer chains can be considered to be independent of the deformation and can be well described under the framework of tube model proposed by de Gennes(1971) and developed by Doi-Edwards(Doi and Edwards 1986). When the deformation is large or rapid, the polymer chains respond to the deformation in a nonlinear relation. That means the rheological response of the polymer chains in nonlinear regime becomes dependent on the magnitude, the rate and the kinematics of the deformation. Unfortunately, the nonlinear rheology of well-defined polymers that involves in transient regime are still far less explored and understood with respect to the unclear relations between flow and structure(Iza and Bousmina 2000;Snijkers, et al. 2013). In general, step strain experiments and step strain rate experiments in shear flow and/or extensional flow are of interest for the rheologists to study the nonlinear rheological features of polymer chains. However, the theoretical interpretation for the nonlinear rheology is still a complex open problem since hitherto no universal constitutive equations are available to describe all the nonlinear behaviors. Due to such theoretical immaturity in the field of nonlinear rheology, the studies on the nonlinear viscoelasticity of multiphase polymer systems are even sparser. In this section, some brief reviews on the stress relaxation after step strains, transient rheology in simple shear and in uni-axial extension are addressed, especially regarding the multilayer polymer systems.

I.3.1 Stress relaxation after step strains

A single step shear relaxation experiment with a shear deformation γ_0 is one of the most illustrative methods to obtain information about the viscoelastic character of a material. After the step deformation, polymer is rested to record the variation of the

shear stress $\sigma(t,\gamma_0)$ caused from the deformation versus time (Figure I-10). The measured shear stress in the test could be expressed by a material function named nonlinear shear modulus G (t, γ_0), defined as

$$G(t,\gamma_0) = \sigma(t,\gamma_0)/\gamma_0 \qquad\qquad (I\text{-}12)$$

Indeed, it is not possible to impose an ideal step strain to the material due to the inertial problem of the instrument and the fluids which limits a truly instantaneous acceleration of strain. Normally, a finite rise time, Δt, is required to achieve the experimentally desired strain value, with the time length depending on the rheometer and materials. When the motor controller is tuned to give a very fast response, there will be an overshoot and ringing in the actual strain history. It is more convenient to model the "step" as a ramp in the initial transient within the duration of Δt, hence the actual shear rate is $\gamma_0/\Delta t$ rather than infinity (Figure I-10). It is universally deemed that only the results with t>10Δt can represent the true behavior of the melt (Dealy and Larson 2006;Rolon-Garrido and Wagner 2009;Yu 2013).
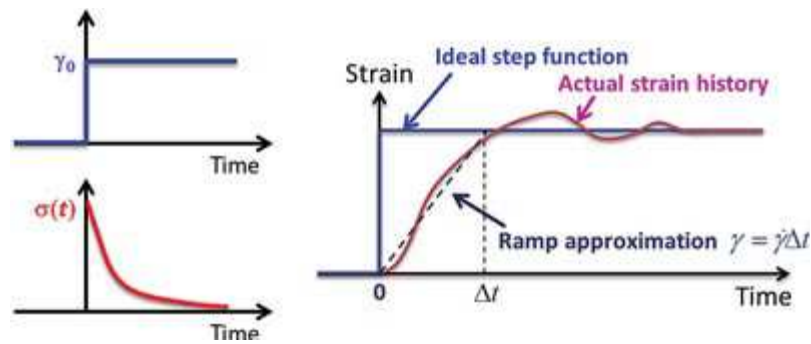
Figure I- 10 Schematics of transient strain and stress, while the actual strain in not an ideal step function. (from Yu 2013)

When the deformation is very small or very slow that lies in the linear regime, the G(t, γ_0) reduces to be linear-viscoelastic relaxation modulus G(t), which is only a function of time. Above a critical strain, the G(t, γ_0) of an entangled polymer drops to successively lower levels as strain magnitude of shear is increased (Figure I-11).
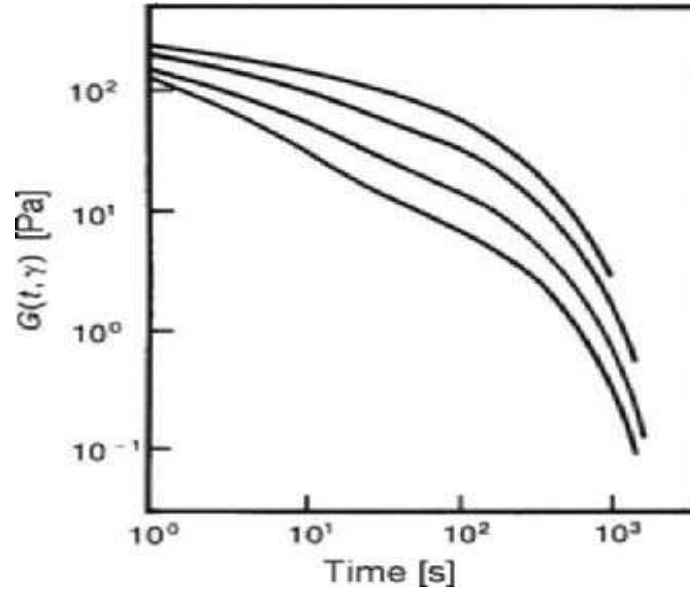
Figure I- 11 Relaxation moduli at several step-strain amplitudes for a polystyrene solution with cM = 5 ×10^5 g cm^{-3}. At the smallest strain (top curve), the behavior is linear, but as the strain increases, the modulus is reduced except at very short times (off scale). (From Osaki 1993)

At long times, the nonlinear stress modulus curve versus time appears to be superposable by the vertical shift on the log-log plot. That is the so-called time-strain separability. In other words, the G(t, γ₀) could be separated into time-dependent and strain-dependent factors as

$$G(t, \gamma_0) = G(t)h(\gamma_0) \tag{I-13}$$

with $h(\gamma_0)$ being called damping function, representing the intensity of nonlinearity.

To date, it appears that there are different theoretical arguments for the nonlinear phenomena. The tube model of Doi-Edwards (DE) theory that simplified the constraints of surrounding chains on the test chain into a tube having a characteristic length and diameter interpreted the nonlinear stress relaxation as a new relaxation mechanism of chain retraction within its tube. In response to a sudden large deformation, the tube is deformed affinely whereby the chain segments are stretched beyond its equilibrium tube contour length, followed by a retraction of the chain segments within its tube to the original length. The fast relaxation process of retraction gives rise to an early, rapid decrease in the relaxation modulus curve and once it is completed the remainder of the relaxation process of stress arising from the chain segment orientations occurs via reptation as in the case of linear viscoelastic regime. This is the main idea of two-step relaxation behavior of the tube model, that is, a fast relaxation of contraction before the second step of orientational relaxation. This idea explained the time-strain separability appeared in relaxation modulus curve of entangled polymer chains subjected to large deformations. Thus,

- 32 -

the damping function deduced from the DE model, $h^{DE}(\gamma_0)$ represents a decrease of a number of the entanglement segment per chain due to the chain contraction. This $h^{DE}(\gamma_0)$ which is universal as no adjustable parameters is needed in its deduction agrees well with the experimental data of $h(\gamma_0)$ for many monodisperse linear entangled polymers.
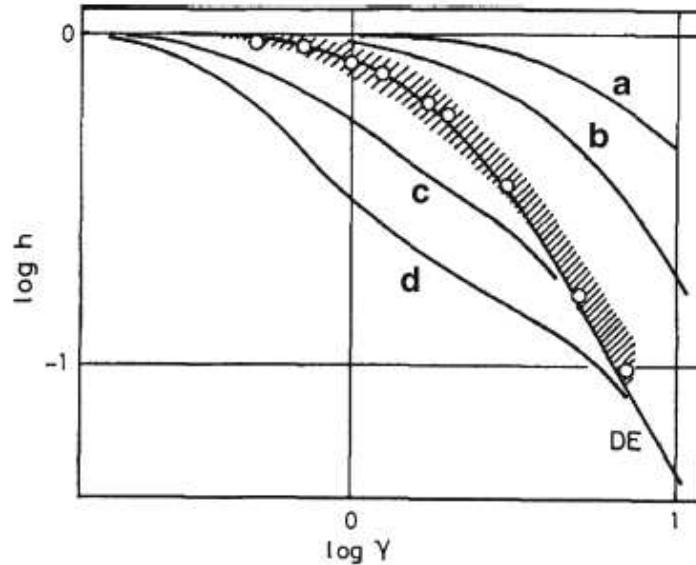
Figure I- 12 Classification of damping function behavior according to Osaki. Type A: described by the DE model (*dashed area*); type B: weaker damping function than the DE model (*a* and *b*); type C: below the tube model prediction (*c* and *d*) (from Osaki, 1993)

Osaki (1993) classified the damping behaviors of polymers into three types, i.e., type A, type B and type C using the $h^{DE}(\gamma_0)$ of DE prediction as a reference. Materials with experimental data $h(\gamma_0)$ lying in the zone of DE model as shown in Figure I-12 were classified into type A, which was supposed to be valid for linear entangled polymers with narrow molecular weight distribution and $M/M_e<50$; The cases that with weaker damping function than DE model like the curves a and b in Figure (I-12) are denoted as type B. Materials with board molecular weight distribution or multiple branch points per molecule appeared to behave such type of damping behavior. Experimental data defined as type C like the curves c and d in Figure I-12 are those exhibit severe damping functions than the DE prediction. Example of this type has been found in polystyrene solutions with $M/M_e>60$ by Marrison and Larson(1992). In this case, an anomaly appears in a plot of shear modulus versus time after the sufficiently large step strain as the nonlinear modulus experiences a very sharp decrease followed by a sudden reversion to the superposable behavior, which sometimes is described as a "kink"(Dealy and Larson 2006). Such kink-like type C is now widely accepted to be caused from experimental artifacts rather than material structures. The critical reason for the type C behavior is the interfacial slip occurs between the bulk polymer and the molecules absorbed at the wall of the rheometer (wall slip) (Ravindranath and Wang 2007;Sanchez-Reyes and Archer 2002;Venerus

.

A serious failure of the original Doi-Edwards theory on nonlinear rheology was that while the orientation tensor of the DE model correctly describes the effect of shear strains on molecular orientation in step shear, it predicts excessive levels of molecular alignment in steady shear flow(Sanchez-Reyes and Archer 2002). A new relaxation mechanism "Convective Constraint Release"(CCR) which was first clearly recognized and modeled by Marrucci (1996) is able to remedy the failure of the original DE model. In response to a large affine deformation, a test chain experiences retraction process, meanwhile the matrix chains surrounding the test chain also undergoes chain retraction which too must lead to constrain release. The flow convects the matrix chains past the test chain and so releases the constraints imposed by the matrix chains on the test chain at a rate proportional to the flow rate, as schemed in Figure I-13. This CCR relaxation mechanism forms the basis for most new DE constitutive models for entangled polymers.
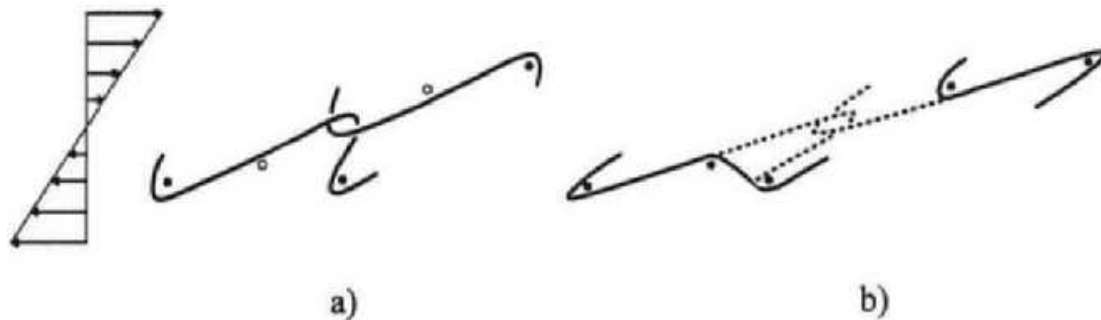
Figure I- 13 Convective constraint release mechanism as envisioned by Ianniruberto and Marrucci. A simple shear field is shown at left and has the effect of sweeping away entanglements originally present in a) allowing the test chain to relax to a new, less constraining entanglement. Filled dots are matrix chains providing active entanglements; unfilled dots become entanglements after the constraint release.

Indeed, the tube model of Doi-Edwards is a mean-field theory in which the complicated intermolecular interactions of many-body surrounding chains on the test chain are averaged by using a tube confinement. In addition to this mean-field theory, the other fundamental theoretical treatment for the entangled polymers is "transient network" models which offers an explicit role of the intermolecular interactions as "cross-link" in a network strand (Lodge 1964; 1995). The cross-links in the transient network models are stress-dependent, having finite lifetimes, differing from the assumption of infinite strength of tube confinement in DE theory. There has been a long ongoing debate about whether the tube confinement is of finite strength or is of infinite strength, i.e., whether or not the tube diameter should couple to deformation (Sussman and Schweizer 2012b). Some scientists argue that the competition between tube dilation and contraction should cancel in a step strain deformation with the tube diameter unchanged(Doi and Edwards 1986;Marrucci

1996). In contrast, other researchers argue that either tube dilation or contraction depends on the deformation as stress increases (McLeish 2002) or decreases (for extensional deformation) (Wagner 1994) tube diameter. Hence, under a large applied deformation, tube dilation, transverse entropic barrier reduction and ultimately tube destruction can subsequently happen beyond a critical level of stress or strain that exceeds the intrinsic entanglement force localizing the polymer in a tube. In fact, the first step of contraction relaxation in DE model as remedied by incorporating the CCR effect is conceptually equivalent to the disentanglement by deformation of a network strand as proposed by Wagner and Meissner (1980)(Rolon-Garrido and Wagner 2009;Wagner and Meissner 1980).

It is worthy to mention that recently Wang and coworkers (Wang, et al. 2007;Wang, et al. 2013;Wang and Wang 2009) proposed a macroscopic dynamic network picture for the phenomena of nonlinearities based on a physical idea about force imbalance in entangled chain liquids as shown in Figure I-14. They argued that the entangled polymers at Weiseenberg number W_i >1 could be regarded as a dynamic network formed by localized intermolecular interactions. Upon an external deformation with Rouse Weissenberg number W_{iR}>1, an intermolecular gripping force f_{img} arises from chain uncrossability, which in turn leads to buildup of an intrachain elastic retraction force $f_{retract}$. When the $f_{retract}$ within the strand, which is proportional to entanglement force f_{ent}, reaches the f_{img} , the original entanglements are lost in a massive amount by a way of chain sliding past other chains at the entanglement points. This entanglement network breakdown, which is analogy to a microscopic "elastic yielding" process, is asserted by them to be the molecular mechanism for the nonlinearity phenomena observed during startup or after stepwise deformation based on their rheology experiments coupled with particle tracking velocimetry.
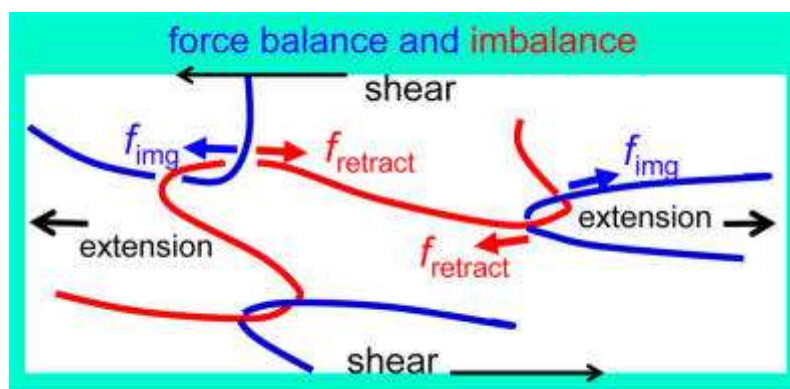
Figure I- 14 The dynamic network picture proposed by Wang and coworkers with an idea of force imbalance to depict an entangled polymer under deformation either in shear or in extension. The elastic retraction force $f_{retract}$ originates from the molecular deformation that occurs in absence of chain sliding at the entanglement points because of the intermolecular gripping force f_{img} .

Meanwhile, Sussman and Schweizer (2011b; 2012a;2012b; 2013) developed a new self-consistent microscopic theory for rigid rods by considering an anharmonic nature of the quiescent dynamic tube potential to describe the nonlinear relaxation of stress after instantaneous step-strain and the continuous startup shear deformations. This theory considers two parallel competing (and coupled) time-dependent relaxation mechanisms under stress: deformation-modified reptative rotational motion and stress -assisted activated transverse barrier hopping (tube breaking). It accounts for a time- and deformation-dependent (dilated) tube diameter, a maximum confinement force and a transverse entropic barrier. According to this theory, after a sufficiently large deformation, the entanglement network is predicted to break down, and the tube is destroyed in a manner akin to the microscopic yielding event. More recently they have qualitatively extended their microscopic theory to the case of topologically entangled melts of flexible polymer chains (Sussman and Schweizer 2012a).

I.3.1.1 Stress relaxation in relation to multiphase systems

To date, due to its readily accessible and its industrial relevance as well as academic significance, multiphase systems including polymer blends or polymer/filler composites are of high interest among researchers(Ares, et al. 2009;Lv, et al. 2013;Silva, et al. 2010;Silva, et al. 2012;Takahashi 2007;Yu, et al. 2002). Compared to the relative maturity in the linear rheology, nonlinear rheology is still an open complex problem that involves transient regime for the multiphase system with no very clear relations between flow and structural evolutions(Iza and Bousmina 2000;Yu, et al. 2002). Stress relaxation process of multiphase system has been demonstrated to be very sensitive to the interfacial properties and the morphology evolution especially the drop deformation in the case of immiscible blend during the flow. For linear relaxation, emulsion model, namely Palierne model (Palierne 1990) can be applied to fit the experimental results of immiscible blends. For the relaxation in nonlinear regime, the Doi-Ohta theory (Doi and Ohta 1991) was developed to couple between the flow and the structure by considering the complex interface as a third phase. Lee and Park (1994) extended the Doi-Ohta theory by introducing another interfacial relaxation process and considering the mismatch in viscosity of the components. Despite of its imperfect inconsistency with experimental data, the Doi-Ohta/Lee-Park theory has been often used for discussions of the interface contribution to the excess relaxaton modulus (Iza and Bousmina 2000;Lv, et al. 2013). Moreover, Vinckier et al. (1997) suggested that stress relaxation can be served as a microstructural probe for immiscible blends. As argued by them, various structural relaxation mechanisms such as retraction, breakup and Rayleigh instabilities could be identified from the shape of the relaxation curves. In the case of compatibilized blend system, experimental evidences indicated the existence of an additional relaxation time (Silva, et al. 2010). For instance, to describe the component contribution to the stress relaxation behavior of immiscible polymer blends, the

linear additivity rule has been normally used in literatures by incorporating an additional item of interface contribution (Takahashi et al. 2007; Lv et al. 2013):

$$G(t,\gamma) = [(1-\phi)G_m(t,\gamma) + \phi G_d(t,\gamma)] + G_{int}(t,\gamma) \qquad \text{(I-14)}$$

It was supposed to be the relaxation of Marangoni stress tangential to the interface between the dispersed phase and the matrix. The additional relaxation has also been observed in the relaxation process of compatibilized blend system under extensional flow (Mechbal and Bousmina 2007).

In brief, the stress relaxation behavior of multiphase polymer systems is sensitive to the interfacial properties. However, to our knowledge, experimental studies on relaxation behavior of multilayer systems are less abundant in quantity even though multilayer structure can be taken as blend system with interfacial area well-controlled. Qiu et al. (2002) carried out step strain experiments on PS/PS bilayers after being annealed for various times to determined the coupling between flow and diffusion kinetics. Besides, recently Silva et al.(2012) demonstrated that the step strain experiment was a sensitive tool to detect the presence of the interphase based on a coextruded elastomeric and amorphous glass thermoplastic polyurethanes. Despite all of these, it is still far lacking with regard to the quantitatively modeling of the contribution of the interface/interphase relaxation based on the final relaxation behavior of multilayer structures.

I.3.2 Transient rheology in simple shear

Transient rheology in simple shear is usually obtained by a fast start-up of steady shear with the strain rate instantaneously stepped from zero to a desired value $\dot{\gamma}$ at time zero as shown in Figure I-15. The response of the material to the strain rate step is the transient stress $\sigma(t,\dot{\gamma})$ and the first normal stress difference $N_1(t,\dot{\gamma})$ recorded over time. In a step test, the strain increases linearly with time and the transient stress and first normal stress difference grows from zero.
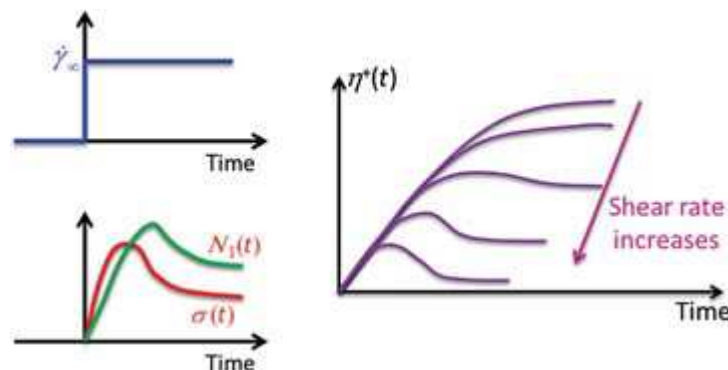
Figure I- 15 Schematics of the start-up in simple shear experiments (from Yu 2013)

Transient viscosity, $\eta^+(t,\dot{\gamma})$, also called as stress growth coefficient and the first

normal stress difference coefficient $\psi^+(t,\dot{\gamma})$ are defined as

$$\eta^+(t,\dot{\gamma}) = \frac{\sigma(t,\dot{\gamma})}{\dot{\gamma}} \qquad \text{(I-15)}$$

$$\psi^+(t,\dot{\gamma}) = \frac{N_1(t,\dot{\gamma})}{\dot{\gamma}^2} \qquad \text{(I-16)}$$

when the shear rate is sufficiently low, the stress growth coefficient can reduced to a linear viscoelastic property, which can be related to the relaxation modulus by:

$$\eta^+(t,\dot{\gamma}\to 0) = \eta^+(t) = \int_0^t G(s)ds \qquad \text{(I-17)}$$

As shown in Figure I-15, in transient shear flow, nonlinear response involves overshoots could be found in stress growth coefficient curve. At short times when the strain is very small, the $\eta^+(t,\dot{\gamma})$ follows the linear viscoelastic envelop (LVE) curve as the case of very low shear rates. As the shear rate increases, nonlinear feature appears at shorter and shorter times with the $\eta^+(t,\dot{\gamma})$ falling below the LVE. The overshoot peak was reported to emerge in the stress growth coefficient and the first normal stress difference coefficient curves when the Wi>1. As for step strains, various theoretical arguments and constitutive equations have been developed for the nonlinear features like overshoot in start-up shear deformation. They are mostly based on either the orientation/retraction mechanism of DE models (Doi and Edwards 1986;Marrucci 1996) or entanglement- disentanglement transition (tube break) mechanism akin to transient network models claiming existence of lateral motions (Rolon-Garrido and Wagner 2009;Sussman and Schweizer 2012b;Wang, et al. 2007).

In addition to instrument compliance, gap spacing and wall slip, etc., one more main experimental difficulty in rotaional rheometer for start-up shear measurements is the appearance of viscous flow instabilities like edge fracture which limits melts to a low strains or strain rates, not very far into the nonlinear regime (Dealy and Larson 2006). Use of a partitioned plate was reported to be possible to avoid the edge fracture in a commercial polystyrene to a shear rate up to 100s^{-1} (Schweizer, et al. 2004).

I.3.2.1 Start-up shear in relation to multiphase systems

Transient flow experiments in start-up have been widely used to examine nonlinear rheological response of solutions, melts, wormlike micelles (Berret 1997), concentrated suspensions (Watanabe, et al. 1999), blends (Chopra, et al. 2000) and nanocomposites (Hassanabadi and Rodrigue 2012), etc. Issues more relevant to the present study are the multiphase systems especially the multilayered structures. In

general, for the rheology-morphology relationships in fully immiscible systems, the Doi-Ohta (1991) theory has been demonstrated to be successful in describing the nonlinear response in steady conditions for mixtures of varying viscoelastic contrast as well as during startup of simple shear (Vinckier, et al. 1997). Chopra et al. (2000) probed the thermorheological complexity of partially miscible polyer blends of poly(styrene-co-maleic anhydride)/poly(methyl methacrylate) during startup of simple shear flow. In that study, they argued that the evolution of shear, normal stress and morphological changes could be understood at a first approximation based on the respective behaivor of immiscible blends as described by the Doi-Ohta theory. More importantly, it was stated that the slip relaxation effects might become important under transient flows (Hatzikiriakos 2012;Mhetar and Archer 1998). Kazatchkov and Hatzikiriakos (2010) demonstrated a significant wall slip in LLDPE melt at very high shear rate in the start-up of steady shear experiment and a dynamic multimode slip model was proposed to predict the experimental shear stress. Likewise, start-up shear experiment has been found to be sensitive to the interfacial slippage taking place at multilayer samples especially under high shear stress (Lee, et al. 2009;Zartman and Wang 2011). As demonstrated in the work of Lee et al. (2009), at high rates, the shear stresses as well as normal stresses and the transient viscosity of polypropylene(PS)/polystyrene(PS) coextruded multilayers appear to be significantly lower than the average values of the constituent polymers. Such negative deviation becomes even more severe as the layer number is increased. Interfacial slippage velocity was determined base on the nominal viscosity of the multilayer systems, which was reported to be a function of the shear stress. By virtue of start-up shear measurement in conjunction with particle tracking velocimetry(PTV), Zartman and Wang(2011) have examined how interfacial slip is produced during and after large deformations. They have observed the interfacial slip upon start-up shear and arrested slip after shear cessation. All these indicate a hint that the chain entanglements lying at the interface/interphase would be significantly weaker than each of constituent bulk polymers, which are prone to produce interfacial yielding as long as external stress is sufficiently high.

I.3.3 Transient rheology in uni-axial extension

For elongation rheology, the measurement of extensional viscosity accurately is a more challenging task in comparison to the shearing deformations. In the present study, we are only interested in the uni-axial extension, with other types of elongation like biaxial extension and planar extension put aside. Many of the experimental difficulties encountered in the extensional measurements have been addressed in the work of Schweizer (2000) and that of Barroso et al. (2002) as well as a more early review article of Meissner (1985). For instance, as extensional force should be transferred from solid fixtures to the test fluid, end effects related non-pure extension can often be a problem near the solid fixtures. One very common important challenge is sample sagging due to gravity followed by melting the sample

especially for those of less viscosity. Supporting mediums are often used to suspend in the sample during the measurement by employing a heating oil bath or an inert gas cushion. Moreover, non-uniformities in deformation and temperature throughout the experiment constitute another error source in such type of measurement. Undoubtedly, good specimen preparation also takes a very important place for an accurate measurement as inhomogeneity in specimen could be amplified during stretching. Besides, the ultimate limits of the total strain are determined by followings: length of the rheometer, flow insability, surface tension, necking and rupture and de-adhesion from end plates (Barroso, et al. 2002;Dealy and Larson 2006). Despite of its high complexity of experimental operation, the extensional measurements are particularly emphasized due to its high sensitivity to the molecular structure of the polymeric system being tested and its high significance in many types of processing like blow molding, film blowing and fiber spinning, etc.(Andrade and Maia 2011).

In uni-axial extension, the experiment usually carried out is start-up of steady simple extension at a constant Hencky strain rate $\dot{\varepsilon}_H$ which is defined in term of sample length L as

$$\dot{\varepsilon} = d \ln L / dt \qquad \text{(I-18)}$$

Note that the velocity of the end of the sample and the sample length increase exponentially with time when a constent Hencky strain rate is commanded. i.e.

$$L(t) = L(0) \exp(\dot{\varepsilon} t) \qquad \text{(I-19)}$$

The material function that usually measured in a start-up uni-axial extension at a Hencky strain rate is the tensile stress growth coefficient as defined from the net tensile stress σ_E by:

$$\eta_E^+(t, \dot{\varepsilon}) = \sigma_E(t, \dot{\varepsilon}) / \dot{\varepsilon} \qquad \text{(I-20)}$$

with the limit of steady extensional flow ($\lim_{t \to \infty} \eta_E^+(t, \dot{\varepsilon})$) being extensional viscosity, $\eta_E(\dot{\varepsilon})$. Newtonian fluid behavior could be denoted in the case of vanishing strain rate or very short time at high strain rate, with the transient extensional viscosity in these linear viscoelastic limits, $\eta_{E,0}^+(t)$, being related to the zero-shear transient viscosity, $\eta_0^+(t)$ as $\eta_{E,0}^+(t) = 3\eta_0^+(t)$. The quantity $\eta_E(\dot{\varepsilon})/(3\eta_0)$ is sometimes referred as Trouton ratio, used to normalize extensional viscosity data.

I.3.3.1 Experimental Methods

Several different extensional setups have been available to date for the measurement of uni-axial extension. The first reliable and accurate setup for extension should be the Meissner-type rheometer (Meissner 1979) in which the sample strip is mounted in horizontal position on an oil bath and extended between rotary clamps. The

commercial version of this setup, i.e., Rheometrics melt extensionmeter (RME: Meissner and Hostettler 1994) which is widely used around the word supports the sample by inert gas flow and stretches it by rotating metal belts. The major challenge is the accurate determination of the strain rate since the actual strain rate could be 20% lower than that directly calculated from the belt velocity (Dealy 2006). The Munstedt tensile rheometer (MTR: Munstedt 1979) and Filament-stretching rheometer (FSR) developed by Mckinley and Seidhar (2002) are two types of end-separation devices. In MTR, the sample is fixed in vertical position in an oil bath before being extended between two grips that displace vertically apart from each other. A strain of $5s^{-1}$ can be reached and creep measurements can be available in the MTR while the temperature is limited to 220 ^{o}C due to the silicone oil used in the bath. In FSR, a cylindrical sample is stretched between two end plates moving apart from each other during which the filament is formed from the small sample. The strain in this device is not uniform and measurement is based on the radius of the filament at the middle position. It is worthwhile to mention that Maia and Binding(1999) proposed a modification to a commercially controlled rate rheometer (MRR) based on a Weissenberg Rheogoniometer to measure transient uniaxial extensional viscosity of polymer melts. Their apparatus takes advantage of the extremely precise driving and measuring systems of the rheogoniometer and it is easy to set-up as well stretching is homogeneous. Several studies of melt rupture conditions have been carried out by them based on the MRR (Aho, et al. 2010).

Recently, a more simple and compact device which can be installed in the oven of a conventional rotational rheometer for uniaxial extension was reported to be Sentmanat extensional rheometer (SER)(Sentmanat 2004). As sketched in Figure I-16, the SER is a dual windup device with a slice of sample attached to the surface of two counter-rotating drums. Thus, the Hencky strain rate applied to the sample specimen can be determined from the drive shaft rotation rate and the force in the sample is calculated from the torque output of the rheometer. The stretching process of the sample can be viewed or recorded through a window in the chamber as the SER fixture is attached to the rheometer. Moreover, the sagging effect in the sample geometry with an upright rectangular cross-section in the case of SER is calculated to be 100 times lower than the flat rectangular cross-section used in the geometries of other extensional fixtures. This SER is the main tool used in the present study for elongation rheology, more details of which could be found in the relevant chapter. Note that one more similar dual windup extension device is the extensional viscosity fixture (EVF) developed by TA Instruments. In this geometry, there is no gear friction, but the sample rotates during stretching due to the fact that one of the drums rotates around the other which makes it difficult to be captured in view(Dealy and Larson 2006).
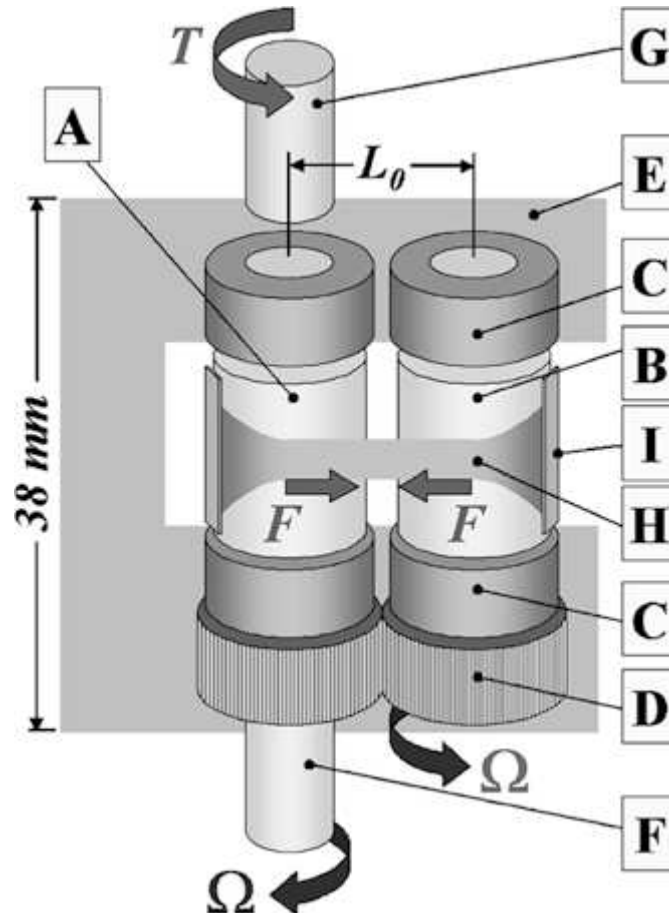
Figure I-16 Schematic view of the Sentmanat extensional rheometer (SER) during operation. Inside squares: A Master drum, B slave drum, C bearings, D intermeshing gears, E chassis, F drive shaft, G torque shaft, H sample, I securing clamps. Other symbols: L$_0$ unsupported length, W drive shaft rotation rate, T torque, F tangential force

Intriguingly, in addition to the greatly interesting strain rate controlled tests via the above-mentioned extensional devices, attentions have been paid to constant force (Wagner and Rolon-Garrido 2012) and constant stress extensional rheometry (Andrade and Maia 2011), especially in the studies regarding the melt failure and rupture under extensional flow. For instance, Maia et al. (2008) developed a novel controlled-stress extensional rheometer (CSER) which uses a feedback loop system to achieve the real controlled-stress conditions.

I.3.3.2 Nonlinear features in elongation rheology

In start-up of uni-axial extension, if the nonlinear data of $\eta_E^+(t, \dot{\varepsilon})$ rise above the linear curve at an inflection point, the melt is classified to have a "strain hardening" behavior. In contrast, when the $\eta_E^+(t, \dot{\varepsilon})$ falls below the linear one, the melt is called "strain softening". Although such extension thickening (strain hardening) or extension thinning (strain softening) is very obvious in the start-up of extensional flow, the physics behind such features seems not yet clear. It is supposed to be

- 42 -

dependent on the extension rate and the molecular characteristic of the polymer, particularly the molecular weight distribution and most especially the presence of long-chain branches. Researchers (Lee et al. 2008, McLeish et al. 1999) commonly perceived that the chain stretching as proposed within tube model is the reason for the observed "strain hardening" behavior. In addition, the apparent "strain hardening" observed in low-density polyethylene (LDPE) is usually thought to be caused from its long-chain branching (McLeish 2008) as theoretically interpreted based on a pom-pom model which describes backbone orientation and stretch for monodisperse polymers that contains two branch points with multiple arms at each branch point. Very recently, Wang and coworkers (Liu et al. 2013) studied the origin of "strain hardening" in extension from a scenario based on the kinematic difference between simple shear and uniaxial extension. They claimed that the "strain hardening" arises from the difficult removal of chain entanglements within the increasingly shrinking area at high Hencky rates during startup extension. As sketched in Figure I-17, a new concept of geometric condensation was proposed illustrating that the number of load-bearing entanglement strands in the cross-section remains unchanged during the initial elastic deformation of uniaxial extension. According to their interpretations, such geometrical condensation that occurs especially in the case of high Hencky strain rates seems to be the underlying reason for the "strain hardening". They attributed the "strain softening" either in the shear or in the uni-axial extension deformation to the microscopic yielding of the entanglement networks. Thus, under their framework, whether or not the "strain hardening" appear depends on which factor between geometrical condensation and massive entanglement yielding plays the dominant role during the extension.
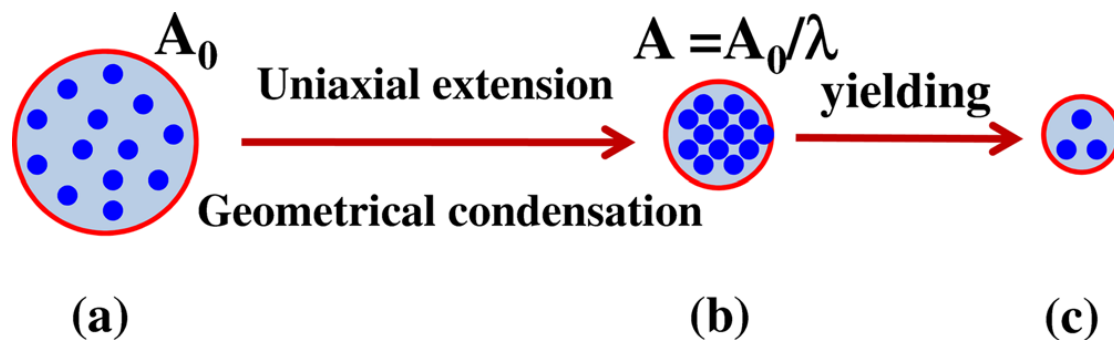
Figure I-17 The molecular picture developed by Wang and coworkers (Liu et al. 2013) on depicting the consequence of startup uniaxial extension. The dots represent the load-bearing entanglement strands in the cross-section. Yielding corresponds to loss of the load-bearing entanglements in the cross-section. A_0, A are cross-section area at initial and stretched states and λ is the stretching ratio.

I.3.3.3 Elongation rheology of multiphase systems

Aside from the interests on the technical methods of extension (Rolon-Garrido and Wagner 2009) and the melt failure or rupture during extension (Andrade and Maia 2011;Wagner and Rolon-Garrido 2012), attentions have also been paid to the

elongation rheology of multiphase systems like miscible (Takahashi, et al. 1999;Wagner, et al. 2004), immiscible polymer blends (Mechbal and Bousmina 2007;Stary, et al. 2012), polymer/filler composites(Hong, et al. 2007) and multilayer structures (Levitt et al. 1997; Silva et al. 2012). For instance, Levitt et al. (1997) studied the extensional behavior of a multilayer polymer system under uni-axial extension and suggested a direct method to measure the interfacial tension in the two-phase blend system. Under extension of a multilayer structure, the interfacial area is amplified and the amount of interface is well-defined which is possible to be calculated at every point of time. Hence, the interfacial effect could be very significant if the layer number is increased. They considered that the measured tensile force is composed of the volumetric contribution of each constituent and of the interfacial tension. This concept for interfacial tension in immiscible multiphase system has been cited by Hong et al. (2007) to study the interfacial tension change on polybutylene terephthalate (PBT)/polyethylene (PE)] immiscible polymer blends with organically modified nanoclay (organoclay) as a compatibilizer. In their study, extensional force of the nanocomposite was found to be significantly reduced due to the reduction of the contribution of the interfacial tension after the addition of the organoclay. In addition, as a common flow pattern involved in various processing, the uniaxial elongation flow has also been widely used to investigate the morphological evolution especially the dispersed droplet deformation in multiphase system under presence or absence of compatibilizers (Mechbal and Bousmina 2007;Stary, et al. 2012).
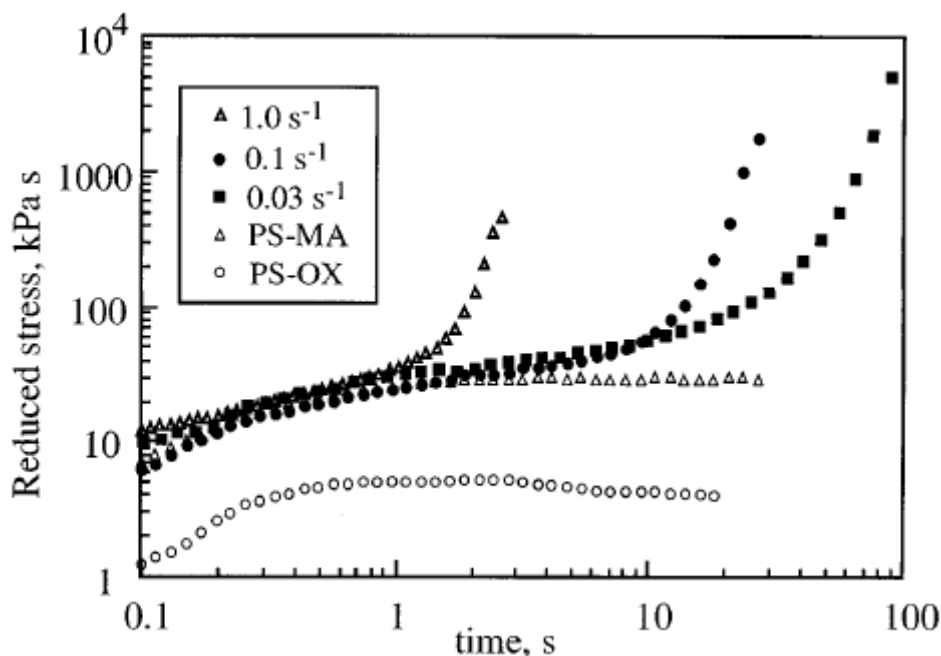
Figure I- 18 Reduced stress (stress/strain rate or apparent viscosity) of PSMA/PSOX pair. Great increase was observed in the layered samples while both homopolymers do not exhibit strain hardening.

Moreover, Levitt et al. (1997) has also demonstrated the extensional rheometry to

be a sensitive probe to the graft reaction at the interface with a result of pronounced strain hardening caused by coupled and even cross linked chains at the interface. Figure I-18 shows the elongation results of the cross-linked system of Polystyrene-co-maleic anhydride (PS-MA)/Polystyrene-oxazoline (PS-OX) pair reported in their study. Dramatic effect on the tensile force resulted from interfacial cross-linking has been observed as indicated by the great increase in reduced stress with time (evident strain hardening) in contrast to the homopolymers. Slower rate results in a higher effect. A 200-fold increase in apparent extensional viscosity compared with the homopolymer average was reported at the slowest strain rate, $\dot{\varepsilon}$ =0.03s^{-1}. As suggested by them, the significant rise of the total stress of the multilayered system is mainly caused from the interface component which is believed to be strain related only instead of the strain rate dependent bulk components as:

$$\sigma = \sigma_{bulk}(\dot{\varepsilon}) + \sigma_{int}(\varepsilon)$$

(I-21)

In a further step, Saito et al. (2001) attempted to extract the interfacial stress from the extensional force increment on a coextruded multilayer sheets of a pair of polyethylenes that can crosslink and correlate it to the extent of interfacial crosslinking. Recently, uni-axial extension has also been employed by Silva et al. (2012) to probe the type and characteristic of the interface/interphase in coextruded thermoplastic urethanes (TPUs).

I.3.4 Partial concluding remarks

In summary, nonlinear rheology in transient regime including stress relaxation after a step strain, start-up in simple shear and start-up in uni-axial extension have been focused in this section. Note that nonlinear rheology also covers other test methods such as nonlinear creep, biaxial as well planar extensions and large-amplitude oscillatory shear (LAOS) with various shear patterns, etc. which are out of scope in the present study. Different from the linear viscoelasticity of polymer chain which could be well described by the tube model of Doi-Edwards, various theoretical arguments have come up to interpret the physics of the nonlinear viscoelasticity due to that so far no completely general molecular theory could explain all the nonlinear phenomena. Main apparent nonlinearities include nonlinear stress damping in stress relaxation curves after large step strains; "strain softening" and stress overshoot appear at high Weissenberg numbers and "strain hardening" emerges at high Hencky strain rates in uni-axial extension for most of polymers. Although having some differences on regarding the effect of intermolecular interactions on a test chain, both the tube models incorporating CCR mechanism and those transient network models agree on that flow induces displacement of chains relative to each other and consequent loss of entanglements between chains in nonlinear regime.

Due to its close relevance to the processing conditions, the field of nonlinear

rheology goes on as a hot issue in the experimental studies among the scientists. When it comes to the multiphase structures, focuses are on correlations among component rheology, microstructural morphology evolution and interfacial properties coupling to the flow situation. Despite some advances have been achieved, it is still far from full understanding of the nonlinear rheology of multiphase systems especially the contribution of the interface/interphase. Till now, multilayer structure, as a model system with interfacial area well-defined to study the multiphase polymer system, has been rarely focused in the field of nonlinear rheology. This intrigues our interests to study the interfacial rheology in nonlinear regime based on such multilayer structure.

I.4 Coextrusion Process of Multilayer Polymers

I.4.1 Principle and applications of multilayer polymer coextrusion

I.4.1.1 Application

The manufacture of multilayer objects by coextrusion is a new and relatively complex technology that is expected to be used for a growing amount of industrial applications in the future. Such a process offers a unique opportunity to combine different layers in order to make large and hollow objects in a single step. Each component of such a multilayer structure provides its own end-use characteristics, such as mechanical insulation, thermomechanical, optical and barrier properties. The fabricated multilayer objects can be used for applications in a very wide variety of fields ranging from barrier films, cabling, garden furniture to smart materials, optical lenses, etc.(Dooley 2002b;Lamnawar, et al. 2013)(Figure I-19). Generally, to get the required solid phase adhesion and avoid peeling and delamination, one needs to use either a modified base or barrier polymer or copolymers thereof as a tie layer (Figure I-19)(Mitsoulis, et al. 1988). Another attractive application of coextrusion is the manufacture of microlayer or even nanolayer films with film thicknesses reduced to a nano-scale(Lai, et al. 2012).
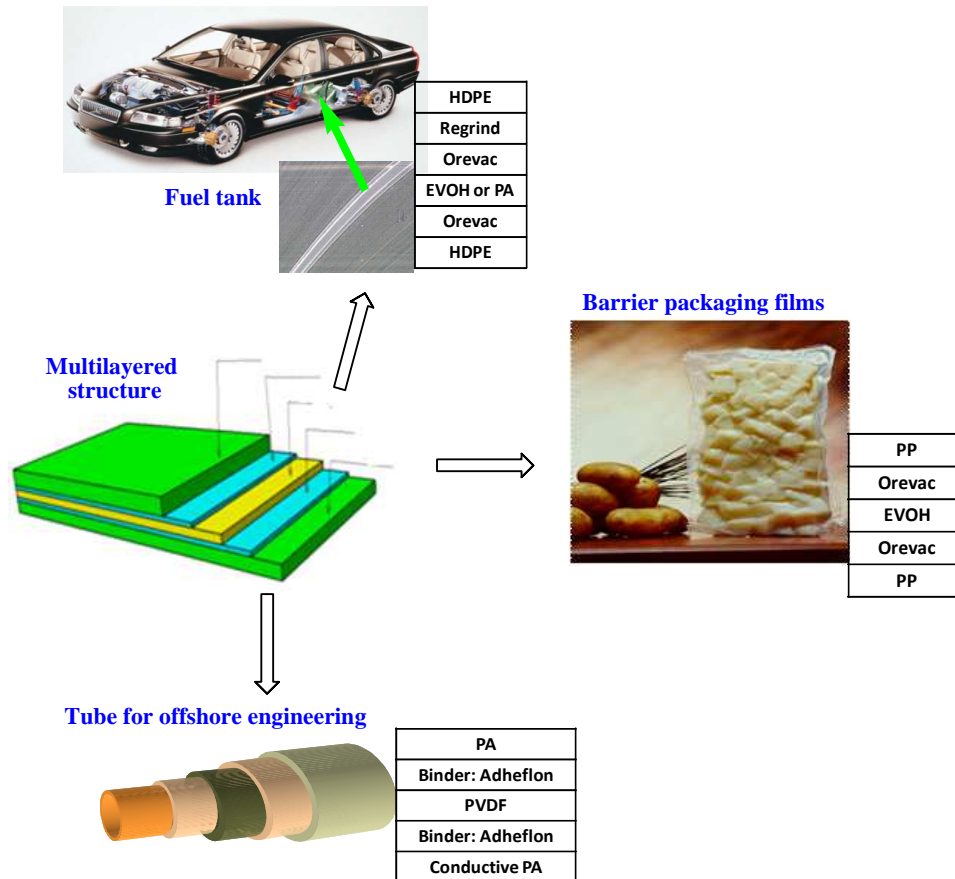
Figure I- 19 Examples of applications of multilayered structures

I.4.1.2 Die system

Coextrusion is realized by a combination of no less than two extruders using a multimanifold die or a feedblock system within which polymer melts from separate extruders are brought together and a specific multilayer assembly is created. The multimanifold die and the feedblock system are two different families of die designs, with their own specific requirements.

-Multimanifold dies

In this design, different fluids are distributed in individual manifolds that are separated from each other (Figure I-20). Each manifold is similar to the type of die used for the extrusion of a monolayer product. Each polymer layer is distributed uniformly in its individual manifold before being combined with other layers outside or inside the die prior to the final die land. The principal advantages of coextrusion with multimanifold dies are that it can maintain the form and the thickness of each layer in a definite way and renders it possible to co-extrude polymers of different rheological properties as the layers are not superposed before exiting the manifolds. On the other hand, the difficulties of this design involve producing multilayers that require strong bonds like the ones where an adhesive layer is required to bond two dissimilar polymers due to the very short residence time of combination. Another issue is adjusting the configuration and the thickness of layers in light of the high

- 47 -

cost of changing to a new manifold.
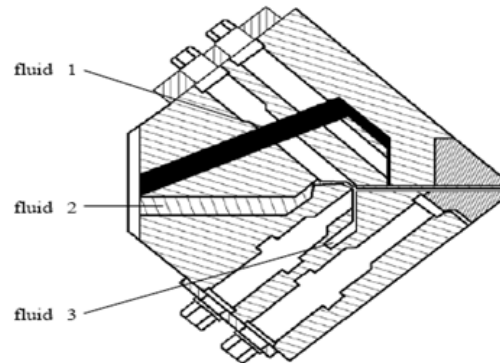
Figure I- 20 Example of a multimanifold die forcast-film coextrusion of multilayer polymer films

-Feedblock systems

In this kind of design, the superposition of different layers can be realized in a feedblock system before being extended to a conventional single-manifold die (Figure I-21). The polymer melt stream from each extruder is subdivided into as many layers as desired in the final product and prearranged with those from other extruders in desired sequence and thickness proportions within the feedblock system that is installed ahead of the die inlet. The feedblock system offers a great flexibility of utilizations. Indeed, as the characteristics of the flow (stacking order of the layers, layer number, relative thickness, etc.) are realized in the feedblock system, they can be modified by merely a simple intervention on the feed rate/output of the flow and/or a change of the geometry of the feedblock. Note also that the geometry of the feedblock significantly reduces the size of the coextruder setup as compared to a situation with a multimanifold die. Moreover, it is easily interchangeable. More details can refer to some earlier work of Dooley(2002b).
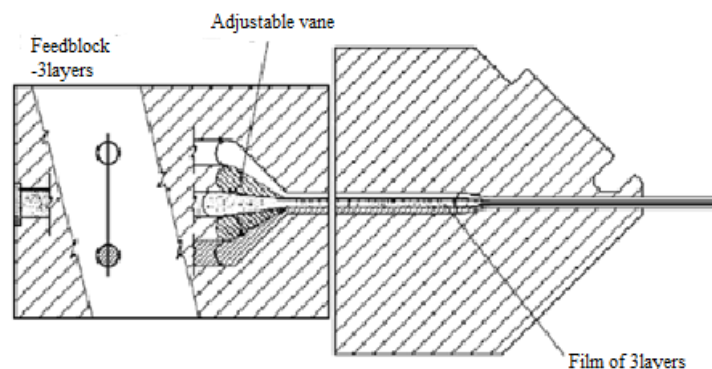
Figure I- 21 Example of a feedblock system designed for a trilayer film

There are two kinds of feedblock geometries, namely, a fixed feedblock geometry and a variable feedblock geometry. The variable design is the most flexible, and is becoming more and more commercially common, as shown in Figure I-22.

- 48 -

However, it is difficult to obtain reproducibility. By varying the configuration of the feedblock, it is possible to form two layers (AB), three layers (ABA), five (such as ABCBA), and even up to eleven layers.
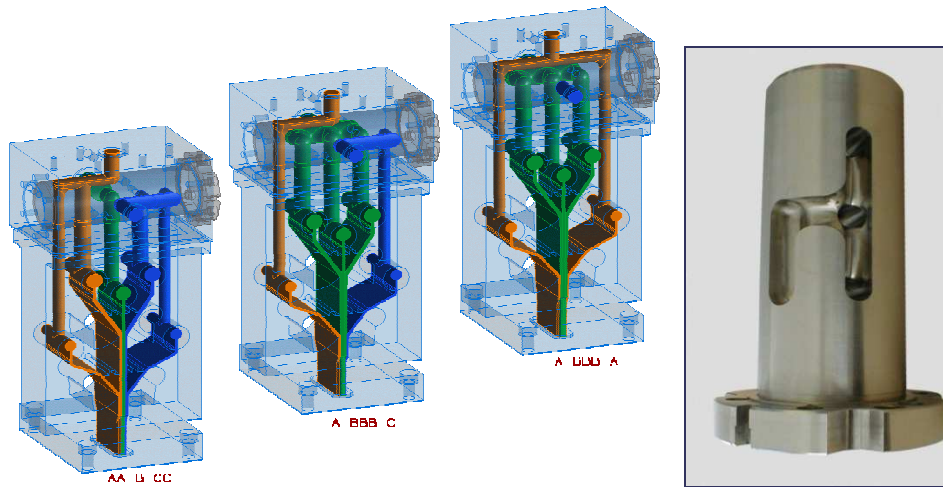
Figure I- 22 Example of a variable feedblock geometry

It is worthwhile to mention that recently an assembly of layer multiplication dies has been used by Baer et al(Mueller, et al. 1997), Macosko et al.(Zhao and Macosko 2002) and Guo et al.(Xu, et al. 2008) to get a multilayer structure of a very high number. This way, a sheet or film with hundreds or even up to thousands of layers can be obtained. Initially, two polymer melts are brought together in a feedblock and arranged into two (or more) layers. If the initial number of layers is N_0 and the number of multiplication dies is n, the final number of layers is simply $N_0 * 2^n$. The layer multiplication dies are now commercially available and run by industry. This layer multiplication technique has been widely used by them to investigate various properties like barrier(Gupta, et al. 2010), electrical property(Xu, et al. 2008) and crystallization(Wang, et al. 2009), etc. of multilayer materials at micro- and nano-scale.

The versatility of the feedblock has made it the most popular type of coextrusion; it is estimated that of over 95% of flat-die coextrusion systems use a feedblock(Dooley 2002b).The main challenge encountered in feedblock-type coextrusion is that the interfacial flow instabilities and some defects of layer non-uniformity like encapsulation phenomena may appear when polymers with severe rheological differences are coextruded. This brings about the hot subject of controlling interfacial defects (including flow instabilities and encapsulation, etc.), via various means such as selecting rheologically matched polymer pairs, adjusting experimental variations, shaping the feedblock geometry, etc. For example, as pointed out by Maia et al.(Patrick et al. 2013), in the original multiplier dies used in layer multiplication technique of coextrusion, large stress and pressure drops occur due to cross section reduction and flow asymmetry during the compression-then-expansion step, thus readily yield viscous encapsulation for the

rheologically dissimilar polymers. In order to overcome such defect, Maia (2012) invented a new die which simultaneously compresses the material in one direction and expands in another while keeping the cross-sectional area constant, whereby better layering performance can be achieved.

I.4.2. Main interfacial defects of coextrusion

I.4.2.1 Encapsulation

The encapsulation subject is old in principle, but very few theoretical studies have been carried out (Karagiannis, et al. 1990;Khomami 1990) and also there are only a very limited number of experimental studies dealing with such encapsulation phenomena(Lamnawar, et al. 2013;Wilson and Khomami 1992). Most of these research efforts have suggested that, irrespective of the stability of the interface, the more viscous fluid tends to push into its less viscous counterpart, eventually leading to the less viscous fluid encapsulating the more viscous components. This phenomenon is illustrated in Figure I-23a, where the top image shows a two-layer structure flowing down a tube with the viscosity of layer B lower than that of layer A. Likewise, the schematic of encapsulation phenomenon in coextrusion of layered films is shown in Figure I-23b, with an appearance of layer thickness nonuniformity at the die exit.

A persuasive mechanism found in literature for this phenomenon of encapsulations is that the more viscous fluid tends to push into the less viscous one in order to minimize viscous dissipation. In other words, the less viscous fluid tends to enter the region of high shear (i.e., the wall with the highest shear stress) and the more viscous fluid locates within the lower shear region, thus minimizes viscous dissipation (the integral involving the dot-product between the stress tensor tau and the velocity gradient tensor) for a given flow rate or, equivalently, maximizes the volume flux for a given pressure gradient. Differences in wall adhesion and viscoelastic characteristics of polymers and weak secondary flows caused by viscoelastic effects have been demonstrated to be the contributing factors (Schrenk, et al. 1978). Moreover, Lee and White (Lee 1974) observed that the more elastic fluid tends to push into the less elastic one. However, examples of coextruded structures with non-uniform layer thicknesses have also been observed even when the viscoelastic properties of the materials are very similar (Lamnawar and Maazouz 2009;Lamnawar, et al. 2013) such as in the case of PE/PA bilayerz films.
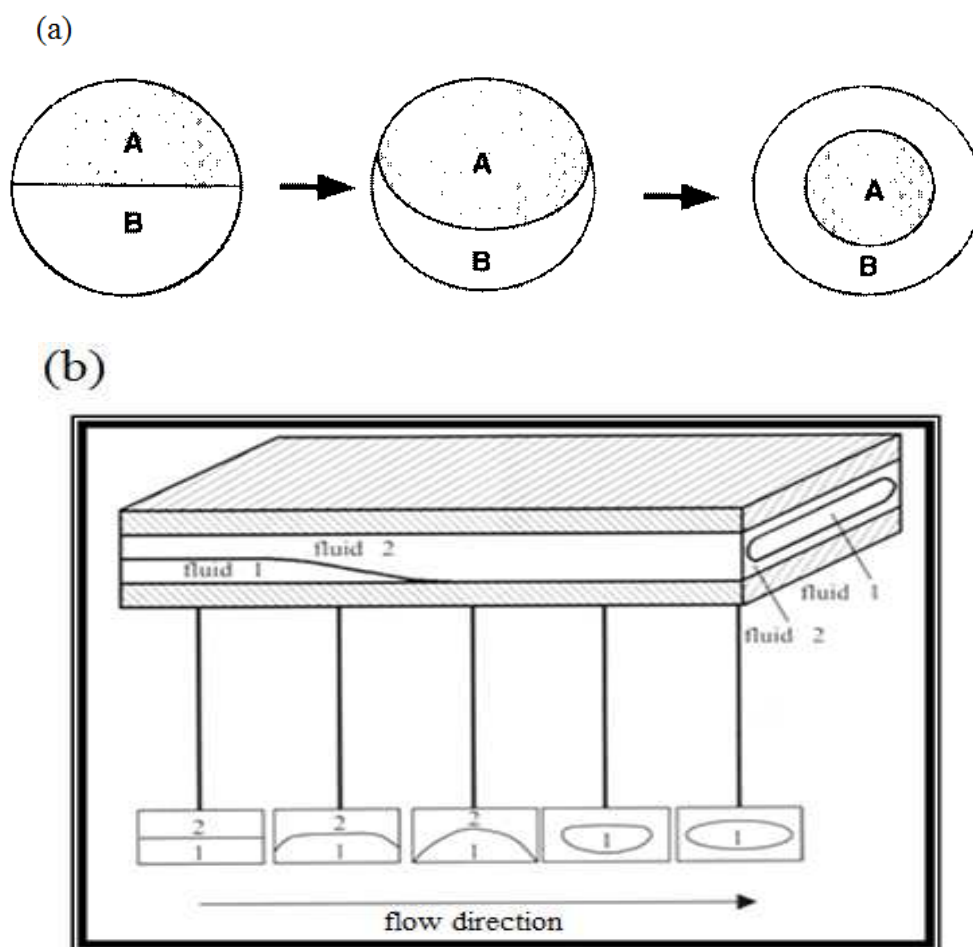
Figure I- 23 Schematic of encapsulation phenomenon in a tube (a) (from Agassant *et al.*(Puissant, et al. 1996)) and in coextrusion (b) (Han 1981)

With an aim to gain a thorough understanding on the effect of full set of rheological parameters as well as physicochemical affinity on the encapsulation phenomenon, Lamnawar et al. (2012) recently carried out some original experiments based on well-characterized model polymer fluids. The model polymer fluids include: (i) Newtonian poly (dimethylsiloxane)(PDMS) polymers of varying molar masses, (ii) high molecular weights, viscoelastic and compatible polymer pairs of PVDF and PMMA as well as two pairs of asymmetrical reactive polymers based on PE-GMA (glycidyl methacrylate)/PVDF-g-MA (maleic anhydride) and PE/PVDF to investigate the effect of physico-chemical affinity. The encapsulation kinetics of two drops was recorded using a lab-built optical device and the results were rationalized as a function of the effect of the viscosity, elasticity ratios, drop geometry, interfacial tension and physicochemical affinity.

Their obtained results indicated that the phenomenon of viscous dissipation minimization as mentioned before is not the sole mechanism; rather, experimentally, the encapsulation can occur even at a low shear or strain rate and that it is governed by surface and viscous forces. Moreover, the coupling between rheological and

optical studies showed that the viscosity of the material is a key parameter that has a considerable influence on the encapsulation kinetics. The high viscosity ratio seems to be the principal parameter and the motor of the encapsulation phenomenon in the PDMS systems. In addition, the drop geometry of the material was also found to have some effects. On the other hand, the encapsulation appeared to be hindered by the interdiffusion process in the case of PMMA/PVDF system despite of their contrast in elasticity and surface tension. Likewise, the encapsulation kinetics could be reduced or eliminated by the creation of a copolymer at the interface in a reactive system (PVDF-g-MA/PE-GMA).

I.4.2.2 Interfacial instabilities

The objective in vast literatures is to - from a more fundamental viewpoint -obtain a better understanding of the physics of the multilayer flow, to identify the mechanisms and the origins of what triggers the instabilities, and to propose solutions in view of controlling or even eliminating such instabilities. Generally, the interfacial instability is notably evidenced by an appearance of an irregular, wavy and/or zig-zag type interface. A typical sample of the interfacial instability with a wave-like interface for a PVDF/ PE bilayer film,as experimentally observed by Lamnawar et al. (2013), is shown in Figure I-24. Over the past decades, numberless studies concerning the interfacial flow instability have been carried out from both theoretical and experimental aspects.

Figure I- 24 An example of a wavy interface observed in a PVDF/PE bilayer film

Theoretical studies are mainly based on linear stability theory, neutral stability analysis as well as asymptotic and numerical methods. Multilayer Couette and Poiseuille flows with plane geometry and axisymmetric geometry for both Newtonian and non-Newtonian fluids have ever been investigated in the fruitful literatures. The poineering work must belong to Yih(1967) who considered both

plane Couette and Poiseuille flows of two superposed layers of Newtonian fluids of different viscosities submitted to very long waves using a linear stability theory and demonstrated that viscosity stratification could lead to instabilities. Li(1969) first applied the linear stability theory to a non-Newtonian fluid by introducing an elastic component (relaxation and retardation time) and proposing an Oldroyd model for the flow of Oldroyd-B fluids. Su and Khomami (1992) demonstrated in the case of a stratified plane Poiseuille flow that a jump in the first normal stress difference between two fluids can induce an unstable interface, like in the case of a stratified axisymmetric flow. So far, numerous factors like viscosity stratification, elasticity difference, capillary and density difference, etc. have been considered to be reasons for the interfacial instabilities. The different mechanisms involved in the interface instability can either add their effects or compensate one another. It seems problematic to separate the contributions offered by each phenomenon. However, stability maps with stable and unstable domains could be elaborated by taking into account the layer thickness ratio, viscosity ratio and elasticity ratio, etc. In the case of coextrusion of polymers, viscous and elastic stratifications account for a more weight than other factors like capillary and gravity forces. For clarity purpose, more details regarding the theoretical advances in the literature are given in Appendix-I.

From an experimental viewpoint, the studies dedicated to the interfacial instabilities in coextrusion are of two types. One aimed to examine the occurrence of interfacial instability and visualize the transition from an unstable to a stable mode of the obtained extrudates. This kind of study, which corresponds more to what is done in industry, attempted to relate the appearance of the instabilities to the physical parameters of the materials, the processing conditions, the flow configurations, etc (Schrenk, et al. 1978; Han and Shetty 1976). The other concerned observations of the development of instabilities in the die by using a partially transparent die or a die mounted with an accessory consisting of an optical window for observation. In these studies, a temporally external perturbation was introduced by imposing a periodic oscillation with a controllable amplitude and frequency to the flow. (Valette, et al. 2004; Wilson and Khomami 1992; 1993a;1993b).

In the industrial studies carried out by Han and Shetty(1976,1978) and by Schrenk et al.(1978), the authors argued that there exists a critical interfacial shear stress for a given polymer system, above which the interfacial instability sets in and appears to be independent of the layer thickness ratio. Therefore, stability maps using the viscosity ratio and elasticity ratio versus the layer thickness ratio were constructed by them according to the conditions for the onset of the interfacial instability. With regard to the studies with imposing controlled perturbations, one example is the comprehensive work carried out by Wilson and Khomami (1992; 1993a;1993b). Their facilities introduced temporally regular disturbances with controllable amplitudes and frequencies. They measured the growth rate or decay rate of the disturbance amplitude along the downstream die position to examine the

interfacial stability regarding materials and geometrical parameters (e.g., layer thickness ratio, wavenumber, etc.). The interfacial flow is unstable if the growth rate is high and it is stable if the growth rate is low, lacking or even negative. The authors have carried out their work on both incompatible (i.e., PP/HDPE) and compatible fluids (i.e., HDPE/LDPE) as well compared the experimental results to those predicted by the linear stability theory. More details about the experimental studies are attached in the Appendix-I. Despite the interesting nature of this kind of research, it is of no help in full understanding either the generation of instabilities or its connection with the physicochemical affinity and the resulting final properties of multilayer polymers.

I.4.3 Importance of the interphase in relation to the interfacial defects

In the comprehensive work of Wilson and Khomami(1993b), the authors first investigated flows of immiscible fluids (PP/HDPE) and found that theoretically predicted growth rates agreed with their experimental data. Subsequently, they considered a plane Poiseuille flow of a compatible polymer system (HDPE/LLDPE). In such a system, there is no interfacial tension, and polymer chains are able to diffuse across the original interface, forming a diffuse interface (i.e., an interphase). In comparison with the high growth rate in the cases of incompatible PP/HDPE systems, the growth rate for the compatible LLDPE/HDPE system was significantly lower despite the fact that the viscosity ratio for the LLDPE/HDPE system was higher (Figure I-25). That is, the interfacial flow in the LLDPE/HDPE system is more stable than the PP/HDPE system. This suggested that the interphase triggered from interfacial diffusion may improve the interfacial stability of coextrusion.
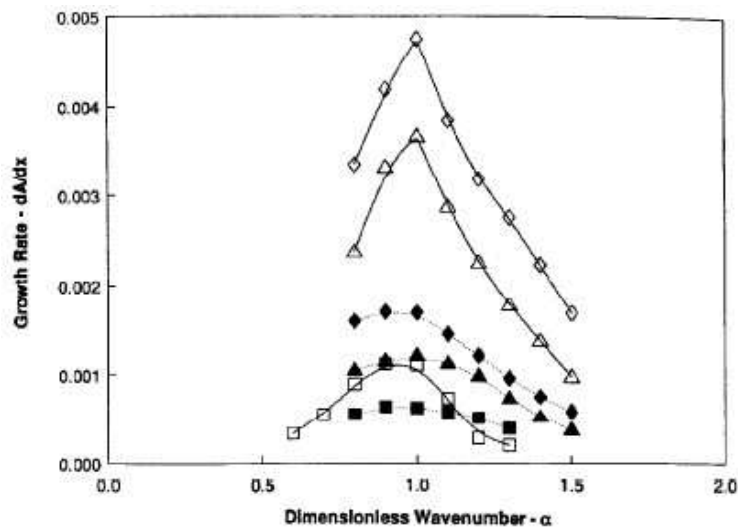
Figure I- 25 Experimental disturbance growth rates versus the dimensionless wave number for LLDPE/HDPE (filled symbols) and PP/HDPE (open symbols) at varying layer depth ratios (from Wilson and Khomami 1993b)

To disclose the underlying mechanisms of the weak sensitivity to disturbances,

the authors proposed two possibilities: the reduction of the effective viscosity ratio in the vicinity of the interface arose from the interfacial diffusion as well as convection and energy dissipation at the interphase which resulted in less energy being available to the growing wave. On the other hand, the energy dissipation by mixing and diffusion processes gives rise to the reduction of the unstable regions at low Reynolds numbers but it was noted that the interaction parameter has a weak effect on stability maps.

In fact, in order to improve the compatibility between neighboring layers, commonly a tie layer is introduced in a coextrusion process of incompatible polymer systems. For instance, Lamnawar et al.(2010b) used rheological and morphological tools to investigate some new generations of tie layers based on PE/PE-COC blends for packaging applications. More interestingly, Lamnawar and Maazouz(2006; 2008, 2010a) performed a large amount of work dealing with the physicochemical affinity (corresponding to the interdiffusion/reaction zone) triggered from reaction between functionalized incompatible polymers of the neighboring layers and its influence on interfacial instabilities. They experimentally confirmed that the weak disturbance can be predicted by considering an interphase of non-zero thickness instead of a purely geometrical interface between the two reactive layers. In their work, multilayer coextruded cast films of polyamide (PA6)/polyethylene-grafted (GMA) or pure PE were studied with different viscosity and elasticity ratios. In order to quantify the contribution of the effect of the interface/interphase with a specific interfacial area, an expression was developed in their study to estimate its thickness $h_I(t)$ at a specific welding time and shear rate:

$$h_I(t) \propto \frac{\dfrac{H}{\eta_{SR}(t)} - n_a h_a / \eta_a - n_b h_b / \eta_b}{\left[\dfrac{n_a + n_b - 1}{\eta_{I\infty} + (\eta_{I0} - \eta_{I\infty})e^{-Kt}} - \dfrac{n_a}{\eta_a}(1 - \dfrac{1}{n_a + n_b}) - \dfrac{n_b}{\eta_b}(1 - \dfrac{1}{n_a + n_b}) \right]} \tag{I-22}$$

where η_{SR}, η_a and η_b denote the viscosities of a multilayer system and of layers a and b; n_a and n_b are the number of layers of polymer (a) and (b); the parameters h_a and h_b represent the thicknesses of each layer; H is the total layer thickness; and η_{I0} and $\eta_{I\infty}$ are the initial and saturation viscosities of the interphase, respectively. Figure I-26 displays the thickness of the interphase as a function of the reaction time of a trilayered PE-GMA/PA6/PE-GMA structure, and as can be seen, the interfacial region increased with the healing time, reaching a maximum value of 35 nm.
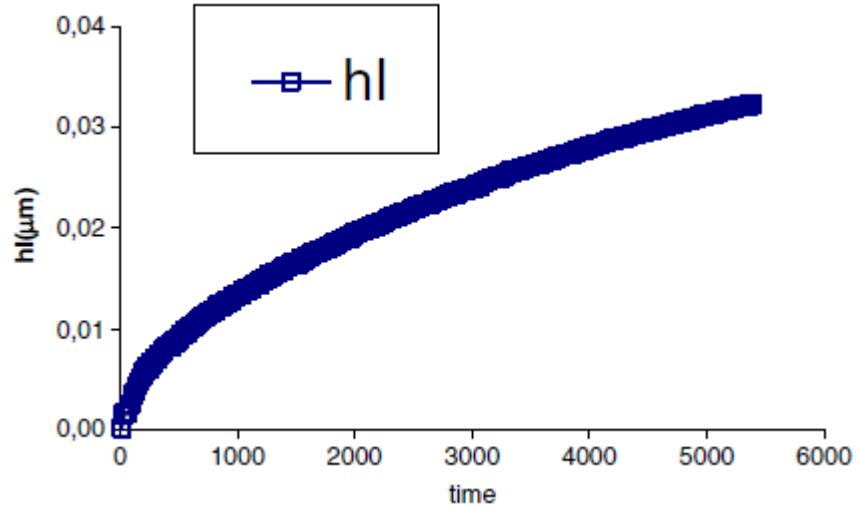
Figure I- 26 The thickness of the interphase as a function of time for a 3 layers PEGMA/PA6/PEGMA at 240°C (from Lamnawar and Maazouz 2008)

After presenting such an upstream rheological study on the interphase, the authors formulated an experimental strategy to optimize the interfacial defects of the reactive multilayer coextrusion process by listing the classical influential parameters and taking into account of effect of the interphase (Lamnawar and Maazouz 2009). Two grades of Polyamides (PA), namely, PA (1) and PA (2), with PA (1) having lower viscosity and PA (2) having similar viscosity as PE (or PE-GMA) were considered in their work.

Figure (I-27a) shows a photograph of the wavy instabilities (i.e., a highly irregular or sometimes regular waviness) observed along the flow direction in the case of the PA6 (2)/PE bilayer system at a flow ratio of 1, i.e., $Q_{PA6\ (2)}$ = Q_{PE}=2 kg/h) and 150s of residence time. However, under some conditions, a stable bilayer system based on the reactive system PE-GMA/PA6 (2) (Figure I-27b) in comparison with the unstable PE/PA6(2) bilayer system was obtained. Independent of the flow rate ratio, this configuration was found to be very stable: the longer the contact time to enhance the amount of reaction at the polymer/polymer interface in the feedblock/die (150 s), the better was the resultant stability. Despite the short contact time during the process, the compatibilization reaction took place at a high temperature and under a high shear rate, as evidenced by rheology and spectroscopic techniques in their studies.

Figure I- 27 Photographs of (a) the instabilities in the case of the PA6 (2)/PE bilayer system observed at T = 240°C with a coat hanger die and a flow rate ratio equal to 1 ($Q_{PA6(2)}$ = Q_{PE}=2 kg/h); (b) a stable bilayer system based on PEGMA/ PA6 (2) obtainedunder equivalent conditions.(The red pigmented sample correspond to PE-GMA and PE).(from Lamnawar and Maazouz 2009)

Indeed, for a reactive multilayered system, the interfacial flow instability can be reduced or eliminated, for example, by (i) increasing the residence time or temperature in the coextrusion feed block (for T > reaction temperature) and (ii) reducing the total extrusion flow rate. Besides, elaboration of experimental stability charts for various non reactive and reactive systems plotted as the viscosity ratio (m_0) versus the thickness ratios could be constructed to guideline a stable coextrusion of reactive functionalized polymers (Figure I-28). In the chart, the empty and hachured small rectangles indicate respectively the stability and instability of the bilayer systems.
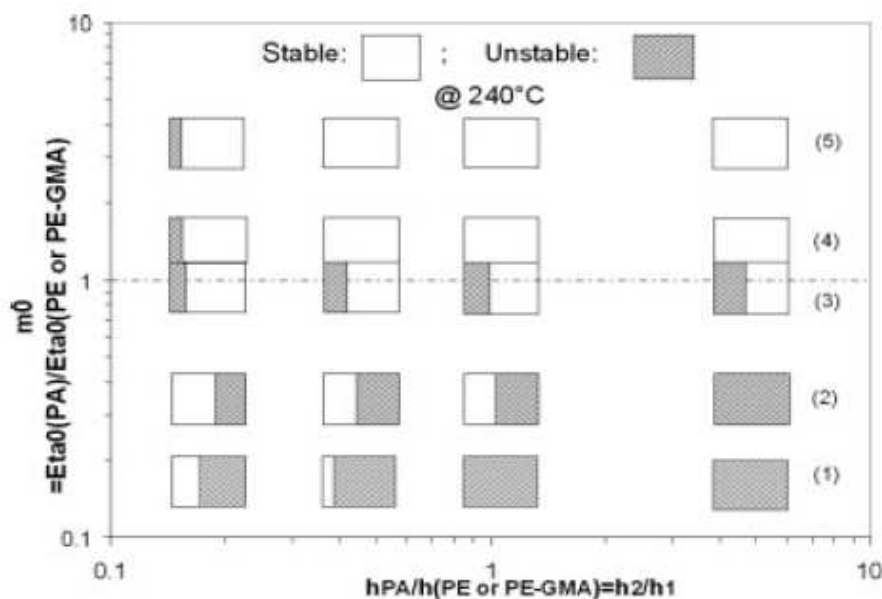
Figure I- 28 A comparison of the stability/instability observed experimentally at 240°C with various viscosity and layer thickness ratios (evolution of the PA/Polyolefin viscosity ratio (m_0) vs. their corresponding thickness ratio) for several bilayer systems: (1) PA6(1)/PE, (2) PA6(1)/PE-GMA, (3) PA6(2)/PE, (4) PA6(2)/PEt20%PE-GMA, and (5)PA6(2)/PE-GMA. (from Lamnawar and Maazouz 2009)

As displayed in Figure I-28, under their conditions, the resulting films of PA6 (1)/PE and PA6 (1)/PE-GMA bilayer were always unstable independently of the process parameters (viscosity ratio, die gap, contact time to enhance the reaction amount at the polymer/polymer interface in the feedblock/die), presenting somewhat chaotic interfacial defects. In the case of PA6 (2)/PE where the viscosity ratio is close to one, the obtained films are more stable especially for a slow PA6(2) flow rate (i.e., $h_{PA}/h_{PE} \leq 1$). Indeed, PE is more elastic than PA(2), and the use of a thin layer of PA was found to lower the rate of elastic instabilities. Moreover, the PE-GMA/PA6(2) structure presented a much higher stability at the temperature of 240°C compared with the PE/PA6(2) bilayer system, even they have higher contrast in terms of viscosity and elasticity. When only 20% of PE-GMA was used, the flow was more stable compared to the PE/PA6(2) system. The PE-GMA would react with the NH_2/COOH groups at the end of the PA6 chains, thus creates certain amounts of interphase with reaction kinetics depending on the contact time and temperature. Consequently, the interfacial instabilities that arise in the case of non-reactive systems can be reduced by the creation of a copolymer at the interface.

On the other hand, beside its role in controlling the flow instabilities, the interphase (the physicochemical affinity) has also been found to be able to hinder the encapsulation kinetics. In the study of Lamnawar et al.(2012) on encapsulation kinetics of drops determined by rheological and optical tools, the authors assessed the encapsulation kinetics of a compatible PVDF/PMMA polymer pair at several temperatures, as given in Figure (I-29). As reported, both PVDF and PMMA were

more viscous at 190 °C as compared to 240 °C. It was noted that the kinetics of coalescence in was slower at 190 °C. The faster kinetics at the higher temperature was attributed to a higher mobility of chains which can be represented by the lower viscosity. The coalescence at 240 °C was nearly complete (x/r = 0.9) compared to that of 190 °C. At 240°C, PVDF and PMMA have a similar viscosity and contrast of elasticity. As indicated in Figure (I-29), no encapsulation phenomenon could be seen in the different experimental conditions, despite of the difference in elasticity and surface tension. Here the observed coalescence development represented the signature of the kinetics of diffusion where the macromolecular chains intertwined and gradually became replaced by a more robust interphase. The encapsulation appeared to be hindered by the interdiffusion process in the case of a miscible pair system despite the contrast in elasticity and surface tension.
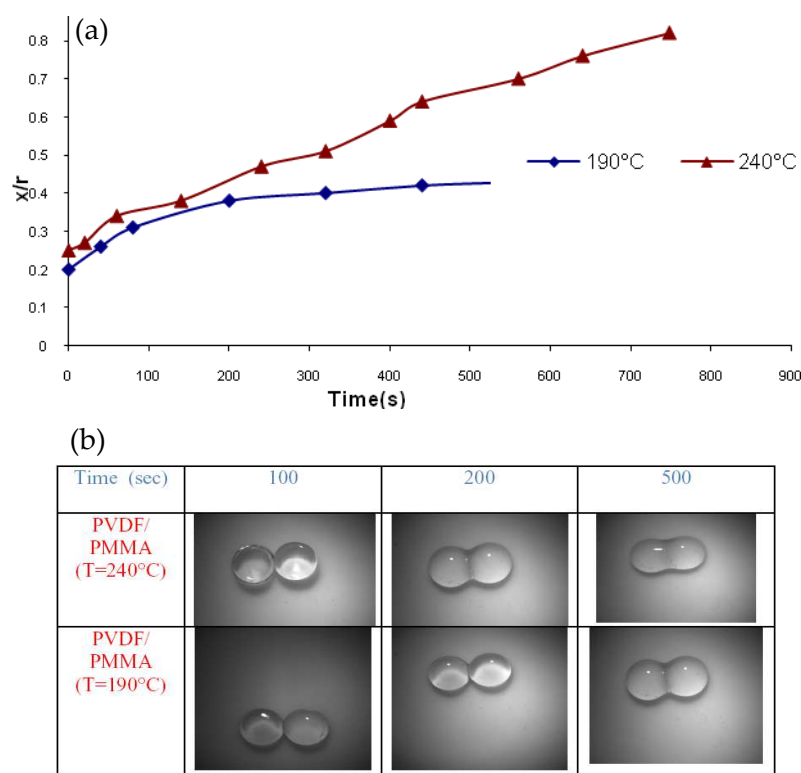
Figure I- 29 (a) Coalescence curves of PVDF/PMMA drops at 190°C and 240°C (r and x are radius radius and neck radius of the drop); (b) An illustration of the coalescence/encapsulation kinetics of PVDF/PMMA drops at 190°C and 240°C. (from Lamnawar et al. 2012)

Moreover, the same approach was applied to functionalized polymers to investigate the effect of reactive compatibilization on the encapsulation phenomenon by the authors. Two pairs of reactive polymers at interfaces based on PE-GMA (glycidyl methacrylate)/PVDF-g-MA (maleic anhydride) as well as a nonreactive material at an interface based on PE/PVDF were selected. Figure (I-30a) shows a comparison of the encapsulation kinetics of these systems at 240 °C. The interfacial

reaction between the MA and GMA functions certainly attenuated the coalescence kinetics. No encapsulation was noted in these cases despite that the zero shear viscosity ratio of PE-GMA/PVDF-g MA was close to 1.5 (Figure I-30b). The triggered copolymer at the interface thus hindered the encapsulation kinetic. On the contrary, the nonreactive PE/PVDF system with a higher viscosity ratio (close 3.2) confirmed that the PVDF tended to encapsulate the PE.

This seemed to affirm that it was essential to couple the viscosity ratio to the physicochemical affinity and viscoelastic parameters in order to gain a better understanding of the encapsulation phenomenon in multiphase systems. In addition, the role of the viscosity ratio, elasticity ratio, and layer ratio should also be investigated, thereby coupling to the reaction rate/compatibilization phenomena of the polymer/polymer interface. Indeed, for a reactive system, the encapsulation phenomenon could be reduced or eliminated by the creation of a copolymer at the interface.
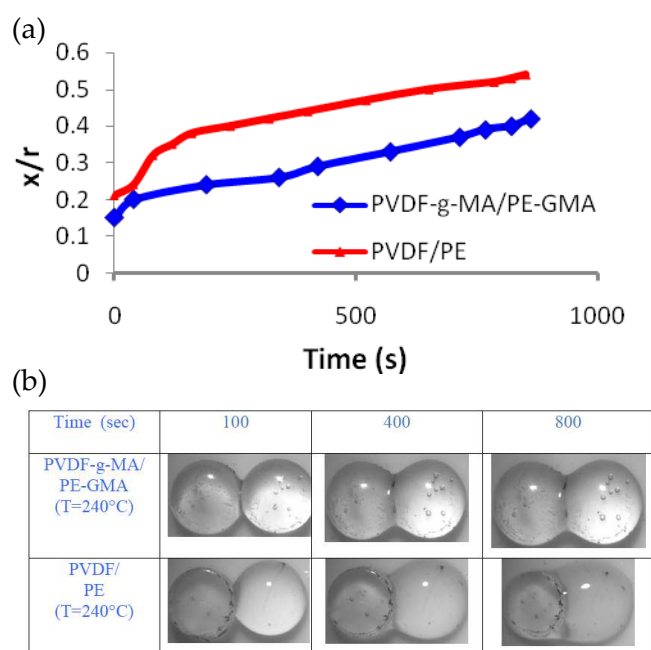
Figure I- 30 (a) An illustration of the coalescence kinetics of PVDF-g-MA/PE-GMA and PVDF/PE drops at 240°C; (b) A comparison of coalescence curves at 240°C featuring PVDF-g-AM /PE-GMA and PVDF/PE drop systems. (from Lamnawar et al. 2012)

I.4.4 Partial concluding remarks

In the coextrusion of multilayer polymers, a core part of feedblock or multimanifold die is required to realize the technique. In practice, the feedblock system takes a prevailing advantage over the multimanifold die system due to its more versatility of the former. The main challenge is to simultaneously process polymers of high different rheological properties as interfacial defects including interfacial instability with wave-type distortion and encapsulation phenomenon may appear between neighboring layers in certain conditions.

Some important theoretical and experimental advances with regard to the interfacial flow stability have been achieved during the last decades especially for incompatible polymers. Most of them are based on mechanical and numerical approaches. One the one hand, the encapsulation phenomenon has been theoretically and experimentally demonstrated to happen as the lower viscous polymer tending to encapsulate the higher viscous polymer due to viscosity dissipation minimization, though which was recently revealed to be not the sole mechanism. On the other hand, generally it is very difficult to have a very thorough view on the stability of the interface in coextrusion since numerous parameters are involved. Normally, the distortion of the interface is due to numerous reasons: viscosity stratification, elasticity difference, capillarity, density difference, etc. The different causes of the instabilities can be additive in certain cases and compensated in others. But it is also highlighted that domains of stability exist and can be predicted in order to make the process stable.

It has been realized that the physicochemical affinity (i.e., interphase) resulted either from interdiffusion in compatible system or from reaction in reactive incompatibel system may have some positive effect on the interfacial flow stability. Thus, it is essential to couple the role of the interphase and its viscoelasticity to classical factors such as the viscosity ratio, elasticity ratio and interfacial tension, etc. in order to give a better understanding of the interfacial flow instabilities and the encapsulation phenomenon in multiphase systems as well as the coextrusion of multilayer structure. Despite of this, the quantitative correlations of the interphase to the interfacial flow stability are not fully understood and the underlying mechanisms of the interphase on improving the interfacial defects are still not very clear.

I.5. Conclusion

An overview of bibliography has been stated in this chapter with regard to the interfacial phenomena at at a polymer/polymer interface of multilayer structures and coextrusion processing as well as their interplays. Firstly, literature work on interdiffusion, interfacial slippage as well as interfacial reaction has been respectively focused. To date, dynamics of self diffusion of polymer chains is able to be described under the framework of Doi-Edwards theory. However, since the mobility, volume, miscibility of dissimilar polymer chains are involved, problem becomes more complicated for the mutual diffusion between different chains. Two divergent theories, that is, fast-mode theory and slow-mode theory, emerged concerning on whether the slower species or the faster specis is dorminant on the mutual diffusion kinetics. In experiment, various techniques ranging from sophisticated tools to common ones have been utilized for interdiffusion. The sophisticated spectroscopic tools though are precise, need some labeled elements and are expensive as well as not readily for manipulations. In particular, rheometry, as a simple tool has been demonstrated to be an important and feasible technique for interdiffusion problem.

Moreover, the interfacial slippage in multiphase system has also been reviewed from aspects of experimental observation and theoretical interpretation. Interfacial reaction, as a very important way for introducing compatibilization effects and suppressing the interfacial slippage, has been vastly investigated for a long period. They are mainly dedicated to the interfacial reaction kinetics and the interfacial morphology development. The structure, rheology and properties of the interphase triggered from the interdiffusion/interfacial reaction are attractive due to their close relations to the final performance of mulitphase systems.

Because of the complex relations between flow and structure evolution, the nonlinear rheology at multiphase polymer system, especially for the interface/interphase is still far from fully undstood. After some brief introductions on the nonlinear rheological measurements such as step shear strain, startup in simple shear and uni-axial extension, bibliographic views regarding nonlinear rheolgy of the multilayer polymer systems have been dealt with. The interface/interphase seems to be sensitive to the nonlinear rheolgy of the multilayer system, though a discovery in depth is still lacking.

For coextrusion processing technology with a feedblock system, the main challenge is the interfacial defects involving interfacial flow instabilities and encapsulations especially when polymers of rheological contrast are simultaneously processed. Literatures regarding theoretical and experimental studies of the interfacial defects are fruitful, but most of them are restricted to numerical and mechanical approaches. Several factors like viscosity stratification, elasticity difference, capillary and density difference, etc. have been considered to be reasons for the interfacial defects. Very few attentions have been focused on the correlations of the physicochemical affinity at the neighboring layers to the interfacial defects. As it is known, the interfacial phenomena have more or less favorable or unfavorable impacts on the adhesion, mixing, morphology development, and properties, etc. at the interface of neighboring layers of a multilayer structure. Since this is the case, researchers cannot neglect the importance of the interfacial physicochemical affinity, especially when they are studying the interfacial flow stabilities of coextrusion. As did in earlier literatures, earlier studies in our group indicated signatures of favorable effect of the interphase generated from interfacial reaction on controlling the interfacial defects. Systematical studies regarding this point are still far from enough.

Chapter II: Rheological Modeling of the Diffusion Process and the Interphase of Symmetrical Bilayers Based on PVDF and PMMA with Varying Molecular Weights

II.1 Abstract

The diffusion process in the molten state at a polymer/polymer interface of symmetrical and model bilayers has been investigated using a small-amplitude oscillatory shear measurement. The polymers employed in this study were poly (vinylidene fluoride) (PVDF) and poly (methyl methacrylate) (PMMA) of varying molecular weights and polydispersities. The measurements were conducted in the linear viscoelastic regime (small deformations) so as to decouple the effect of flow from the diffusion. The focus of this paper has been to investigate the effects of healing time, angular frequency (ω), temperature and molecular weight on the interdiffusion and the triggered interphase between the neighboring layers. The kinetics of diffusion, based on the evolution of the apparent diffusion coefficient (D_a) versus the healing time, was experimentally obtained. The transition from the non-Fickian to the normal Fickian region for the interdiffusion at the interface was clearly observed, qualitatively consistent with the reptation model, but it occurred at a critical time greater than the reptation time (τ_{rep}). In non-Fickian region, effects of frequency and temperature were studied with regard to the ratio of the apparent diffusion coefficient to the self diffusion coefficient (D_a/D_s). The D_s determined in the Fickian region was found to be consistent with Graessley's model as well as with the literatures. And the dependence of the D_s on the frequency agreed well with the Doi-Edwards theory, in particular, scaling as $D_s \sim \omega^{1/2}$ at $\omega > 1/\tau_e$ and $D_s \sim \omega^0$ at $\omega \ll 1/\tau_{rep}$. Our experimental results also confirmed that the dependence of the D_s on the temperature for PMMA and PVDF can be well described by the Arrehnius law. Moreover, blends of PMMAs have been proposed in order to be able to change the $\overline{M}_w$. The rheological investigations of these corresponding bilayers rendered it possible to monitor the effect of $\overline{M}_w$ on the diffusion process. The obtained results gave $D_s \sim \overline{M}_w^{-1}$, thus corroborating some earlier studies and some experimental results recently reported by Time-Resolved Neutron Reflectivity Measurements (TR-NR). At last, the thickness of the interphase and its corresponding viscoelastic properties could be theoretically determined as a function of the healing time.

II.2 Introduction

Up to date, what is known of the polymer diffusion process across an interface is based on the chain dynamical theory developed by de Gennes (1971), and later improved by Doi and Edwards (1986). This so-called tube theory involves each polymer chain crawling like a snake, since its motion is constrained by the topological entanglement structure formed by the surrounding chains. According to this theory, several characteristic time regimes can be delimited considering the general motion behavior of the polymer chains. At very short times, $t<\tau_e$, known as the Rouse relaxation time between entanglements, a quite small motion takes place on a single statistical segment, without being subjected to topological constraints. For $\tau_e < t < \tau_R$, i.e., the Rouse relaxation time of the whole chain, the chain starts to feel the topological constraints of the tube and thus the motion of Rouse segments perpendicular to the tube contour is restricted whereas free motion is allowed along the curvilinear axis of the tube. For $\tau_R < t < \tau_{rep}$, i.e., the reptation relaxation time, the defects are equilibrated along the total length of the tube and the chain moves as a whole along the fixed tube. For $t > \tau_{rep}$, the chain motion is governed by reptational dynamics that allow the chain to renew the tube by escaping completely from the first tube without memory of its initial conformation. Moreover, the displacement ($\Phi_n(t)$) of Rouse segments of entangled polymers has been found to be time dependent, which can be expressed in the terms that $\Phi_n(t)=<(r_n(t)-r_n(0))^2>^{1/2} \sim t^{1/4}$ for $t \leq \tau_e$; $\Phi_n(t) \sim t^{1/8}$ for $\tau_e \leq t \leq \tau_R$; $\Phi_n(t) \sim t^{1/4}$ for $\tau_R \leq t \leq \tau_{rep}$ and $\Phi_n(t) \sim t^{1/2}$ for $t > \tau_{rep}$ which is expected as normal Fickian diffusion.

Nevertheless，one cannot take for granted that the self diffusion mechanism in the bulk is valid for the diffusion at the interface. Indeed, the latter greatly depends on the configuration of chain ends at the initial state of diffusion. Many authors (Karim, et al. 1990;Reiter and Steiner 1991) have attempted to distinguish the same time-dependent zones for the inter-diffusion process at the interface as for self-diffusion in the bulk, but with no absolutely perfect coincidences obtained. Among these, only the reptation-to-Fickian transition at $t=\tau_{rep}$ involve segment displacements on the order of the radius of gyration was clearly observed, as indicated by a strong change of slope in the displacement-time logarithm curve. Wool(1995) argued that only the Fickian diffusion region, i.e., $\Phi_n(t) \sim t^{1/2}$, still holds for the diffusion at the interface, whereas in the Rouse and reptation regions, a mixing and repartition of Rouse and reptation contributions should be considered due to the effect of the interface configuration. These may blur the transitions between characteristic times, with the average inter-diffusion distance increasing smoothly and monotonically over most of the dynamic regions.

The sophisticated methods based on spectroscopical measurements like forward recoil spectroscopy (Composto, et al. 1988;Crist, et al. 1989), secondary ion mass spectroscopy (Wool 1995), small-angle neutron scattering (SANS) (Hellmann, et al.

1991), neutron reflectivity (Kunz and Stamm 1996) etc. have given us deep insights into the inter-diffusion at the interface. Nevertheless, the labeled or marked elements required in these spectroscopic techniques have been indicated to be able to slow down the mass transport process during diffusion (Green and Doyle 1987). It is worth meantioning that very recently, Kawaguchi et al. (2011) have published an interesting paper allowing to follow the time evolution of concentration profiles based on interdiffusion of polystyrene/deuterated polystyrene bilayer by time-resolved neutron reflectivity(TR-NR) measurements. But this technique, though with a high spatial resolution, is a very expensive, sophisticated and un-versatile tool. Moreover, nearly all the techniques above -mentioned deal with polymer-polymer interdiffusion under static conditions, however, for the realistic polymer processings, interdiffusion occurs more often in a shear flow field.

At the end of last century, a simple and rapid research technique, consisting in using a rheological tool, was firstly developed by Bousmina and his coworkers (Bousmina, et al. 1998;Qiu and Bousmina 1999; 2000; 2002;Qiu, et al. 2002) to quantify the inter-diffusion process across polymer/polymer interfaces. The principle of this method is based on the macromolecular dynamics theory. Several specific quantitative models relevant to rheological functions like the storage modulus *G′* or complex modulus *G** have been proposed to determine the self-diffusion coefficients of neat polymers and mutual diffusion coefficients between chemically dissimilar polymers, respectively. The researchers in question observed an anomalous scaling law of the time transition of *G** increments and confirmed the effect of excess chain ends at the interface. Furthermore, they pointed out that the time transition is washed out by a polydispersity effect in polydisperse polymer couples. The rheological tool was later adopted by Lamnawar and Maazouz (2006; 2008; 2009, 2010a) to study the role of the interphase between incompatible polymers (including interfacial diffusion and reactions), and was expanded to the mutual diffusion of coextruded multilayers systems by Zhao and Macosko(2007) and Yang et al. (2010). In fact, this rheological tool has also been successfully extended to the diffusion process between low molar mass molecules, like plasticizers, and polymers (Bella, et al. 2006;Joubert, et al. 2002;Msakni, et al. 2007). Recently, role of diffusion on the encapsulation behavior of two drops has been highlighted from a rheological and optical viewpoints, on the model system based on poly(dimethylsiloxane)(PDMS) of varying molecular weights, PVDF/PMMA and PE-GMA(glycidylmethacrylate) / PVDF-g-MA (maleic anhydride) (Lamnawar, et al. 2012).

Even so, to the best of our knowledge, very few papers have been published on the topics of (i) monitoring the diffusion, by a rheological tool, on high molecular weight, polydisperse polymers; (ii) performing modeling, using a theoretical and experimental approach, to determine the effect of M_w, I_p on the diffusion phenomena; and (iii) using rheology as a suitable tool to investigate the effect of temperature and time on the diffusion process. In order to understand polymer processing like

coextrusion (Lamnawar and Maazouz 2009;Xu, et al. 2008) and relevant interfacial phenomena (Lamnawar, et al. 2010a;Li, et al. 2011;Rahim, et al. 2011), it is very important to determine and quantify the apparent diffusion and self diffusion, and especially their kinetics versus time, temperature, frequency and structural properties (M_w, I_p, etc.). To this end, this paper is devoted to determining the inter-diffusion process between similar polymers with a symmetric bilayer structure by a parallel plate rheometer.

II.2.1 Determining the diffusion coefficient from rheological functions

The most important question we wish to answer is how one can determine the diffusion coefficient from time-dependent rheological functions of a bilayer assembly. A connective relationship between these functions has been derived by Qiu and Bousmina (1999) from Boltzmann's integral form

$$\tau(t) = \int_{-\infty}^{t} G(t - t^{'})\gamma(t^{'})dt^{'}$$

(II-1)

where the stress $\tau(t)$ measured at the time t is a function of the whole history of past deformation $\gamma(t^{'})$ at anterior times t', and the shear relaxation modulus $G(t-t')$, which contains the whole past history of the deformation, can be related to the mass transport across the interface that occurred at previous times. In the linear regime, the complex modulus $G^*(\omega)$ can be obtained by

$$G^*(\omega) = i\omega \int_{0}^{\infty} e^{-i\omega t}G(t)dt$$

(II-2)

and the relaxation modulus $G(t)$ for the motions of Rouse dynamics ($t<\tau_e$) is given as

$$G(t) = \frac{\rho RT}{M} \sum_{n=0}^{\infty} \exp\left(\frac{-6n^2\pi^2 k_B Tt}{\zeta N^2 b^2}\right)$$

(II-3)

Here, ρ is the density, RT the temperature defined in energy units, M the molecular weight, k_B the Boltzmann constant, ζ the monomeric friction coefficient, N the number of segments per chain and b the effective bond length. And the $G(t)$ for the motions of reptation dynamics ($t>\tau_e$) is

$$G(t) = G_N^0 \sum_{n=0}^{\infty} \frac{8}{(2n+1)^2 \pi^2} \exp\left(\frac{-(2n+1)^2 \pi^2 k_B Te^2 t}{\zeta N^3 b^4}\right)$$

(II-4)

where G_N^0 denotes the plateau modulus, and e represents the step length.

The self-diffusion coefficients of macromolecular chains with Rouse dynamics and reptation dynamics developed by Doi-Edwards theory as

$$D_R = \frac{k_B T}{\zeta N} \tag{II-5}$$

and

$$D_{rep} = \frac{k_B T e^2}{3\zeta N^2 b^2}, \tag{II-6}$$

were utilized to relate the diffusion coefficient to the rheological functions.

Omitting the higher terms in Eqs. (II-3) and (II-4) that render negligible contributions, and substituting Eqs. (II-5), (II-3) and (II-6), (II-4) into eq. (II-2), respectively, one can attain the related expressions between the complex modulus $G^*(\omega)$ and diffusion coefficients as follows:

$$G^*(\omega) = \frac{\rho RT}{M}\left(\frac{Nb^2\omega}{24D_R}\right)^{1/2} \tag{II-7}$$

$$\left[G^*(\omega)\right]^2 = \left(\frac{8G_N^0}{\pi^2}\right)^2 \frac{1}{1+\left(\frac{3\pi^2 D_{rep}}{\omega Nb^2}\right)^2} \tag{II-8}$$

which amounts to

$$D_R = \left(\frac{Nb^2}{24}\right)\left(\frac{\rho RT}{M}\right)^2 \frac{\omega}{\left[G^*(\omega)\right]^2} \tag{II-9}$$

for the Rouse model, and

$$D_{rep} = \frac{Nb^2\omega}{3\pi^2}\left[\left(\frac{8G_N^0}{\pi^2 G^*(\omega)}\right)^2 - 1\right]^{1/2} \tag{II-10}$$

for the reptation model. It is worth mentioning that the Rouse model applies to the motions of short chains in the melt, corresponding to the case of chains with relaxation times shorter than τ_e. It is suggested that in the linear regime (of small γ), the relaxation for $t > \tau_e$ is due only to the disengagement from the deformed tube since the relaxation of the contour length can be neglected to the first order in γ according to reptation dynamics. From this viewpoint, the reptation model of the diffusion coefficient is applicable for $\tau_e \leq t \leq \tau_R$ and $t > \tau_R$.

II.3 Experimental Section

II.3.1 Materials and Characterizations

The poly (methyl methacrylate) (PMMA)s and poly(vinylidene fluoride) (PVDF) used in this study were commercial grades supplied by the Arkema Corporation, namely PMMA-V825T, PMMA-V046 and PVDF-Kynar 720. The main characteristics of the materials are listed in Table II-1. To expand the molecular weight range, three more PMMA samples were prepared in our laboratory by melt blending PMMA-V046 and PMMA-V825T in a twin screw extruder at weight ratios of 30/70, 50/50 and 70/30. For clarity, details on the experimental procedures have been given elsewhere (Lamnawar and Maazouz 2009). Note that for a blend consisting of two miscible components with an identical chemical structure, the corresponding weight-average molecular weight $\overline{M}_{wb}$ can be determined by the following expression (Han and Kim 1989a;Struglinski and Graessley 1985):

$$\overline{M_{wb}} = \sum w_i \overline{M_i} \qquad \text{(II-11)}$$

in which w_i and $\overline{M_i}$ are the weight fraction and weight-average molecular weight of component *i*. Accordingly, the number-average molecular weight is expressed as

$$\overline{M_{nb}} = 1 \bigg/ \sum \frac{w_i}{M_i} \qquad \text{(II-12)}$$

and the polydispersity index is written as

$$Ip = \frac{\overline{M_{wb}}}{\overline{M_{nb}}} \qquad \text{(II-13)}$$

The glass transition temperature (T_g), melting temperature (T_m) and crystallization temperature (T_c) of the polymers were measured by differential scanning calorimetry (TA Q20) at a heating and cooling rate of 10 ºC/min in an ambient environment of nitrogen gas at a flow rate of 50 mL/min. Nuclear magnetic resonance (NMR) was employed to characterize the tacticity of PMMA. ^{1}H-NMR (250 MHz) spectra were recorded on a Bruker AVANCE 250 spectrometer using chloroform-d (CDCl$_3$) as the solvent. The molecular weight and polydispersity of PMMA were determined via size exclusion chromatography (SEC) equipped with 3 Waters HR5E columns, using tetrahydrofuran (THF) as an eluent at a flow rate of 1 mL.min^{-1} at room temperature. Results were obtained by multi-detectors with sample concentrations of 1.0 mg.ml^{-1}. For PVDF, the molecular weight and polydispersity

were determined via a SEC apparatus running in dimethyl formamide (DMF) (flow rate: 0.8 mL.min^{-1}) equipped with 3 Styragel HR 4E columns, calibrated with polystyrene (PS) standards.

Table II-1 Characteristics of the investigated polymers

Samples	Trademark/ Supplier	$T_g(^oC)$	$T_m(^oC)/$ $T_c(^oC)$	M_w(g/mol)		$M_w/$ M_n	E_a(KJ/mol)
PVDF	Kynar 720/ARKEMA	-42	170/ 136	210,000		2.0	59
PMMA-1	AltuglasV825T/ ARKEMA	114	——	95,000		2.1	169
PMMA-2	AltuglasV046/ ARKEMA	102	——	137,000		2.0	157
PMMA-B 1	PMMA-1/PMMA-2 (70/30)	109	110.3^a	——	105,000	107,000^b	2.3	156
PMMA-B 2	PMMA-1/PMMA-2 (50/50)	107	107.9^a	——	119,000	116,000^b	2.5	160
PMMA-B 3	PMMA-1/PMMA-2 (30/70)	105	105.5^a	——	122,000	124,000^b	2.5	155

^{a} theoretical value calculated from Eq.(II-14); ^{b}theoretical value calculated from Eq.(II-11)； Ea -activation energy of viscous flow obtained from master curve at a reference temperature of 200 ºC.

II.3.2 Samples preparation and rheological measurements

All the resin granules were dried at 80 °C under vacuum to remove any moisture before use. The samples for rheological measurements were prepared by compression molding at 180 ºC between two Teflon films to obtain a smooth surface. During the stages of heating and cooling under compression, nitrogen purging was introduced to protect the polymers from oxidation. The obtained samples were then cut into round disks with a diameter of 25 mm. All samples were fabricated under identical processing conditions to eliminate sample-to-sample errors. Subsequently, the disks were annealed at 80 ºC under vacuum for at least 24 h to relax the surface orientation caused by the compression molding.

Rheological measurements of the neat polymers were carried out by a small-amplitude oscillatory rheometer, i.e., ARES (Advanced Rheometrics Expansion System), in strain-control mode with a parallel-plate geometry (Φ=25 mm) at different temperatures from 180 °C to 240 °C. Sample disks were loaded and melted between the upper and lower plates that had been preheated to the measurement temperature prior to the testing. The gap between the plates was set to 1.2 mm, which was the thickness of the bulk disk. To ensure that the viscoelastic measurements were performed within the linear regime, a dynamic strain sweep test was first conducted in the range from 0.1% to 100% with the maximum angular frequency (ω) amplitude of 100 rad/s. Moreover, in rheological measurements

especially in steady shear flow and high shear rate, wall slip is very important to be taken into account (Ansari, et al. 2011;Hatzikiriakos 2012;Mhetar and Archer 1998;Mooney 1931). However, in linear viscoelasticity regime of small-amplitude oscillatory shear measurement (SAOS), the small shear stress and the strong contact of polymer bulk to the stainless steel plates makes wall slip negligible. In our present work, we have performed measurements on monolayer and bilayer with a given gap varying from 1.0 mm to 1.8 mm and the good agreement between the obtained rheological properties of the component measured in different gap geometries is strong evidence against any wall slip.

The healing process across the polymer/polymer interface was tracked by a dynamic time sweep test with a bilayer assembly melted between the parallel plates at a given temperature in the oven of the ARES rheometer. Before they were loaded in the oven, two symmetric disks with individual thicknesses of 600 μm were brought into intimate contact at room temperature. It should be noted that the loading of the assembly should be rapid to avoid a too significant reduction of the oven temperature. The tests were started when the oven temperature reached the equilibrium state of the measured temperature, ~ 3 minutes. The deviation of the oven temperature was within ± 0.5 °C. The gap was set to 1.2 mm, corresponding to the total thickness of the bilayer assembly. An external compression, which is believed to accelerate the diffusion process, was not expected in the experiments by using same sample dimensions and gap geometry for all tests. Moreover, purging with dry nitrogen was warranted during all the measurements to exclude the effects of oxidation and/or cross-linking.

II.4 Results and Discussion

II.4.1 Polymer characterization

II.4.1.1 DSC and ^{1}H-NMR characterizations

The DSC results of the investigated polymers are listed in Table II-1 and the glass transition temperatures (T_g) of the PMMAs are plotted in Figure II-1. The value of the glass transition temperature was taken as the inflection of the curve. It should be noted that, unlike the common growth relationship between T_g and molecular weight, PMMA-1 (of lower M_w) unexpectedly had a higher T_g than PMMA-2 (of higher M_w). Moreover, the PMMAs obtained from the melt blending (from PMMA-B1 to PMMA-B3) demonstrated a single T_g, lying between those of the two corresponding neat polymers. This was in agreement with the predictions of the well known Fox equation for miscible blends (Fox 1956):

$$1\!\!\Big/\!{Tg_b} = {w_A}\!\!\Big/\!{Tg_A} + {w_B}\!\!\Big/\!{Tg_B} \tag{II-14}$$

where T_g and w are the glass transition temperature and the weight fraction;

subscripts *b*, *A* and *B* designate the blend, and its components *A* and *B*, respectively.
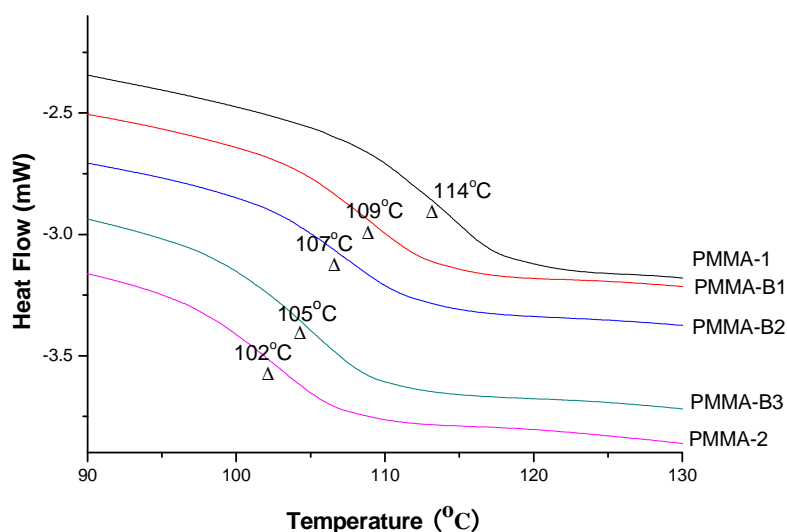
Figure II- 1 DSC thermograms (2nd heating) of neat PMMAs and PMMA blends

With respect to the deviations from the common growth relationship between T_g and M_w, it is possible that for PMMA, besides being related to the molecular weight, the T_g may also be related to its tacticity. The tacticity of PMMA can be experimentally estimated from the α-methyl proton region (0.5-1.2 ppm) of the ^{1}H-NMR spectra in a way that determines the amounts of syndiotactic (st), heterotactic (ht), and isotactic (it) triads by integration over the peaks at 0.85 ppm, 1.02 ppm and 1.21 ppm, respectively. The results obtained for PMMA-1 and PMMA-2 are given in Figure II-2. It is evident that the higher amount of the syndiotactic triad as opposed to the lower amount of the isotactic triad of PMMA-1 gave rise to its higher T_g compared with PMMA-2. It is also worth mentioning that the tacticity of PMMA has been reported in the literature to have a possible effect on its diffusion process. Considering that the differences in tacticity of the PMMAs investigated in this study were not very great, the effect of tacticity has not been taken into account in the following discussions.

Tacticity	PMMA-1	PMMA-2
st	50%	42%
ht	39%	39%
it	11%	19%
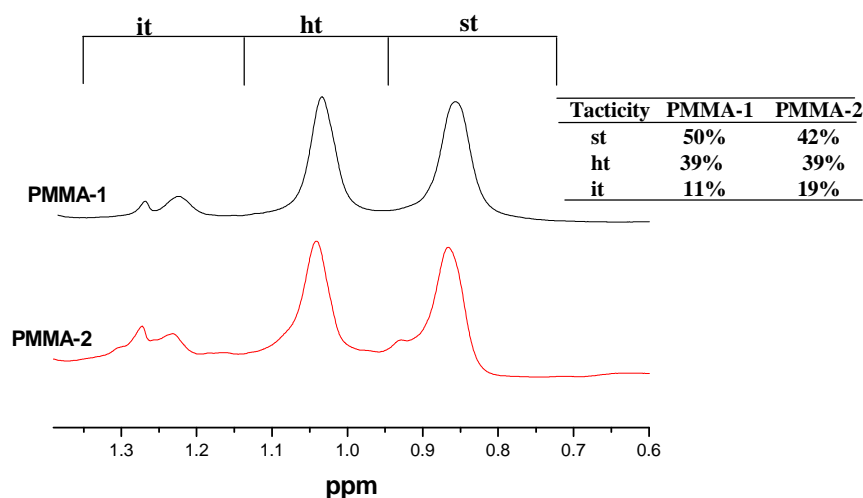
Figure II-2 ^{1}H-NMR spectra of PMMA-1 and PMMA-2and their determined tacticities, it:isotactic; ht: heterotactic; st: syndiotactic

II.4.1.2 SEC characterization

The results of the size exclusion chromatography (SEC) experiments are shown in Figure II-3 and the corresponding molecular weights and polydispersities are listed in Table II-1. As stated before, three of the PMMAs were achieved by melt blending to change their molecular weights. The feasibility of this method can be verified by examining the molecular weights and polydispersities of the blended PMMAs under SEC. The unimodal and lightly broadened molecular weight distributions of the blended PMMAs in Figure II-3 imply that these blended PMMAs can to a certain extent be used as specimens of given $\overline{M}_w$ for investigations of the effect of the molecular weight on the diffusion process. Moreover, the experimentally determined $\overline{M}_w$ values were consistent, within experimental errors, with those theoretically calculated by Eq. (II-11).
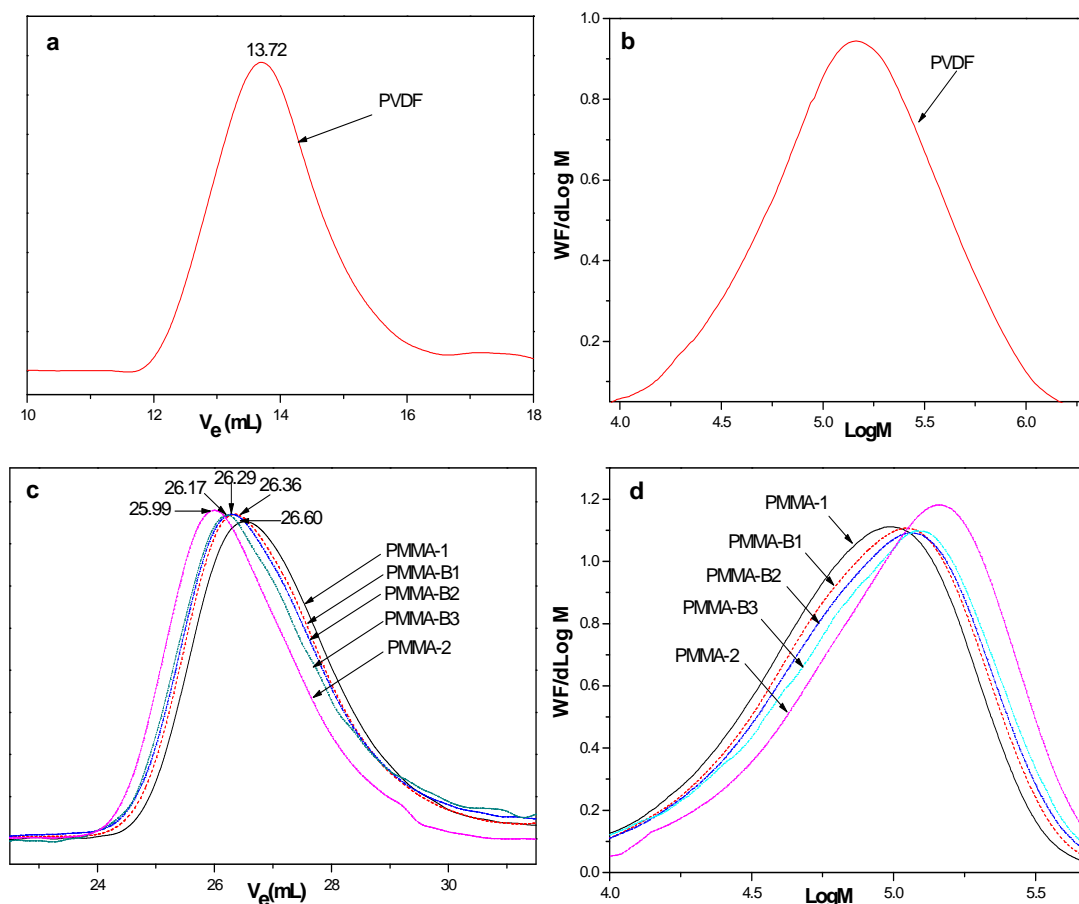
Figure II-3 (a) and (c) SEC chromatographs of PVDF (DMF) and PMMAs (THF), respectively; (b) and (d) Their corresponding WF/dLog M versus Log M curves after calibrations

II.4.1.3 Rheological characterization

II.4.1.3.1 Dynamical shear viscoelasticity

Rheological properties of the neat polymers in the molten state were measured in a parallel-plate geometry using monolayers with a thickness around 1.2 mm (corresponding to the total thickness used for the bilayers in order to minimize possible errors caused by geometry). The master curves were created by time-temperature superposition from dynamic frequency sweep tests obtained at temperatures ranging from 160 °C to 260 °C for the PMMAs, and temperatures ranging from 180 °C to 240 °C for the PVDF. The temperature-dependence of the shift factors followed an Arrhenius-type equation, and their corresponding values of the activation energies are given in Table II-1. For clarity, Figure II-4 shows only the storage modulus *G′*, loss modulus *G″* and dynamic viscosity *η** as functions of frequency obtained at the reference temperature of 200 °C for these three neat polymers. From the curves of *η** versus frequency, noticeable shear thinning behaviors can be observed at high frequencies, especially for the PMMAs. Moreover, these variations can be well fitted by the Carreau model, where the zero shear viscosities *η₀* are produced. Commonly, polymers with molecular weights above the critical molecular weight of entanglement *Me* show a plateau with regard to the *G′*

curve. In the present work, the plateau zone of the G' curve of PMMA was well perceivable when the frequency was above 100 rad/s within the superposed frequency range as shown in Figure II-4-b and Figure II-4-c. The plateau modulus G_N^0 of PMMA was determined at the reference temperature 200 °C as equal to the storage modulus G' at the frequency where tanδ was at its minimum in the plateau zone, (Fuchs, et al. 1996;Wu 1989) i.e.,

$$G_N^0 = \left[G^{'} \right]_{\tan \delta \to \min}$$ (II-15)

For PVDF, on the other hand, the plateau zone of G' could not be completely obtainable within the limited superposed frequency range as shown in Figure II-4a. This was due to the dynamical measurement in the melted state not being available at lower temperatures as the material tended to crystallize below its melting point 170 °C (determined by DSC).

Thus, the plateau modulus G_N^0 of PVDF was calculated as (Dealy and Larson 2006)

$$G_N^0 = \eta_0 \Big/ \tau_{0n}$$ (II-16)

where τ_{0n} is number-average relaxation time, reciprocal of the critical frequency ω_c corresponding to the crossover modulus G_c of the G' and G'' curves. The corresponding values of the molecular weight of entanglement, M_e, were calculated by the following equation

$$M_e = \frac{\rho R T}{G_N^0}$$ (II-17)

Table II-2 Material parameters of PMMA and PVDF

Polymer	ρ(g/cm³) at 200°C	η_0(Pa.s) at 200°C	G_N^0 (Pa)	M_e (g/mol)	b [a] (Å)	$(R_{ee}^2)/M$ (Å²mol/g)	τ_{0w}(s) at 200°C
PMMA-1	1.097	6.4×10^4	3.6×10^5	1.2×10^4	4.41	0.425[b]	0.965
PVDF	1.471	4.0×10^3	6.5×10^5	8.9×10^3	3.64	0.410[c]	0.178

[a] effective bond length b was determined by $b= (C_\infty b_0^2)^{1/2}$ with the characteristic ratio C_∞=8.2 for PMMA (Wool 1995), and C_∞=5.6 for PVDF (Welch 1974)

[b] see reference (Fetters, et al. 1994); [c] see reference (Welch 1974)
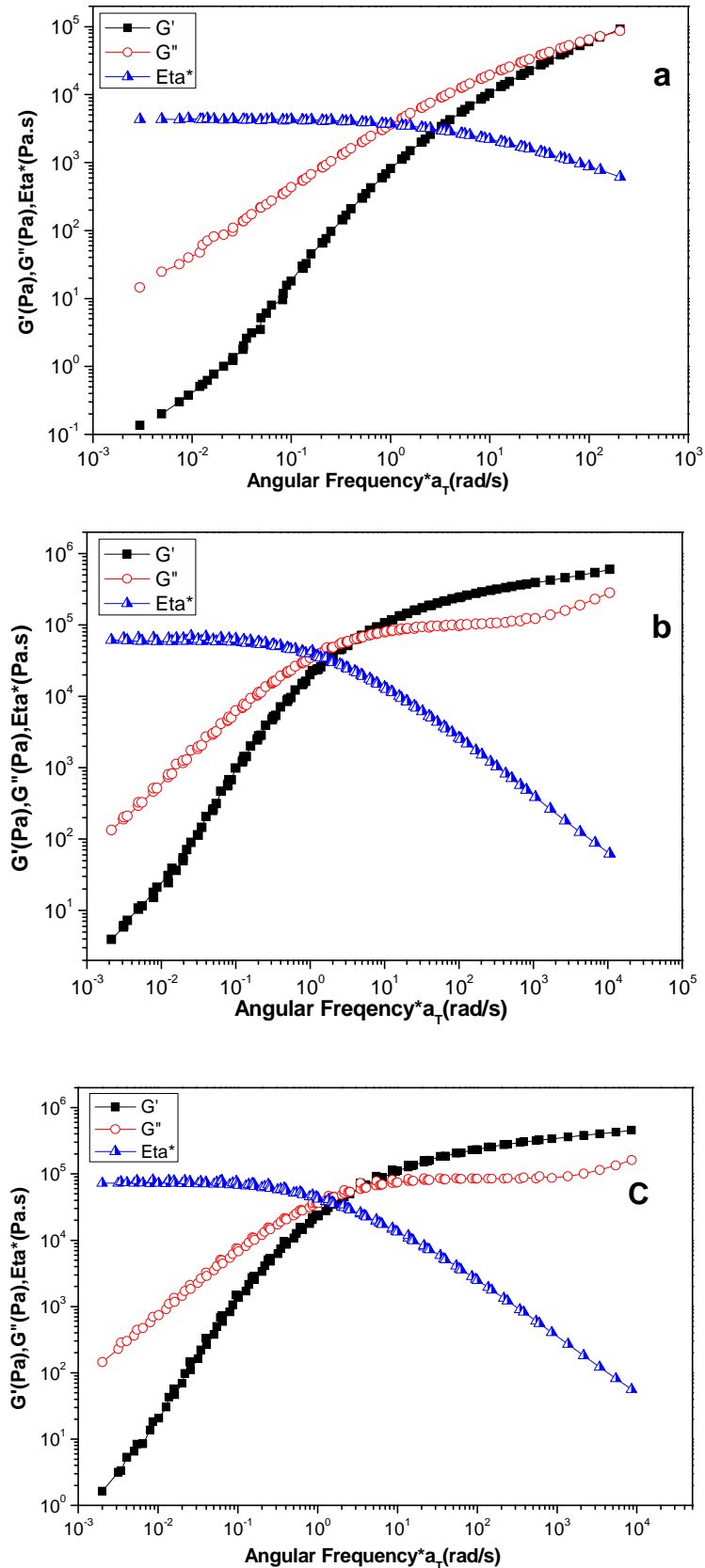
Figure II-4 Master curve of *G′*, *G″* and *Eta** as functions of frequency at the reference temperature 200 °C for neat polymers: a-PVDF; b-PMMA -1; c-PMMA -2

II.4.1.3.2 Relaxation behavior of the PMMAs

A Cole-Cole curve is a useful plotting technique to obtain some important viscoelastic properties of polymers. For example, the imaginary versus real components of the complex viscosity function can give the characteristic relaxation time of the polymer and can also show contributions from the constituent components of a blend, indicating a homologous behavior of the blend (Dealy and Larson 2006). Figure II-5a presents the η'' versus η' curves of neat and blended PMMAs at 200 °C. From the frequency corresponding to the maximum value of η'' at the circular arc, one can determine the weight-average relaxation time τ_{0w}, as given in Table II-2. The Cole-Cole plot of the blended PMMA exhibited a smooth and single semicircle like the one of neat PMMA. The fact that it was without deviation or divided into two arcs indicates a good homogeneity of the blended PMMA. This result may also be supported by the weighted relaxation spectra $H(\lambda)*\lambda$ versus λ of the blended PMMAs as shown in Figure II-5b. The linear relaxation spectrum $H(\lambda)$ was calculated based on the work of Mead(1994) and Honerkamp and Weese (1993) according to Eq.(II-18)

$$G^{*}(\omega) = \int_{-\infty}^{+\infty} \frac{H(\lambda)i\omega\lambda}{\lambda(1+i\omega\lambda)}d\lambda \qquad \text{(II-18)}$$

The weighted relaxation spectra $H(\lambda)*\lambda$ reflect the time distribution of the chain relaxation behavior for the neat and blended PMMAs. The single and unimodal relaxation peaks of the blended PMMAs were analogous with those of its PMMA counterparts, as shown in Figure II-5b. This, together with the perfect semicircular shapes in the Cole-Cole curves as well as the monomodal molecular weight distributions in the SEC chromatographs, revealed that the blended PMMA possessed similar characteristics with neat PMMA, evidencing a good feasibility of using blended PMMAs as studying specimens for diffusion process in this study.
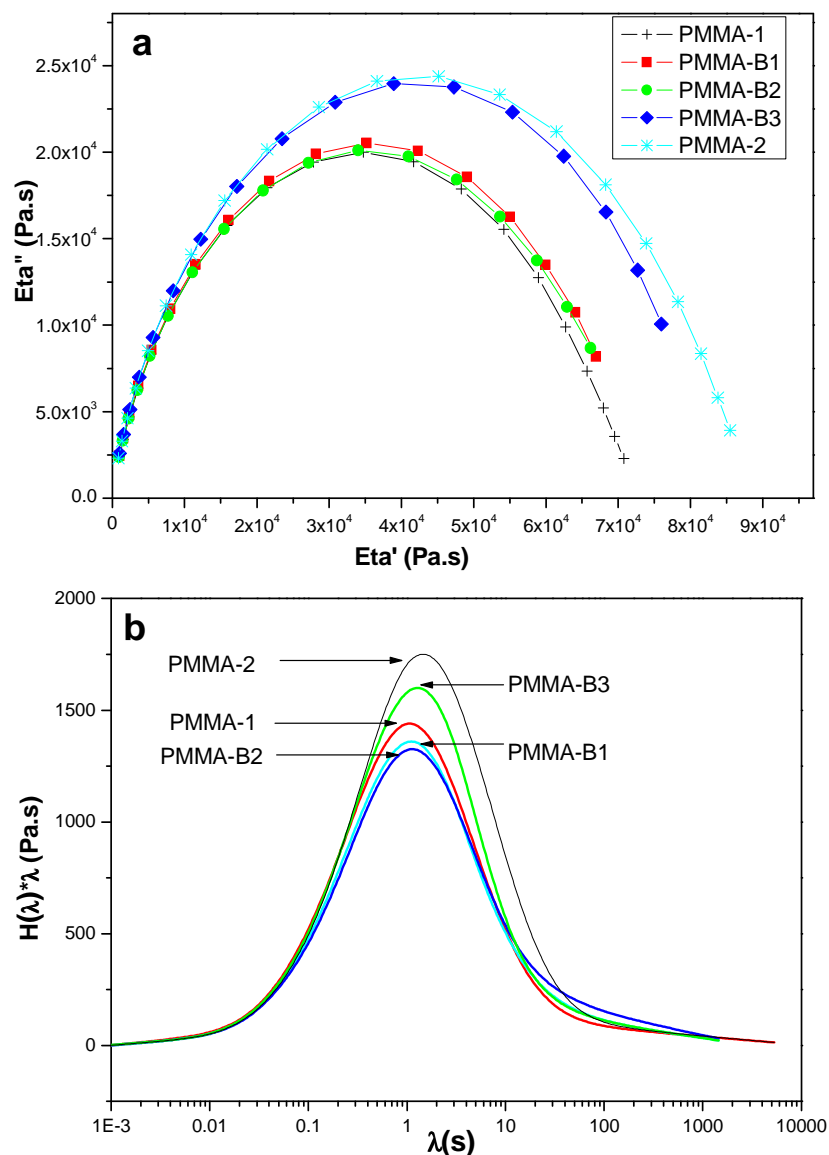
Figure II-5 Relaxation behaviors of the PMMAs: (a) Cole-Cole curves of the neat and blended PMMAs at 200 °C; (b) weighted relaxation spectra of neat and blended PMMAs at 200 °C

II.4.1.3.3 Thermal stability of the investigated polymers

Prior to probing the diffusion process of polymer bilayers in the molten state by rheology, it was indispensable to examine the thermal stability of the used pure polymers at the measured temperatures. Hence, dynamic time sweep tests for the pure polymers were conducted in advance under the same conditions as for the bilayer systems. For the sake of clarity, only the rheological results obtained at the maximum temperature 240 °C and angular frequency (ω) = 1 rad/s are given here. The invariability of the rheological properties with time, as presented in Figure II-6, sufficiently indicated the thermal stability of these investigated polymers at the employed conditions. Thus, the increments of the G^* (or G') in the following work may be attributed solely to the diffusion process.
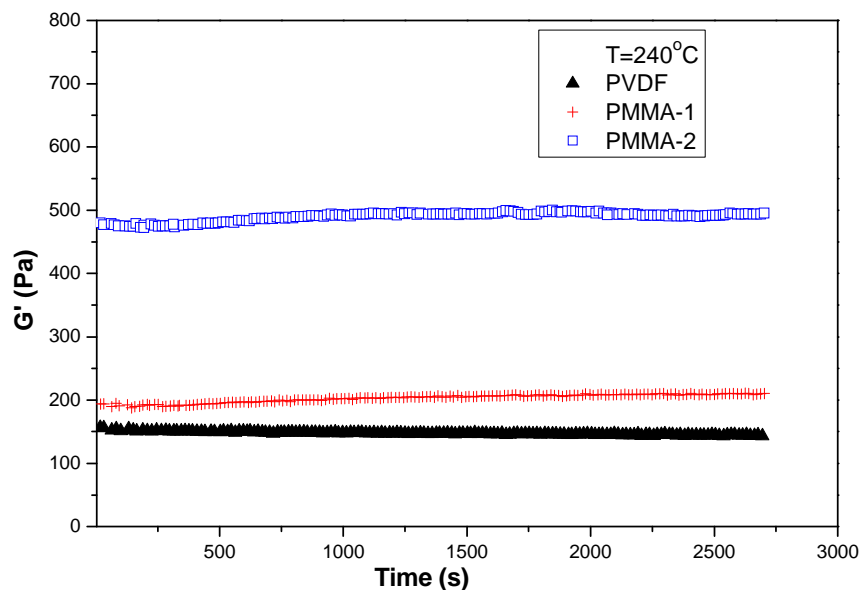
Figure II-6 Evolution of *G'* versus time at T=240 °C and ω = 1 rad/s for neat polymers

II.4.2 Kinetics of the interdiffusion process at polymer/polymer interface

The healing process of polymer/polymer interfaces was followed by dynamic time sweep tests in the linear viscoelastic regime by small-amptitude oscillatory rheometry. As stated by Wool and O'Connor (1981), the healing process has five stages, i.e., surface rearrangement, surface approach, wetting, diffusion and randomization (Figure II-7). By the end of the wetting stage, namely the first moments of diffusion, the characteristic strength of the polymers appeared. In the present work, the variations of rheological properties (e.g, the storage modulus *G'* and/or complex modulus *G**) can be seen as the indications of such characteristic strength. It should be noted that at the very beginning of our experiments, instead of a pronounced direct increment with time, the viscoelastic properties of bilayers underwent a short period of fluctuations that can be seen as the interference of the relaxation and the thermal equilibrium process of the sample. During this period, potential barriers associated with inhomogeneities at the interface disappear and the chains were consequently free to move across it. Here, we define the time at which the viscoelastic functions (*G'* or *G**) start to increase as the start of the diffusion process (*t* = 0).
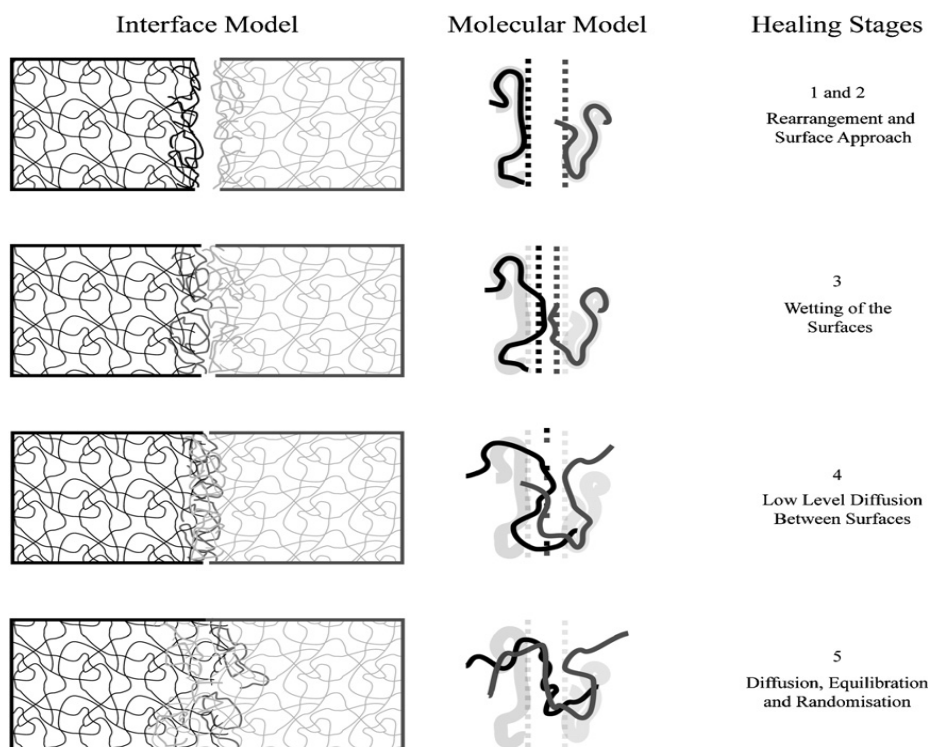
Figure II- 7 Scheme of the healing process across a polymer interface via molecular inter-diffusion (adopted from reference (Wu et al. 2008))

Figure II-8 depicts the evolution of the complex modulus G^* and the apparent diffusion coefficient (D_a) of the PMMA-1/ PMMA-1 symmetric bilayer versus healing time at 200 °C and ω= 0.1 rad/s. The apparent diffusion coefficient (D_a) was determined by Eq. (II-10) or Eq. (II-9) from the complex modulus (G^*) depending on the types of the motion dynamics. In addition to the parameters listed in Table-2, other numerical parameters involved in D_a calculations are κ_B = 1.380×10^{-23} J/K, R = 8.314 J/mol.K, N_{PMMA-1} = 949, N_{PMMA-2} = 1368 and N_{PVDF} = 3279. It is noteworthy that our pre-calculations based on the experimental data of the present work indicated that the D_a results calculated from the complex modulus (G^*) differed from the ones calculated from the storage modulus (G') by Eq. (II-8) of Reference (Qiu and Bousmina 1999) as did by Qiu and Bousmina. In their studies, one can notice that the temperatures used were much lower than ours, 115 °C for PS/PS, which is only slightly above its T_g. It may thus be reasonable to use G' to calculate the diffusion coefficient since the dissipating fraction G'' at low temperature is relatively minor. However, in our study, experiments were performed at higher temperatures (ranging 180 °C to 240 °C), corresponding to the molten state of the polymers. The elastic behavior contribution G' accounted for a smaller fraction, and the difference between results determined from G^* and that from G' became wider at higher temperature. Consequently, we suggest that it would be better to utilize G^* rather than G' to determine the D_a at higher temperatures.
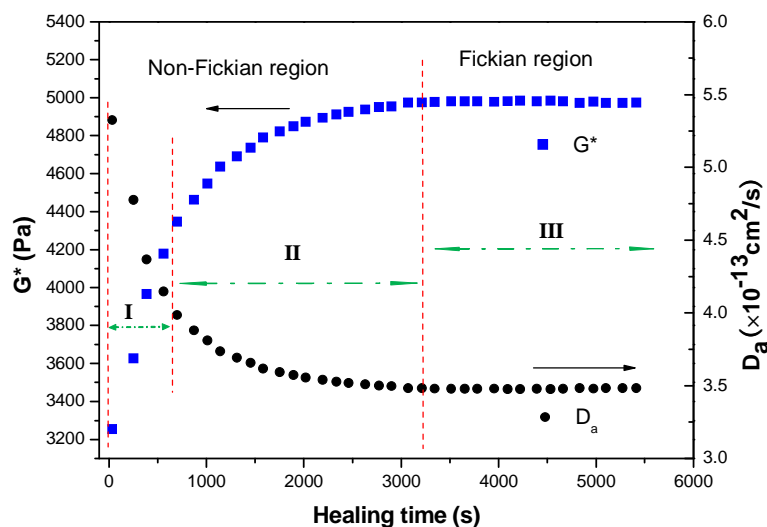
Figure II- 8 Complex modulus G^*(■) and apparent diffusion coefficient D_a(●) versus healing time for a PMMA-1/PMMA-1 symmetric bilayer at ω = 0.1 rad/s and T = 200 ºC

We can see from Figure II-8 that the evolution of G^* (or D_a) with time exhibited three clear stages: at the beginning, G^* increased (or D_a decreased) monotonically with time at a rapid rate, then the increase (or decrease) slowed down and gradually transformed into the third stage, where a plateau occurred. The G^* (or D_a) approached a saturation value, within experimental errors, expected to be close to the G^* value (or the self diffusion coefficient D_s) of the neat polymer. The low beginning value of G^* of the bilayer assembly was resulted from the gap at the interface plane at the beginning of healing process. The gap represents regions of the interface plane that have not been threaded through by reptating chains, and thus lacking bridges and entanglements.

As the diffusion proceeds, the polymer chains on both sides begin to penetrate into each other's sides. As time elapses, the original sharp interface plane decays to disappear, replaced by an interfacial zone (interphase) consist of entanglements newly established by polymer chains transported from the bulk at both sides. From this viewpoint, the diffusion process across the interface can be seen as a process of entanglement establishment at the interfacial zone (Figure II-9). As more and more chains cross the interface, the entanglement density at the interfacial zone increases, thus the interphase becomes strengthened. And the more torque is required for shear, hence the higher the complex modulus of the system becomes. The increment of the rheological functions is only attributed to the strengthening brought about by the inter-diffusion process. After a critical time (t_c), the two layers completely merge into one homogenous layer as indicated by the arrival of plateau stage of $G^*(t)$. From a microscopic viewpoint, now the diffusion at the interfacial zone is, identical to the center-of-center motion in the bulk, independent of the surface conformation. As a

consequence, the rheological results at the plateau stage can give us the information upon the self diffusion of polymer involved in a symmetrical bilayer structure or the mutual diffusion of polymer mixtures involved in an asymmetrical bilayer structure.
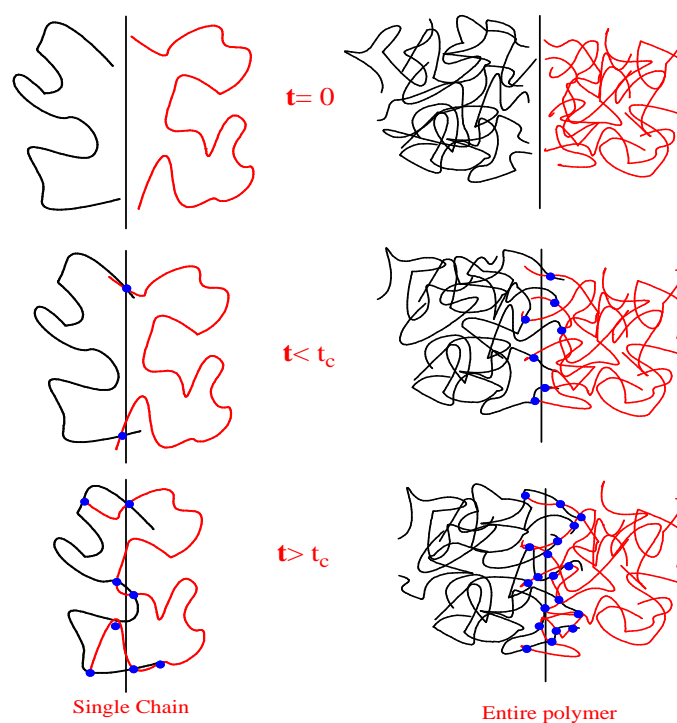
Figure II-9 Schematic diagram of diffusion process at polymer/polymer interface (a process of entanglement establishment)

Based on the reptation and minor chain model, Wool (1995) pointed out that the kinetics of the chain diffusion process at the interface can approximately be divided into two parts: the non-Fickian region and the normal Fickian region with a crossover at $t = \tau_{rep}$, the characteristic time of reptation dynamics. Moreover, the scaling law for the average monomer interpenetration distance $X(t)$ as a function of time, has a transition from $t^{1/4}$ to $t^{1/2}$ at the reptation time (τ_{rep}). Likewise, the apparent coefficient decay from high values at $t < \tau_{rep}$ to a constant value at $t > \tau_{rep}$. In our study, there was an excellent qualitative consistency with this theoretical prediction with respect to the striking transition of the diffusion coefficient from a high value to a constant versus time. But the transition occured at a critical time (t_c) greater than the reptation time. Recently Kawaguchi et al. (2011) also reported similar experimental findings (i.e. transition occurred at a $t_c > \tau_{rep}$), and they argued that the diffusion process after reptation time is still strongly affected by an early stage of diffusion obeying Rouse model, and a hypothesis proposed for this argument is that the interfacial layer is formed by early stage of diffusion obeying Rouse model and the number density of entanglement in the interfacial region reaches the bulk value and the transition from Rouse to reptation occurs. The high D_a values at $t < t_c$ were largely due to the significant contributions from segmental motion of chains in non-equilibrium conformations rather than the motions of whole chains. It is noted here, in the molten

state, for the sake of approximation, τ_{rep} is taken as the order of terminal relaxation time, determined from a Cole-Cole curve (η'' vs η'). This is the weight-average relaxation time, which is verified as larger than the relaxation times determined from other methods (Wu 1989).

II.4.3 Dependence of the interdiffusion process on angular frequency

In rheological measurements, the rheological properties of polymers vary when the employed angular frequency changes. Consequently, the diffusion coefficient calculated in Eqs. (II-10) and (II-9) should be a function of the angular frequency used in the measurements. As we know, the interval time between two sequentially exerted oscillations, i.e., the reciprocal of the corresponding angular frequency, can be regarded as the time allowed for the chains to relax. Thus, in different scopes of the angular frequencies, the measured rheological properties correspond to the relaxation behaviors of chains of different sizes. It is worthwhile to mention that unlike steady shear, in the case of linear viscoelastic regime in SAOS flow, since the deformation is infinitesimal and its influence on chain confirmation is insignificant, the possible shear-induced structural evolution (like orientation or stretching) of the interphase is unlikely to occur. The shear effects on interdiffusion process at different angular frequencies can be ruled out and the diffusion process may be considered as pure Brownian motion. In other words, the diffusion coefficients detected at different frequencies reveal the diffusion processes of different chains: short chains at high frequencies and longer chains at lower frequencies. Especially, when $\omega < 1/\tau_{rep}$ (terminal zone), all chain types are involved.

Figure II-10 portrays the variations of the apparent diffusion coefficient (calculated by the reptation model) versus healing time at different angular frequencies ranging from 0.05 rad/s to 100 rad/s at 200 ^{o}C for assemblies of PMMA-1/PMMA-1 and PVDF/PVDF. Strikingly, for both polymers, the diffusion coefficients remained nearly independent of frequency at the terminal zone ($\omega < 1/\tau_{rep}=1.036$ rad/s for PMMA-1 and $\omega < 1/\tau_{rep}=5.631$ rad/s for PVDF), whereas it increased pronouncedly with frequency at $\omega >1/\tau_{rep}$. This result was similar to those of Qiu and Bousmina (1999) on polystyrene/polystyrene.
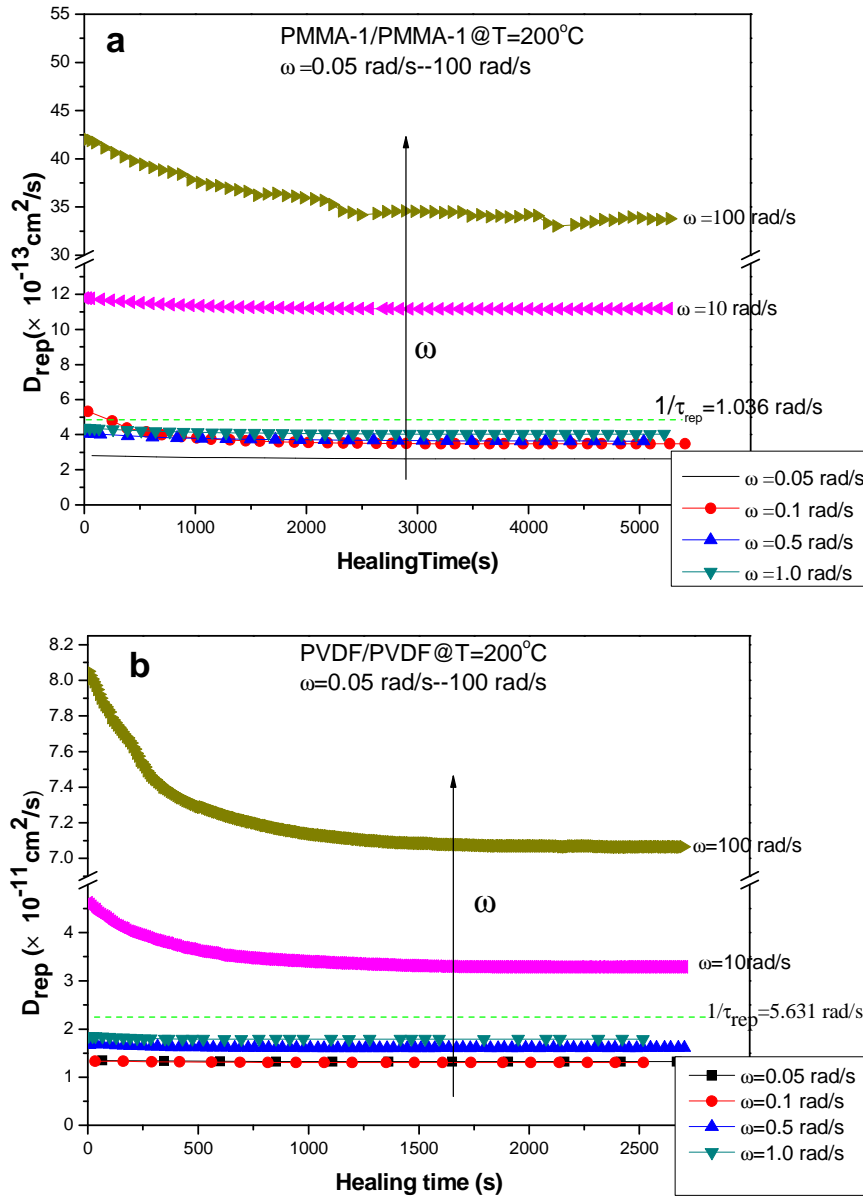
Figure II-10 Apparent diffusion coefficient as a function of healing time at various frequencies ranging from 0.05 rad/s to 100 rad/s at 200 °C for (a) PMMA-1/PMMA-1 and (b) PVDF/PVDF. (The dotted line is a virtual line used to delimit the frequency zone at $1/\tau_{rep}$)
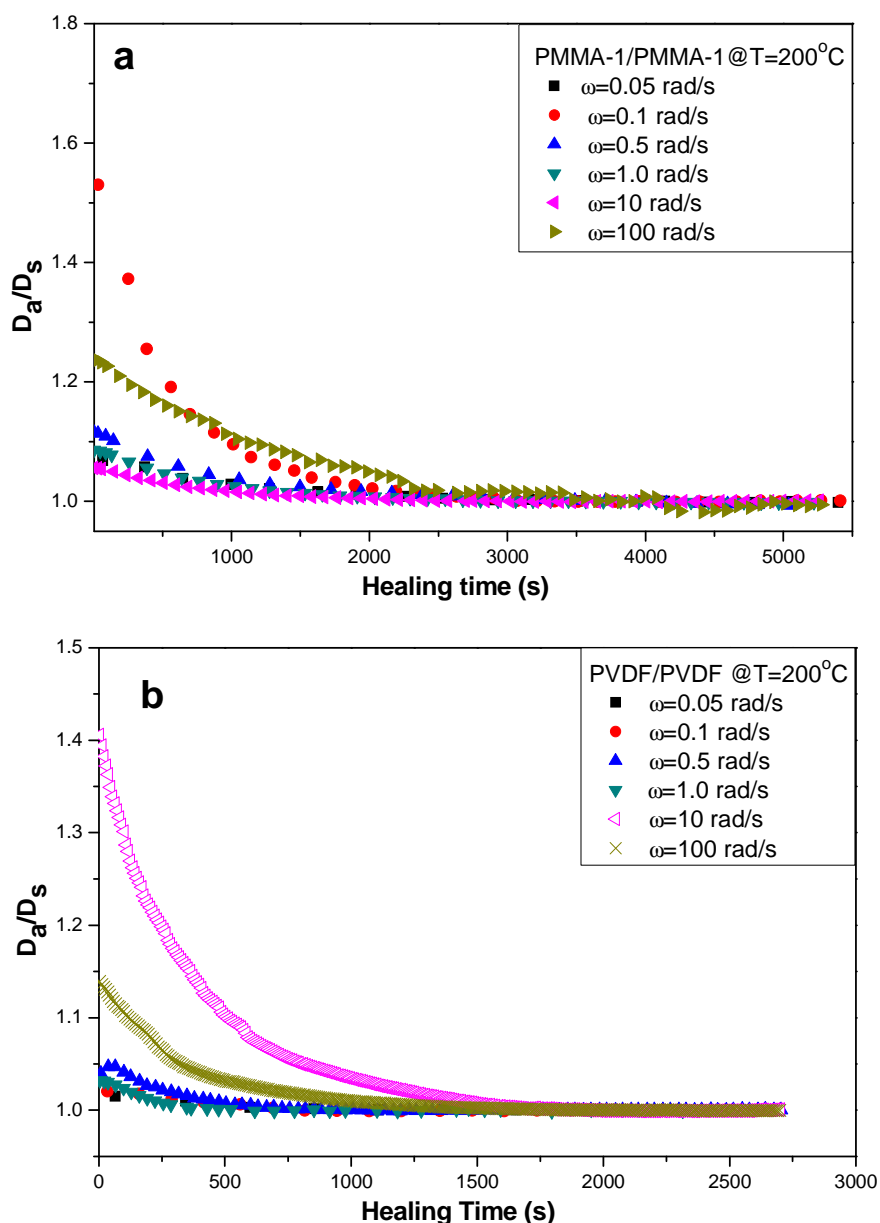
Figure II- 11 *D_a/D_s* versus healing time for (a) PMMA-1/PMMA-1 and (b) PVDF/PVDF at varying frequencies

As mentioned above, the inter-diffusion process at the interface versus time can be divided into two parts: non-Fickian and normal Fickian regions. To get an idea of the kinetics in the non-Fickian region, the ratio of the apparent diffusion coefficient to the self diffusion coefficient (*D_a/D_s*) is here used to exclude the window effect caused by the different order of magnitude of the diffusion coefficients under different conditions. In this region, the diffusion is mostly dominated by segmental motions and the relaxation of the compressed configurations, corresponding to a mix of Rouse and reptation contributions. A macroscopic scope of the frequency is correlated with a microscopic scope of motion units. One may thus imagine greater changes of small motion units during the inter-diffusion process across an interface reflected at higher frequencies and smaller changes of large motion units like whole

chains during the interdiffusion process across an interface reflected at lower frequencies. This imagination was met, within reasonable errors, by the experimental results presented in Figure II-11, considering the complexity of the experiments.

Moreover, in the normal Fickian region, for a more detailed variation, Figure II-12 plots the D_s obtained from the equilibrium stage against the angular frequency in log-log scale. In this case, since it represents the self-diffusion of bulk polymers, the time dependency of the diffusion coefficient was expected to be in accord with the Doi-Edwards theory (Appel, et al. 1994;Doi and Edwards 1986;Pahl, et al. 1997), i.e.

$$D = \frac{\left(\left\langle \Phi_n(t)\right\rangle\right)^2}{6t} \propto \begin{cases} t^{-1/2}, t \leq \tau_e \\ t^{-3/4}, \tau_e \leq t \leq \tau_R \\ t^{-1/2}, \tau_R \leq t \leq \tau_{rep} \\ t^0, t \geq \tau_{rep} \end{cases}$$
(II-19)

As we can see in Figure II-12, for PMMA-1/PMMA-1, following a plateau over the terminal zone ($\omega < 1/\tau_{rep}$), we observe that D_s calculated from the reptation model (i.e. Eq. (II-10)) was related with the frequency by an exponent of ~1/2 in the $\omega > 1/\tau_{rep}$ region. As pointed out above, for the diffusion that occurred at a frequency $\omega > 1/\tau_e$, the self diffusion coefficient should be determined by the Rouse model (i.e., Eq. (II-9)) rather than the reptation model. Apart from the difference in absolute values, a similar relation $D_s \sim \omega^{1/2}$ was also observed for Rouse model at $\omega > 1/\tau_e$, which was in perfect accord with the Doi-Edwards theory. One should note that the Rouse relaxation time between entanglements (τ_e) was here calculated by the following expression:

$$\tau_e = \frac{e^4\zeta}{k_B T b^2}$$
(II-20)

with the step length e determined as

$$e = (4/5(M_e/M_0))^{1/2}b$$
(II-21)

and the monomeric friction ζ obtained by

$$\zeta = \frac{3}{\omega_c kT}\left(\frac{4M_0 G_c}{b\rho N_0}\right)^2$$
(II-22)

from the crossover modulus G_c of the G' and G'' curves and its corresponding frequency ω_c (Ferry 1980).

However, we also have to point out that the transition regime at $1/\tau_R < \omega < 1/\tau_e$

may be washed out due to the polydispersity effect (M_w/M_n~2.0). For PVDF, a qualitative accordance was also achieved, but with D_s displaying a lower exponent 0.33 at a frequency ω>$1/\tau_{rep}$. Since $1/\tau_e$ (=145.62 rad/s) exceeded the maximum frequency (100 rad/s) that can be determined by the ARES, and its superposition was limited due to its crystallinity at low temperatures, the diffusion coefficients at higher frequencies are not available here.
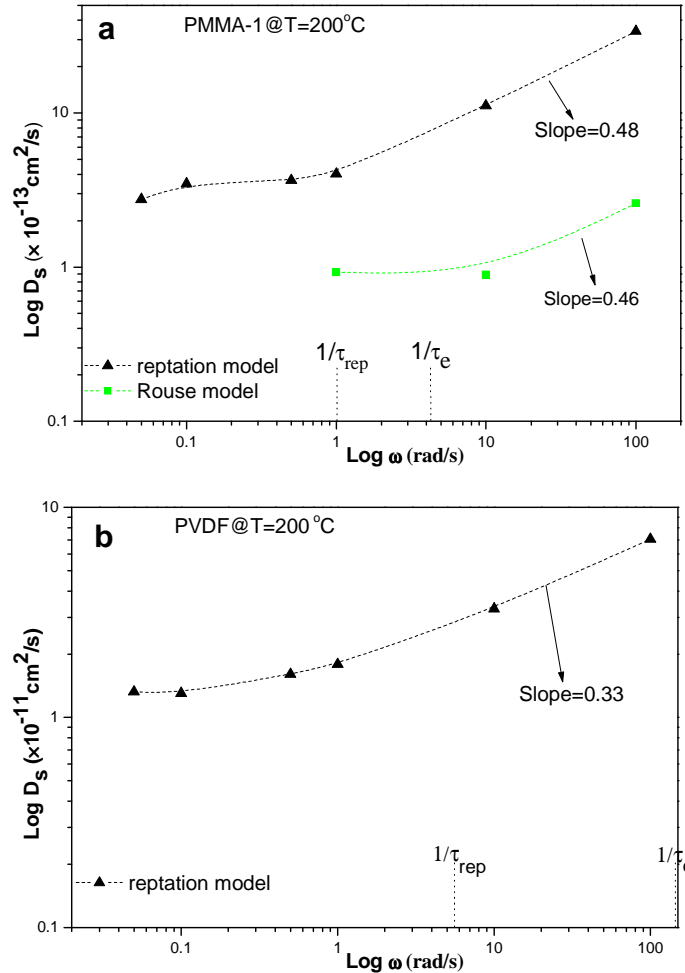
Figure II- 12 Self- diffusion coefficient of (a) PMMA -1 and (b) PVDF as a function of the angular frequency ranging from 0.05 rad/s to 100 rad/s at 200 ℃ in log-log scale

The above discussion have made it clear that only the diffusion coefficient determined at the terminal zone represents the self-diffusion coefficient of the entire material. So, in the following sections, the discussions are based on the rheological results determined at frequencies ω<$1/\tau_{rep}$.

II. 4.4 Dependence of the interdiffusion process on temperature

This section describes the dependence of the interdiffusion process on the healing temperature. Time sweep tests of PMMA -1/PMMA-1, PMMA -2/PMMA-2 and PVDF/PVDF symmetric bilayers were measured at given temperatures ranging from 180 ℃ to 240 ℃. The frequencies selected for these tests were in the terminal zone for

every given temperature, i.e., ω=1.0 rad/s for PVDF throughout the whole temperature range (1/τ_{rep}= 2.865 rad/s at 180 ºC); ω =1.0 rad/s for PMMAs at 240 ºC and 220 ºC (1/τ_{rep}= 3.69 rad/s at 220 ºC for PMMA -2); ω = 0.1 rad/s for PMMAs at 200 ºC (1/τ_{rep} = 0.746 rad/s at 200 ºC for PMMA -2) and ω = 0.05 rad/s for PMMAs at 180 ºC (1/τ_{rep} = 0.104 rad/s at 180 ºC for PMMA -2). To follow the interdiffusion process before reaching the equilibrium stage (normal Fickian region), the variation of the ratios of D_a/D_s versus healing time were considered, as plotted in Figure II-13. At higher healing temperature, chains need less energy to overcome the chemical potential barrier to diffuse. Furthermore, the shorter the chains that were activated, the faster the segments and chains moved across the interface. Figure II-13 displays the shorter times needed for the motion units to arrive at an equilibrium configuration from the pseudo-equilibrium configuration at the interface, which accounts for the decrease in critical time (t_c) as the healing temperature increased.

At the initial period of diffusion at low temperature, only short chains or segments such as Rouse- or reptation-type motion units (especially chains ends) preferred to move. This corresponded to the initially higher ratios of D_a/D_s, as indicated by Wool (1995), and the ratio D_a/D_s can be much larger, especially at times lower than the Rouse time. As the temperature increased, an increasing number of motion units of larger size participated in the diffusion at short times, smearing out the contribution of smaller units, and reducing the ratio of D_a/D_s with time. For this reason, the closer the healing temperature was to T_g, the more significant the decrease in D_a (which also means a more significant increase in G^*). This was well evidenced by the experimental results of PVDF/PVDF shown in Figure II-13c. It should be noted that the exception of PMMAs at 180 ºC may be somewhat attributable to the unique temperature dependence of the viscoelastic behaviors concerning PMMA (Plazek 1982). In addition, the very low frequency (i.e., 0.05 rad/s, with long time intervals between two adjacent oscillations) at 180 ºC may also have had some effects. Anyway, the influence of temperature on the interdiffusion process at the interface was prominent.
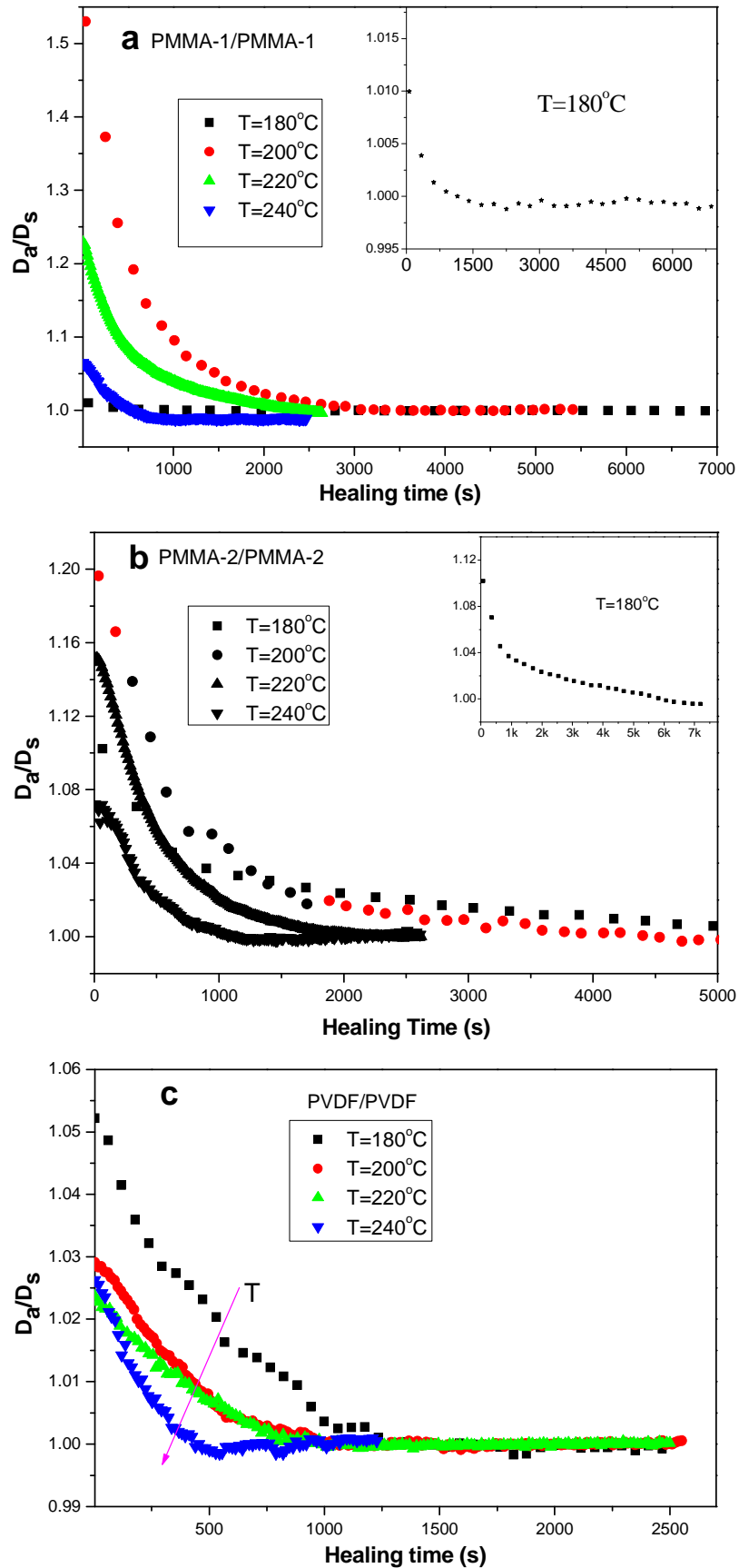
Figure II-13 D_a/D_s versus healing time at different temperatures for (a) PMMA -1/PMMA-1; (b) PMMA-2/PMMA-2; and (c) PVDF/PVDF polymer bilayers

Table II-3 lists the D_s of PMMAs and PVDF determined from the G^* of the corresponding assemblies at the equilibrium stage at different temperatures. In fact, the self diffusion coefficient of the neat polymers can also be calculated from the zero shear viscosity by a model developed by(Graessley 1980):

$$D_s = \frac{G_N^0}{135}\left(\frac{\rho RT}{G_N^0}\right)^2\left(\frac{R_{ee}^2}{M}\right)\frac{M_c}{M^2\eta_0(M_c)}$$
(II-23)

in which R_{ee}^2 represents the unperturbed mean-square end-to-end distance, M_c is the

critical molecular weight for a viscosity satisfying $M_c = 2M_e$, and $\eta_0(M_c)$ is the

zero-shear viscosity for the molecular weight M_c. Since the numerical value was not available, the estimated relationship

$$\frac{\eta_0(M_c)}{\eta_0(M)} = \left(\frac{M_c}{M}\right)^{3.4}$$
(II-24)

was used for the calculations, as also carried out by Kim and Han(1991). The calculated results (listed in Table II-3) were consistent with the data obtained in our work, with the exception of minor discrepancies.

Table II-3 Self-diffusion coefficients from Graessley's model and our present work for PMMAs and PVDF

Polymers	Self-diffusion coefficient, D_s (cm^2/s)			
	180 ℃	200 ℃	220 ℃	240 ℃
PVDF-Graessley	3.31×10^{-12}	6.45×10^{-12}	1.16×10^{-11}	1.98×10^{-11}
PVDF-Present	1.52×10^{-11}	2.46×10^{-11}	3.88×10^{-11}	5.96×10^{-11}
PMMA-1 –Graessley	3.12×10^{-14}	2.36×10^{-13}	1.15×10^{-12}	4.59×10^{-12}
PMMA-1 –Present	3.68×10^{-14}	3.48×10^{-13}	2.71×10^{-12}	7.89×10^{-12}
PMMA-2 –Graessley	1.23×10^{-14}	9.06×10^{-14}	3.38×10^{-13}	1.43×10^{-12}
PMMA-2 –Present	4.57×10^{-14}	3.46×10^{-13}	1.58×10^{-12}	6.35×10^{-12}

In addition, Figure II-14 presents a semi-log plot of the experimentally obtained self-diffusion coefficients versus the reciprocal temperature. Undoubtedly, we can draw the conclusion that the self diffusion coefficients of these three polymers obey the Arrhenius law:

$$D(T) = D_0 \exp(-Q/RT)$$
(II-25)

where Q is the activation energy and D_0 is a pressure-dependent constant.

Such a temperature dependence of the diffusion coefficient has been generally acknowledged in the literature (Yang et al. 2010). The activation energies of diffusion

(*Q*) for these polymers in the measured temperature range as obtained from the slope of the linear curves were 55.03 KJ/mol for PVDF, 185.90 KJ/mol for PMMA -1 and 154.63 KJ/mol for PMMA -2. The lower *Q* of PVDF as opposed to PMMA can be readily understood due to the difference in (T-T_g) between the two materials. But the fact that Q_{PMMA-1} was larger than Q_{PMMA-2} was unexpected, since PMMA-1 has a shorter chain length than PMMA-2.

Figure II-15 reviews the rheological properties of PMMA-1 and PMMA-2 at different temperatures as determined in the present work. A difference in the dependence on temperature for PMMA-1 and PMMA-2 can be observed, and even Eta* of PMMA-1 was higher than for PMMA-2 at 180 ºC. This further confirms the confusing findings on the rheological properties of PMMA in the literature. For PMMA, diffusion coefficients may also depend on the material's tacticity and water context (plasticizer), as noted earlier (Jud, et al. 1981). For comparisons with the literature, we converted the results obtained above to the conditions in the literature by relationships of the Arrhenius law Eq. (II-25) and $D{\sim}M^{-1}$ as shown below.

To the best of our knowledge, there is limited data in the literature available for the self diffusion coefficient of PVDF. The one reported by Kim and Han (1991) was also theoretically estimated from the Graessley model (Eq. (II-23)), which provided a result similar to ours. For PMMA, results have been widely determined in the past decades (Green, et al. 1988;Jud, et al. 1981;Kunz and Stamm 1996;Liu, et al. 1993;Shearmur, et al. 1998;Vanalsten and Lustig 1992). For example, Jud et al. (1981) reported on a self diffusion coefficient of PMMA (T_g= 101 ºC) of 1.2×10^5 g/mol at 116 ºC to be 10^{-17}cm²/s. In our work, a similar value of 7.16×10^{-17} cm²/s was obtained by scaling from PMMA-2 (T_g =102 ºC, M_w =1.37×10^5 g/mol) to the same condition. In addition, Liu et al (1993) reported a value of 2.36×10^{-16} cm²/s for PMMA (T_g=116.4 ºC, M_w=8.55×10^4 g/mol) at 145 ºC according to X-ray measurements. As a comparison, we reduced that of PMMA-1 (T_g = 114 ºC, M_w = 9.5×10^4 g/mol) to similar conditions, obtaining an equivalent value of 7.25×10^{-16} cm²/s. For the sake of simplicity, the many comparisons of our results with those in the literature are not detailed here, but significant agreements were observed.
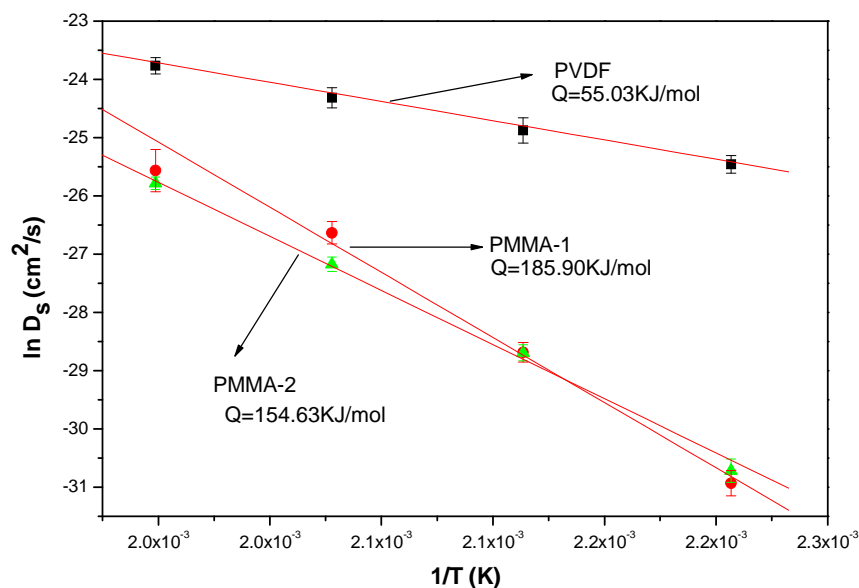
Figure II-14 Temperature dependence of the self diffusion coefficient for PVDF (■), PMMA -1 (●) and PMMA -2 (▲). The solid lines correspond to the fitting of the curves to the Arrhenius law
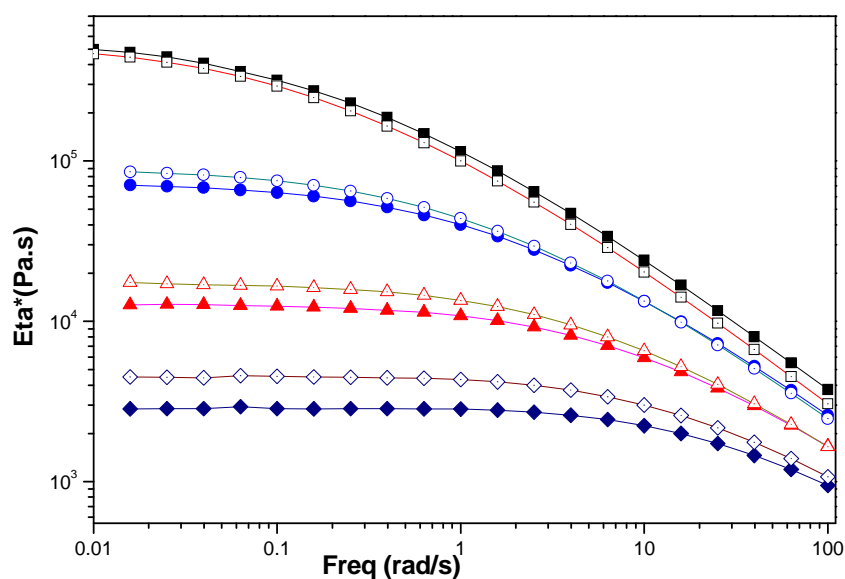
Figure II-15 *Eta** versus angular frequency for PMMA-1 (filled symbols) and PMMA-2 (open symbols) at different temperatures: (■,□) 180 °C; (●,○) 200 °C; (▲,△) 220 °C; (◆,◇) 240 °C

II.4.5 Dependence of the interdiffusion process on molecular weight

This section discusses the average molecular weight influence on the diffusion process. Considering the special nature of the temperature dependence of PMMA, we here only consider the high temperatures (220 °C and 240 °C). At long times of healing, the chain motion is independent of the chain conformation at the surface but identical to the center-of-center motion in the bulk. Extensive studies by various

techniques have in the past confirmed their common agreements with the results of reptation dynamics, i.e., the center-of-mass diffusion coefficient behaved according to $D \sim M^{-2}$. Qiu and Bousmina (1999) theoretically confirmed this dependence in their paper but experimental verifications have not been given.

In our present work on PMMA-1 (M_w = 95,000 g/mol), PMMA-2 (M_w = 137,000 g/mol) and their blends of different ratios, we attempted to experimentally determine the applicability of this molecular weight dependence law in our system. Figure II-16. presents log-log plots of the self diffusion coefficients calculated from the average value of the equilibrium G^* by Eq. (II-10) versus molecular weight. Unexpectedly, the slope was around -1.0, thus showing a discrepancy with regard to the dependent exponent -2 predicted by the reptation model. Rather, it agreed more with the Rouse theory that $D \sim M^{-1}$. Indeed, we have to point out that in our work the investigated range of molecular weight was limited (albeit above the critical entanglement molecular weight) and the polydispersity would be greater for the M_w enabled by blends.
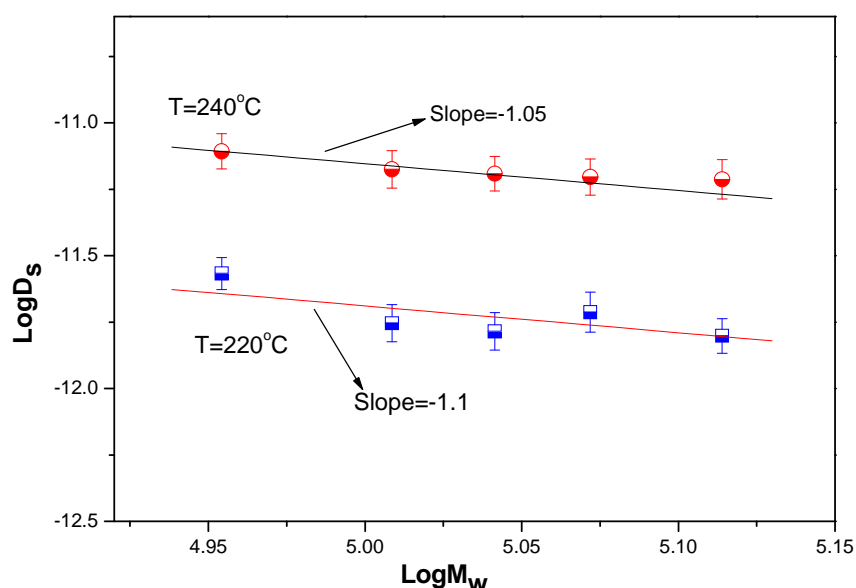
Figure II- 16 Self diffusion coefficient versus molecular weight for PMMA at T=220 ºC(■) and T=240 ºC(●)

Despite this point, the trends of our experimental observations were in agreement with some other older findings. For instance, Kumagai et al. (1979) measured the diffusion between tagged and untagged polystyrene and found the dependence of the diffusion coefficient upon $M^{-1.0}$, a result consistent with our study. Gilmore et al. (1980) reported on a similar observation, i.e., that the diffusion coefficient was proportional to $M^{-1.0}$, in their case for the interdiffusion of poly(vinyl chloride) and polycaprolactone with an assumption that the interdiffusion coefficients of the two components were the same and that the interfacial profile was symmetrical. Coincidentally a latest experimental finding reported by Kawaguchi et al. (2011) also supports mobility being proportional to N^{-1}, a pattern consistent with

segmental relaxation model (i.e. Rouse model). In addition, considering the broadening of the polydispersity effect that may have been brought on by the blending, the discussion of molecular weight dependence on the anomalous diffusion regions is not specified here.

II.4.6 Properties of the diffuse interphase

II.4.6.1 Interfacial (Interphase) thickness

In compatible polymer pairs, particularly for *A/A* symmetrical couples, an interphase is spontaneously generated at the interface during the interdiffusion process. The thickness of this interphase increases with the elapsed time. Extensive experimental studies (Reiter and Steiner 1991; Crist et al. 1989; Kunz and Stamm 1996) have tracked such increases of the diffusion distance using deuterated or labeled polymers under spectroscopic techniques to determine the time-dependent regimes of segment displacements theoretically predicted by the Doi-Edwards theory, i.e., $\Phi_n(t) \sim t^{1/4}$, $t^{1/8}$, $t^{1/4}$ and $t^{1/2}$ at different dynamic regions, respectively. Generally, for symmetric systems, the interfacial thickness can be estimated by the well-known relation (Crank 1975)

$$h_I(t) = 2(2Dt)^{1/2} \tag{II-26}$$

In the present work, after having employed the above equation and the apparent diffusion coefficient obtained previously, we could theoretically estimate the evolution of the thickness of the interphase with time. The estimated results for the PMMA-1/PMMA-1 and PVDF/PVDF assemblies are shown in Figure II-17, and we can again see the distinct difference in diffusion rate between PMMA and PVDF. Obviously, the PVDF diffusion distance was significantly larger than that of PMMA at the same healing conditions, with the interfacial thickness reaching 10 μm after annealing for 45 min at 240 ºC whereas for PMMA only 4 μm were reached under identical conditions. This distinguishing difference on the self-diffusion rate gives rise to an asymmetry of the concentration profile, reported in the literature for mutual diffusion between PMMA/PVDF couples (Kim and Han 1991;Wu, et al. 1986). This gives us some references for our coming studies on mutual diffusion on PMMA/PVDF asymmetric bilayers.
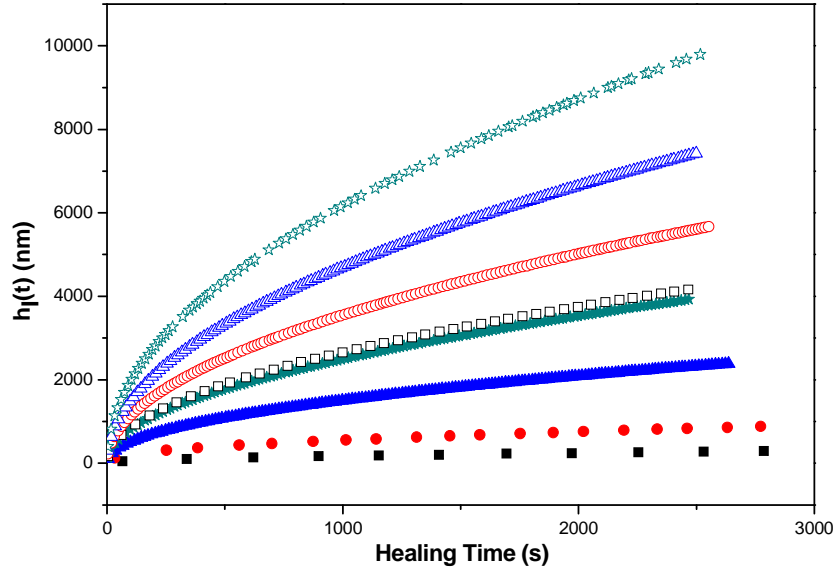
Figure II-17 Interfacial thickness vs. healing time for PMMA-1 (filled symbols) and PVDF (open symbols) at different temperatures: (■,□) 180 ℃; (●,○) 200 ℃; (▲,△) 220 ℃; (★,☆) 240 ℃

II. 4.6.2 Rheological properties of the interphase

If we take the interfacial zone where chains interplay from each side as a separate phase with distinct properties, we can use Eq. (II-8) in Reference (Lamnawar and Maazouz 2008) proposed for multilayers, to readily relate the rheological property of the interphase with the apparent rheological property of an *A/B* bilayer by the following expression:

$$\frac{1}{G_{bi}^*(t)} = \frac{\left[h_A - 1/2\, h_I(t)\right]/H}{G_A^*} + \frac{\left[h_B - 1/2\, h_I(t)\right]/H}{G_B^*} + \frac{h_I(t)/H}{G_I^*(t)} \qquad \text{(II-27)}$$

in which $G_{bi}^*(t)$ represents the complex modulus of the bilayer, G_A^* and G_B^* represent the complex moduli of neat polymer *A* and *B*, respectively, h_A, h_B, H correspond to the thickness of layer *A* , *B* and the total thickness of the bilayer, and $G_I^*(t)$ is the complex modulus of the interphase. Notice that here we assume that the interphase is broadening symmetrically, which is reasonable for the symmetrical bilayered structure of same polymers (*A=B*) used in the present work.

By taking *B=A* for a symmetrical bilayer and replacing h_A (=h_B) and H with 0.6 mm and 1.2 mm, Eq. (II-27) becomes

$$\frac{1}{G_{bi}^*(t)} = \frac{\left(0.6mm - \frac{1}{2} h_I(t)\right)/1.2mm}{G_A^*} + \frac{\left(0.6mm - \frac{1}{2} h_I(t)\right)/1.2mm}{G_A^*} + \frac{h_I(t)/1.2mm}{G_I^*(t)} \qquad \text{(II-28)}$$

After rearrangements, one can derive an empirical equation for the evolution of rheological properties of interphase $G*_I(t)$ versus time for an *A/A* symmetrical bilayer as follow:

$$G_I^*(t) = \frac{h_I(t)}{\dfrac{1.2mm}{G_{bi}^*(t)} - \dfrac{1.2mm}{G_A^*} + \dfrac{h_I(t)}{G_A^*}} \tag{II-29}$$

Thus, with the interfacial thickness obtained above, one can easily follow the evolution of rheological properties of the interphase generated at the interface with healing time. Figure II-18 gives the corresponding example curves of $G*_I(t)$ as a function of time for PMMA-1/PMMA-1 and PVDF/PVDF bilayers at *T* = 220 °C. Interestingly, we can see that with a thinner interfacial thickness, the interphase generated at the PMMA-1/PMMA-1 bilayer had lower rheological properties than its PVDF/PVDF counterpart. It seems that the property of the interphase triggered at the polymer/polymer interface is an important issue valuable for one to take into account.
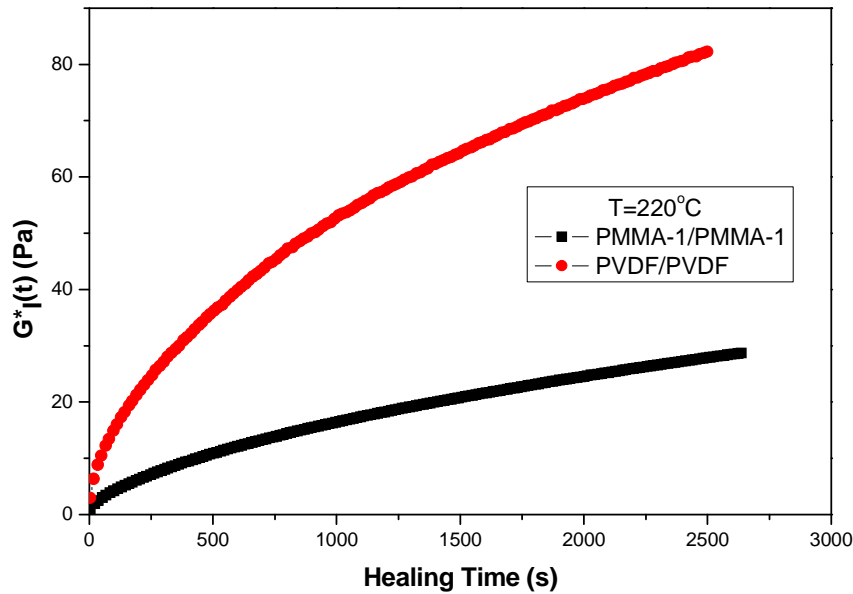
Figure II-18 Evolution of the rheological properties of the interphase $G*_I(t)$ versus healing time at 220 °C for PMMA-1/PMMA-1 and PVDF/PVDF bilayers, respectively

II. 5 Conclusions

We have employed a rheological tool in the linear viscoelastic regime to investigate the interdiffusion process in the molten state which occurs at the symmetric polymer/polymer interface of PMMA/PMMA and PVDF/PVDF bilayers. Rheometry proved to be a reliable and feasible method for monitoring the diffusion process at a polymer/polymer interface. The quantitative model for the self diffusion coefficient determined from the complex modulus *G** was experimentally confirmed. During

the interdiffusion process at the interface, the non-Fickian and Fickian regions were clearly divided but the transition occurred at a critical time t_c greater than the reptation time.

The influences of the angular frequency and temperature on the kinetics of inter-diffusion were analyzed based on the reptation theory. The ratios of the apparent diffusion coefficient to the self-diffusion coefficient (D_a/D_s) were used to follow the interdiffusion process in the non-Fickian region. We arrived at the conclusion that rheological results at different frequencies mirror the diffusions of the different motion units, with a higher D_a/D_s at higher frequencies, i.e., $\omega > 1/\tau_{rep}$, but a similar behavior at $\omega < 1/\tau_{rep}$. The self diffusion dependence on the angular frequency in a normal Fickian region was found to agree well with the Doi-Edwards theory. In particular, the D_s remained constant at $\omega < 1/\tau_{rep}$, and $D_s \sim \omega^{1/2}$ at $\omega > 1/\tau_e$.

The closer the temperature was to the T_g, the greater was the change of D_a/D_s and the longer was t_c. This can be interpreted as a greater contribution of the small motion units at lower temperature. The temperature dependence of the self diffusion coefficient demonstrated a good fit to the Arrhenius law, with activation energies of Q_{PVDF}=55.03 KJ/mol, Q_{PMMA-1}=185.90 KJ/mol, Q_{PMMA-2} = 154.63 KJ/mol. Moreover, the results of the self-diffusion coefficient were in accord with what can be found in the literatures.

When it came to the blends of PMMAs prepared with different chain lengths, the dependence of the self diffusion coefficient on $\overline{M}$ behaved more according to the Rouse theory as opposed to agreeing with the theoretical prediction given by Qiu and Bousmina. It was scaled as $D_s \sim \overline{M}^{-1}$, in agreement with some earlier achievements given in the literature and some reported recently by TR-NR.

Ultimately, the interfacial thickness of the symmetric bilayer was theoretically determined and reached 10 μm for PVDF/PVDF and 4 μm for PMMA/PMMA after annealing for 45 min at 240 ºC. Moreover, on the basis of such theoretical results of the interfacial thickness, the corresponding rheological properties of the interphase can be obtained as a function of healing time developed from a model proposed previously by our group.

Chapter III: Rheological Modeling of the Mutual Diffusion and the Interphase Development for an Asymmetrical Bilayer Based on PMMA and PVDF Model Compatible Polymers

III.1. Abstract

The mutual diffusion process and interphase development taking place at an asymmetrical polymer-polymer interface between two compatible model polymers, poly (methyl methacrylate) (PMMA) with varying molecular weights and poly(vinylidene fluoride) (PVDF) in the molten state were investigated by small amplitude oscillatory shear measurements. Rheology method, Lodge-McLeish model and test of the time-temperature superpositon (tTS) principle were employed to probe the thermorheological complexity of this polymer couple. The monomeric friction coefficient of each species in the blend have been examined to vary with composition and temperature and to be close in the present experimental conditions and the failure of tTS principle was demonstrated to be subtle. These were attributed to the presence of strong enthalpic interaction between PMMA and PVDF chains that couples the component dynamics. Hence, a quantitative rheological model modified from a primitive Qiu–Bousmina's model that connectted the mobility in mixed state to the properties of matrix was proposed to determine the mutual diffusion coefficient (D_m). The modified model takes into account the rheological behavior of the interphase for the first time. In turn, viscoelastic properties and thicknesss of the interphase have been able to be quantified on the basis of the modified model. Effects of the annealing factors like welding time, angular frequency, temperature and the structural properties as well molecular weight and Flory-Huggins parameter (χ) on the kinetics of diffusion and the interphase thickness and its viscoelastic properties were investigated. On one hand, D_m was observed to decrease with frequency till leveling off at the terimnal zone; to depend on temperature obeying the Arrhenius law and to be nearly independent of PMMA molar mass, corroborating the prediction of the fast-mode theory. On the other hand, the generated interphase which reached dozens of microns was revealed to own a rheological property approaching its equivalent blend. Scanning electron microscopy coupled with energy dispersive X-ray analysis (SEM-EDX) and transmission electron microscopy (TEM)

were also carried out and confronted to the rheological results. Comparisons between mathematical modeling of concentration profile based on the D_m obtained from rheology and the experimental ones of SEM-EDX and TEM were conducted. Thus, a better correlation between theory and experimental results in term of mutual diffusion and the interphase properties was nicely attained. The obtained data are in good agreement with literatures using other spectroscopical methods.

III.2. Introduction

Aside from its academic and practical significances in phase separation and morphology in polymer blends (Kwei 1978), adhesion (Wu 1982), welding and crack healing (Wool 1995), etc, mutual diffusion between polymers is also very important in polymer processing like co-extrusion (Mueller, et al. 1997), co-injection molding(Jiang, et al. 2009), etc. With respect to such processing techniques, mutual diffusion that occurs in the vicinities between polymers is of critical significance in mixing, homogenizing and control of the disappearance rate of a composition gradient(Mueller, et al. 1997). This is especially true in the case of reactive processing(Macosko, et al. 2005), and it may even affect the rate of interfacial reactions at reactive polymer couples and the formation rates of an interphase generated at the interface by dominating the transport of reactants from the bulk to the reacting sites. Moreover, it is worth mentioning that mutual diffusion process also appeared to have an effect on governing the kinetics of encapsulation phenomenon in the multiphase systems (Lamnawar, et al. 2012). Besides, recently the interdifusion of two materials was reported to affect the optical properties of multilayerd films, specially, the refrective index (Lai, et al. 2012). Hence, for the purpose of understanding these phenomena during polymer processing, it is essential to firstly probe and quantify the kinetics of the mutual diffusion process between polymers and how they control the interfacial phenomena, especially in chemically dissimilar mixtures or multiphase systems.

Hitherto, extensive studies have been performed regarding the mutual diffusion between polymers by various sophisticated techniques like secondary ion mass spectrometry (SIMS) (Yokoyama and Kramer 2000), neutron reflectivity (NR) (Karim, et al. 1990;Kawaguchi, et al. 2006;Kawaguchi, et al. 2011;Kunz and Stamm 1996;Schnell, et al. 1998), forward recoil spectroscopy (FRES) (Composto, et al. 1988), X-ray microanalysis in scanning electron microscopy (SEM-EDX) (Jones, et al. 1986), nuclear reaction analysis(Klein 1990), transmission FTIR spectroscopy(High, et al. 1992), etc. By virtue of some of these methods (Composto, et al. 1988;Yokoyama and Kramer 2000), concentration profiles can be directly obtained. Through fitting of a theoretical profile computed from Fick's equation (III-1) to an experimentally achieved counterpart, one can receive a mutual diffusion coefficient D_m of the two species at a given time t and position z.

$$\frac{\partial \phi(z)}{\partial t} = \frac{\partial}{\partial z}\left[D(\phi)\frac{\partial \phi(z)}{\partial z} \right] \qquad \text{(III-1)}$$

However, many of these spectroscopical techniques need labed or marked elements on the specimens which were confirmed to affect the diffusion process (Green and Doyle 1987). Additionally, these measurements are limited to a static fashion at a certain time, rather than conducting a time evolution. It is worth meantioning that very recently, Kawaguchi et al. (2011) have published an interesting paper allowing to follow the time evolution of concentration profiles based on interdiffusion of polystyrene/deuterated polystyrene bilayer by time-resolved neutron reflectivity(TR-NR) measurements. But this technique, though with a high spatial resolution, is very expensive, sophisticated and un-versatile. Moreover, the static conditions, mostly used by the above-mentioned tools for polymer-polymer interdiffusion, are still far from simulating the real shear flow field happened in polymer processings. Nowadays, thanks to the highly developed knowledge, diffusion processes can also be investigated and quantified by a rheological tool (Bousmina, et al. 1998;Qiu and Bousmina 1999; 2000; 2002;Qiu, et al. 2002). Qiu and Bousmina(2000) put forward a quantitative model for a mutual diffusion coefficient for a PMMA/SAN bilayer system from a molecular dynamics viewpoint based on the rheological functions of the polymer bilayer. It should also be mentioned that Zhao and Macosko (2007) proposed a different model for the mutual diffusion coefficient in their multilayer system of HDPE/LLDPE by fitting the complex viscosity variation theoretically calculated from Fick's law to experimetal data.

Different from self-diffusion of same polymers, the mutual diffusion coefficient has been widely recognized to being closely related to the miscibility of diffusing species ranging from accelerated interdiffusion (for strongly compatible mixtures) to its suppression below the critical point for phase separation (Klein 1990), as well as the nature, structure and molecular weight of the respective polymers. It has been pointed out that the mutual diffusion of chemically dissimilar polymers is dominated by the excess enthalpy and entropy of segment-segment mixing, and an expression for mutual diffusion coefficient D_m of species A and B can be given by (Composto, et al. 1988)

$$D_m = 2(\chi_s - \chi)\varphi_A\varphi_B D_T = \left(\frac{\varphi_B}{N_A} + \frac{\varphi_A}{N_B} - 2\chi\varphi_A\varphi_B \right) D_T \qquad \text{(III-2)}$$

in which χ_s is the interaction parameter at the spinodal of A/B mixture

$$\chi_s = \frac{1}{2}\left[\frac{1}{\varphi_A N_A} + \frac{1}{\varphi_B N_B} \right] \qquad \text{(III-3)}$$

χ is the Flory-Huggins interaction parameter, φ_i, N_i represent the volume fraction and the weight-average degree of polymerization of component *i*, respectively. Note that $\varphi_A + \varphi_B = 1$. D_T is a transport coefficient which is related to the mobility of the segments $B_{0,i}$ or the molar monomeric friction coefficient ζ_i of the involved components. Regarding D_T, two divergent theories have emerged, known as the fast-mode model with a faster moving species dominating the mechanism, proposed by Kramer et al. (1984) and the slow-mode model with a slower moving species dominating the mechanism, proposed by Brochard et al. (1983). The main distinction between these two modes lies in whether the vacancy flux is taken into consideration or not. Details of the theory of polymer-polymer mutual diffusion are given in next section. Both the experimental results that are favorable for the fast-mode model and those favorable for the slow-mode model have been reported in the literature. The weight of experimental evidence today supports the original observation by Kramer: that mutual diffusion between two entangled polymers with different diffusivities is indeed largely controlled by the diffusivity of the more mobile chains. In a molecular picture, the faster diffusing polymers reptate into the region of the more sluggish chains, they do so within an entangling environment, i.e., "tubes", due to constraints imposed by the slower molecules, who themselves move in the opposite direction by a convective mechanism, providing the net bulk flow(Klein 1990).

It is necessary to note that in a mixed state, the mobility of polymer chains could be affected by blending, which make them different from the situation in bulk system. The origin of the difference was partly attributed to distinct sgemental and global dynamics of each component in the blend resulted from the presence of thermal concentration fluctuation and dynamical heterogeneity(Kumar, et al. 1996;Lodge and McLeish 2000). Investigation on the component dynamics in blend concerning a composition and temperature dependent monomeric friction coefficient $\zeta_i(\varphi,T)$ has come into a big focus in the past two decades. Generally, the $\zeta_i(\varphi,T)$ was determined via various techniques ranging from direct measurements of tracer diffusion coefficient (Composto, et al. 1990;Kim, et al. 1995a), NMR relaxation measurements(Chung, et al. 1994;He, et al. 2003) to rheo-dielectric studies (Chen, et al. 2008;Roland, et al. 2006;Watanabe, et al. 2011;Watanabe, et al. 2007), rheo-optical measurements (Arendt, et al. 1997) and rheological methods (Pathak, et al. 2004;Yang, et al. 2001;Zeroni, et al. 2008), etc. Most of the attentions were shed on the miscible polymer mixtures of substantial dynamic asymmetry (large difference in glass transition between pure components) but restricted to those of weak or no specific interaction with those of strongly interactions like PMMA/PVDF used in this work out of intensive focus. Very recently, Yang and Han (2008) conducted a comprehensive investigation on the viscoelasticity of miscible polymer blends with hydrogen bonding and concluded that the presence of concentration fluctuations and

dynamic heterogeneity in the miscible blends forming hydrogen bonds (strong intermolecular attractive interactions) between the constituent components might be very small, if not negligible. Meanwhile, Lodge and coworkers (Gaikwad, et al. 2010), after examined the viscoelasticity of miscible polymer blends with tuned amounts of hydrogen bonds, also confirmed that the dynamic response of two polymers can be effectively coupled in the presence of strong specific interactions (sufficient hydrogen-bonding interactions), whereby the temperature dependences of the two-component relaxation times become equivalent. More theoretical details on this part are to be given in next section. Therefore, to the end of probing the interdiffusion kinetics occurred at polymer/polymer interface and exploring the interfacial rheology of the interphase, it is very important first to examine the component dynamics of this polymer couple in mixed state at the studied conditions before implementing relevant rheological modelings.

On rheological modeling of mutual diffusion at polymer/polymer interface, for instance, Qiu and Bousmina (2000) suggested a model relating the mobility of the polymers to the evolution of the rheological properties of a polymer bilayer structure versus annealing time. Nevertheless, in their study, on one hand, examination of the motional dynamics of each component in mixed state for their polymer couple was neglected; on the other hand, they straightly direct the complex modulus (G^*) of the total polymer bilayer to determine the D_m of the polymer pair, which, as pointed out by Zhao and Macosko (2007), may overestimate the contribution of the interphase. As a matter of fact, the total rheological properties of a bilayer structure were contributed mostly from the part of polymer bulks rather than the interphase as the region of interphase where mutual diffusion occurs was very limited. From this view, their model cannot be considered to be very perfect. This motivated us to first examine the variation of $\zeta_i(\varphi,T)$ for each component in mixed state before taking an attempt to give some modifications to their primitive model by taking the real rheological properties of the interphase into account in the present study.

In addition, the interphase triggered between neighboring layers is also of great academic and industrial interest (Ajji and Utracki 1996;Liao, et al. 2007;Liu, et al. 2004; 2005;Liu, et al. 2003;Zhang, et al. 2006a), especially for the systems of reactive compatibilization of blends or multilayer structures. The performance of the interphase is closely related to the interfacial structure; exactly speaking, local entanglements that are gradually established via interchain penetration during the interdiffusion process. However, the detailed topological image of such an interfacial structure has yet to be fully understood as a result of it being experimentally unobtainable. To reveal the properties of the interphase of immiscible polymers, Liu et al (2003, 2004; 2005) made up an interphase material with a multilayer structure through decreasing the layer thickness to a comparable size of the interphase realized in a forced assembly way by layer multiplying coextrusion. And the interphase strength was examined in a term of delamination strength measured by T-peel test.

In miscible polymer pairs, in order to investigate the properties of the interphase formed via interdiffusion, a common practice in literatures (Ajji and Utracki 1996;Liao, et al. 2007;Liu, et al. 2004; 2005;Liu, et al. 2003;Zhang, et al. 2006a) is to evaluate the interface fracture toughness by asymmetric double beam cantilever (ADBC) testing, which causes propagating cracks within the interphase zone. However, since cracks are not always perfectly produced, especially in highly adhered interphases, no accurate experimental data can be achieved.

Finally, as briefly summarized above, significant progress in understanding and quantifying the mutual diffusion in bilayer structure has been obtained over the past decades. To the best of our knowledge, few papers have been dedicated to the coupling between rheology, spectro and microscopical tools to quantify and modelize the mutual diffusion depending of temperature, welding time, angular frequency and structural properties as well the average molecular weight and the Flory-Huggins parameters. Despite the interesting nature of this kind of research especially in the work of Bousmina et al. (2000), it is of no help when attempting to comprehend either the generation of the interphase triggered between the neighboring layers and also quantify its proper rheology taking into account the mutual diffusion in this phase. In our previous work, we have studied the competition between interdiffusion and reaction using incompatible and compatibilized higher molecular weight and asymmetrical bilayers (Lamnawar, et al. 2010a;Lamnawar and Maazouz 2006; 2008). However, the systems were very complex with higher polydispersity which limited the real quantification and modeling of the rheological behavior of the triggered interphase. The present study focused on original rheology experiments in small amplitude oscillatory shear measurement (SAOS) of multilayer with well-characterized model asymmetrical and compatible bilayer polymers of different molar masses. The aims of this work thus involved on (i) giving a full analysis on the component dynamics of PMMA/PVDF blend via rheology method, Lodge-McLeish model and test the validity of tTS principle before rheological modeling; (ii) modifying the Qiu and Bousmina's model to take into account of the viscoelastic properties of the interphase on the mutual diffusion and (iii) highlighting the effect of welding time, temperature, angular frequency and structural properties as well molecular weight and the Flory-Huggins parameters on the kinetic of diffusion and the interphase thickness and its viscoelastic properties. Furthermore, scanning electron microscopy coupled with energy dispersive X-ray analysis (SEM-EDX) and transmission electron microscopy (TEM) were employed to achieve a concentration profile as a function of position, as well as the microscopic morphology of the interphase formed after the diffusion process for the purpose of confirming the validity of the rheological tool on the interdiffusion investigations. A good agreement between rheological modeling and EDX analysis has been achieved in terms of the interphase thickness and the concentration profile. This study renders it possible from a rheological aspect to probe the kinetics of the mutual diffusion and to disclose the rheological behavior of the interphase.

III.3. Theory

Both fast-mode theory (Kramer, et al. 1984) and slow-mode theory (Brochard, et al. 1983) agreed that the chemical potential gradient is the driving force for interdiffusion and both were derived from Flory-Huggins Lattice theory using Onsager formalism. Relations of flux J_i to chemical potential μ_i are:

$$J_A = -\Lambda_A \nabla(\mu_A - \mu_V) \tag{III-4}$$

$$J_B = -\Lambda_B \nabla(\mu_B - \mu_V) \tag{III-5}$$

$$J_V = \Lambda_A \nabla(\mu_A - \mu_V) + \Lambda_B \nabla(\mu_B - \mu_V) \tag{III-6}$$

where Λ_i is Onsager coefficient of lattice i, subscript A, B, V denote molecule A, molecule B and vacancy, respectively.

The chemical potential gradient was yielded from Flory-Huggins theory:

$$\nabla \mu_i = \frac{k_B T}{\varphi_i} \left[\frac{\varphi_B}{N_A} + \frac{\varphi_A}{N_B} - 2\varphi_A \varphi_B \chi \right] \nabla \varphi_i \tag{III-7}$$

where $k_B T$ is the temperature in a term of Boltzman constant.

The difference between fast-mode and slow-mode theory lies in the treatment of the flux of vacancy J_V. The slow-mode theory assumed no vacancy flux, i.e. $J_V = 0$, which leads to

$$J_A = -J_B = \frac{-\Lambda_A \Lambda_B}{\Lambda_A + \Lambda_B} \nabla(\mu_A - \mu_B) \tag{III-8}$$

Combination of eqs.III-7, 8 and the eq. III-9 of continuity for component A:

$$\frac{1}{\Omega} \frac{\partial \varphi}{\partial t} = \nabla(-J_A) \tag{III-9}$$

gives:

$$\frac{\partial \varphi}{\partial t} = \nabla(D_m \nabla \varphi) = \nabla(-\Omega J_A) = \nabla \left[\frac{\Omega k_B T}{\varphi_A \varphi_B} \frac{\Lambda_A \Lambda_B}{\Lambda_A + \Lambda_B} \left(\frac{\varphi_B}{N_A} + \frac{\varphi_A}{N_B} - 2\varphi_A \varphi_B \chi \right) \nabla \varphi \right] \tag{III-10}$$

and thus D_m can be yielded:

$$D_m = \frac{\Omega k_B T}{\varphi_A \varphi_B} \frac{\Lambda_A \Lambda_B}{\Lambda_A + \Lambda_B} \left[\frac{\varphi_B}{N_A} + \frac{\varphi_A}{N_B} - 2\varphi_A \varphi_B \chi \right] \tag{III-11}$$

where Ω is the volume of a quasi-lattice site.

Nevertheless the fast-mode theory assumed $J_v \neq 0$ but rather $\nabla \mu_v = 0$, which leads to the total flux J_A^T of A:

$$J_A^T = -\Lambda_A \varphi_B \nabla \mu_A + \varphi_A \Lambda_B \nabla \mu_B \qquad \text{(III-12)}$$

Likewise, an expression of D_m can be given:

$$D_m = \Omega k_B T \left(\frac{\varphi_B}{\varphi_A} \Lambda_A + \frac{\varphi_A}{\varphi_B} \Lambda_B \right) \left[\frac{\varphi_B}{N_A} + \frac{\varphi_A}{N_B} - 2\varphi_A \varphi_B \chi \right] \qquad \text{(III-13)}$$

The slow-mode theory assumes that the fluxes of the two polymers are equal and opposite, which means that the interface remains symmetric as interdiffusion proceeds for symmetric boundary condition. However, the fast-mode theory describes the interdiffusion with a moving interface by unequal fluxes of polymers which are balanced by a net flux of vacancies across the interface. It concludes a movement of the interface towards the faster-diffusion component and a broadening of concentration profile in the slower-diffusion component side, which was experimentally confirmed in the concentration profile obtained by EDX (Figure III-20) in the present work. This demonstrates the accuracy of our determination of D_m on the basis of the fast-mode model in this study.

Comparing eq.（III-13）to eq.（III-2）and making some arrangements, one can obtain

$$D_T = \varphi_B N_A D_A^* + \varphi_A N_B D_B^* \qquad \text{(III-14)}$$

with the tracer diffusion coefficient of component i, D_i^* as:

$$D_i^* = \frac{\Omega k_B T}{N_i \varphi_i} \Lambda_i \qquad \text{(III-15)}$$

The Onsager coefficient Λ_i can be given in a term of the curvilinear Rouse mobility $B_{0,i}$ or in a term of the monomeric friction coefficient ζ_i of the segment i:

$$\Lambda_i = \frac{B_{0,i} N_i^e}{\Omega N_i} \varphi_i = \frac{N_i^e}{\zeta_i \Omega N_i} \varphi_i \qquad \text{(III-16)}$$

in which N_i^e is the number of repeat units per entanglement length of component i, respectively.

Herein, two monomeric fricition coefficients, ζ_A, ζ_B of the segment A and B are

included. On this point, one convergent question was arised: can one use a single mobility to describe the dynamics of compatible binary mixture?

Some authors (Jabbari and Peppas 1995;Qiu and Bousmina 2000) considered a single mobility for completely miscible blends and emphasized the only monomeric friction coefficient was strongly dependent on compositions, which could be used to describe the interdiffusion process. Though this is empirical, it could greatly provide an easy route to relate the mobility of the polymers in the mixed state to the properties of the matrix (Jabbari and Peppas 1995;Kawaguchi, et al. 2011;Qiu and Bousmina 2000).

Some others addressed an opinion of distinct component dynamics in miscible blend even the system is statically homogenous at a molecular level, which is likely due to a combination of factors, including intrinsic differences in mobility between the components, and local variations in composition. This thermalrheological complexity seems to be confirmed by more direct experimental observations using a wide range of techniques. One appealing physical picture for the distinct component dynamics lies in that each component in the miscible blend effectively experiences a richer local environment with its own local composition quite different from the average composition of the blend. On discussing the origin of these biased local compositions and the relevant length scale for such a local region, some interesting approaches have been proposed, like "thermal concentration fluctuation" of Ficher/Kumar models(Kumar, et al. 1996;Lodge and McLeish 2000) which incorporated a cooperative volume concept. This model is more applicable for the segmental dynamics considered at temperatures closer to T_g since the cooperative volume is small at temperatures far above the blend T_g. An alternative approach involves a concept of "self concentration" caused by chain connectivity with an idea that a local region around an A segment is always somewhat enriched in A segments(Chung, et al. 1994). Recently Lodge and McLeish proposed a simple implementation of the idea of "self concentration" by assuming the relevant length scale to be the Kuhn length of the chain(Lodge and McLeish 2000). Thereafter the Lodge-McLeish model has been tested in various miscible polymer mixtures to be adequate to predict the component segmental and terminal dynamics in miscible polymer blends.

Among the intensive investigations of component dynamics in miscible blends in the past decades, a general consensus can be drawn is that the concentration fluctuations and the dynamic heterogeneity are related to the broadness of glass transition and the failure of time-temperature superposition (tTS) in the miscible blends without specific interaction when the constituent components had a large difference of T_g, with an empirical threshold of $\Delta T_g \approx 25$°C(Yang and Han 2008). Today, despite the vast amount of studies focused on the local dynamical heterogeneity both at segmental and global level, the measurements are mostly restricted to the miscible blends with weak or without specific interactions ($\chi \approx 0$), while few attentions have

been paid to the ones with strong interactions.

Back to this work, to have an idea on the mobility difference of PMMA and PVDF in the mixtures, we expand a section on the component dynamics of PMMA/PVDF blend before continuing our work to explore the mutual diffusion kinetics and the interphase development versus healing time occurred at a bilayer system.

The component dynamics of the blends have been examined by rheology on the basis of the Tsenoglou version of "double reptation" model (Tsenoglou 1991) modified by Haley et al (2003)and have been compared to the predictions of the Lodge-McLeish models(Lodge and McLeish 2000). On one hand, the difference of the intrinsic frictions of PMMA and PVDF appears to be too small to give a large effect on the global dynamics of polymer chains; on the other hand, the strong specific interactions (probably resulted from hydrogen-bonding(Leonard, et al. 1985) and dipole-dipole intermolecular interactions(Paul and Barlow 1980), etc.) between PMMA and PVDF ($\chi \sim$ -0.07 as detailed later) may minimize the dynamical heterogeneity and couple the dynamic response of the two polymers. Under the conditions examined in the present work, the friction coefficients of PMMA and PVDF component in the blend, ζ_{PMMA} (φ,T), ζ_{PVDF}(φ,T), were observed to be close, at least, in the same order of magnitude.

In consequence, with an aim to explore the interfacial rheology at polymer-polymer interface and to relate the rheological behavior of the interphase evolving with healing time to the mutual diffusion coefficient of different polymers, it would be reasonable to assume an apparent friction coefficient for the mixture in this work as a first approximation. In this case, using an apparent friction coefficient ζ_b, eq16 can be reduced to (Arendt, et al. 1997)

$$\Lambda_i = \frac{N_b^e}{\zeta_b \Omega N_i} \varphi_i \tag{III-17}$$

Here, the ζ_b is strongly composition-dependent for a polymer pair; N_b^e is the average number of repeat units between entanglements for the blend, which is also a function of composition. In this way, after integration of eq.（III-17）into eq.（III-13）and some necessary arrangements, eq. （III-13）can be reduced to:

$$D_m = \frac{k_B T N_b^e}{\zeta_b} \left(\frac{\varphi_B}{N_A} + \frac{\varphi_A}{N_B} \right) \left[\frac{\varphi_B}{N_A} + \frac{\varphi_A}{N_B} - 2\varphi_A \varphi_B \chi \right] \tag{III-18}$$

So now the mutual diffusion coefficient D_m can be related to the structural properties of the matrix of A and B via eq.（III-18）. In particular, the first term in the right hand of eq.（III-18）is greatly related to the dynamics of blend (interphase), i.e., a part representing the strongly composition- dependent mobility of the blend, which is reasonable as the $\zeta_i(\varphi,T)$ for each component were demonstrated to be close

in the studied experimental conditions.

III.3.1 Determination of D_m from a rheological viewpoint

III.3.1.1 Review of a premitive Qiu-Bousmina's model

A quantitative model coupling viscoelastic functions with the mutual diffusion coefficient on the basis of polymer dynamics theory and fast-controlled mode theory has been proposed by Qiu and Bousmina (2000). They derived the relation from Bolzmann's integral form

$$\tau(t) = \int_{-\infty}^{t} G(t - t')\gamma(t')dt' \tag{III-19}$$

where the stress $\tau(t)$ measured at the time t is a function of the whole history of past deformation $\gamma(t')$ at anterior times t', and the shear relaxation modulus G(t-t') that contains the whole past history of the deformation can be related to the mass transport across the interface having occurred at previous times. Under small amplitude oscillatory deformation, the complex modulus G*(ω) can be given by

$$G^{*}(\omega) = i\omega \int_{0}^{\infty} e^{-i\omega t} G(t)dt \tag{III-20}$$

From the reptation theory, one has

$$G(t) = G_N^0 \sum_{n=0}^{\infty} \frac{8}{(2n+1)^2 \pi^2} \exp\left(\frac{-(2n+1)^2 \pi^2 k_B T e^2 t}{\zeta N^3 b^4}\right) \tag{III-21}$$

where G_N^0 denotes the plateau modulus, *e* represents the step length, on the order of the gyration radius of entanglement, and *b* is the effective bond length. By omitting the higher terms in eq.（III-21） and substituting it into eq. （III-20）, one can after arrangements obtain an expression for monomeric friction coefficient as:

$$\zeta = \frac{\pi^2 k_B e^2 T}{N^3 b^4} \frac{1}{K^{1/2}} \tag{III-22}$$

with

$$K = \omega^2 \left[\left(\frac{8G_N^0}{\pi^2 G^{*}(\omega)}\right)^2 - 1\right] \tag{III-23}$$

Thus, integrate eq. （III-22） into eq. （III-18） via the apparent mobility parameter ζ_b, one can reach a new expression for the mutual diffusion coefficient relating to the complex modulus as

$$D_m = \frac{N_b^e N_b^3 b_b^4 K^{1/2}}{\pi^2 e_b^2} \left(\frac{\varphi_B}{N_A} + \frac{\varphi_A}{N_B} \right) \left(\frac{\varphi_B}{N_A} + \frac{\varphi_A}{N_B} - 2\chi\varphi_A\varphi_B \right) \tag{III-24}$$

Here, this equation was used to present the mobility of the interphase (regarded as an equivalent macroscopic miscible blend with a fraction φ_A of component A), with the plateau modulus of the interphase (or equivalent blend) $G_{N,b}^0$ given in eq. （III-23） expressed as (Graessley and Edwards 1981)

$$G_{N,b}^0 = \left[\varphi_A \left(G_{N,A}^0 \right)^{1/2} + \varphi_B \left(G_{N,B}^0 \right)^{1/2} \right]^2 \tag{III-25}$$

and N_b^e, the average number of repeat units per entanglement of the interphase, expressed as

$$\frac{1}{\left(M_{0,b} N_b^e \right)^{1/2}} = \frac{\varphi_A}{\left(M_{0,A} N_A^e \right)^{1/2}} + \frac{\varphi_B}{\left(M_{0,B} N_B^e \right)^{1/2}} \tag{III-26}$$

where $M_{0,i}$, N_i^e denote the monomer molecular weight and repeat unit numbers per entanglement of component i. Moreover, the repeat unit numbers of blend N_b can be given by

$$N_b = \frac{1}{M_{0,b}} \left[\varphi_A M_A + \varphi_B M_B \right] \tag{III-27}$$

Evidently, all the above deductions are based on the molecular dynamics and rheological behavior of a blend with a given fraction φ of component A. For a bilayer system, an interphase at the interfacial area is created as diffusion occurs at the polymer/polymer interface, whereafter the bilayer converts to a sandwich-like trilayer structure. The interphase can be considered as a macroscopic blend with its own specific compositions and properties developing with time, which essentially governs the overall time evolution of the viscoelastic properties of the sandwich.

Based on this point, the above model can be adequate for determining the mutual diffusion coefficient at the interphase (equilivalent blend), and its evolution with time can also be established when the variations with time of the concentration and rheological properties of the equivalent blend are known. For this sake, Qiu and Bousmina (2000) suggested a normalization procedure to determine the concentration variation with time for the interphase. Nevertheless, for the sake of

simplicity, they used the time evolution of the viscoelastic properties ($G_s^*(t)$) of the overall sandwich instead of those ($G_I^*(t)$) of the real interphase for calculations in eq. （III-23）. In fact, to some extent, the viscoelastic properties of the interphase did not straightforwardly equal to the ones of the overall sandwich. This was particularly true for the bilayer system, where the bulk phases of the constituents accounting for a great proportion should not be ignored. For this reason, an attempt was made to modify the model, details of which are described below.

III.3.1.2 Modifications to Qiu-Bousmina's model

As mentioned above, it would be more plausible to use the viscoelastic properties of the interphase instead of the ones of the overall sandwich for calculating the mutual diffusion coefficient. The viscoelastic properties of the interphase can be obtained as follows(Bousmina, et al. 1999;Lamnawar and Maazouz 2008;Vaudreuil, et al. 2000):

$$\frac{1}{G_{s,t}^*} = \frac{\varphi_{A,t}}{G_{A,t}^*} + \frac{\varphi_{B,t}}{G_{B,t}^*} + \frac{\varphi_{I,t}}{G_{I,t}^*} = \frac{h_A^{'}/H}{G_{A,t}^*} + \frac{h_B^{'}/H}{G_{B,t}^*} + \frac{h_I^{'}/H}{G_{I,t}^*} \tag{III-28}$$

with the initial state

$$\frac{1}{G_{s,0}^*} = \frac{\varphi_{A,0}}{G_{A,0}^*} + \frac{\varphi_{B,0}}{G_{B,0}^*} = \frac{h_A/H}{G_{A,0}^*} + \frac{h_B/H}{G_{B,0}^*} \tag{III-29}$$

where $G_{i,t}^*, \varphi_{i,t}, G_{i,0}^*, \varphi_{i,0}$ represent the complex modulus and volume fractions of layer i at a diffusion time $t>0$ and initial state $t=0$; $h_i^{'}$ represents the thickness of layer i, developing with the elapsed time, as shown in Figure III-1, and H is the total thickness of the sandwich (1.2 mm for the PMMA/PVDF assembly in question).
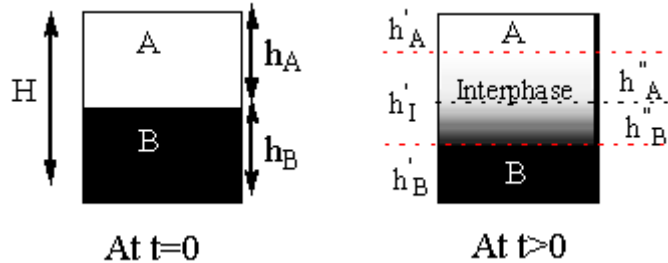
Figure III- 1. A schematic of the mutual diffusion taking place at the interface of an A/B bilayer.

Considering that the volume fractions of component i within the interphase can be expressed by $\varphi_{i,t}^{'} = h_i^{''}/h_I^{'}$ and $\varphi_{i,0} = \varphi_{i,t} + \varphi_{i,t}^{'}\varphi_{I,t}$, eq. （III-28） leads to

$$\frac{1}{G_{s,t}^*} - \frac{1}{G_{s,0}^*} = \left[\frac{1}{G_{I,t}^*} - \left(\frac{\varphi_{A,t}'}{G_{A,0}^*} + \frac{\varphi_{B,t}'}{G_{B,0}^*} \right) \right] \frac{h_{I,t}'}{H} \tag{III-30}$$

By replacing the fraction of component A, B in the interphase $\varphi_{A,t}', \varphi_{B,t}'$ with φ_A and φ_B used in the above section, and relating the interphase thickness to the mutual diffusion coefficient by eq.（III-31） (Kunz and Stamm 1996;Yukioka, et al. 1992)

$$h_I' = 2(D_m t)^{1/2} \tag{III-31}$$

one can obtain

$$\frac{1}{G_I^*(t)} = \frac{H}{2(D_m t)^{1/2}} \left(\frac{1}{G_{s,t}^*} - \frac{1}{G_{s,0}^*} \right) + \left(\frac{\varphi_A}{G_{A,0}^*} + \frac{\varphi_B}{G_{B,0}^*} \right) \tag{III-32}$$

If we substitute $G^*(\omega)$ in eq. (III- 23) by $G_I^*(t)$ from eq.（III- 32） and rearrange eq. （III- 24）, we get a new expression for the mutual diffusion coefficient:

$$D_m = \left[\frac{(2/3)^{1/3}\, p}{\left(9q + \sqrt{3}\sqrt{-4p^3 + 27q^2}\right)^{1/3}} + \frac{\left(9q + \sqrt{3}\sqrt{-4p^3 + 27q^2}\right)^{1/3}}{2^{1/3}3^{2/3}} \right]^2 \tag{III-33}$$

with

$$p = \frac{8\delta\omega G_N^0}{\pi^2} \left(\frac{\varphi_A}{G_{A,0}^*} + \frac{\varphi_B}{G_{B,0}^*} \right) \tag{III-34}$$

$$q = \frac{8\delta\omega G_N^0}{\pi^2} \frac{H}{2t^{1/2}} \left(\frac{1}{G_{s,t}^*} - \frac{1}{G_{s,0}^*} \right) \tag{III-35}$$

where

$$\delta = \frac{N_b^e N_b^3 b_b^4}{\pi^2 e_b^2} \left(\frac{\varphi_B}{N_A} + \frac{\varphi_A}{N_B} \right) \left(\frac{\varphi_B}{N_A} + \frac{\varphi_A}{N_B} - 2\chi\varphi_A\varphi_B \right) \tag{III-36}$$

For the sake of clarity, the specific procedures of arrangements are listed in the Supporting information A. In consequence, with the time evolution of the component concentration in the interphase and the time evolution of viscoelastic properties ($G_s^*(t)$) of the known sandwich, we can adequately determine a time variation of the mutual diffusion coefficient of A/B within the interphase.

III. 4. Experimental Section

III. 4.1. Materials

The polymers used in this study were supplied by Arkema. A thorough characterization of the polymers has been performed in our laboratory and the corresponding characteristics are listed in Table III- 1. It is noted PMMA-3 in Table III-1 was obtained by blending PMMA-1 and PMMA-4(50/50 w/w) in a twin-screw extruder. For clarity, details on the processing procedures were given elsewhere (Lamnawar and Maazouz 2008). Glass transition temperature (T_g), crystallization temperature (T_c) and melting temperature(T_m) were measured by differential scanning calorimetric (DSC), with a TA Instrument (Q20), at a heating and cooling rate of 10 ºC/min under N_2. Molecular weights were determined by size exclusion chromatography (SEC) with tetrahydrofuran (THF) as the eluent for PMMA and dimethyl formamide (DMF) for PVDF. Specifically, Figure III-2 presents the SEC chromatographs of the polymers for reference, where unimodal molecular weight distributions were observed for all polymers used. In addition, the tacticity of PMMAs were detected via ^{1}H-NMR (250 MHz) using chloroform-d (CDCl$_3$) as the solvent by integrating over the peaks at 0.85 ppm, 1.02 ppm and 1.21 ppm for syndiotactic (st), heterotactic (ht) and isotactic (it) conformations, respectively. The data are presented in Figure III-3. It is worthy to mention that the inverse relationship of T_g with M_w of PMMA as shown in Table III-1 is related to the difference in tacticity of the PMMAs. Higher amount of the syndiotactic triads give rise to a higher T_g of PMMA.

Table III-1. Characteristics of the investigated polymers

Samples	Trademark/Supplier	T_c(ºC)	T_g(ºC)	T_m(°C)	M_w (g/mol)	M_w/M_n	Ea(KJ/mol)[a]
PVDF	Kynar 720/ARKEMA	136	-42	170	210,000	2.0	59
PMMA-1	V825T/ ARKEMA	——	114	——	95,000	2.1	169
PMMA-2	V825T/ ARKEMA	——	112	——	100,000	1.9	160
PMMA-3[d]	Homemade	——	107	——	119,000	2.5	160
PMMA-4	V046/ ARKEMA	——	102	——	137,000	2.0	157

[a] energy of activation of the viscous flow (Ea) obtained from a master curve at a reference temperature of 220 ºC.
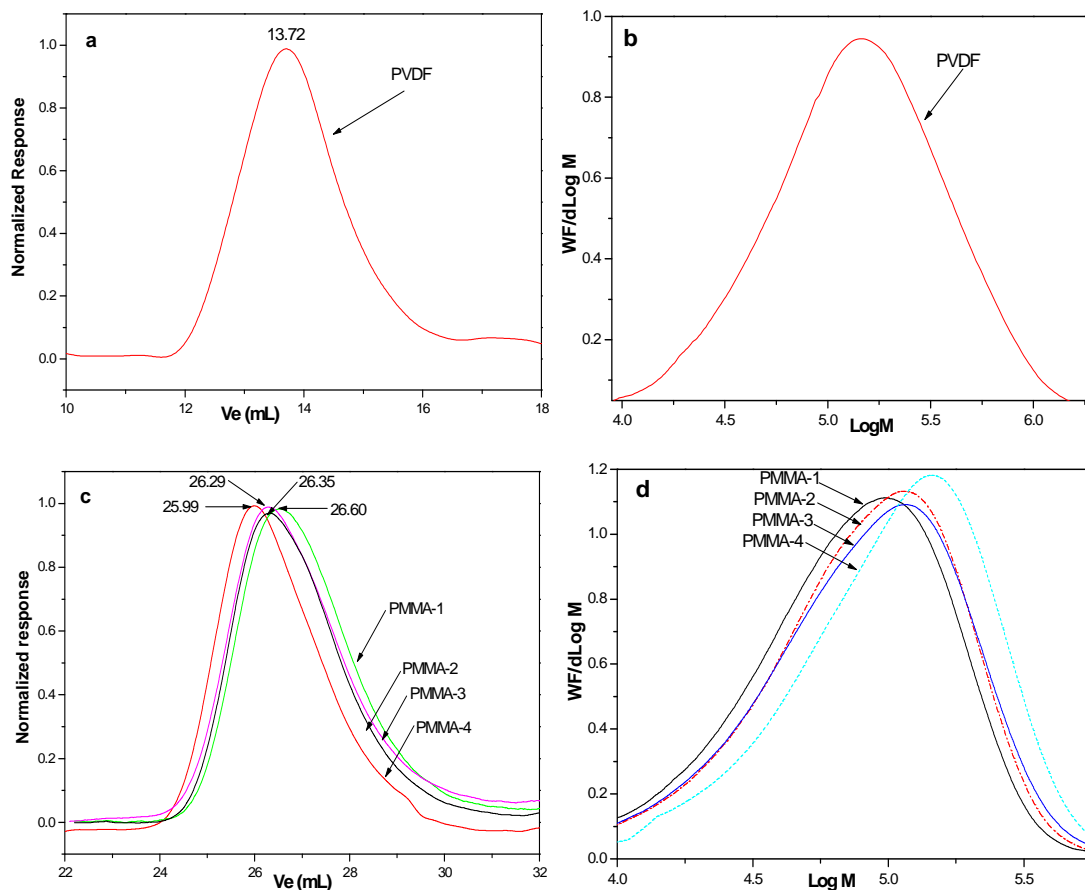
Figure III- 2. (a) and (c) are SEC chromatographs of PVDF (DMF) and PMMAs (THF), respectively; (b) and (d) are their corresponding WF/dLog M versus Log M curves after calibrations.

Tacticity	PMMA-1	PMMA-2	PMMA-4
st	50%	45%	42%
ht	39%	42%	39%
it	11%	13%	19%
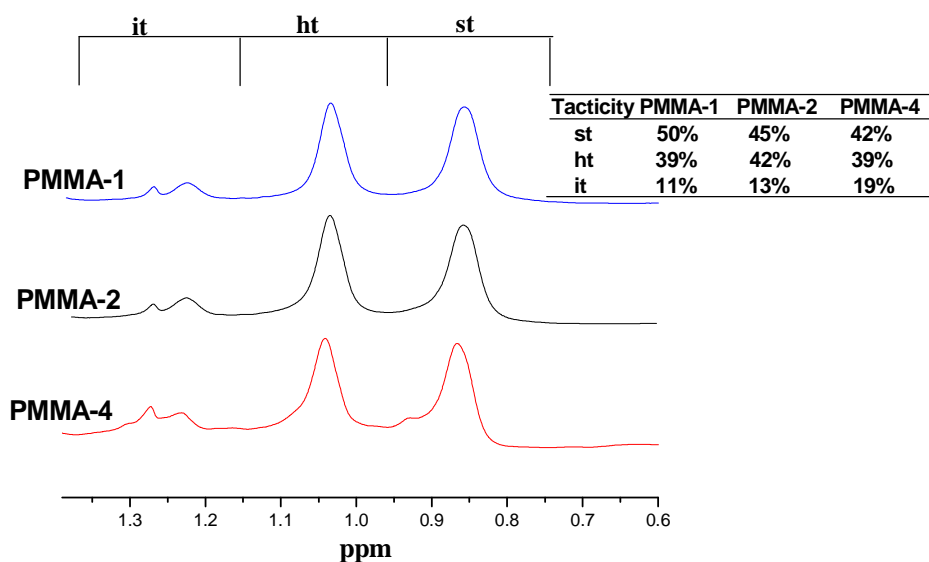
Figure III- 3. ^{1}H-NMR spectra of PMMA-1, PMMA-2 and PMMA-4 and their determined tacticities, it:isotactic; ht: heterotactic; st: syndiotactic.

III. 4.2. Sample preparation and rheological measurements

All the resin granules were dried at 80 °C under vacuum to remove any moisture before use. Samples for the rheological measurements were prepared by compression molding at 180 °C with a pressure of 200 bar between two Teflon films to obtain a smooth surface. The required thicknesses of the disks were achieved by using several molds. The thickness of the disks were measured by micrometer and rugosimeter at various points of the disc for at least three times to make sure the disks used are of no difference on thickness. During the heating and cooling stages of the compression, nitrogen (N$_2$) purging was introduced to protect the polymers from oxidation. The obtained samples were then cut into round disks with a diameter of 25 mm. After verifying the effect of the configuration, samples with thicknesses of 1.2 mm and 0.6 mm were used for rheological measurements of the neat polymers and a bilayer system, respectively. All samples were prepared under identical processing conditions to eliminate sample-to sample errors. To eliminate the possible effect of surface orientation brought about by the compression molding, all the disks were annealed at 80 °C under vacuum for at least 24h before measurements.

Rheological measurements were carried out under a strain-controlled rheometer: ARES (Advanced Rheometrics Expansion System) with a parallel-plate geometry (Φ=25 mm) at varying temperatures from 180 °C to 240 °C under a nitrogen atmosphere. Sample disks were placed between the parallel plates and melted before the tests. To ensure that all the oscillatory measurements were performed within the linear viscoelastic regime, a dynamic strain sweep test was first conducted in the range from 0.1% to 100% with a maximum angular frequency (ω) amplitude of 100 rad/s. Dynamic frequency sweep tests were carried out under a fixed strain amplitude of 5%, which was in the linear viscoelastic region, and an angular frequency range of 100-0.01 rad/s.

The bilayer assembly for the diffusion process was prepared by bringing round disks of PMMA and PVDF with individual thicknesses of 0.6 mm into intimate contact at room temperature with a desirable configuration before loading them between the plates and annealing them in the oven. Dynamic time sweep tests were performed at a given temperature from 180 °C to 240 °C under a fixed strain that lies in the linear viscoelastic region and a given angular frequency amplitude for a certain time with a 200FRTN1 transducer in the range from 0.02 g cm to 200 g cm.

It is worth mentioning that, for the bilayer configurations, the manner of loading the samples (the more viscous component on less viscous one or vice versa) may have an influence on the final results due to the viscosity difference of the materials (Bousmina, et al. 1998;Lamnawar and Maazouz 2006; 2008). In the present work, prior experiments were carried out in both two configurations, and the errors observed between the results were minimized by selecting a better gap between the upper and lower plates. The details are given below. It is noticed that the gap was set to be equal to the total thickness of bilayer in this part of experiments is for the sake

of avoiding the effects of external compression pressures, which are indeed believed to strengthen the diffusion process, making the investigation more complicated. For all oscillatory shear measurements, nitrogen purging was maintained throughout the tests to avoid the potential degradation and oxidation of the polymers. After the annealing processes, the specimens were first cooled down *in situ* within the rheometer chamber to a low temperature (<100 ^{o}C) at a rapid speed under N_2 by unscrewing the joint of upper plate and torque transducer, then they were quenched in liquid N_2. The quenched specimens were for the following EDX analysis and morphology observations. It should be mentioned that the manipulation of unscrewing must be done carefully in order to avoid any damage to the transducer.

III. 4.3 Determination of composition in the interphase

For the purpose of determining the composition of the interphase (equivalent to a macroscopic blend), we applied a similar method of normalization from the rheological properties of the corresponding blends as that developed in the work of Qiu and Bousmina (2000). Firstly, PMMA/PVDF blends with various volume fractions ranging from 10/90 to 90/10 with a step of 10 were prepared by melt blending at 220 °C in a twin-screw extruder. For the sake of clarity, the details of the processing procedures of the twin-screw extruder were given elsewhere (Lamnawar and Maazouz 2008). Subsequently, the rheological properties of blends were determined via small-amplitude oscillatory shear measurements in dynamic frequency sweep test. Thus, a calibration curve of the complex modulus (G*) or complex viscosity (Eta*) versus composition of the blend could be established. By comparing the rheological data of the sandwich assembly to that in the calibration curve and after a normalization procedure, the composition of the interphase can be available with a reasonable approximation.

III.4.4 SEM-EDX analysis and TEM observation

In an attempt to further verify the accuracy of the rheological modeling, a technique combining SEM and energy dispersive x-ray analyzer (EDX) was employed to determine the concentration profile across the interphase after the annealing process of the PMMA/PVDF assembly. This technique which makes use of the characteristic x-ray fluorescence of characteristic atoms present in the sample, has been demonstrated to be more than adequate for measuring the interdiffusion of compatible polymer systems (Gilmore, et al. 1980;Jones, et al. 1986). The quenched specimens were microtomed normal to the interfacial plane using an ultramicrotome before being exposed in a Hitachi S800 FEG Scanning electron microscopy (SEM) with an EDX microanalysis system. After a magnification suitable for obtaining an accurate representation of the concentration profile was selected, a line scan of electron beam was conducted along the diffusing direction from one bulk (e.g. PVDF)

to the other (e.g. PMMA) in a desired field where a cursor was placed at the beginning and the end of the chosen path for analysis. The EDX analyzer collected the x-ray data across this path (20 analysis points) and at each point   the number of x-ray events of given energy generated within a fixed time period was recorded as a function of x-ray energy and at the same time the position of the path was photographically recorded. For comparison purpose at varying points, analyses were performed at the same magnification, the same electron beam tension (5 kV) and the same number of counts. This procedure was repeated at different successive distances across the interface on the sample, giving replicate measurements. As the number of x-ray counts is directly proportional to the number of atoms (and hence the amount of characteristic element of the polymer) from which they originate, a concentration profile can be developed for the characteristic element, and the involved polymer across the interphase in the annealed specimen. In addition, to observe the morphology of the interfacial zone, the cross section of the quenched diffusion specimens were examined in a Philips CM 120 transmission electron microscopy (TEM) operating at an accelerating voltage of 80 kV.

III. 5. Results and Discussion

III.5.1 Rheology of neat polymers and PMMA/PVDF blend

III.5.1.1 Viscoelasticity of neat polymers

The storage modulus (G′), loss modulus (G″) and dynamic viscosity (η*) of neat polymers were measured as a function of frequency at given temperatures ranging from 180 °C to 240 °C. For the sake of clarity, only PMMA-2 was explored in the discussion, unless other specifications are given. Curves of η* versus frequency of PMMA-2 and PVDF are shown in Figure III-4a, where one can observe a shear-thinning behavior at higher frequencies and a Newtonian behavior at lower frequencies for the two neat polymers. PVDF exhibited a more moderate shear-thinning behavior than PMMA at any given temperature. Moreover, the turning point between these two regions moved towards higher angular frequencies when the temperature increased. It is worth mentioning that PMMA is more viscous than PVDF at the same temperature, but as the temperature is raised, their viscosities approach each other. Master curves of the polymers obtained by time-temperature superposition at a reference temperature of 220 °C are shown in Figure III- 4b,c. The rheology at terminal zone was observed to keep the typical relations G′~ω^2, G″~$\omega^1$for the neat polymers. The temperature dependence of the rheological behavior followed the Arrhenius equation and the activation energies of viscous flow calculated from the master curve at such a reference temperature are given in Table III-1. The other rheological parameters like plateau modulus G_N^0, terminal relaxation time τ, zero shear viscosity η_0, etc. of the polymers have been given in our earlier work (Zhang, et

al. 2012).
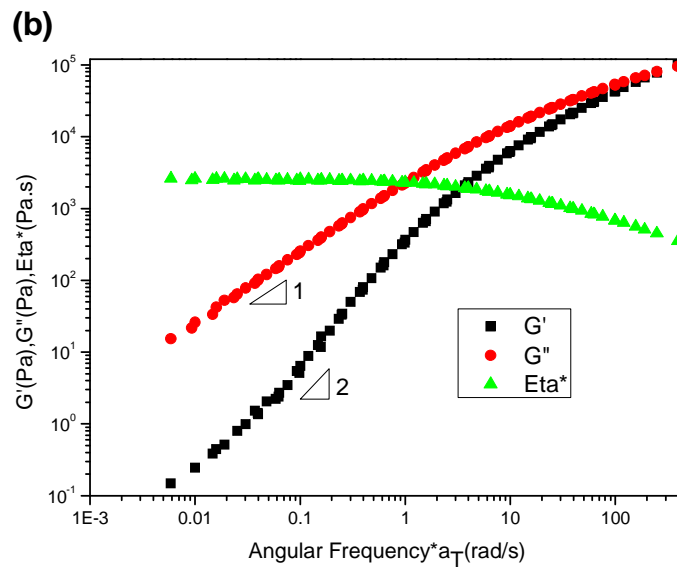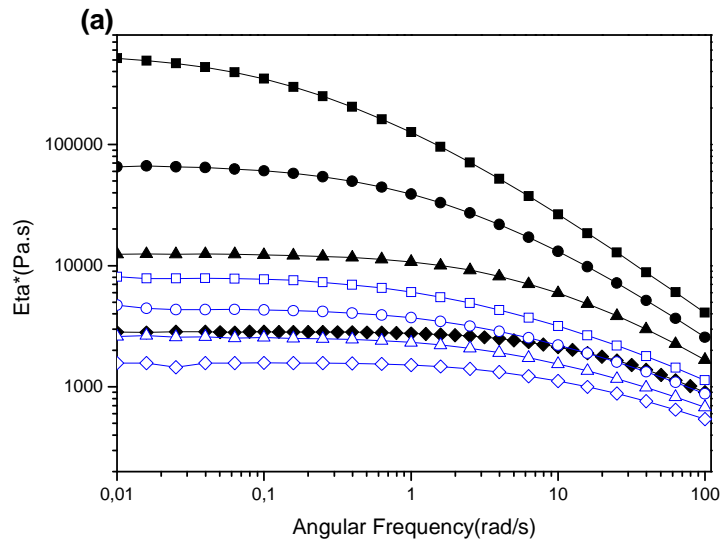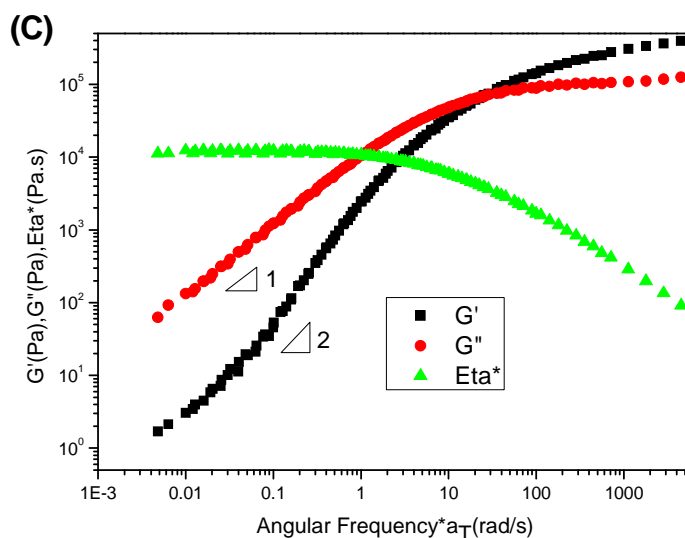
Figure III-4. (a) Plots of η* versus frequency for the neat polymers PMMA-2 (filled symbols) and PVDF (open symbols) at different temperatures:(■,□) 180 °C; (●,○) 200 °C; (▲,△) 220 °C; (◆,◇) 240 °C. (Dynamic viscosity fitted by the Carreau model)   (b) and (c) Master curves of G′, G″, η* as a function of angular frequency at the reference temperature of 220 °C for PVDF and PMMA-2, respectively

III.5.1.2 Component dynamics of PMMA/PVDF blend

PMMA and PVDF are polymers of industrial and academic importance and their blends are also of great interest. Various studies with respect to the miscibility of PMMA/PVDF blends have already been reported several decades ago and this material couple has been found to be miscible at a molecular level over the whole composition range in the melt (Schmidt 1969) below a lower critical solution temperature (LCST) of 350 °C (Bernstein, et al. 1977) (a theoretical temperature, which in practice is above the degradation temperature). Up to date, thanks to the progress made on the research of polymer mixtures, some blends, even though they are found to be thermodynamically miscible, are demonstrated to be dynamical heterogeneous at segmental and global chain level, particularly for the groups without or with weak specific interactions. These are considered to be the origin of features of broad glass transition and failure of time-Temperature superposition (tTS), etc. observed in miscible blends, indicating distinct component dynamics. And the dynamics (terminal dynamics and segmental dynamics) of each component behaved in the mixed state have been able to be disclosed over a wide temperature and composition range with the aids of various approaches from direct measurements of tracer diffusion coefficient (Composto, et al. 1990;Kim, et al. 1995a)to the component relaxation measurements by NMR (Chung, et al. 1994;He, et al. 2003), rheo-dielectric tools (Chen, et al. 2008;Roland, et al. 2006;Watanabe, et al. 2011;Watanabe, et al. 2007) and rheo-optical techniques (Arendt, et al. 1997) and some other rheological methods (Pathak, et al. 2004;Yang, et al. 2001;Zeroni, et al. 2008), etc. Among the approaches,

rheological methods offer an appealingly simple route to extract the component dynamics in a blend. In particular, a solution rheology method (Yang, et al. 2001) and a rheological measurement in a tracer blend (Zeroni, et al. 2008) were used to directly resolve the component terminal or segmental relaxations in blends. Besides, an alternative rheological tactic proposed by Haley et al. (2003) by fitting a double reptation model to the dynamic moduli of the blend has also been demonstrated to be quantitatively reliable on determining the component dynamics in comparison to other techniques. This is the main methodology adapted here. In this section, for clarity purpose, only the blends of PMMA-2/PVDF are considered.

III.5.1.2.1 Estimation of monomeric friction ζ_i (φ,T) from Rheology of blend

For the purpose to gain some understandings on the mutual diffusion kinetics occurred at the interphase and on the development of the interfacial rheology, it is of great significance to first examine the component relaxation behavior (variation of the $\zeta_i(\varphi,T)$ for each component) in mixed state under the conditions used here. So far, though no completely reliable rheological models have been established to describe the viscoelasticity of the miscible blend, however, fortunately, some advances have been achieved, in particular, the "double reptation" model proposed by Tsenoglou(1991) has been found to be a good choice to predict the linear viscoelasticity of miscible blend under some assumptions (Haley, et al. 2003;Haley and Lodge 2005;Yu, et al. 2011). Within the framework of such modified "double reptation" model, the ζ_i (φ,T) for each component of the blend is more facile to be determined, which has been demonstrated to be quantitatively reliable in comparison to other usual methods like tracer diffusion measurement, dielectric spectrums, rheo-optical birefirence measurements, etc(Haley, et al. 2003).

In a miscible blend system of polymer A,B, if the relaxation modulus of polymers can be each treated as single-exponential relaxation functions, then a mixing rule originated from "double reptation" model can be approximated for G' and G": (Haley, et al. 2003)

$$G'(\omega) = \varphi_A^2 G'_A (a_{T,A}\omega) + \varphi_B^2 G'_B (a_{T,B}\omega) + 2\varphi_A\varphi_B \sqrt{G_{N,B}^0 \Big/ G_{N,A}^0} \, G'_A (a_{T,A}x\omega) \qquad \text{(III-37)}$$

$$G''(\omega) = \varphi_A^2 G''_A (a_{T,A}\omega) + \varphi_B^2 G''_B (a_{T,B}\omega) + 2\varphi_A\varphi_B \sqrt{G_{N,B}^0 \Big/ G_{N,A}^0} \, G''_A (a_{T,A}x\omega) \qquad \text{(III-38)}$$

where $x = 2/\left(1 + \tau_{1,A}/\tau_{1,B}\right)$ and components A and B are specified such that $\tau_{1,A} \leq \tau_{1,B}$.

$a_{T,A}$ and $a_{T,B}$ are composition and temperature dependent shift factors, which are defined as:

$$a_{T,i}(\varphi,T) = \tau_{1,i}(\varphi_i,T)/\tau_1(\varphi_i = 1, T_{ref}) \qquad \text{(III-39)}$$

PVDF and PMMA homopolymer master curves shifted to a reference temperature of 220°C were used as the functions $G'_A(\omega)$ and $G'_B(\omega)$ for the fittings.

The longest relaxation times $\tau_{1,i}(\varphi_i, T)$ of each component in the blends were extracted by fitting G' and G'' data of blends via the above modified Tsenoglou mixing rules(Haley, et al. 2003), and converted to monomeric friction coefficients within the context of the reptation model(Ferry 1980).

$$\zeta = \frac{24\pi^2}{15} \frac{\tau_1 k_B T}{b^2} \left(\frac{M_e}{M}\right)^{1.4} \left(\frac{M_0}{M}\right)^2 \qquad \text{(III-40)}$$

For clarity purpose, representative examples of these fittings of the modified "double reptation" model to the experimental data of PMMA/PVDF at selected temperatures are shown in the Supporting information B-1.
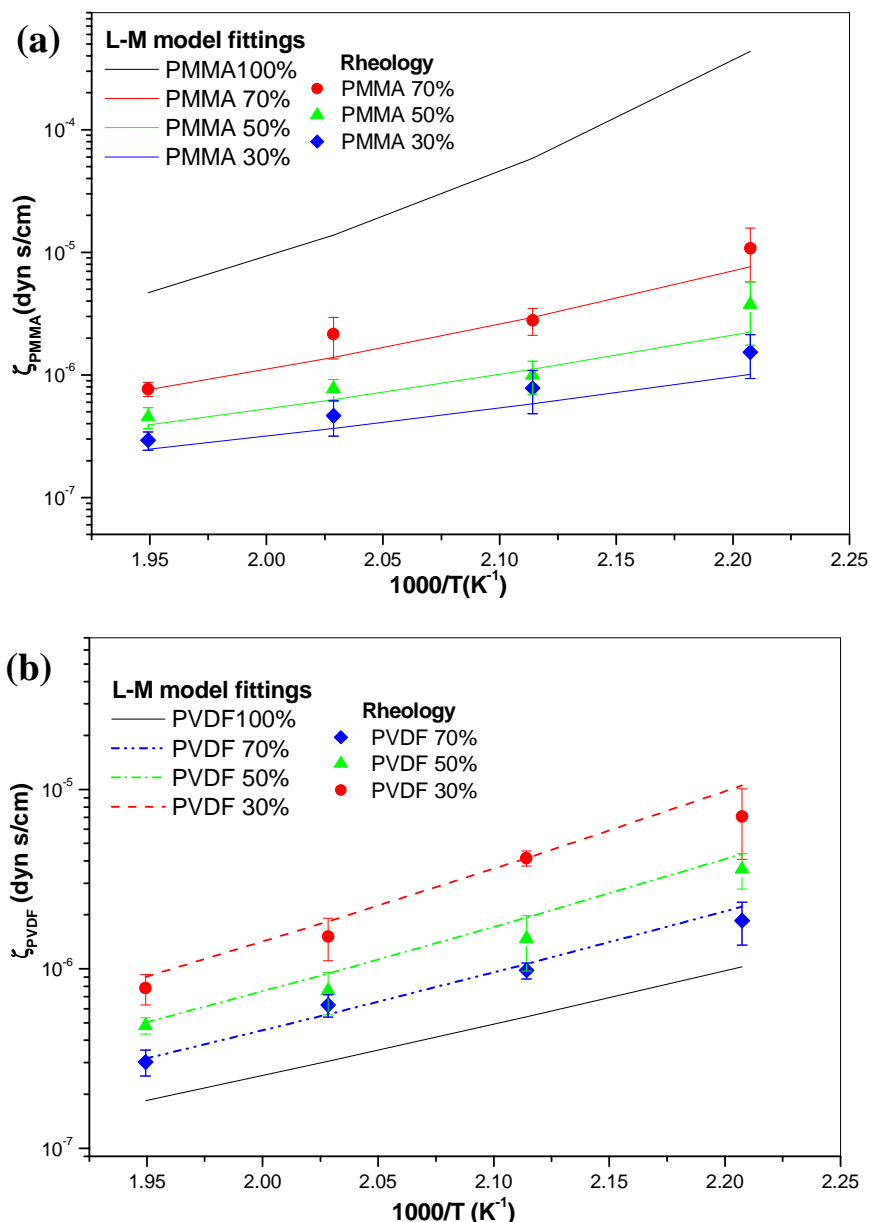
Figure III-5. ζ(φ,T) extracted from rheology experiments of blends plotted versus temperature for (a) PMMA and (b) PVDF; solid lines and dashed lines are the predicted results for each component in bulk and in mixed state using Lodge-McLeish model with relevant length of Kuhn segment, respectively.

The values of ζ (φ,T) for both PMMA and PVDF extracted from the rheological data are plotted in Figure III-5, in which both the ζ of PMMA and PVDF increase with decreasing temperature as expected. Meanwhile, both the ζ of PMMA and PVDF vary with composition: ζ$_{PMMA}$ decrease when increase the fraction of PVDF while ζ$_{PVDF}$ increase as the fraction of PMMA is increased. More interestingly, from a quantitative aspect, at the same condition in the mixed state used in the present study, the PMMA and PVDF components experience similar friction resistance, with friction coefficients ζ (φ,T) owning close values, at least, lying in the same order of magnitude. Take the composition of PMMA/PVDF 50/50 as an example,

ζ_{PMMA}(φ=0.5,T=220°C)= 7.72±0.1×10^{-7} dyn.s/cm; ζ_{PVDF}(φ=0.5,T=220°C)= 7.55±0.1×10^{-7} dyn.s/cm; ζ_{PMMA}(φ=0.5,T=180°C)= 3.75±0.1×10^{-6} dyn.s/cm; ζ_{PVDF}(φ=0.5,T=180°C)= 3.58±0.08×10^{-6} dyn.s/cm. This gives hints of weak thermorheological complexity of PMMA/PVDF, different from pairs of grave thermorheological complexity where the ζ_i(φ,T) of constituent component differ significantly as reported for literatures like poly(ethylene oxide)(PEO)/PMMA(Haley, et al. 2003),1,4-polybutadiene/poly(vinyl ethylene)(PB/PVE) (Yang, et al. 2001). and Polyisoprene/Polyvinylethylene (PIP/PVE) (Arendt, et al. 1997).

III.5.1.2.2 Comparison to the predictions of Lodge-McLeish model

Before introducing the Lodge-McLeish model (2000) concerning the dynamical heterogeneity in miscible blend, it is very important to point out that in the experimental conditions of this work, that is, temperatures far above from the T_g of blend, the part of dynamic heterogeneities that possibly induced from the thermal concentration fluctuation incorporating the concept of cooperative volume (Kumar, et al. 1996)can be negligible as the cooperative volume is small in such conditions as well concentration fluctuations are suppressed in the case of strong interactions between components (making χ<<0) (Pathak, et al. 1998). Hence, the main origin of dynamic heterogeneities remains in the contribution of chain connectivity. Bearing the idea of influences of chain connectivity on segmental dynamics, the model of Lodge-McLeish (L-M) provides a concept of "self-concentration" for the miscible blend system that indicates an excess of monomers of the component of interest within a region on the scale of a Kuhn segment. According to this theory, the effective concentration φ$_{eff,i}$ of monomers of type *i* can deviate significantly from the average of the bulk composition φ, and it can be calculated as:

$$\varphi_{eff,i} = \varphi_{s,i} + (1 - \varphi_{s,i})\varphi \qquad \text{(III-41)}$$

with the "self-concentration" (φ$_{s,i}$) of monomers of type *i* determined as:

$$\varphi_s = \frac{C_\infty M_0}{n_b \rho N_{av} V} \qquad \text{(III-42)}$$

where C_∞ is the characteristic ratio; n_b is the number of backbone bonds per repeat unit; volume V is assumed to be defined as the volume occupied by the Kuhn length (l_k)'s worth of monomers, expressed by $V = l_k^3$.

Many miscible blends have been found to have an anomalous broadened width of the glass transition temperature, which could be able to be interpreted from the dynamic heterogeneity using this new concept of self-concentration in the segmental length scale. Without exception in this work, the DSC traces of PMMA/PVDF blends and the bulk polymers shown in Figure III- 6a evidence a broader width of glass transition temperatures for the blends than the bulks. It is worthy to note that in a

miscible blend system including crystallizable component, the calorimetric response can be complicated, as the melting/crystallization transitions of the component can overlap with the glass transition of the other and the composition of the amorphous regions is not readily accessible. This situation is clearly true in this case. For those of high PVDF fractions where crystallization would happen, the presence of a significant glass transition temperature observed in low PVDF blends are replaced with two subtle transition zones which separated to be closer to that of the bulk polymers, respectively (Figure III- 6a). The calorimetric T_g of the corresponding PMMA/PVDF blends determined as the inflection point in the dsc trace are displayed in Figure III-6b. This anomaly of two T_gs of high PVDF blends has also been widely reported in literatures (Hahn, et al. 1985;Wu, et al. 1986). This did not necessarily indicate immiscibility. In fact, as pointed out by earlier researchers (Hahn, et al. 1985), the observation of a T_g of the PVDF component that was largely independent of blend composition even if is intimately mixed with PMMA, was taken as a signature of a nearly pure PVDF amorphous "interphase" immediately adjacent to the crystalline lamella fold surface.

(a)

(b)
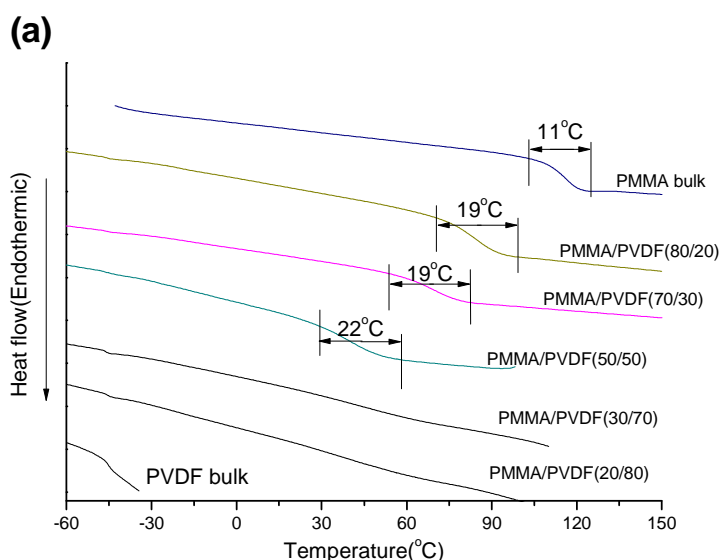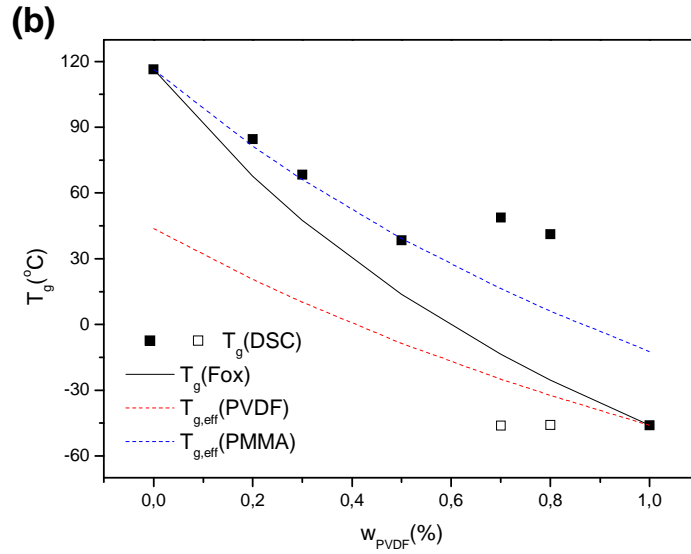
Figure III-6. (a) DSC traces for PMMA/PVDF blends and bulk PMMA and PVDF systems; (b) Lodge-McLeish predictions for the effective glass transition temperature for each component in a PMMA/PVDF blend as a function of composition. The solid line is the Fox prediction for the T_g of the blend, while the dashed lines are the predicted $T_{g,eff}$ for each component. The solid data points are calorimetrical T_g of blends determined by DSC

With the idea that an effective concentration is experienced by the local environment of monomer *i*, an effective glass transition temperature was also introduced to reflect the local dynamics of polymer chains in such a length scale of monomeric segment. It was implemented via Fox equation by replacing the average composition φ_i with the effective concentration $\varphi_{eff,i}$ of the blend component:

$$\frac{1}{T_{g,eff,i}} = \frac{\varphi_{eff,i}}{T_{g,i}} + \frac{1-\varphi_{eff,i}}{T_{g,j}} \qquad \text{(III-43)}$$

On calculating the $T_{g,eff,i}$, self-concentrations of PMMA and PVDF are taken as 0.31 and 0.32, the theoretical values predicted using cube of Kuhn length, with $l_{k,PMMA}$ =12.6 Å, $l_{k,PVDF}$ =8.6 Å, respectively(Zhang, et al. 2012). As shown in Figure III-6b, the anticipation of the Lodge-McLeish model meets the physics that the dynamics of higher T_g component in the mixture is more representative of the average blend composition (say that, the $T_{g,eff}$ of PMMA well accord with the experimental T_g of blend), on the other hand, the lower T_g component shows a glass transition that may be quite similar to its pure polymer, only weakly dependent on concentration over much of the composition range(Gaikwad, et al. 2008;Lodge, et al. 2006).

According to this model, the component dynamics in the blend were assumed to follow the same Vogel-Fulcher-Tammann (VFT) temperature dependence like its pure homopolymer, with only the Vogel temperature T_0 varies with composition through the parameter of $T_{g,eff,i}(\varphi)$. The resulting VFT equation is as follow:

$$\log\left(\frac{\zeta_i(\varphi,T)}{\zeta_{\infty,i}}\right) = \frac{B_i}{T - \left(T_{0,i} + T_{g,eff,i}(\varphi_{eff}) - T_{g,i}\right)} \qquad \text{(III-44)}$$

Here i represents component A or B, $\zeta_{\infty,i}$, B_i and $T_{0,i}$ are the VTF parameters that describe the temperature dependence of terminal relaxation times for pure homopolymer i.

The predictions of $\zeta(\varphi,T)$ of Lodge-McLeish model are consistent with those extracted from rheology by "double reptation" model (Figure III- 5). Furthermore, as indicated in Figure III- 5a, the $\zeta(\varphi,T)$ of PMMA was significantly reduced from that of the PMMA bulk after the addition of PVDF, with a tendency to approach that of PVDF, which can be ascribed to the fact that PVDF tends to soften the constrains on the overall long-range segmental motion and thus change the structural environment. As detailed in the above section, in the mixed state of the conditions used in this study, PMMA and PVDF chains undergo similar friction resistance or similar mobility though they cannot be exactly identical. It is necessary to mention that for miscible blends of no specific interaction, a large difference between the glass transition temperatures of the pure component polymers (ΔT_g) means strong thermorheological complexity, which results in large broadening of glass transition or even two distinct transitions in the blend. PMMA and PVDF, though $\Delta T_g \approx 150$ºC, the glass transition widths of their blends (~20 ºC) are only a bit broader, in comparison to some large broadening transitions observed for other pairs. In light of this fact, if the blend of PMMA and PVDF cannot be characterized by dynamic symmetry, it can be deemed to be a pair of weakly dynamic asymmetry, though they own some different structural characteristics. This similarity on the monomeric friction coefficient of these two components in the mixture and the characteristics of weak thermorheological complexity would be due to the contributions of coupling effects caused from the strong intramolecular forces on the rheological response of PMMA and PVDF chains(Carini, et al. 2002;Es-Haghi, et al. 2007;Mijovic, et al. 1997). The intramolecular forces probably include hydrogen bonding(Leonard, et al. 1985), dipole-dipole interaction(Paul and Barlow 1980), van der Waals interaction, etc..

III.5.1.2.2 Test of time-Temperature superposition

To further confirm the weak thermorheological complexity of PMMA/PVDF mixture, the success or failure of application of the empirical principle of tTS which is a good indicator of local rheological heterogeneity, has also been examined. To check the validity of TTS for the blends, the dynamic moduli were plotted according to Han(Han and Kim 1989a;1989b)(Figure III- 7a). This kind of plot employs raw data that are not shifted. If the data points of the different isotherms fall on a common line in a log G' versus log G'' presentation and if the scatter in the data or the linewidth is not too broad, then the time-temperature superposition should be valid and miscibility is assumed. Obviously, the Han plot for neat PMMA and that for neat PVDF exhibited quite small spreads, and the plots for all of the blend compositions

lay between those of these two constituents. This indicated a quite good miscibility between PMMA and PVDF. Meanwhile, the plots of shift factors (log a_T) versus temperature (Figure III- 7b) indicate similar temperature dependence of relaxation dynamics of the blends particularly for the ones of high PVDF fractions though no complete smooth linearity was obtained remaining some discrepancies. The linearity holds especially at high temperatures. For sure, representative master curves of blends are plotted at a reference temperature of 220 °C (Figure III- 8), it is clear that the tTS principle works well for the PMMA/PVDF blends, with only a subtle discrepancy at the terminal zone for blends of high PMMA content.
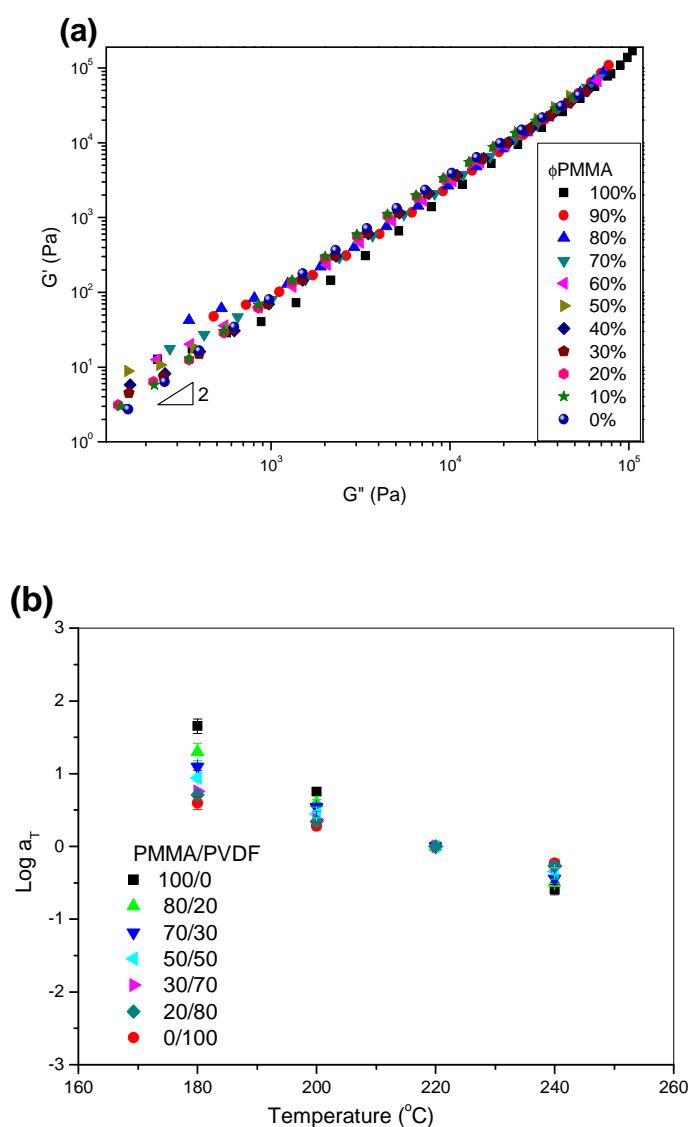
Figure III-7. (a) Plots of log G'versus log G" for the PMMA/PVDF blends over a wide composition range at 220 °C; (b) Plots of log a_T versus temperature for the PMMA/PVDF blends over a wide composition range using a reference temperature of 220 °C
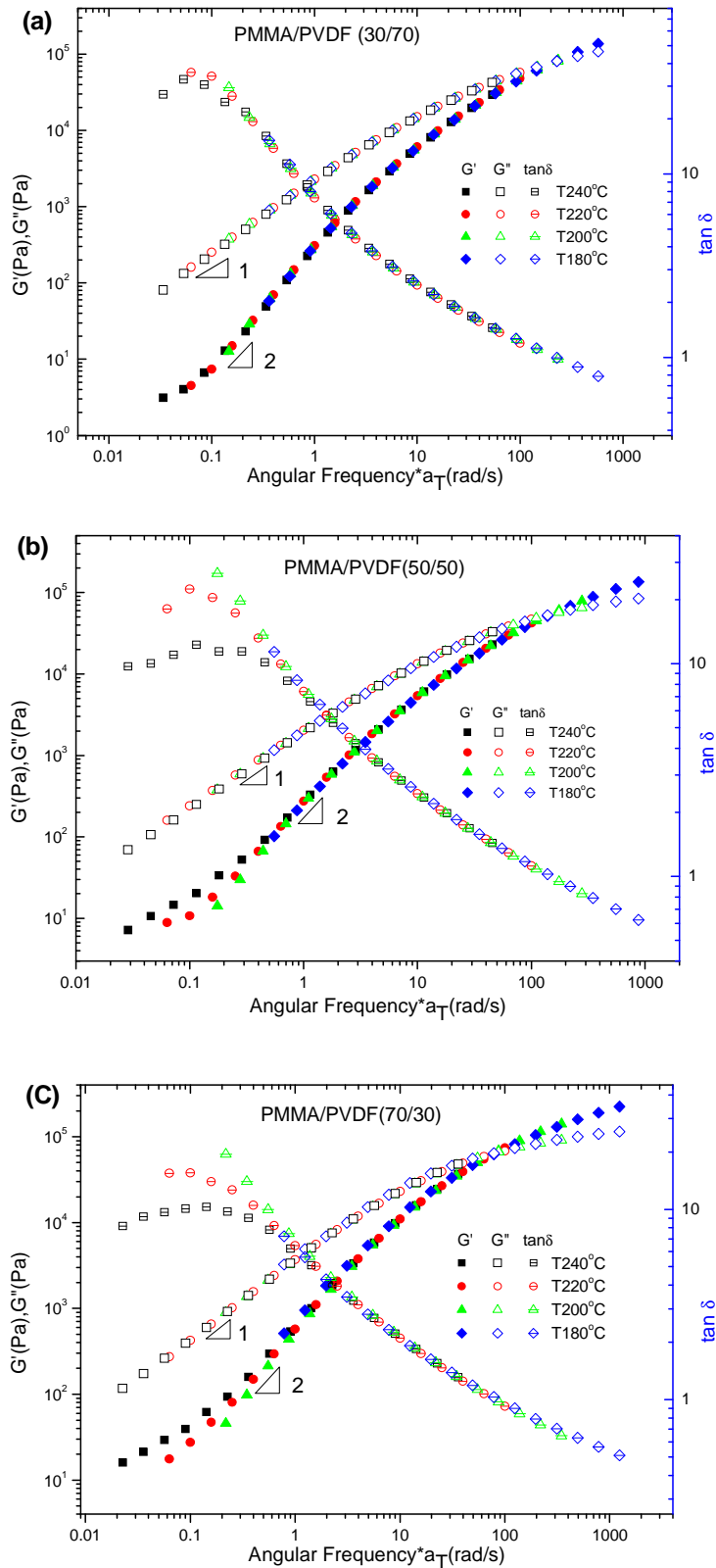
Figure III-8. Time-temperature superposition of PMMA/PVDF blends shifted to a reference temperature of 220 ºC. (a)PMMA/PVDF (30/70); (b) PMMA/PVDF (50/50); (c) PMMA/PVDF (70/30);

Another tactic by plotting the Van Gurp and Palmen curve (Van Gurp and

Palmen 1998)of delta versus logG* to confirm the success or failure of tTS was also used, which as well gives the similar conclusion of the weak failure of tTS application for PMMA/PVDF blends. For clarity purpose, the curves are added in the Supporting information B-2. Although some deviation of tTS principle obedience are observed, the failure is quite subtle when they are compared to the prominent departure from tTS of the PEO/PMMA blends studied by Colby(1989)in view of the similar characteristics and dynamic asymmetry (close ΔT_g) between these two pairs. This difference only appears to be due to the fact that the enthalpic interaction between PMMA and PEO is very weak ($|\chi|$ is quite small) whereas PMMA and PVDF has a strongly interacting one.

Though few attentions have been given to the miscible blends of strong specific interaction like PMMA/PVDF pair regarding the local dynamic heterogeneity in the past decades, very recently some authors (Gaikwad, et al. 2010;Yang and Han 2008) have demonstrated that the strong intermolecular interactions (particularly the forming of hydrogen bonds) between the constituent components in such miscible blend would restore thermorheological simplicity to some extent as the presence of concentration fluctuations and dynamic heterogeneity in the miscible blends might be very small, if not negligible. For the present system of PMMA/PVDF, strong dipole-lipole intermolecular interactions have been reported to occur between the carbonyl group of PMMA and the fluorines of PVDF(Paul and Barlow 1980). Besides, some earlier studies on the miscibility of the PMMA/PVDF blends indicated that the H-bonds are possible to be formed and they can even exist in the melt state (Kim, et al. 1995b;Leonard, et al. 1985;Mijovic, et al. 1997). After all, these intermolecular associations that give the strong interaction effectively coupled the rheological response of the PMMA and PVDF chains. Even though the complete restoring of thermorheological simplicity has not been reached, the thermorheolgical complexity for this blend is significantly reduced to be weak.

From this aspect, provided the similar friction coefficient of each component in the PMMA/PVDF mixtures resulted from the weak thermorheological complexity in the studied conditions, it is reasonable to assume an apparent parameter to simplify the description of the friction resistance in such a mixture and using the mutual diffusion coefficient which incorporates the enthalpic interaction to describe interdiffusion process occurred at polymer/polymer interface.

III. 5.2 Mutual diffusion at a polymer/polymer interface of an asymmetric bilayer

III. 5.2.1 Evolution of the mutual diffusion process with time

As a first step, it is of importance to take into account the configuration of the asymmetric bilayer used for investigation, i.e., whether the more viscous component

(here PMMA) is loaded above the less viscous one (here PVDF) (denoted as PMMA/PVDF (t-b)) or vice versa (denoted as PVDF/PMMA (t-b)). Besides the fact that the less viscous component may flow out from the parallel plates during experiments when it was loaded at the bottom, one more important principle one should consider is that the less viscous component should be placed adjacent to the motor to have a good dissipation of strain and the more viscous one close to the transducer(Lamnawar and Maazouz 2008). In the present work, a pre-study of the viscoelasticity variation versus healing time was given to the two reverse bilayer configurations at 180ºC,ω=1.0 rad/s for 45mins. The error between the two configurations was examined in a set of experiments elaborated by varying the gap between the parallel plates (i.e. the bilayer thickness) from 0.8mm (400 μm/400 μm) to 1.6 mm (800 μm/800 μm) with an interval of 0.1 mm. The errors observed were not pronounced, particularly for the case of 1.2 mm (600 μm/600 μm), the error could be negligible. It is the configuration that PVDF at the bottom close to the motor, PMMA on the top adjacent to the transducer with a gap of 1.2 mm employed in this study.
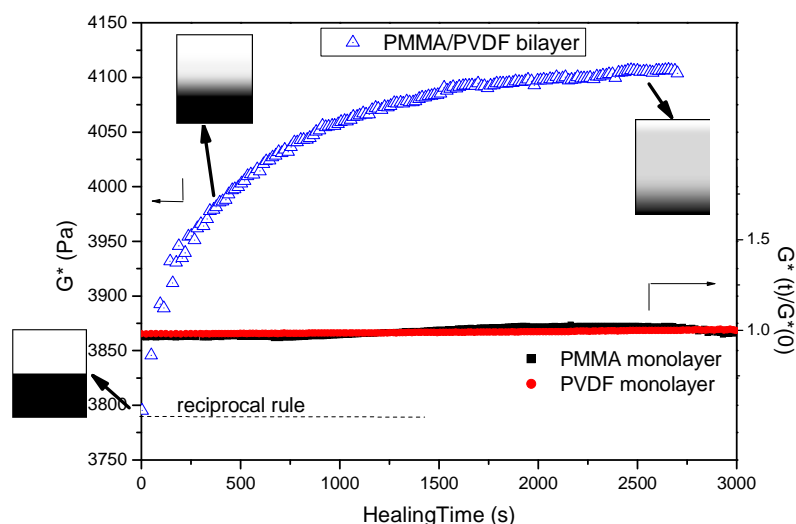
Figure III-9. Evolution of the complex modulus of a PMMA-2/PVDF sandwich with time at 220 ºC, ω=1.0 rad/s.

Figure III- 9 portrays a typical plot of the evolution of viscoelastic properties (we here used the complex modulus G*) with time for a PMMA-2/PVDF bilayer at T=220 ºC, ω = 1.0 rad/s (at the terminal zone of both components). It exhibits a rapid initial increase after which the increase gradually slows down before eventually approaching an equilibrium plateau. This pronounced increase can essentially be attributed to the mutual diffusion process of PMMA and PVDF chains having occurred at the interface of the bilayer. For more clarity, G* variation versus time for monolayers of neat polymers were examined in the same experimental conditions. Results are plotted in a term of G*(t)/G*(0) in a smaller inserted window in Figure III-

9 for comparison, where the near linearity of G*(t)/G*(0) to 1.0 of the neat polymers through the whole measuring time indicates their thermal stability at the measuring temperature. Thus the increase in complex modulus (G*) of bilayer is a signature of the diffusion process across the interface. After a surface rearrangement, surface approach and wetting stages within the short period during the healing process stated by Wool et al (1995), chains on both sides began to invade the interface, with a motion pattern generally considered to be governed by repation kinetics put forward by de Gennes (1971) and developed by Edwards (1986). Differing from the case of symmetrical system, in asymmetrical system, the chemical potentials of vacancies in the two continuous phases remain unequal for dissimilar polymers, with excess vacancies formed in the faster-diffusing phase. Such chemical potential gradients should, as pointed out by Kramer et al. (1984), vanish in virtue of viscous melt flow, which is the driving force for mutual diffusion.

As chains on both sides uninterruptedly penetrate into the other side and entanglements in the interfacial region continuously become established, the sharp interface decays as the time elapses. It is replaced by a broadening interphase, which can be considered as a macroscopic blend composed of PMMA and PVDF chains. From a microscopic viewpoint, in the interphase, in addition to constraining tubes constructed by neighboring chains of the same polymer, the interactions between a wriggling chain and its neighboring chains of the other polymer also contribute to the establishment of new entanglements. Based on this aspect, a molecular model can be schematized (Figure III-10) to describe the chain behavior at an asymmetric bilayer interface brought about from mutual diffusion.
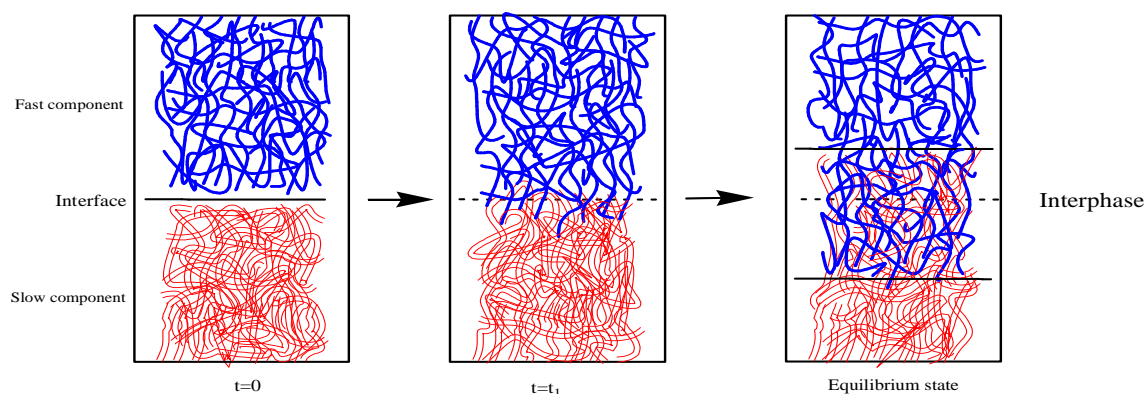
Figure III-10. Molecular model of entanglements development at the interface as a result of mutual diffusion (t_1, a certain time after diffusion but before reaching the equilibrium state)

The interphase is believed to posses its own characteristics, with thickness, composition and properties developing with time. The emergence and development of such an interphase provoked by mutual diffusion at the interface mainly contribute to an increase in G* of the sandwich with healing time, assuming that the

mass transport is independent of flow under small amplitude shear measurements. In fact, eq. III- (30) also gives us a concept from a theoretical aspect that the variation in viscoelastic properties of the sandwich with time is caused by the time evolution of the viscoelastic properties, composition and thickness of the interphase. Moreover, it is worth noting that the measured G* value of the bilayer at the initial period of diffusion when the interphase still remains negligible was close to the value predicted by the reciprocal rule as indicated in eq. III- (29), similar to the results reported in the literature(Yang, et al. 2010;Zhao and Macosko 2007).

III. 5.2.2 Calculation of the mutual diffusion coefficient

Bousmina et al. (2000) did mounts of works on polymer-polymer interdiffusion from rheology, which provides us some interesting basis to understand the D_m from a rheological aspect. Despite this, it is still far from enough for us to calculate D_m of the mutual diffusion within the interphase on the basis of the rheology of real interphase. Exactly speaking, in an asymmetrical bilayer, the loci of mutual diffusion situates in the broadening interfacial region (interphase), the only zone containing both diffusing elements. This is the reason why it would be more accurate to employ the viscoelasticity of the interphase rather than that of the entirety of the total sandwich to determine the D_m.

As indicated in the model developed in the section of theory, D_m is dependent of the composition in the interphase. Hence, in a first step, it is essential to determine the variation of the composition with time. In fact, from a rigorous viewpoint, the component concentration in the interphase is a time and position function, varying from 1 to 0 from one side of the moving boundary to the other side and the concentration profile can be determined by a solution of Fick's equation (eq. III-1) assuming the diffusion belongs to normal Fick's type. In solution, nonlinear partial differential equations that cannot be solved analytically will be encountered when D_m is considered to be concentration-dependent. To solve them, Zhao and Macosko (2007) used a finite element method to give a concentration profile for HDPE and LLDPE multilayers. In the present paper, for the sake of simplicity of discussing the development of the interphase, the interphase was assumed as a first approximation to be a homogenous blend with composition changing with the diffusion time. Indeed, the concentration profile versus position within the interphase was also examined at a given time by spectroscopic tool EDX as shown below. To determine the time evolution of the composition in the interphase, Qiu and Bousmina (2000) suggested a normalization method by comparing the G* of the sandwich to a calibration curve of corresponding blends with various compositions and using a normalizing equation to remove the effect of polymer bulks in the sandwich assembly: $\varphi = [C(t) - C_0]/[C_1 - C_0]$. Here, $C(t)$ and C_0 are the volume fraction of PMMA in the sandwich at the healing times t and 0 (at which state their viscoelasticity equals that of a blend with composition 50%), $C_1 = 1$.

A similar normalization procedure was used in this study to determine the concentration of PMMA-2 in the time-developing interphase, assuming that the validity of this method was adequate. The difference remains that our experimental data indicated that the initial G* value of the PMMA-2/PVDF sandwich when that interphase was trivial coincided more closely with that given from the reciprocal rule in eq. (III-29), as reported by Zhao and Macosko (2007)and Yang et al. (2010). The concentrations of PMMA-2 in the interphase as a function of time at different temperatures are depicted in Figure III-11. We can observe that the PMMA concentration increased rapidly at the beginning of the diffusion before reaching an approximate steady state, except at 180 ^oC where the plateau period had not arrived within the sweep time length. The dotted lines in Figure III-11 were used to compensate the possible rapid diffusions occurring during the period before the first experimental result collected at high temperatures. The phenomenon of a sudden increase observed at the very initial period of diffusion has also been reported in the literature (Qiu and Bousmina 2000;Yukioka, et al. 1992). Another important point reflected in the figure is that the PMMA concentration remained below 0.5, approaching 0.5 with the raise in temperature, which was in accord with the prediction of the fast-mode theory (the faster-moving species being dominating).

It should be mentioned that due to the great negative deviation of the blend curve from that of the reciprocal rule at 240 ^oC, which was also observed in the literature(Han and Kim 1989a;1989b), the normalization of φ_{PMMA} behaved inaccurately at this temperature. For this reason, a virtual scattering curve (open diamonds) was plotted under an assumption that the interphase underwent a final saturation concentration (steady state) of 0.5 at long diffusion times. In addition, it is worth pointing out that the different angular frequencies used at different temperatures intended to guarantee that the measurements were conducted in the terminal zone, details of which will be shown below. The varying concentration profiles that appeared at different temperatures can be easily understood in a more vivid manner when taking into accont the viscosity ratio and weight-average relaxation time τ_w (determined from Cole-Cole curves) ratio of PMMA-2 to PVDF at the same experimental conditions, cf. Figure III-12. As the temperature was increased, both the viscosity ratio and τ_w ratio decreased sharply from a rather large value at 180 ^oC to a value close to 1 at 220 ^oC and 240 ^oC, thus giving rise to the monotonic increase of φ_{PMMA} from low values at 180 ^oC to values approaching 0.5 at 220 ^oC and 240 ^oC. The information of rheological behavior of components in mixed state, as detailed in section III.5.1.2, also can give the same conclusions.
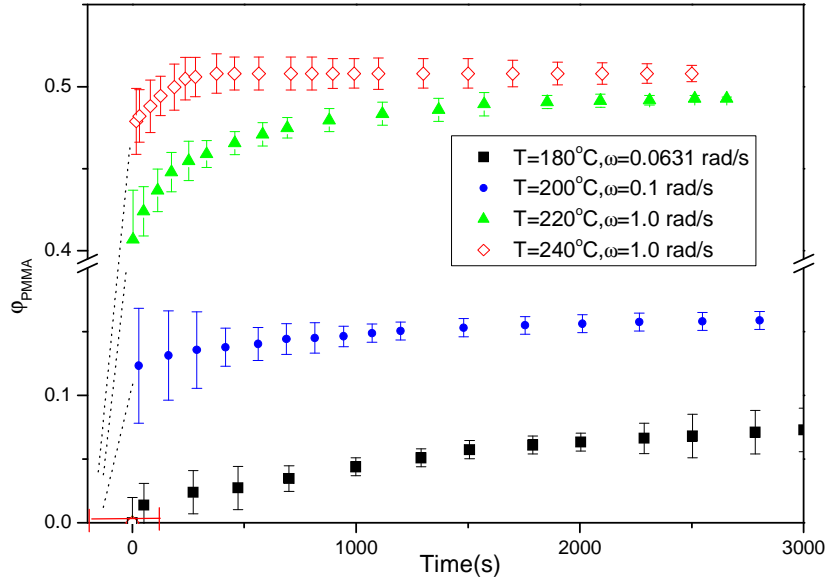
Figure III-11. Evolution of the normalized concentration of PMMA-2 in the interphase with time at different temperatures in the terminal zone ($\omega < 1/\tau_{rep}$)
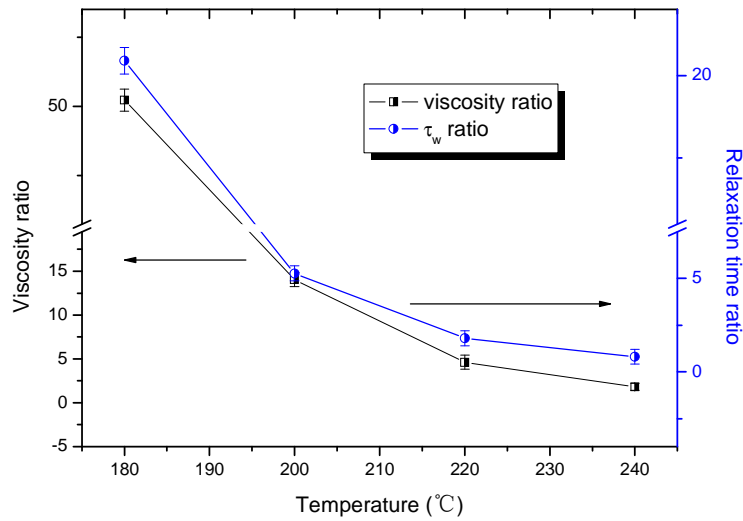
Figure III-12. Viscosity ratio and relaxation time ratio of PMMA-2 to PVDF at the experimental conditions of annealing processes

Furthermore, to eventually achieve the result of the mutual diffusion coefficient by eq. (III-24) or eq. (III-33), one another important factor needed was the Flory-Huggins interaction parameter χ of the relevant couple, which has been demonstrated to play a vital role(Composto, et al. 1988;Jones, et al. 1986;Klein 1990). The value of χ of the PMMA/PVDF pair was reported to be from -0.02 to -0.7, depending greatly on the measuring techniques (melting point depression; SAXS; SANS; Inverse chromatography and Dilatometry etc.) and the composition (Dipaolabaranyi, et al. 1982;Riedl and Prudhomme 1984;Sasaki, et al. 1995;Wendorff

1980), whereas some papers have reported it to be independent of concentration(Canalda, et al. 1995;Nishi and Wang 1975). Moreover, it should be mentioned that at present there is no systematical experimental data available to describe the dependence of χ on temperature for the PMMA/PVDF blend (Han and Kim 1989a;1989b). For this reason, in many previous studies of PMMA/PVDF interdiffusion by other researchers (Han and Kim 1989a;1989b) they also used a constant value obtained by Nishi and Wang (Nishi and Wang 1975) for their D_m. Nevertheless, Takahashi et al(1995) pointed out that the χ value obtained from melting temperature depression using the Nishi-Wang equation contained large errors compared with values obtained by other methods (Sasaki, et al. 1995). As did by other researchers, in the present case we also used a constant χ but a value χ =-0.07 determined from small-angle x-ray scattering (SAXS) (Wendorff 1980). Meanwhile, we have tried several different values of χ (χ = 0.0; χ =-0.07; χ =-0.3; χ =-0.5) to calculate the D_m value in the rheological approach and the corresponding interphase thickness. The results obtained from rheology were compared to that of EDX results in a term of concentration profile. For the simplicity purpose of comparing differentχ, the concentration profile was approximated by the simple Fickian solution (Composto, et al. 1988;Crank 1975):

$$\varphi_{(z,t)} = \frac{1}{2}\left[erf\left(\frac{(h-z)}{2(D_m t)^{1/2}} \right) + erf\left(\frac{(h+z)}{2(D_m t)^{1/2}} \right) \right] \tag{III-45}$$

where *erf* is the error function, *h* is the thickness of the layer, *z* is the spatial axis of the diffusion direction with the contact interface of bottom layer and lower plate of rheometer as z=0.

The comparisons between different χs are displayed in Figure III-20c, from where we can observe that χ =-0.07 gives a better agreement between rheology and EDX. This evidences the rationality of using χ =-0.07 for PMMA/PVDF couple. For blends exhibiting an LCST, it is generally expected that the value of -χ will increase when decreasing the temperature and χ can be expressed in a term of $\chi = A + B/T(K)$. Using χ=-0.07 at T=473K and χ=0.0 at T=623K (cloud point), a relation $\chi = 0.2207 - 137.52/T(K)$ can be obtained. We have calculated D_m from the χ values of this relationship and found that the obtained results of D_m in the temperatures involved in the present work are in the same order and within the error of those calculated with constantχ =-0.07. So in this case, it is reasonable to use a constant χ =-0.07 for the rheological analysis as well it has given a better agreement between rheological modelling and EDX results.

Mutual diffusion coefficients calculated from the primitive model of Qiu and Bousmina (i.e., eq. III-24) as well as our modified model (i.e., eq. III-33) are displayed in Figure III-13 as a function of diffusion time. The apparent D_m gradually decreases

with annealing time, reducing to a constant in the longer time limit. Similar time dependence of diffusion coefficient has also been observed very recently by Kawaguchi et al. (2011) based on PS/deuterated PS bilayer films via time-resolved neutron reflectivity measurements. The higher D_m values at shorter diffusion time are supposed to be attributable to the segmental relaxation. At the first beginning of diffusion, the dynamics is dominated by short chains or segmental motions in a Rouse behavior with a higher diffusion coefficient, then more and more long chains participate into the diffusion, resulting in a decrease of D_m to a plateau stage where is a sum of contributions from species of different chain lengths. This was clearly demonstrated in Figure III-13. When compared to D_m calculated from the primitive model using $G_{s,t}^{*}$ of the total sandwich assembly, D_m calculated from the modified model basing on the concept of $G_{I,t}^{*}$ of the interphase displayed a greater value but with a similar order of magnitude. The latter is believed to mirror the mutual diffusion process in the interphase in a more reasonable manner.

The ensuing discussions are based on the data of D_m determined by the modified model. The D_m value (7.08×10^{-9}cm^2/s) at the equilibrium state is considerably greater than both the self-diffusion coefficients of PMMA-2 (2.35×10^{-12}cm^2/s) and PVDF (3.88×10^{-11}cm^2/s) as computed in our earlier work (Zhang, et al. 2012) from symmetrical bilayer systems at 220 ºC. This implies that the enhanced mutual diffusivity, which is also known as thermodynamically accelerated interdiffusion, or the so called "speed up" effect, was due to the favored segment-segment interactions ($\chi < 0$) as first predicted by de Gennes (1971). It is also pointed out that mutual diffusion is controlled by enthalpic driving forces which favor mixing whereas self-diffusion is controlled by entropic driving forces (Garbella and Wendorff 1988). The D_m value obtained for the PMMA/PVDF mixture in the present work is in good agreement with those reported in the literature as shown below.
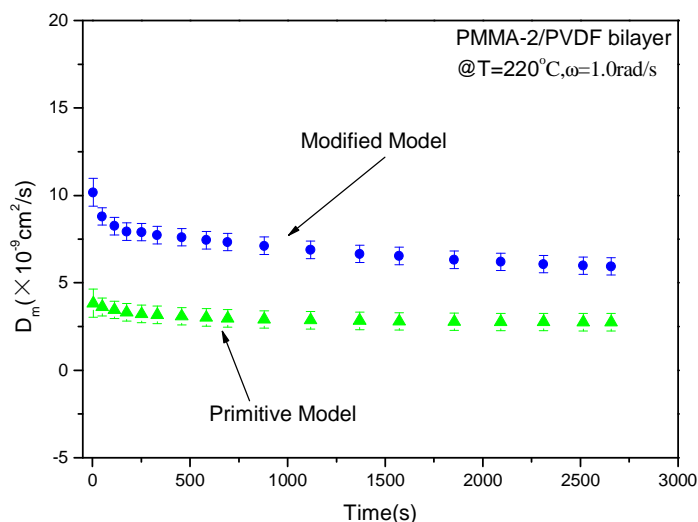
Figure III-13. Mutual diffusion coefficient versus time for the PMMA-2/PVDF bilayer at 220 °C,ω=1.0 rad/s

III. 5.3 Dependence of D_m on annealing and structural factors

III.5.3.1 Dependence on angular frequency

Through a macroscopic window of frequency, one can look into the motion behaviors of various sizes of chains in a microscopic window. Figure III-14 displays mutual diffusion coefficients determined at different angular frequencies at 220 °C. As elucidated, the lower the frequency applied, the motion of the longer size of chains was reflected out, and the lower the diffusion coefficient values that would be perceived. In particular, when ω was below the reptation relaxation time, τ_{rep}, all chain sizes (both long and short) were involved, and the diffusion coefficient came close to being invariable. Here, τ_{rep} of PVDF and PMMA-2 were ~0.18s and ~0.27s at 220 °C, respectively. Details on determining this characteristic time have been given in our previous work (Zhang, et al. 2012). In order to reflect the real motion of the whole polymer chain, the ensuing discussions are based on the data measured in the terminal zone (ω<1/τ_{rep}).
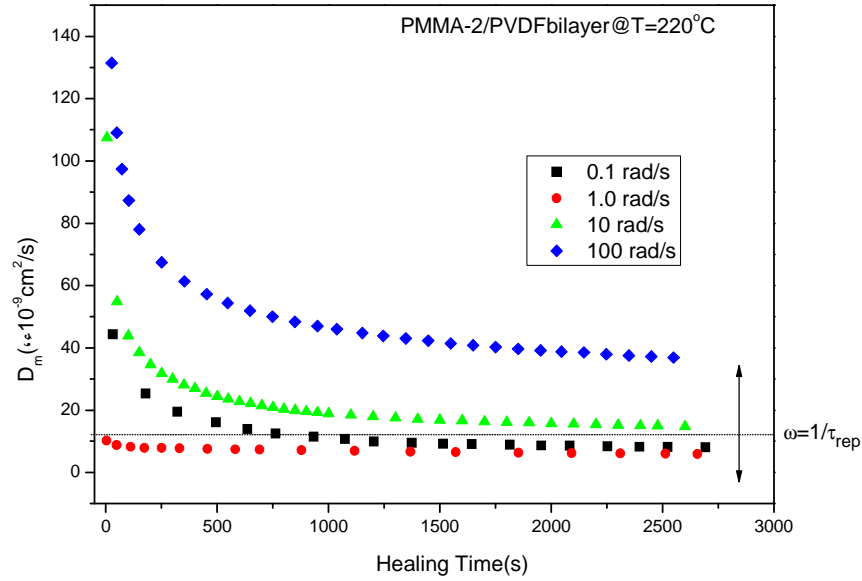
Figure III-14. Mutual diffusion coefficient at the interphase of a PMMA-2/PVDF sandwich as a function of time at 220 ºC under various frequencies from 0.1 rad/s to 100 rad/s

III.5.3.2 Dependence on temperature
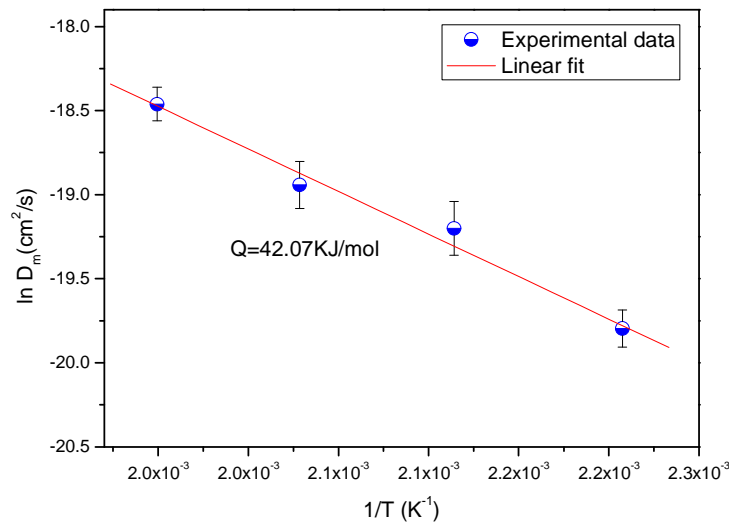
Figure III-15. Dependence of the mutual diffusion coefficient on temperature as determined in the terminal zone ($\omega < 1/\tau_{rep}$)

From the expression of the mutual diffusion coefficient in eq. (III-2), one can easily understand that the variation of the mutual diffusion coefficient D_m with temperature must be accounted for by the temperature dependence of the mobility D_T and the thermodynamic factor $S(0) = (\chi_s - \chi)\varphi_A\varphi_B$. The former should exhibit an Arrhenius

- 136 -

temperature dependence similar to that observed for the shear viscosities. On the other hand, the variation of the thermodynamic factor with temperature can become important only for temperatures close to the coexistence curve (i.e., $\chi \sim \chi_s$) (Kanetakis and Fytas 1989). Considering the uncertainties of the temperature dependence of χ for the PMMA/PVDF pair and for measuring temperatures T<<Ts (350ºC), here, the thermodynamic dependence on temperature can be decoupled using an invariable χ value of -0.07 for all compositions at all temperatures in the study. The temperature dependence of the mutual diffusion coefficient is therefore expected to be determined by the mobility D_T term.

Figure III-15 depicts the temperature dependence of the mutual diffusion coefficient of PMMA-2/PVDF at the equilibrium state, which well exhibits an Arrhenius temperature dependence:

$$D(T) = D_0 \exp(-Q/RT)$$

(III-46)

where D_0 is a pressure-dependent constant and Q is the activation energy, equal to 42.07 KJ/mol. This is much closer to the self diffusion of PVDF (55 KJ/mol) than that of PMMA-2 (185.9 KJ/mol) as determined in our previous work(Zhang, et al. 2012). This laterally implies that the mutual diffusion is controlled by the fast PVDF component as predicted by the fast-mode theory (Kramer, et al. 1984).

III.5.3.3 Dependence on molecular weight

Numerous studies on mutual diffusion carried out by various spectroscopic tools have given insight into the dependence of the mutual diffusion coefficient on molecular weight. On the basis of a forward recoil spectrometry (FRES) study of the mutual diffusion in entangled PS/PXE blends, Composto et al. (1988) reported that the mutual diffusion coefficient was a function of the chain length of the faster-moving PS chains, scaling approximately as N_{PS}^{-1}. Likewise, Kanetakis and Fytas (1989) have come to a similar conclusion supporting the fast-mode theory that the mutual diffusion coefficient decreases monotonically as the chain length of the faster PEO component increases. Their study involved dynamic light scattering of the mutual diffusion in PEO/PPO blends. On the contrary, some results have been reported to be in favor of the slow-mode theory. For example, for the mutual diffusion between PMMA and SAN, on the basis of ellipsometric studies, Yukioka et al. (1992) argued that the molecular weight dependence of D_m can be well interpreted in the framework of the 'slow theory', which claims that D_m is mostly governed by the slower moiety. According to the fast-mode governed kinetics(Composto, et al. 1988;Kanetakis and Fytas 1989;Kramer, et al. 1984), the mutual diffusion coefficient should be inverse proportional to the chain length of the faster species but be

independent of the chain length of the slower species. In the present study, the slower species (PMMA) with varying chain lengths were used to examine the effect of chain length on D_m. Figure III-16 shows the mutual diffusion coefficients determined from the rheological data at different chain lengths of PMMA, where we can observe that the mutual diffusion coefficient demonstrates a very slight dependence on the chain length of 'slow' species (here PMMA), in accordance with the prediction by the fast-mode theory. It should be noted that the results are calculated at a given concentration (φ_{PMMA}=0.4) in the interphase.
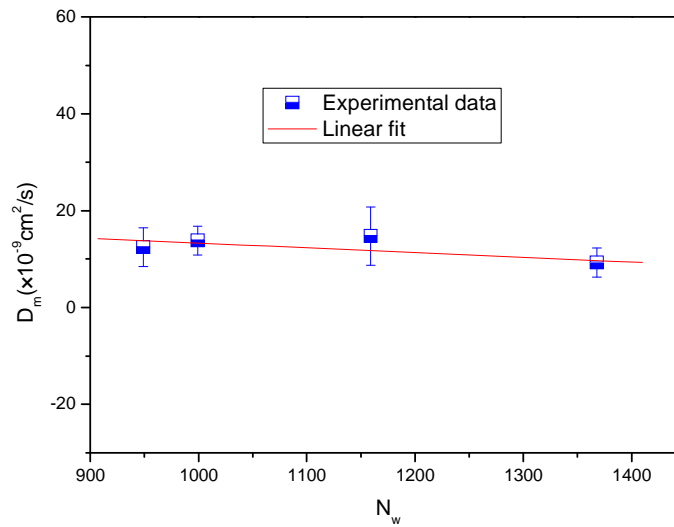
Figure III-16. Dependence of the mutual diffusion coefficient on the chain length of PMMA at T=220 °C, ω=1.0 rad/s, with a given concentration of φ_{PMMA}=0.4 in the interphase.

III.5.3.4 Comparison to literatures

The mutual diffusion coefficient D_m obtained in the present study was taken into comparison with the literature data. For this purpose, results of present study (T=220 °C and $\overline{N_{w(PVDF)}}$ = 3279) are shifted to the experimental conditions of literaturesusing the Arrhenius temperature dependence (i.e. eq. III- 46) by an activation energy of 42.07KJ/mol and $D_m \sim \overline{N_{w(PVDF)}}^{-1}$. As in some literatures(Kim and Han 1991;Wu, et al. 1986), only intrinsic diffusion coefficients D_i (i=A, B) are available, D_m was calculated by the fast-mode theory using $D_m = \varphi_B D_A + \varphi_A D_B$ with φ_i being the volume fraction of component *i*. The comparisons are presented in Table III- 2, where a good agreement

between our experimental results with the literatures can be found considering the fact that the presence of heavy marker has been demonstrated to slow down the diffusion process(Green and Doyle 1987).

Table III- 2. Mutual diffusion coefficient of PMMA/PVDF couple (present work and literature data)

Methods	M_{w-PMMA}/M_{w-PVDF}	D_m, cm^2/s (reported in literature)	D_m, cm^2/s(present work) (shifted to literature condition)
TEM+gold marker[Wu, et al. 1986]	$1.5\times10^5/1.88\times10^5$	$1.91\times10^{-10}(190\,^oC)$	4.07×10^{-9}
Theoretically simulation[Kim and Han 1991]	$1.075\times10^5/1.45\times10^5$	$4.45\times10^{-10}(230\,^oC)$	9.60×10^{-9}
Small angle X-ray[Garbella and Wendorff 1988]	$1.20\times10^5/1.0\times10^5$	$3.75\times10^{-9}(180^oC)$	6.01×10^{-9}
Rheology[present study]	$1.0\times10^5/2.1\times10^5$	$7.08\times10^{-9}(220^oC)$	7.08×10^{-9}

III.5.4 Development of the interphase with time

III.5.4.1 Rheological aspect

As demonstrated before, the newly modified model of the mutual diffusion coefficient extracted from the concept of the interphase in this study allows us to gain insight into the feature of the interphase. From the mutual diffusion coefficient obtained above, we can in turn determine the viscoelastic behavior of an interphase through eq. (III-32). From Figure III-17 we can see that the complex modulus G* of the interphase of a PMMA-2/PVDF assembly first experiences a rapid initial increase before rising at a moderate rate and then approaching a steady state. This implies that a short-time interdiffusion along with the establishment of entanglements by interchains within the interphase give rise to greatly enhanced properties of the interphase. It is suggested that polymer chains need only to interpenetrate by roughly an entanglement distance to provide an optimum adhesion, which then remains constant with further interdiffusion(Wu 1982).

Since the amplitudes of G* differ considerably at the different frequencies and temperatures measured, comparisons between temperatures have not been performed here. As mentioned before, the interphase can be seen as an equivalent blend, and it is hence expected that it should possess properties comparable to those of its equivalent blend. Here, for the sake of comparison, Figure III-17 presents the complex modulus (G*) of a blend (in a dashed line) with a similar composition to the interphase at steady state (as shown in Figure III-11) and determined under identical experimental conditions. As expected, as the time elapsed, G* of the interphase asymptotically approached the corresponding value of its equivalent blend,

indicating that the assumption was valid and that the rheology of the interphase is accessible.
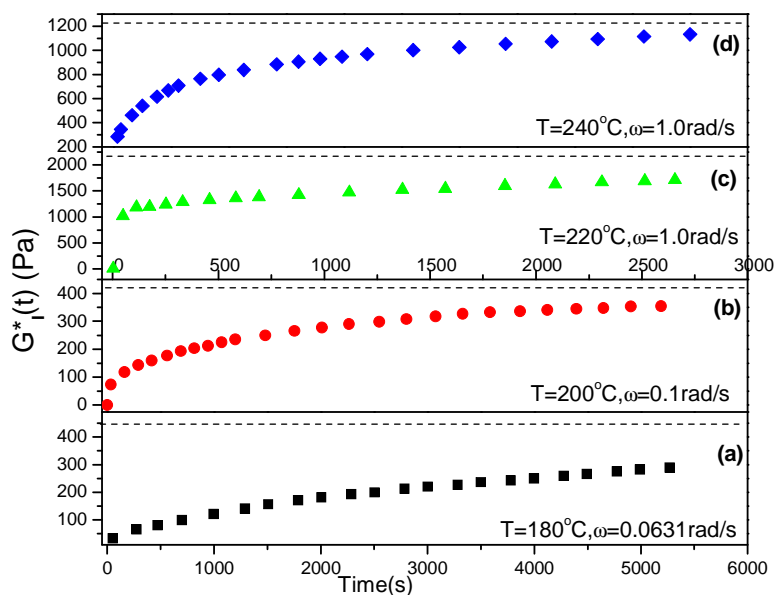
Figure III-17. Evolution of G*$_I$(t) of the interphase with time for a PMMA-2/PVDF sandwich assembly at various temperatures and ω at terminal zones: (a) 180 ºC, 0.0631 rad/s; (b) 200 ºC, 0.1 rad/s; (c) 220 ºC, 1.0 rad/s; (d) 240 ºC, 1.0 rad/s (the dashed lines indicate the G* value of corresponding blends under the same conditions)

Likewise, the variation of the interphase thickness with time can be obtained from the mutual diffusion coefficient determined by eq. (III-31). The resulting thicknesses of the interphase of a PMMA-2/PVDF assembly obtained at different temperatures are shown in Figure III-18. We can observe after mutual diffusion for 45 min that the thickness of the interphase can reach several dozens of microns (e.g. ~77 *µm* at 200 ºC), a similar order of amplitude as that found in the literatures. The numerically evaluated interfacial thickness of PMMA (M_w=1.5×10⁵ g/mol) and PVDF (M_w=1.88×10⁵ g/mol) reported by Wu et al. (1986) reached more than 40 µm after diffusion for around 1h at 190 ºC. The interphase thickness between PMMA (M_w=1.075×10⁵ g/mol) and PVDF (M_w=1.45×10⁵ g/mol) given by Kim and Han (1991) was also several tens of microns after 600s diffusion during coextrusion at 230 ºC. Feng et al. (2002) experimentally determined the interdiffusion distance of a PMMA/PVDF bilayer by time-of-flight secondary ion mass spectrometry chemical imaging (ToF-SIMS), and the interdiffusion distance was greater than 30 *µm* at 200 ºC after 1h. In fact, their interdiffusion distance was defined as the distance between the points at 20% and 80% of the plateau of the ion concentration profile, so the exact width of interphase defined from the migrating front on one side to that on the other side should be much greater than reported. Besides, a much earlier work (Gilmore, et

al. 1980) concerning using x-ray microanalysis as we did in the present study reported an approximate interphase thickness of 20 μm for a PMMA/PVDF sandwich laminate containing 76% PVDF as compression molded at 190 ℃ and 250 psi for 50 min. Overall, our rheological modeling of the interphase thickness gives a good corroboration with the earlier findings.
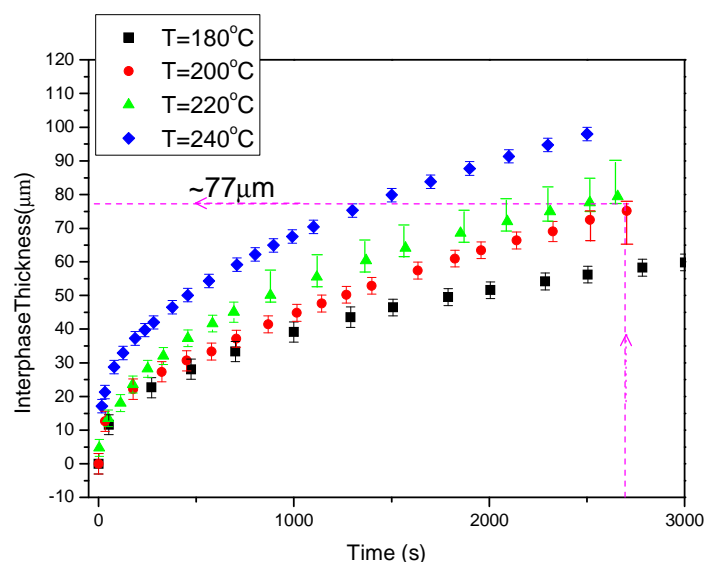
Figure III-18. Evolution of the interphase thickness with time for a PMMA-2/PVDF sandwich assembly at various temperatures

III.5.4.2 SEM-EDX and TEM analysis

In the above discussions, for the purpose of modeling, the interfacial region (interphase) was first assumed to be a homogenous blend. This was in fact an approximation. To further verify the validity of the rheological tool, a sophisticated spectroscopic tool, a combination of scanning electron microscopy and energy dispersive x-ray analysis (SEM-EDX), was employed to determine the concentration profile across the interphase of the specimens quenched from the interdiffusion process. This technique makes use of the phenomenon of electron-beam induced x-ray fluorescence of the characteristic atoms present in the sample, permitting direct measurement of the concentration gradient of one, or both components in the interfacial region. In the investigated mixtures, a unique fluorine (F) element of PVDF and oxygen (O) element of PMMA provided good elemental markers for PVDF and PMMA, respectively. By monitoring the changes of the atomic F and atomic O compositions across the interfacial region (interphase), one could obtain a general picture of the concentration profile of PMMA and PVDF versus their positions in the interphase. A line scan analysis including 20 points was conducted perpendicular to the interphase from an initial point within one bulk region (e.g., PVDF) to a final point lying in the other bulk region (e.g., PMMA). Micrographs

superimposed with a trace of the line scan where the points were collected for analysis are shown in Figure III- 19 for the quenched specimens annealed at ω=0.1 rad/s and ω=100.0 rad/s, respectively. In each point of the line scan, the x-ray data were collected by the EDX analyzer and a spectrum of the number of x-ray events of given energy as a function of x-ray energy was recorded. Since the number of x-ray events is directly proportional to the amount of the atom from where they originate, it can be used to measure the concentration profile of component versus position. A typical experimentally measured concentration profile of F and O element (quantified in portion of peak area, A%) was displayed in Figure III- 20a, with raw data of x-ray spectrum versus x-ray energy collected at 8th point and 13th point appended at left and right side, respectively. In the x-ray spectrum, the peaks of carbon at 0.2keV (Kα), oxygen at 0.5keV (Kα) and fluorine at 0.7keV (Kα) are greatly distinguished. In order to determine the concentration gradient of components more clearly, the concentration profile of element was normalized by removing the influence of background x-ray events and fluorine was used as a tracer element to map the normalized concentration of PVDF across the interface and thus measure the thickness of interphase triggered after interdiffusion. Figure III- 20b displays the concentration profile of two specimens obtained at different frequencies, i.e., 0.1 rad/s and 100 rad/s, at 200 ºC. The asymmetric profile shape indicates that the concentration profile is more broadening in the slower-diffusion component side (PMMA), that means, the distance penetrated by the PVDF phase into the PMMA phase is greater than the distance penetrated by the PMMA phase into PVDF phase. This asymmetry is greatly consistent with the prediction of the fast-mode theory (Kramer, et al. 1984). This supports our original assumption of fast-mode theoy in our theoretical deductions in the rheological part. The interfacial zone of the specimen of 0.1 rad/s (designated by a dashed square) where concentration gradient occurs gives us an approximate value of the interphase thickness of 85 μm, which is consistent with the result (~77 μm) received by the rheological tool (as shown by a purple dash denoted in Figure III-18). Likewise, in Figure III-20c, the good agreement between experimentally obtained concentration profile (diamond symbol) and the theoretical concentration profile (solid line) calculated using eq. III- 45 on the basis of D_m determined usig a χ=-0.07 in the rheological part also confirms a corroboration between the EDX and the rheology. This thus verifies the applicability of the rheological tool and the above modeling.
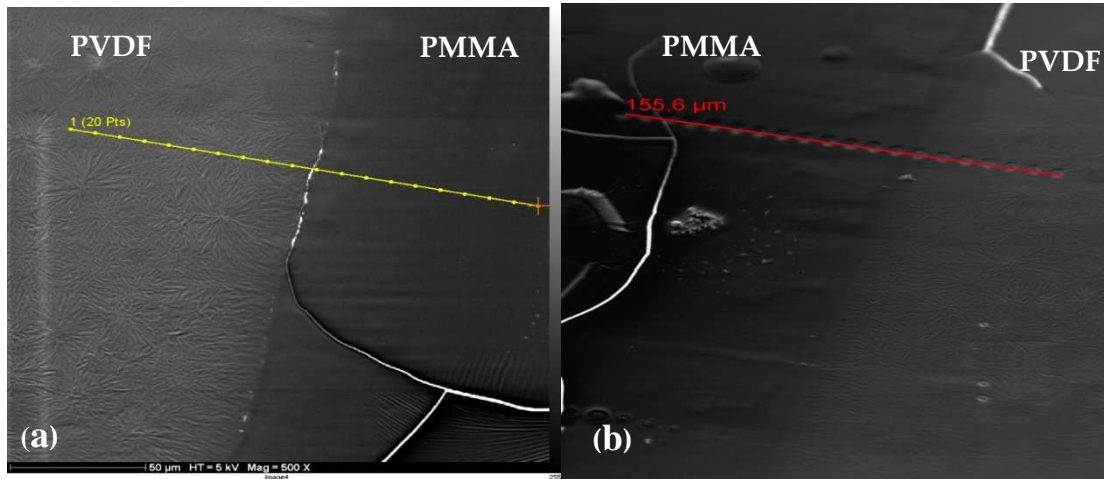
Figure III-19. Micrographs of the quenched specimens of PMMA-2/PVDF assembly with a trace of the line scan of the electron beam positions superimposed : (a) T=200 ºC, ω=0.1 rad/s; (b) T=200 ºC, ω=100.0 rad/s

(b)

(C)
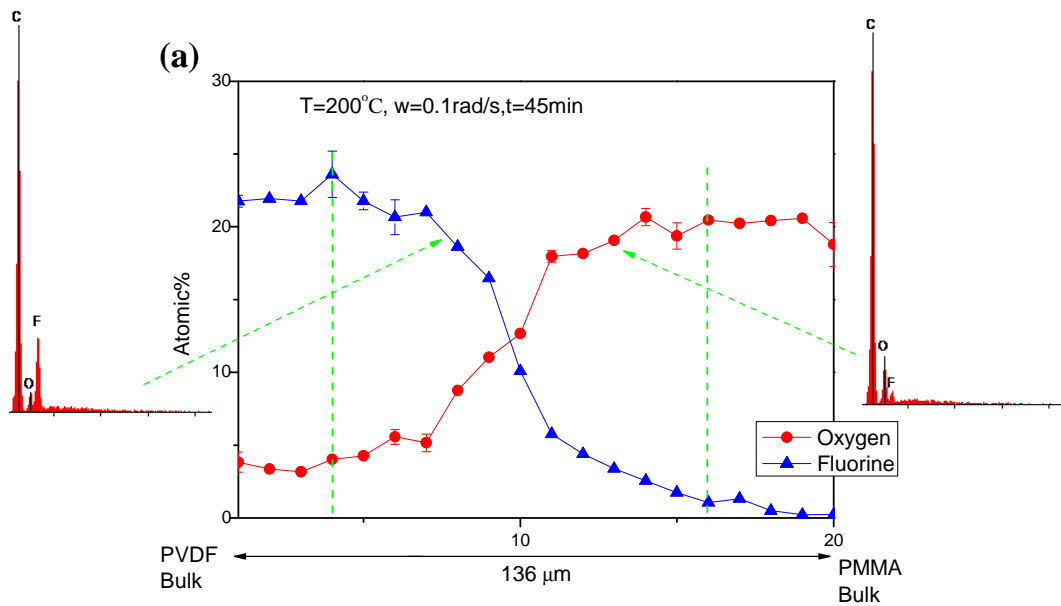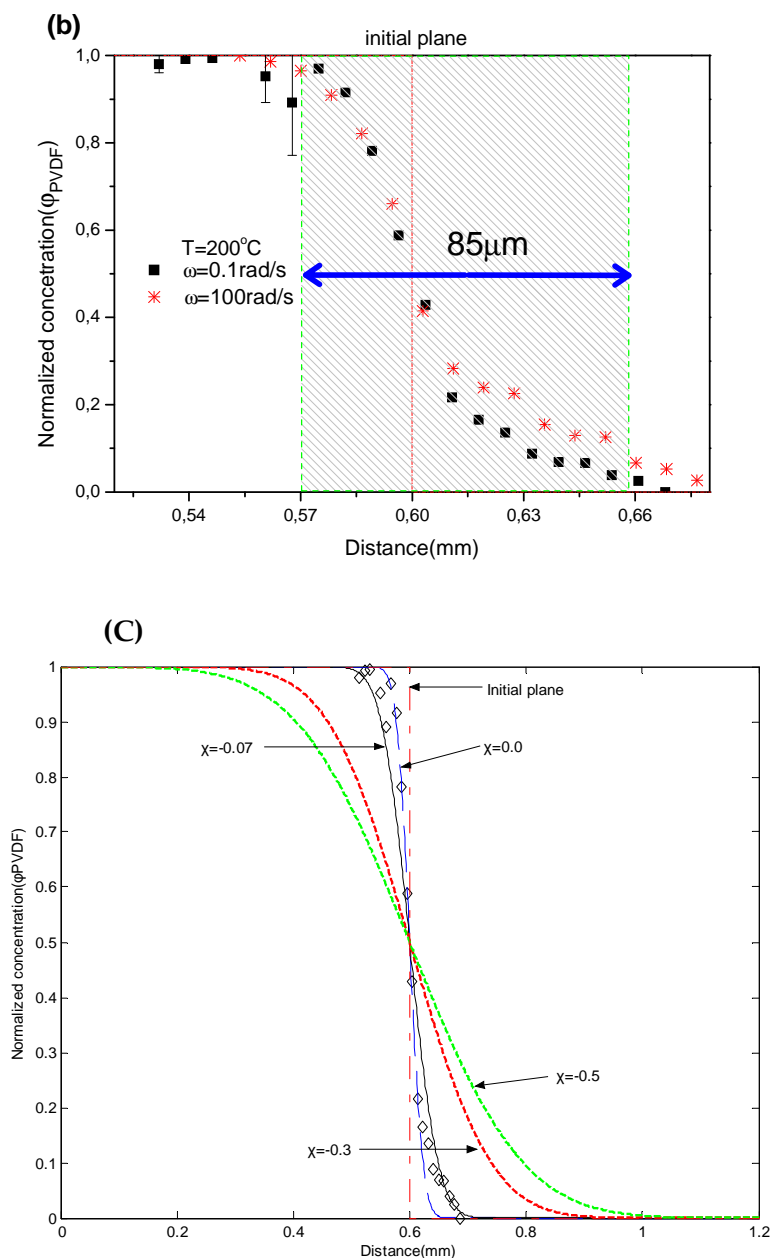
Figure III-20. (a) Example of EDX experimentally measured concentration profile of F and O (in atomic fraction) vs. measured positions for a PMMA-2/PVDF assembly quenched after 45 min diffusion at T=200 ºC, ω=0.1 rad/s; (b) Normalized PVDF concentration profile vs. distance (spatial axis z of the diffusion direction) for quenched specimens at ω=0.1 rad/s and ω =100.0 rad/s, respectively; the shadow zone designates the interphase (~85 *μm*) of the specimen at ω=0.1 rad/s; (c) Normalized PVDF concentration profile versus distance: experimental data from EDX (diamond symbol) and theoretical simulations of eq. (III-45) with D_m obtained from rheological approach using different χ. The thin dashed to thick dashed curves correspond to χ of 0.0,-0.07,-0.3and -0.5, respectively.

In addition, comparing to that of low frequency (0.1 rad/s), the profile shape of specimen with the diffusion performed at a high frequency (100 rad/s) was more

asymmetrical to the PMMA bulk and the interphase thickness was wider. This result implies that a too high angular frequency of the shear may accelerate the mutual diffusion process, perhaps due to that high-frequency shear deformation extracting more chain ends from the polymer bulks to the interface which has been presumed to favor diffusion (Bousmina, et al. 1998;Lamnawar and Maazouz 2006; 2008) and the possible orientation effect if it exists. We will verify the effect of shear deformation more precisely in the near future . One may undoubtedly tend to use the apparent D_m determined at 100 rad/s to calculate the interphase thickness in this case, but one should keep in mind that the rheological functions determined at high frequencies reflect information of small motion units, like segmental motion, chain bonds or chain angles motions, etc. We have indeed tried to determine the theoretical interphase thickness in this way, but obtained a much higher value than that from EDX (which corresponds to diffusion of the whole chain). This again confirms that only the rheological functions determined from terminal zones reveal the truth of the diffusion process of whole chains.

Of additional particular interest, as presented in Figure III-19, is the morphological phenomenon displaying a crystalline phase and an amorphous phase separated by a distinct boundary. A micrograph obtained at higher magnification via transmission electron microscopy (TEM), exhibited in Figure III- 21, gives a clearer view of the morphology of the specimen after 45 min of mutual diffusion. Upon cooling from the melt, PVDF in the interphase can either crystallize or remain amorphous depending on the cooling rate and the composition. The blend (interphase) with a composition of more than 60 wt% PVDF tended to crystallize below the crystal melting point to form spherulites. On the other hand, the blend (interphase) with less than 60 wt% PVDF remained amorphous upon cooling, as also reported in the literature(Wu, et al. 1986). This results in a clear boundary at 60% PVDF in the micromorphology of the interphase, distinguishing the crystalline phase in PVDF-riched side and the amorphous phase in PMMA-riched side. The crystallinity was not expected to affect the measured concentration profile(Gilmore, et al. 1980).
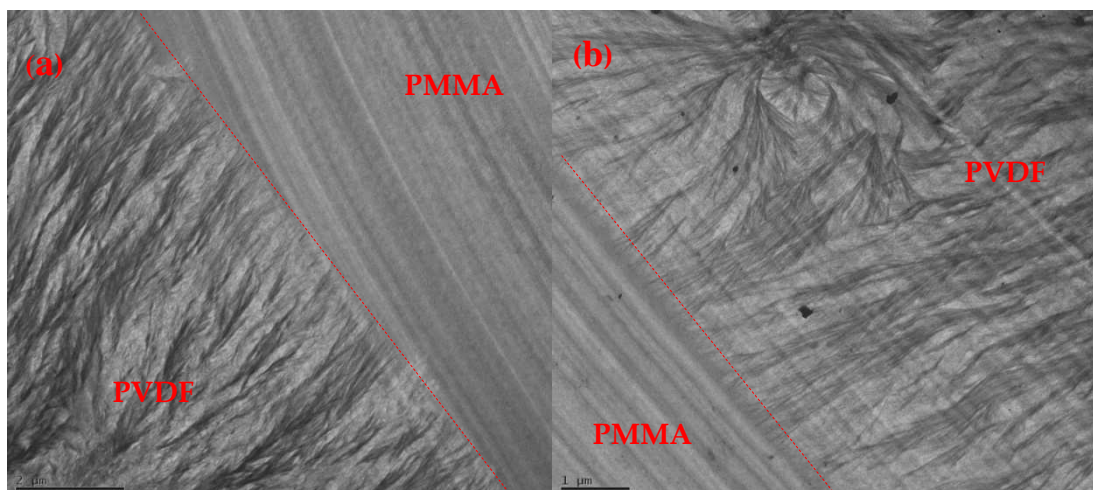
Figure III-21. TEM micrographs of a quenched specimen of the PMMA-2/PVDF assembly after 45 min diffusion at 200 ºC, (a) ω=0.1 rad/s; (b) ω=100.0 rad/s

III. 6. Conclusions

This paper presents investigations of the mutual diffusion process and the interphase (interfacial region) development taking place in the molten state at the interface of an asymmetric model bilayer consisting of well-characterized PMMA with varying molecular weights and PVDF polymers from macro- to molecular scale via a method of rheological modeling in combination with spectro- and microscopical tools. Before this work was done, the component dynamics in PMMA/PVDF blend was examined by rheology and compared to the prediction of Lodge-McLeish model. As well, the validity of tTS principle to such blend was tested over wide composition. Results indicated that despite of a large difference between T_g of PMMA and PVDF (dynamic asymmetry), the failure of tTS principle is subtle and the ζi (φ,T) of each component determined at same conditions are close due to the fact that the strong intermolecular interactions between the components attenuates the dynamic heterogeneity and concentratrion fluctuations. Thus, PMMA/PVDF could be concluded to be a pair of weak thermodynamic complexity, if they were not absolutely thermodynamic simple. Basing on this physics, rheological modeling of the mutual diffusion kinetics at polymer/polymer interface with an aim to explore the interfacial rheology was performed from a viewpoint of the generated interphase by connecting the mobility at the interfacial region to the viscoelasticity of the interphase using a presumably apparent friction resistance factor. The rheological model was modified from a primitive model of Qiu and Bousmina by taking into account of the effect of the viscoelasticity of interphase on the mutual diffusion kinetics, which appears to produce a greater D_m.

With this modified model, the effects of relevant annealing factors like welding time, angular frequency, temperature and other structural properties as well molecular weight and Flory-Huggins parameter on the kinetics of diffusion and the

interphase development have been highlighted. On one hand, the apparent D_m was found to decrease as decreasing angular frequency (ω) until the terminal zone of ω was arrived where the apparent D_m remained invariable. This is related to the motions of different chain sizes revealed by different angular frequency windows, particularly the chains of all sizes were involved in the terminal zone. Arrhenius equation was able to describe the temperature dependence of the D_m with activation energy close to that of the PVDF species. Moreover, the D_m was demonstrated to be nearly independent of the chain length of the slower PMMA species, thus corroborating the fast-mode theory. On the other hand, the modified rheological model allows us to monitor the proper rheological behavior and thickness of the interphase triggered between neighboring layers. The interphase owned similar rheological properties with its equivalent blend and could reach a thickness of dozens of microns under the experimental conditions in the present work.

More importantly, Optical observation and EDX characterization on the quenched specimen after interdiffusion were introduced to validate the rheological modelings in terms of interphase thickness and concentration profile. The EDX analysis gave a concentration profile versus position in the interphase at a high resolution, where the profile shape was asymmetrical on slower species which greatly supported the prediction of fast-mode theory. To compare the experimental results of EDX with the ones of the rheological modeling, a similar theoretical concentration profile based on the D_m of rheological modeling was mathematically established according to a simple solution of Fickian equation. In the mathematical modeling of concentration profile, the D_m calculated from various χs was examined, among which $\chi=-0.07$ gave the best match between the theoretical concentration profile of rheological modeling with the experimental ones of EDX results as well as the interphase thickness and corroboration between rheological modeling and EDX analysis was achieved. Furthermore, both the D_m results and the interphase thickness obtained in rheological modeling were compared to be consistent with those determined by other techniques in literatures. Additionally, from EDX results, it was noted that a higher angular frequency may slightly accelerate the interfacial diffusion process as a result of the excess chain ends at the interface extracted from the bulk. The morphology examined by TEM confirmed the presence of amorphous structure in PMMA-riched side and crystalline structure in PVDF-riched side in the interphase. In sum, on the basis of a full understanding of the miscible blend of weak thermorheological complexity, like PMMA/PVDF couple, the rheological modeling seemed to be a suitable and sufficient tool, as validated by spectra- and optical measurements, to quantify the effects of healing time, angular frequency, chain length and temperature on the interdiffusion kinetics and to probe the geometrical and rheological properties of the triggered interphase between an asymmetrical compatible neighboring polymer layers. This is a key issue in further prospects to give a better understanding and comprehension on the generation of the interphase triggered in the relevant system.

Supporting Information III-A

By substituting eq. (III- 32) into eq. (III-23), we have

$$K \cong \omega^2 \left(\frac{8G_N^0}{\pi^2 G^*(\omega)} \right)^2$$

$$= \omega^2 \left(\frac{8G_N^0}{\pi^2} \right)^2 \left[\frac{H}{2(D_m t)^{1/2}} \left(\frac{1}{G_{s,t}^*} - \frac{1}{G_{s,0}^*} \right) + \left(\frac{\varphi_A}{G_{A,0}^*} + \frac{\varphi_B}{G_{B,0}^*} \right) \right]^2 \qquad \text{(III-S1)}$$

Thus eq. (III-24) can be rewritten as

$$D_m = \delta\omega \left(\frac{8G_N^0}{\pi^2} \right) \left[\frac{H}{2(D_m t)^{1/2}} \left(\frac{1}{G_{s,t}^*} - \frac{1}{G_{s,0}^*} \right) + \left(\frac{\varphi_A}{G_{A,0}^*} + \frac{\varphi_B}{G_{B,0}^*} \right) \right]$$

$$= \left(\frac{8\delta\omega G_N^0}{\pi^2} \right) \frac{H}{2t^{1/2}} \left(\frac{1}{G_{s,t}^*} - \frac{1}{G_{s,0}^*} \right) D_m^{-1/2} + \left(\frac{8\delta\omega G_N^0}{\pi^2} \right) \left(\frac{\varphi_A}{G_{A,0}^*} + \frac{\varphi_B}{G_{B,0}^*} \right) \qquad \text{(III-S2)}$$

where δ is a parameter defined as eq. (III- 36). If we substitute the right-hand side of the above equation by the new parameters p and q defined according to eq. (III- 34) and eq. (III-35), eq. (III-S2) can be reduced to a cubic equation of $D_m^{1/2}$,

$$\left(D_m^{1/2} \right)^3 - p D_m^{1/2} - q = 0 \qquad \text{(III-S3)}$$

with a sole real root:

$$D_m^{1/2} = \frac{(2/3)^{1/3} p}{\left(9q + \sqrt{3}\sqrt{-4p^3 + 27q^2} \right)^{1/3}} + \frac{\left(9q + \sqrt{3}\sqrt{-4p^3 + 27q^2} \right)^{1/3}}{2^{1/3} 3^{2/3}} \qquad \text{(III-S4)}$$

Eq. (III-S4) gives the eventual result of a mutual diffusion coefficient as shown in eq. (III- 33).

Supporting Information III-B

1. Fit the blend rheology by modified "double reptation" model
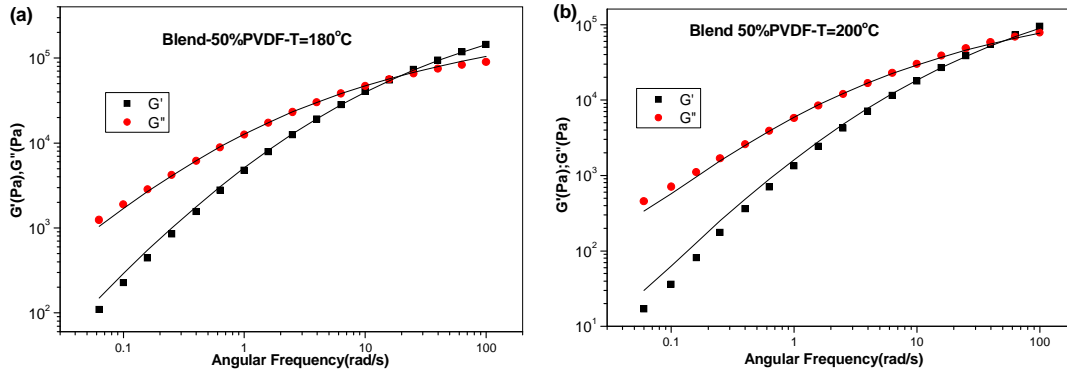
Figure III-S 1. Experimental data of blend fitted by modified Tsenoglou version of "Double reptation"model. Solid lines denote the fiting curve of the double reptation model.

As an example, the fittings of the modified "double reptation" model, i.e. eq. III-37 and eq. III-38 to the experimental data of PMMA/PVDF 50/50 blend at 180 ^{o}C and 200 ^{o}C are shown in Figure III-S1. On fitting, the component shift factors $a_{T,a}$ and $a_{T,b}$ in eq.(III-37) and eq. (III-38) were adjusted until the best fit to the experimental data was obtained.

2. Van Gurp and Palmen curve to test the tTS principle

(b)

(c)
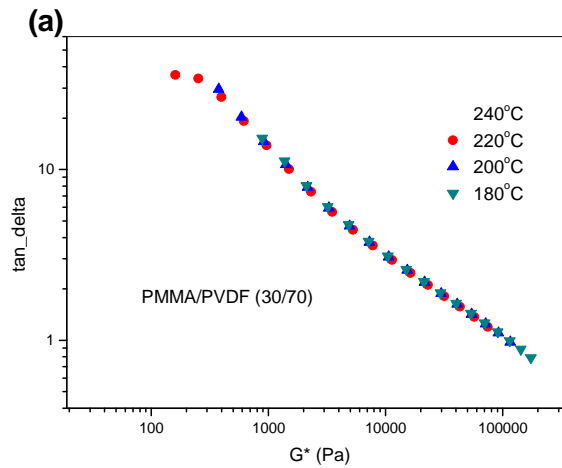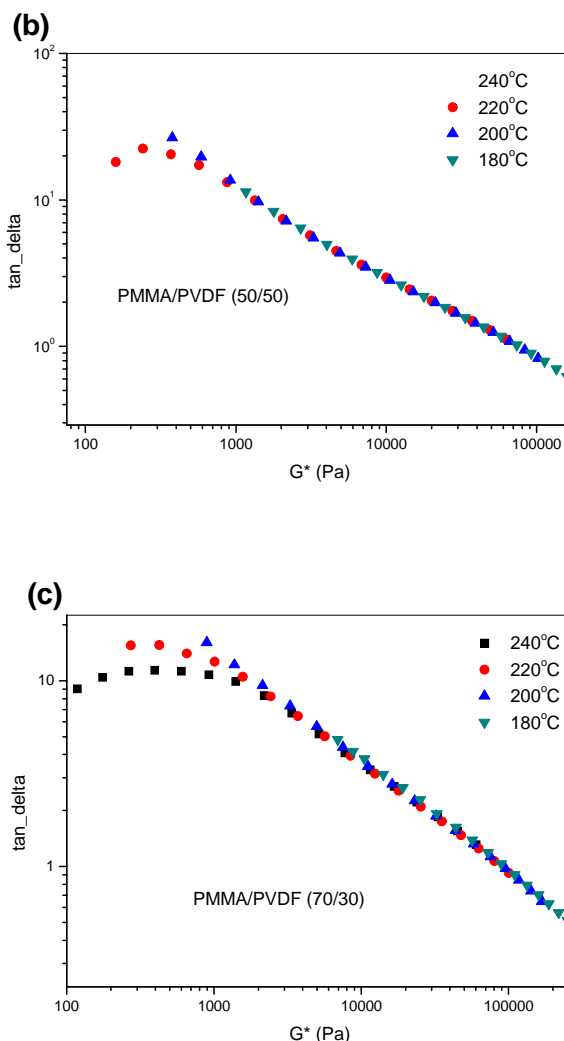
Figure III-S 2. Tan phase angle as a function of absolute value of the complex modulus at various temperatures for: (a) PMMA/PVDF 30/70; (b) PMMA/PVDF 50/50; (c) PMMA/PVDF 70/30

In addition, the tan phase angle was plotted against the absolute value of the complex modulus according to Van Gurp and Palmen method(Van Gurp and Palmen 1998)(Figure III-S2). This way of plotting eliminates the effect of shifting along the frequency axis, and yields temperature independent curves when tTS holds. Moreover, direct insight into the amount of a resulting vertical shift is readily observed, which cannot be seen from a G'-G" plot. Evidently, tTS principle holds well for the blends particularly for that of low PMMA volume, but fails a bit at the terminal zone for the blends of high PMMA volume.

Chapter IV: Nonlinear Rheology of Interphase: Relaxation after a Step Strain, Startup Shear and Uniaxial Extension of PMMA/PVDF Compatible Multilayers

IV.1. Synopsis:

This work aims to examine whether or not nonlinear transient rheology of multilayered polymer structures in both shear and extensional flow are sensitive to the presence of the diffuse interphase generated at neighboring layers. For this, experiments of stress relaxation after a step strain, fast startup in simple shear and in uni-axial extension have been performed to PMMA/PVDF alternating multilayers with presence of well characterized diffuse interphase using multilayers without interphase as a reference. Firstly, nonlinear rheology of the neat PVDF and PMMA melts has been focused. In nonlinear step strain, time-strain factorability was found to occur around the terminal relaxation time. Damping functions were determined for PMMA and PVDF melts, which belong to type A and type B, respectively. In fast startup shear, typical features of stress overshoot and "strain softening" were evident for the neat melts at Weissenberg number $W_i > 1$. In fast startup uni-axial extension, "strain hardening" behavior was found for the PVDF melt whereas the studied PMMA melt displayed a "strain softening". These nonlinear features are interpreted under the framework of Doi-Edwards theory incorporating "convective constraint release" and under some recent theoretical scenarios of entanglement network yielding as well as dynamic tube confinement barrier breakdown under stress. Secondly, an original model has been developed to describe the relaxation behavior of multilayer systems after step strains, which well captures main tendencies of experimental results, and is able to estimate the relaxation modulus $G(t,\gamma)$ of the interphase. For the un-annealed bilayers, interfacial failure happens at intermediate deformations (and intermediate W_i) in both step strain and startup shear measurements. The $G(t,\gamma)$ in relaxation and the transient viscosity η^+ in startup significantly fall down from their theoretical predictions. Meanwhile, for the annealed bilayers, the triggered interphase greatly delays the interfacial failure to a larger deformation in step strain and to a higher deformation rate in startup shear. Such failure at the interface/interphase, as a result of entanglement strands breakdown under stress after and/or during large external deformations, may be due to entanglement lack at the interface and entanglement weak intensity at the

---

This chapter is to be submitted to *Journal of Rheology*

interphase. In startup uni-axial extension, presence of certain interphase that bridges the gap at the interface could enhance the transient extensional viscosity $\eta_E^+(t)$ of the structure. After saturation, as the interphase fraction of the structure was increased as realized by mounting layer number, its weaker entanglement intensity in comparison to the bulks makes the $\eta_E^+(t)$ of the total structure subtly decline, approaching their equivalent blend. Moreover, the elongation rheology was also shown to be sensitive to the "strain softening" weakening with increasing interfacial area. After all, the interface/interphase at multilayer structures is able to be distinguished in nonlinear rheology due to their sequential easy "microscopic yielding" upon external deformations.

IV.2. Introduction

In multiphase systems like blend and multilayer structures, an interphase (a nonzero thickness physicochemical zone as opposed to a purely geometrical plane interface) can be generated either from interdiffusion process in compatible systems or from interfacial reaction in reactive systems or from both of them in some other cases. Literatures reporting on rheology of the multiphase systems with the interphase involved are numberless during the past decades (Utracki 1995; Lamnawar, et al. 2013). A common finding is that presence of an interphase at multiphase systems enables some variations in linear viscoelasticities of the system (Kim, et al. 2003;Lamnawar, et al. 2010a). As did in the literature, we have also observed in our earlier work that generation and growth of the interphase triggered from interdiffusion process is sufficiently sensitive to intrigue variation of linear rheological response (Zhang, et al. 2013).

Nevertheless, effect of the thick interphase on the nonlinear rheological properties is still an open question. To the best of our knowledge, very few researches have been dedicated to the nonlinear rheology especially in transient regime of multilayer system, such as fast startup shear and extensional deformations and stress relaxation after step strains. Levitt et al. (1997) demonstrated extensional rheometry to be a sensitive tool to the interface at reactive multilayer structures. Amount of interface can be well defined using multilayer structures and interfacial effects could be amplified during stretching in extensional measurements since interfacial area per unit volume is increased. In their work, the interfacial tension for the incompatible pairs was able to be determined and strain hardening was found for the reactive pairs via the extensional rheology. Thereafter Saito and Macosko (2002) attempted to extract the interfacial stress from the measured extensional forces and determine the extent of interfacial crosslinkings via extensional rheology based on reactive and compatible coextruded multilayers. It is worthy of mentioning that in a recent work of Silva et al. (2012), the authors gave some experiments including stress relaxation and extensional rheology, etc. to compare sensitivity of different rheometrical techniques to the existence of the interface/interphase in coextruded

thermoplastic urethanes (TPU). Even though the results obtained are very fruitful and inspiring, properties of the interphase have yet been quantitatively revealed and explanations in a deeper level are still needed for the multilayer structures because of the complex structure of TPU. Indeed, hitherto systematical studies of nonlinear rheology of multiphase systems are rather sparse. This is partly attributed to the immaturities of theoretical interpretation at microscopic level for polymers in the field of nonlinear rheology. In other words, rheological response of entangled flexible polymer chains under large external deformations is still far from full understanding, let alone the multiphase systems composed of different polymer chains.

Till recently, linear viscoelastic response of entangled polymer liquids could be well interpreted under the framework of tube model that proposed by de Gennes (1971) and improved by Doi-Edwards(1986). This Doi-Edwards (DE) tube model describes the dynamics of test chain by simplifying the effect of geometrical constrain of neighboring chains (entanglement effect, dynamic consequence of chain connectivity and uncrossability of interpenetrating chains) into a confining tube with a certain contour length and tube diameter. This DE model treats the intermolecular interactions of surrounding chains as an effectively static confining potential that strictly prohibits transverse motion of the test chain within a virtual tube. The dynamic effect of intermolecular forces is simply represented by the tube and the parameter of tube diameter. Indeed, basic features of polymer dynamics at equilibrium state in the linear viscoelastic regime are able to be sketched via the reptation motion of segment and/or full chain within the tube and the one-dimensional curvilinear diffusion along the tube.

In nonlinear viscoelastic regime of large external deformation, the DE model succeeds in its qualitatively description of the nonlinear stress relaxation modulus of linear entangled chains in step strain experiments. The DE model prediction of a universal damping function has good agreements with experimental results for a range of entangled polymer solutions. It also succeeds in predicting the features such as stress overshoot during fast startup shear measurements. Despite of this, failures of the DE model have been widely reported in describing some experimental observations especially in nonlinear regime for entangled polymers. For instance, it is unable to explain the observed difference in polymer rheological behavior in simple shear and extensional flows (Mhetar and Archer 1999)]. Specifically, major disparities between theoretical predictions and experimental observations have been addressed in ref. (Hua, et al. 1999). It also fails to explain some recent observations of various strain localization phenomena such as shear banding and nonquiescent relaxation(Wang, et al. 2013). Recently, numbers of experimental and simulation studies (Sussman and Schweizer 2011a; 2012a;2012b;Tapadia and Wang 2006;Wang, et al. 2011; Larson 2007;Likhtman 2009;Wang, et al. 2007;Wang, et al. 2013) have been emerging to challenge the confining tube concept of the DE model in sense that this model is phenomenological rather than first-principles-based since it lacks

microscopic foundation on delineating the origin of chain entanglement.

Drawback of the DE model in nonlinear rheology lies in its oversimplification of extraordinarily complex many-body system into a single chain picture by treating intermolecular force as infinitely strong tube constraints and restricting the transverse motion to a mesoscopic space known as tube diameter. The stress could be evaluated from the intrachain force. Doi and Edwards assumed for simplicity that stress does not modify the tube diameter. The DE model explains response of the entangled polymer chains to the fast large external deformation on basis of chain orientation and stretching in the tube. In fact, many evidences imply that stress could induce tube dilation and reduction of entanglement upon large fast shear or extensional deformations. One important advance improving the DE theory is the proposal of "convective constrain release"(CCR) mechanism by Marrucci (1996). The CCR mechanism reduces the effectiveness of entanglement constraints, thus remedies the excessive levels of orientation and shear thinnings predicted by the original DE model, and enables to indicate that continuous shearing flows convection accelerates molecular relaxation. The essential idea of the mechanism is that continuous shearing flows convection accelerates molecular relaxation at condition of intermediate shear rates (i.e., Rouse Weissenberg number $W_{iR} \ll 1$ and $W_i > 1$), thus the relaxation is described by a form as $\tau^{-1} = \tau_{rep}^{-1} + \dot{\gamma}$, where $\dot{\gamma}$ is the flow rate.

At this conjunction, to complete the shortcomings of the DE model in the theoretical framework for the entangled polymer in nonlinear rheology regime, Wang and coworkers(2007, 2009, 2013) outline a different picture by treating the entangled polymer system as a dynamic network junction formed by localized intermolecular interactions. Their network-like picture recognizes the explicit role of intermolecular interactions at the entanglement points instead of representing the intermolecular interactions in a smoothed-out, uniform way by using a virtual confining tube as did in the DE theory. In their picture, response of an entangled polymer to external deformation is analyzed from an aspect of forces balance, including the intermolecular gripping forces f_{img} caused from chain uncrossability upon external deformation, intrachain elastic retraction force $f_{retract}$ and entanglement force f_{ent} associated with the entropic barrier that provides the structural integrity or cohesion of the entanglement network. The force imbalance of these forces and the accompanying chain sliding at the entanglement points was asserted to be the molecular mechanism for the observed macroscopic nonlinearity either during startup deformation or after a large stepwise strain. They envision a picture that the stress overshoot during startup shear is a consequence of molecular disentanglement in contrast to the tube model picture of the chain orientation (Wang, et al. 2013).

In parallel to the work of Wang et al., Sussman and Schweizer (2011b; 2012a;2012b; 2013) recently developed a new self-consistent microscopic dynamic theory for the transverse tube confinement potential of topologically entangled rigid polymer chains under quiescent and stressed conditions. Rod-like polymer was

considered in their studies at the first step for analytical simplicity purpose to develop the microscopic theory before extending it to the more practical complex situation of topologically entangled flexible polymer chains (Sussman and Schweizer 2012b). The basic of this theory is its postulation of anharmonic nature of the dynamic tube confinement potential and that the dynamic entanglement force localizing a polymer in a tube is of finite strength. As a consequence, the theory is formulated by taking into account of a time- and deformation-dependent (dilated) tube diameter, a maximum confinement force and a transverse entropic barrier. For the situation under stress, two competing parallel time-dependent relaxation channels were addressed: (i) deformation-modified reptative rotational relaxation and (ii) transverse activated barrier hopping (tube breaking) relaxation process. Under equilibrium conditions, the theory is consistent with the DE theory in describing the reptation relaxation and rotational/transverse center-of-mass diffusion kinetics. Their microscopic theory has been implemented to treat the stress relaxation after a nonlinear step strain(Sussman and Schweizer 2012b) and during a continuous startup shear deformation(Sussman and Schweizer 2013), respectively. It was predicted that tube dilation resulted from external deformation accelerates the terminal rotational relaxation and at sufficiently high deformations the competitive transverse hopping relaxation occurs. In other words, the entanglement network is to breakdown after a large enough strain and the tube is destroyed in a manner akin to a microscopic yielding event. This gives rise to a ultrafast relaxation of stress and orientation in a time shorter than terminal relaxation time. Thereafter the entanglement constraints and confining tube re-forms as stress relaxes and the polymer chain returns to an unperturbed reptative relaxation process at long times. In startup shear deformation, the stress overshoot was interpreted based on an idea that the tube is only transiently destroyed in the vicinity of the stress peak but then re-forms at a very weak level in steady state(Sussman and Schweizer 2013).

At present, the question of whether lateral constraints are still present during fast large deformations and how large deformations soften, or even destroy the confining tube is a frontier issue. Both the pioneering work of Wang and coworkers as well as Sussman and Schweizer give some basic physics for understanding of the nonlinear rheology of entangled polymer liquids. Although the discovery of the microscopic physics for nonlinear rheological response of the entangled polymer chains in bulk system is still on the way, we attempt to extend this type of investigation to the multiphase systems, i.e., multilayered structures in this work. The investigation will be two-folds, that is, nonlinear rheology of neat polymer melts and that response of multiphase systems. We have to remain that for compatible multilayered structures having been studied in our earlier work, a well-defined diffuse interphase could be formed from interdiffusion and here we aim to reveal the nonlinear response of the interphase. For this sake, systematic rheological experiments in nonlinear regime have been carried out to explore the transient rheological responses of the interphase during the fast startup shear and uniaxial

extensional measurements as well as its stress relaxation after a single step strain. Experimental results will be discussed under different theoretical pictures, such as the DE tube theory and the force imbalance concept in the scenario of Wang et al.(2007, 2013) as well as the first principle microscopic theory proposed by Sussman and Schweizer (2011b; 2012b) for the transverse tube confinement potential of topologically entangled rigid polymer chains under quiescent and stressed conditions.

To make a definite microscopically theoretical description of polymer entanglement behavior under large fast external deformation is quite a formidable task, let alone depicting how they behave in mixed state (multiphase systems) where different polymer chains are involved. That is why so far most of the studies of shear stress relaxation behavior are dedicated to monolayer of entangled polymer and/or blend systems, laying a blank in the field of multilayered polymer systems. Hence, in the present study, we only give some exploring work in the field of nonlinear rheology of multiphase systems and attempt to give some potential conclusions. Originality in this study includes: 1) stress relaxation, startup in shear and extensional measurements of PVDF and PMMA melts; 2) discovery about nonlinear rheology of the multilayered structures composed of these melts in both cases with (i.e. annealed bilayer) and without (i.e. unannealed bilayer) interphase; 3) proposal of a more accurate model to describe the stress relaxation behavior of multilayered structre rather than the simple linear additivity and reciprocal rule; 4) introduction of interphase with large fractions (i.e., higher layer number) in multilayered structures to investigate its contribution in extensional measurement.

IV.3. Experimental Section

IV.3.1 Materials

The polymers employed in this study were Poly (methyl methacrylate)(PMMA) and poly(vinylidene fluoride) (PVDF) supplied by ARKEMA. Main material characteristics of these polymers are listed in Table IV-1. More characterization information of the polymers could be found in our earlier work(Zhang, et al. 2012; 2013).

Table IV-1 Characteristics of the investigated polymers

Samples	Trademark/Supplier	$T_c(^oC)^a$	$T_g(^oC)^a$	$T_m(^oC)^a$	M_w^b(g/mol)	M_w/M_n^b	Ea(KJ/mol)[c]
PVDF	Kynar 720/ARKEMA	136.40	-42	170	210,000	2.0	59
PMMA	V825T/ ARKEMA	——	112	——	100,000	1.9	160

[a] measured in our laboratory by a TA Instruments Q20 DSC at a heating and cooling rate of 10 ºC/min under N_2. [b]determined in our laboratory by size exclusion chromatography (SEC) with tetrahydrofuran (THF) as the eluent for PMMA and dimethyl formamide(DMF) for PVDF. [c] energy of activation of the viscous flow (Ea) obtained from a master curve at a reference temperature of 220 ºC.

IV.3.2 Sample preparation

All the polymers were dried at 80 ℃ under vacuum to remove any moisture before use. Samples for the rheological measurements were prepared by compression molding at 180 ℃ with a pressure of 200 bar between two Teflon films to obtain a smooth surface. The obtained samples were then cut into round disks with a diameter of 25 mm. All samples were prepared under identical processing conditions to eliminate sample to sample errors. To eliminate the possible effect of surface orientation brought about by the compression molding, all the disks were annealed at 80 ℃ under vacuum for at least 24h before measurements.

IV.3.2.1 Bilayer systems

The bilayer assembly for the diffusion process was prepared by bringing round disks of PMMA and PVDF with individual thicknesses of 0.6 mm into intimate contact at room temperature with a desirable configuration before loading them between the parallel plates and annealing them at the measured temperature in the oven of the rheometer. It is noticed that the gap was set to be equal to the total thickness of bilayer (1.2 mm) in sake of avoiding effect of external compression pressures, which were indeed believed to strengthen the diffusion process, making the investigation more complicated.

IV.3.2.2 Multilayer prepared from coextrusion

In order to amplify the amount of interphase and hence the interfacial effects, alternating multilayer structures of different layer numbers with a constant composition of 50% were prepared. They are PMMA/PVDF bilayers, PVDF/PMMA/PVDF- 3layers and PMMA/PVDF/PMMA/PVDF/PMMA- 5layers. Coextruded multilayer structures were prepared via a coextruder setup consists of extruder A (d=18mm, L/D=25) (for PMMA) and extruder C (d=15mm, L/D=25) (for PVDF). Variation of the layer number was realized by changing feedblock system in the coextruder setup, whereby the polymers were brought together and arranged into more than two alternating layers. The thickness ratio of the layers was determined by varying the flow rate of each polymer melt, for which a calibration curve was created beforehand by adjusting the screw rate of extruder from 5 to 65 rpm/min. After exiting the die, the multilayer film passed over a water-cooled double chill roll and quenched to room temperature. The total thickness of the coextruded multilayer film is ~250 μm. More details about the processing procedures are to be shown in next chapter.

IV.3.3 Rheological measurements

IV.3.3.1 Small-Amplitude Oscillatory Shear (SAOS) Measurements

Linear viscoelasticities of neat polymer melts have been measured at different temperatures in both strain-controlled rotational rheometer, i.e. ARES (Advanced

Rheometrics Expansion System, Rheometric Scientific, Inc.) and stress-controlled rotational rheometer, i.e. DHR-2 (Discovery Hybrid Rheometer, TA instrument) with a parallel plate geometry(diameter ϕ=25mm). During all the rheological experiments including nonlinear shear and extensional measurements (see below), nitrogen purging was maintained throughout the tests to avoid the potential degradation and oxidation of the polymers. In this chapter, results of linear viscoelasticity are those determined in stress-controlled rheometer. For clarity purpose, details about the annealing process of bilayers as monitored by SAOS measurements have been presented in previous chapters, only some results of which are used in this chapter.

IV.3.3.2 Stress relaxation after a single step strain

Step strain experiments were carried out in both the stress-controlled rotational rheometer, DHR-2 and the strain-controlled rotational rheometer, ARES, for comparisons. In this work, as bilayer structures are involved, a parallel-plate geometry (diameter ϕ=25mm) was used. It was reported that the determination of the relaxation modulus in the parallel-plate geometry requires a correction associated with the nonhomogeneity of the strain at large strains(Soskey and Winter 1984). The corrected moduli may be lower than the apparent moduli especially at large strains, but the deviation is not very significant for those of small and intermediate strains. For simplicity purpose, in this work, no correction is considered, rather, we regard the measured strain as a nominal strain. This does not have fatal effects on our discussions associated with the bilayer structures.

The specimen was lay at rest for few minutes at measurement temperature to eliminate the axial force caused from the loading process and the specimen should be completely relaxed prior to the imposition of the step strain. The purpose of equilibrating the samples for several minutes before measurement is also to avoid wall slip by increasing the adhesion between the polymers and metal. In this work, disposable alunium plates were used for the measurements, as it was reported that polymers are easiser to attach to the alunium plates than that of steels (Ferri and Greco 2006; Gevgilili and Kalyon 2001). Note that as did by Gevgilili and Kalyon (2001), a straight-line marker line could be used to document whether or not the wall slip behavior happens during the step strain experiments. The straight marker line was placed to cover the edges of the fixtures and the free surface of the specimen before the step strain was imposed. During the imposition of the shear strain, the motion of the fixture and the resulting deformation of the specimen at its edge were continuously monitored and recorded with the cameras.
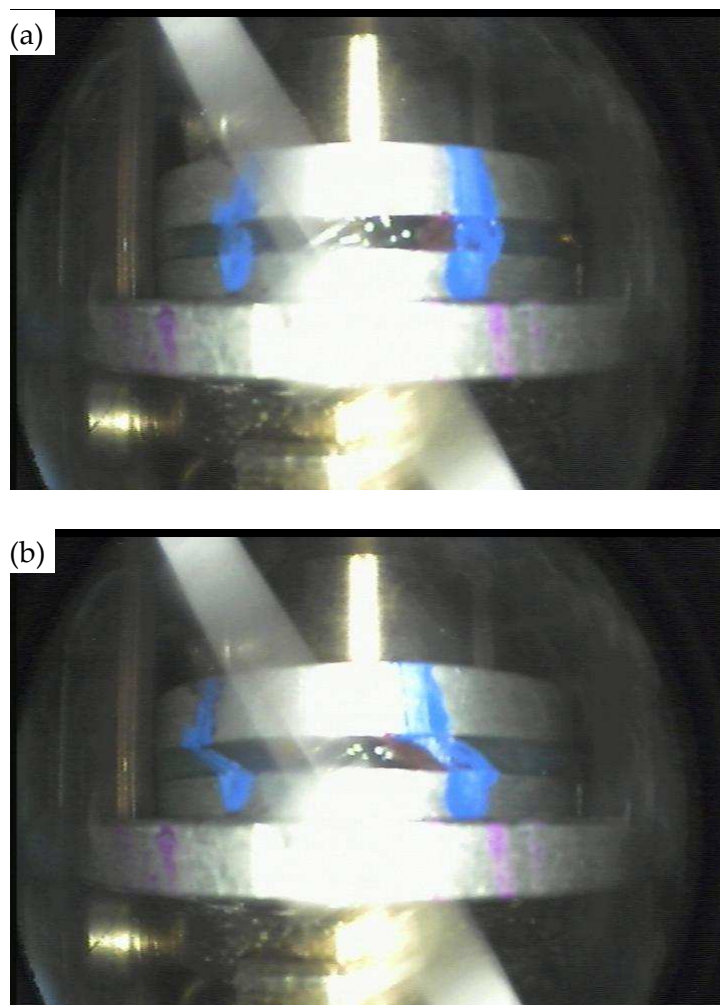
Figure IV-1. Images of the PVDF melt in a step strain experiment with a commanded strain at T200 ℃: (a) before step strain; (b) after a step strain of 5.0. Continuity of the straight marker line indicates no wall slip.

As shown in Figure IV-1 is an example of PVDF melt with a step strain of 5.0 commanded, where continuity in the marker line at the metal/polymer melt interface was clearly observed. This indicates that no wall slip was generated during the imposition of step strains since normally a discontinuity in marker line appears if the wall slip happens. Different strain amplitudes varying from very small values (0.01) at linear viscoelastic regime to large values (6.28) at nonlinear viscoelastic regime were employed. It is worthwhile to mention that for the step strain experiments of PMMA, stress overloading was easy to be reached due to the limitation of the transducer compliance of the rheometer when extreme large strain amplitudes were demanded. Thus, suitable choices of gap were made to make sure the rise time was sufficiently short to generate large step strains. For bilayer systems with presence and absence of interphase, various step strains in small deformation regime, intermediate deformation regime and large deformation regime have been examined.

IV.3.3.3 Startup Shear Experiments

Startup shear experiments (step strain rate tests) were carried out in the same DHR-2 stress controlled rotational rheometer using parallel-plate geometry for neat polymers and bilayer structures. In this test, strain rate is commanded to increase instantaneously at time zero and the transient shear stress is recorded over time. At a constant strain rate the sample strain increases linearly with time. The stress response increases and exponentially approaches a steady state value. The material function is the time-dependent viscosity function (stress growth coefficient) (eq. IV-1):

$$\eta^+(t) = \frac{\sigma(t, \dot{\gamma})}{\dot{\gamma}} \tag{IV-1}$$

In comparison to the monolayers of neat polymers, a serie of step rate tests were performed to the unannealed PMMA/PVDF bilayers and the annealed bilayers (annealed for 45mins at 200 ºC in LVE conditions) to explore the transient rheological sensitivity of the interphase upon the fast startup shear deformation. Different shear rates ranging from 0.01s^{-1} to 30s^{-1} have been attempted.

Wall slip was excluded as in step strain experiments. In addition, the typical minimum value of shear stress for the onset of wall slip was reported to be 10^5 Pa (Lee, et al. 2009), but in our work, the shear stress was limited to be around 6.5×10^4 Pa due to the instrument compliance. The ohter experimental difficulty in such test was the edge fracture caused in the case of particular high shear rates. Measurements were terminated manually when edge fracture appeared, which can be obsered via a camera installed in our rheometer. An image of the typical severe edge fracture observed at PMMA melts is shown in Figure IV-2. Indeed, the onset of the edge fracture corresponds to an abrupt decrease of the viscosity (or stress) from the steady state.
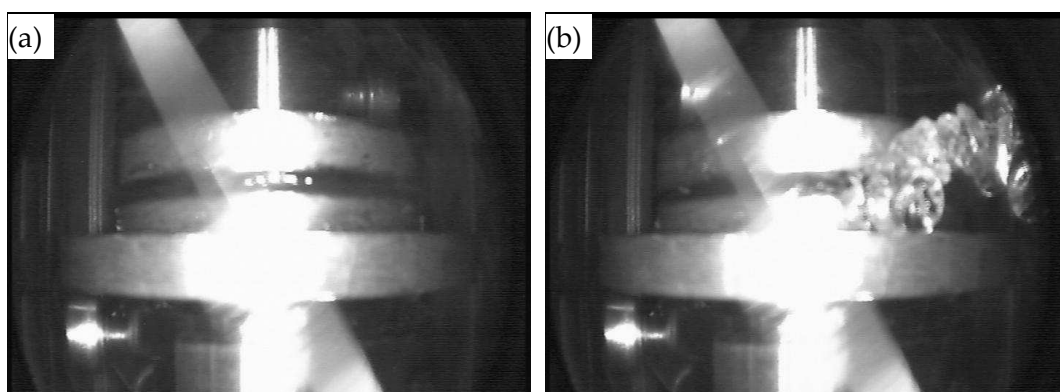
Figure IV-2. Typical images of melt with no edge fracture (a) and melt with great edge fracture (b) observed at different periods during a startup shear measurement of PMMA melts at 30s^{-1}

IV.3.3.4 Extensional rheology

Uniaxial extensional experiments were carried out using a second generation SER2

(Sentmanat Extensional Rheometer Universal Testing Platform) detachable fixture (Xpansion Instruments LLC) mounted on the DHR-2 stress-controlled rotational rheometer. Using this fixture, a constant Hencky strain rate could be easily to be imposed by applying a given angular velocity to turn the dual wind-up drums.

Sheet samples for extensional measurements were prepared either from compression molding or from coextrusion depending on specific purposes, then rectangular-shaped specimens were cut out from the sheets. Typical dimension of a monolayer specimen is 2.0 cm × 1.0 cm × 0.65 mm (Length × Width ×Thickness). Rectangular plates were clamped between the two counter-rotating wind-up drums. The temperature of the located chamber was raised to the measurement temperature (200°C in this study) before starting experiments under nitrogen atmosphere.

In an extensional experiment, dimensions of the specimen are continuously varied versus time during the stretching process. For a molten polymer sample stretched under a constant Hencky strain rate $\dot{\varepsilon}_H$, the cross-sectional area A(t) has been demonstrated to be reduced by an exponential relation with time, which could be theoretically described by following expression:

$$A(t) = A_0 \left(\frac{\rho_s}{\rho_m} \right)^{2/3} \exp\left[-\dot{\varepsilon}_H t \right] \tag{IV-2}$$

where A_0 is the initial cross-sectional area of the un-stretched specimen; ρ_s and ρ_m are density of specimen in solid and melt state, respectively. This factor is used for compensation of volumetric expansion of polymer upon melting.

A procedure of strain validation was carried out during the experiments. This was attained thanks to the camera installed in the oven of DHR2 rheometer, which enabled to continuously record the real width dimension of the sample undergoing stretching. Monitoring of the dimension change rendered it possible to check for a constant strain rate and to determine the real strain rate applied to the polymer as well as their multilayer structures. As depicted in Figure IV-3 is an example showing the evolution of width dimension of a coextruded trilayer subjected to the stretching with a constant Hencky strain rate of 0.01s⁻¹. Experimentally measured width dimensions were compared to the theoretical ones according to eq. (IV-3),

$$W(t) = W_0 \left[\exp\left(-\dot{\varepsilon}_H t \right) \right]^{1/2} \tag{IV-3}$$

in which W_0 is initial width dimension prior to stretch. Good agreement has been obtained between experimental and theoretical results, thus the Hencky strain has been validated from the actual strain over various applied strain rates for both mono and multilayered structures.
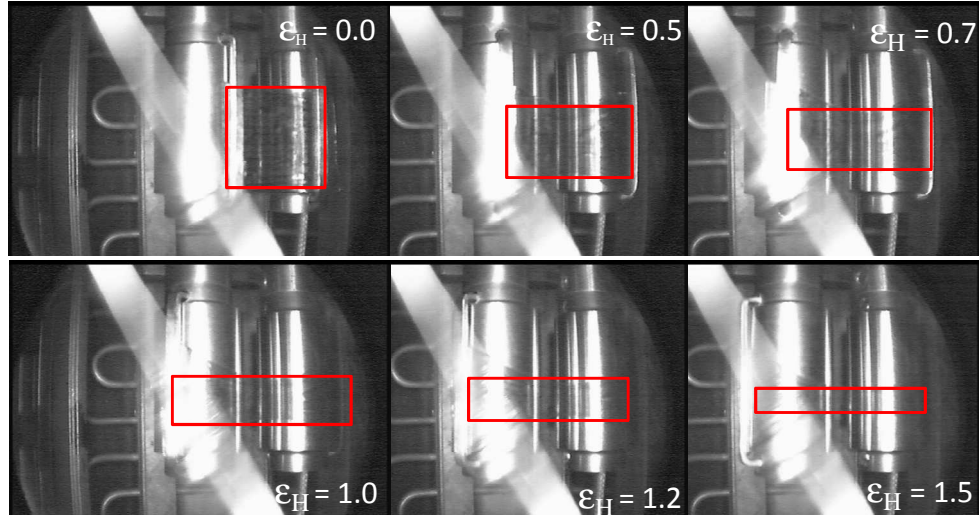
Figure IV-3. Sequential images recorded by built-in camera to show the evolution of actual width dimension of coextruded trilayer undergoing stretching at a constant Hencky strain rate of 0.01s^{-1}

Transient extensional stress growth of the PMMA, PVDF melts and their annealed/coextruded multilayers and unannealed multilayers were measured during the fast startup uniaxial extensional measurements. For a constant Hencky strain rate, the tensile stress growth rate, $\eta_E^+(t)$, of the stretched sample can be expressed as:

$$\eta_E^+(t) = \frac{F(t)}{\dot{\varepsilon}_H A(t)} \qquad (IV-4)$$

where F(t) is the instantaneous extensional force imposed to the sample from stretching at time t.

It is worthy of mentioning that one main shortcoming in such transient startup test of the SER fixture is its limitation of achievable maximum value of Hencky strain, $\varepsilon_H(t)$, since the sample strip can start to wrap around itself before a full revolution of the dual-windup drums. The Hencky strain, $\varepsilon_H(t)$, is determined via following expression:

$$\varepsilon_H(t) = \frac{2R\Delta\theta(t)}{L_0} \qquad (IV-5)$$

where R is the drum radius, 5.155 mm; L_0 is gage length between the centerline distance between the master and slave drums, that is, the initial length of the stretching zone of the specimen, which is 12.72 mm; Δθ(t) is the angular displacement, i.e. deflection angle, with $\Delta\theta(t) = \Omega t$ where Ω is the rotation speed of cylinders. It was reported that the actual test with constant strain rate stops when Δθ(t)>265° (Aho, et

al. 2010). Using these values, it is easy to reach that the achievable maximum Hencky strain is limited to be ~3.75.

IV.4. Results and Discussion

IV.4.1 Linear viscoelasticity of neat polymers

Small-amplitude oscillatory shear measurements (SAOS) of PVDF and PMMA melts were carried out at different temperatures ranging from 180 °C to 240 °C in DHR-2. Master curves of storage modulus (G'), loss modulus (G'') and dynamic viscosity (η*) of these two neat polymers produced via time-temperature superposition at a reference temperature of 200 °C are given in Figure IV-4. Zero shear viscosity, η_0, of these two polymers were determined by fitting Carreau model to the viscosity curve versus angular frequency. Methods to determine the plateau modulus G_N^0 of PMMA and PVDF have been addressed in our earlier work (Zhang, et al. 2012)). The entanglement molecular weights, M_e, were evaluated from G_N^0 by the relation of $M_e = \rho RT / G_N^0$. Weighted average terminal relaxation times, τ_{0w}, were determined from Cole-Cole curve ($\eta'' \sim \eta'$), taken as the order of reptation time, τ_{rep}. The Rouse relaxation times, τ_R, can be estimated according to

$$\tau_R = \frac{6 M_w \eta_0}{\pi^2 \rho RT} \left(\frac{M_c}{M_w} \right)^{2.4} \tag{IV-6}$$

where ρ is the density, RT the temperature defined in energy units, M_c is the critical molecular weight for a viscosity satisfying $M_c = 2M_e$.
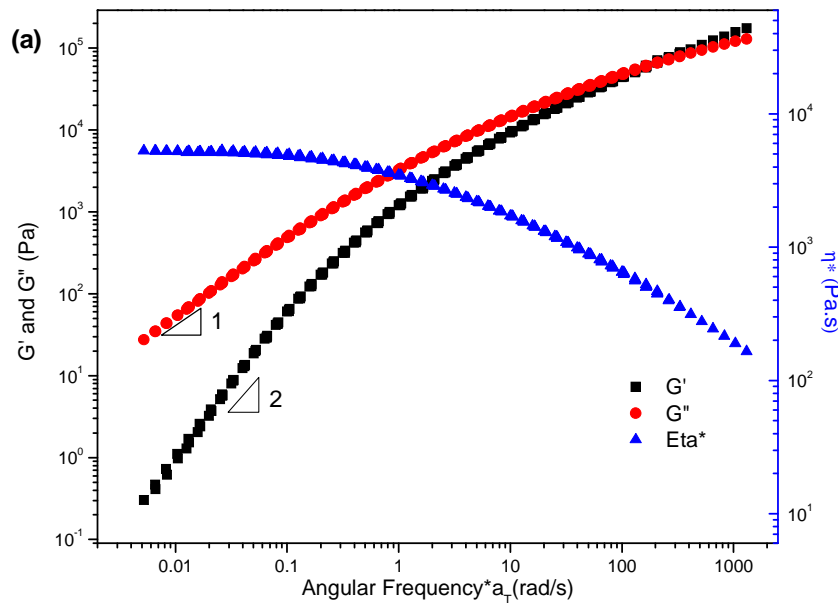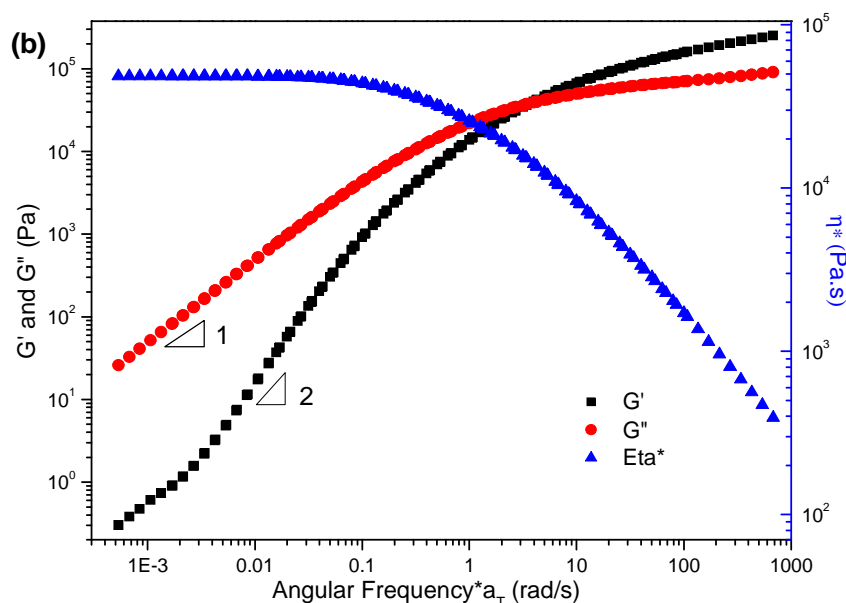
Figure IV-4. Master curves of G', G" and η^* as a function of angular frequency produced at the reference temperature of 200 ^{o}C for PVDF (a) and PMMA (b)

Table IV-2 lists main characteristic material parameters of these two melts. Note that the effective bond length b was determined by $b= (C_\infty b_0{}^2)^{1/2}$ with the characteristic ratio C_∞=8.2 for PMMA (Wool 1995), and C_∞=5.6 for PVDF (Zhang, et al. 2012).

Table IV-2 Characteristic parameters of PMMA and PVDF

Polymer	ρ(g/cm^3) at 200°C	η_0(Pa.s) at 200°C	$G_N{}^0$ (Pa)	M_e (g/mol)	b (Å)	τ_{rep}(s) at 200°C	τ_R(s) at 200°C
PMMA	1.097	6.4×10^4	3.6×10^5	1.2×10^4	4.41	~0.94	~2.7×10^{-2}
PVDF	1.471	4.0×10^3	6.5×10^5	8.9×10^3	3.64	~0.18	~4.7×10^{-3}

IV.4.2 Interphase generated at neighboring layers from annealing and from coextrusion

In our earlier work, great efforts have been devoted to producing and characterizing the diffuse interphase resulted from interdiffusion process between neighboring layers. Both interphase generated by annealing bilayer structures between parallel plates in the rheometer and those generated during coextrusion process for short contact time (see Chapter V) have been examined. Small-amplitude oscillatory shear measurement (SAOS) has been demonstrated to be a reliable tool to monitor the interdiffusion kinetics and to modelize the developed interphase. To attain the objective of probing the nonlinear rheological response of the developed interphase, it is of necessity to first give a brief view on how many amount of interphase could be produced under experimental conditions of interest. Figure IV-5(a) depicts the variation of apparent mutual diffusion cofficient D_m and the corresponding interphase development versus time for a PMMA/PVDF bilayer structure which was annealed at 200 ^{o}C and ω=0.1rad/s for 45mins. As clearly shown in the figure, with a

D_m decreasing from a high value to a constant around 5.0×10^{-9} cm²/s, an interphase with a thickness reaching c.a. *77μm* can be generated after annealing for 45mins. Details about the rheological modeling correlating the D_m and properties of the interphase to the variations of rheological functions of the sandwich structures during annealing process have been given in Chapter III. Such amount of interphase has also been validated by the scanning electron microscopy coupling with energy dispersive X-ray (SEM-EDX) tool, as shown in Figure IV-5(b), where a similar interphase thickness (~85 *μm*) has been observed on the same specimen quenched after annealing.
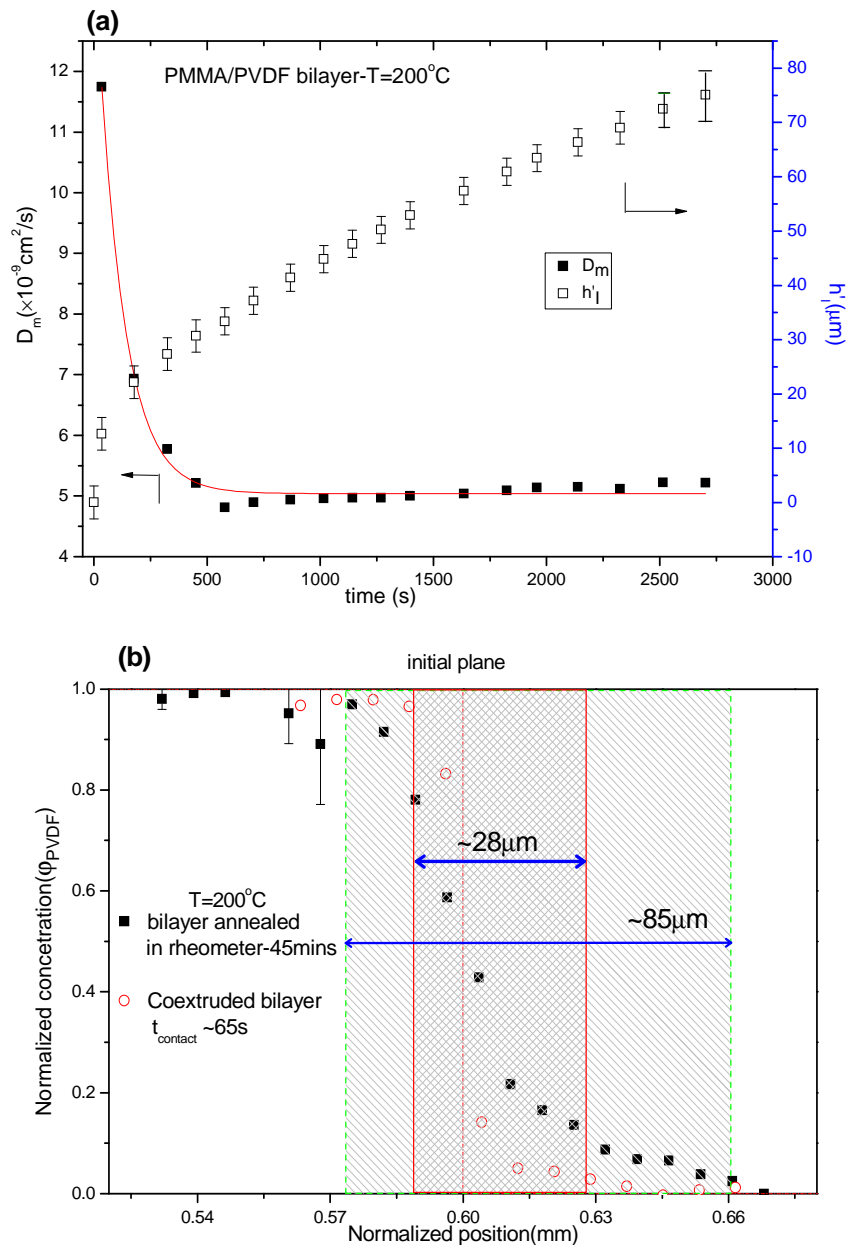
Figure IV-5 (a) Evolution of mutual diffusion coefficient (D_m) and interphase thickness (h'_I) versus time for PMMA/PVDF bilayer annealed at 200 ºC, 0.1 rad/s, as determined from rheological modeling; (b)Normalized PVDF concentration profile versus normalized position for quenched PMMA/PVDF bilayer after annealing in rheometer for

45mins (black solid squares) and for quenched bilayer coextruded at 200 °C, contact time ~65s (red open circles),as determined from SEM-EDX. The sparse shadow and condense shadow zones designate the interphase of annealed bilayer and coextruded bilayer, respectively.

Likewise, SEM-EDX was also used to characterize the interphase on the quenched coextruded bilayers obtained within a short contact time around 65s. As indicated in Figure IV-5(b), an interphase with a thickness around 28 μm could be triggered for a PMMA/PVDF bilayer coextruded at 200 °C. Such a high amount of interphase created within such a short contact time is attributed to a significant positive effect of intermixing on the interphase development under the practical flow field of processing condition. More details about the interphase development during coextrusion process are available in Chapter V of this manuscript. In the present work, focuses are mainly on the nonlinear rheological response of multilayers with interphase and multilayers without interphase. The multilayers with interphase considered in this study are two cases, includingi) PMMA/PVDF bilayer annealed in the rheometer at 200 °C, 0.1rad/s for 45 mins with a generated interphase of 85 μm thickness; and ii) coextruded alternating multilayersobtained from coextrusion at 200 °C and t_contact ~65s, with an interphase thickness around 28 μm between neighboring layers. The multilayers without interphase are combined multilayers without any annealings before use for nonlinear rheological measurements.

IV.4.3 Stress relaxation after a single step strain

IV.4.3.1 Stress relaxation of neat polymers

This study begins with the stress relaxation behavior of neat polymer systems in shear after imposition of a finite step strain before extending to the multilayered systems. Typically, in a stress relaxation measurement for monolayer, experiment is carried out by "instantaneously" applying a finite shear strain of amplitude γ_0 to the sample and laying it at rest to relax the stress resulted from such an instant deformation while the strain amplitude is held constant at the residual times. As a matter of fact, from an experimental viewpoint, the actual strain pattern generated by the rheometer in response to a command for a step strain is not exactly a perfect step function. A finite rise time t_0 is required for the motor to rotate the plate to achieve the prescribed strain, as shown in Figure IV-6a. In principle, t_0 is preferable to be as short as possible, as reported in the literature(Dealy and Larson 2006;Rolon-Garrido and Wagner 2009;Yu 2013), a t_0 less than one tenth of the average relaxation time of the material is prerequisite for obtaining meaningful information of relaxation process in a single step strain test. A too long rise time is difficult to give the information about rheological nonlinearity in the relaxation modulus curve since only time shorter than relaxation time allows for an affine deformation whereby nonlinear phenomena appear. To generate instantaneously a large step strain within a time short enough to be in the order of material's relaxation time is quite a main

challenge. As indicated in some studies (Juliani and Archer 2001), one strength that a stress-controlled rheometer offers is the possibility that a nonlinear step strain could be imposed in less than 0.1 s for even a very high stiff polymer system. More details will be given as follow by showing the actual strain profile during the transient period.
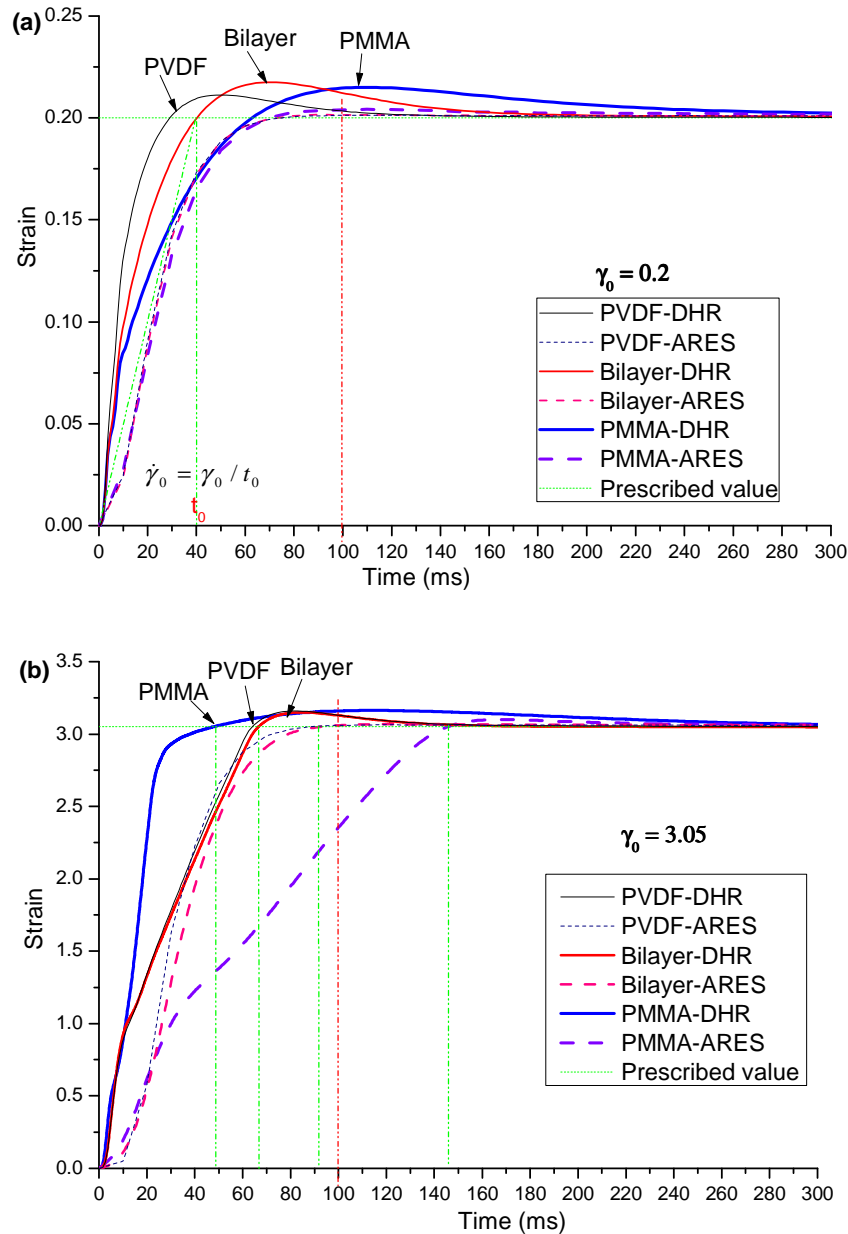
Figure IV-6 Actual strain variation versus time in step strain tests measured respectively in DHR2 and ARES based on PVDF, PMMA melts and PMMA/PVDF bilayer structures with different commanded strain amplitudes: (a) $\gamma_0 = 0.2$ and (b) $\gamma_0 = 3.05$. The actual strain is not a perfect step function.

Indeed, as it is known, in the stress-controlled rheometer an inertia effect may exist on commanding a step strain since the input signal in this type of rheometer is stress rather than strain. In this work, same step strain experiments have been carried out

in both stress-controlled (i.e., DHR-2) and strain-controlled rheometers (i.e. ARES) and a comparison between these two types of rheometers has been performed. As indicated in Figure IV-6(a) and (b) are actual strain variations versus time measured in both DHR-2 and ARES with command of different strain amplitudes, $\gamma_0 = 0.2$ and $\gamma_0 = 3.05$, based on neat polymers and bilayer strucutres. We can see that for a same material, the stress-controlled rheometer, DHR-2, requires shorter rise time to reach the prescribed strain value than the ARES although the strain in DHR-2 lightly overshoots before moving back to the prescribed value due to the inertia effect. It is important to note that for a high stiff material as PMMA melt which has $\tau_w \sim 0.94$ s, to command a large strain step like $\gamma_0 = 3.05$, 146 ms is required for ARES while it needs only 49 ms by DHR-2 to reach the strain value though a following period of strain stabilization ($\leqslant 4\%$) is required (Figure IV-6b). Due to this cause, nonlinear feature of stress damping behavior as a result of the first ultrafast relaxation process of chain retraction fails to appear for the PMMA melt in ARES (see Figure IV-S1b in the supporting information) as opposed to that clearly observed in DHR-2 (see Figure IV-7b). For clarity purpose, more details about the comparisons between these two rheometers are given in the Supporting information of this chapter. For the DHR-2, the rise time in most cases is no more than 70 ms, which enables giving information of rheological nonlinearity for the polymers and even presumably for the interphase. Therefore, unless otherwise specified, results obtained in DHR-2 are used for discussions in the present study. For analysis accuracy, in this work, only the data obtained after times when the actual strain keeps constant are focused and analyzed considering that in this case the step time is supposed to have no relevant influence on the relaxation modulus.

(b) PMMA-T=200°C

$G(t,\gamma)$ (Pa)

- —— γ=0.01
- ----- γ=0.1
- —— γ=0.2
- ----- γ=1.0
- —— γ=2.0
- ----- γ=3.04
- —— γ=6.28

Time (s)

(c) PVDF-T=200°C

λ_k

$G(t,\gamma)h(\gamma)^{-1}$ (Pa)

- ----- γ= 0.05
- ----- γ= 0.3
- ----- γ= 1.0
- —— γ= 1.8
- —— γ= 2.3
- —— γ= 4.4
- —— γ= 5.0

Time (s)

- 169 -
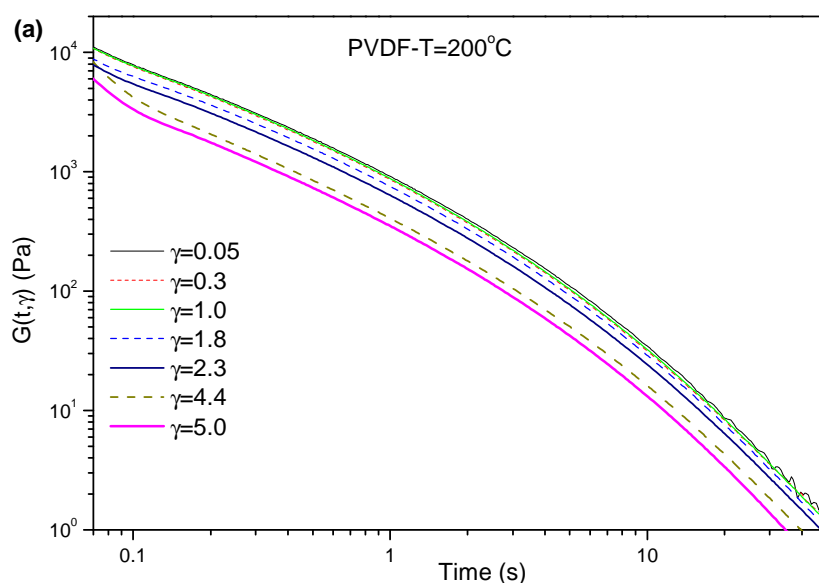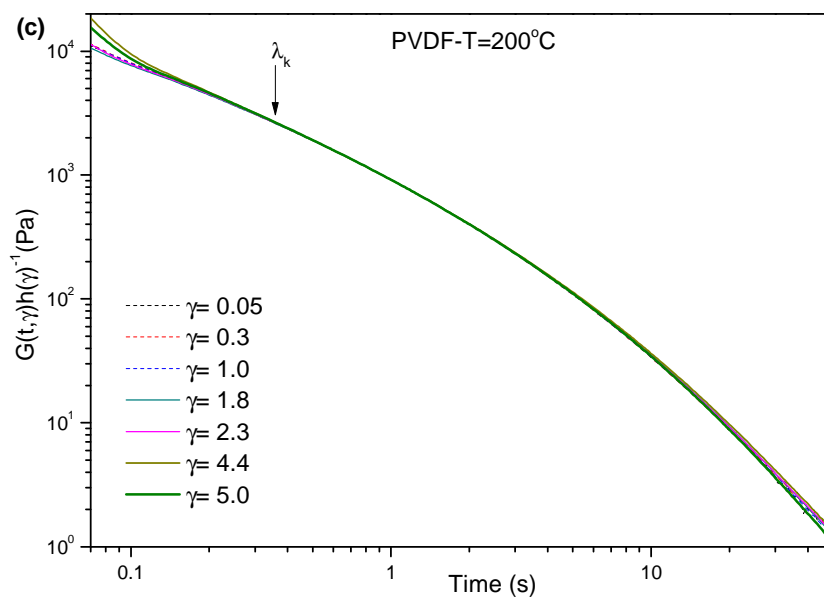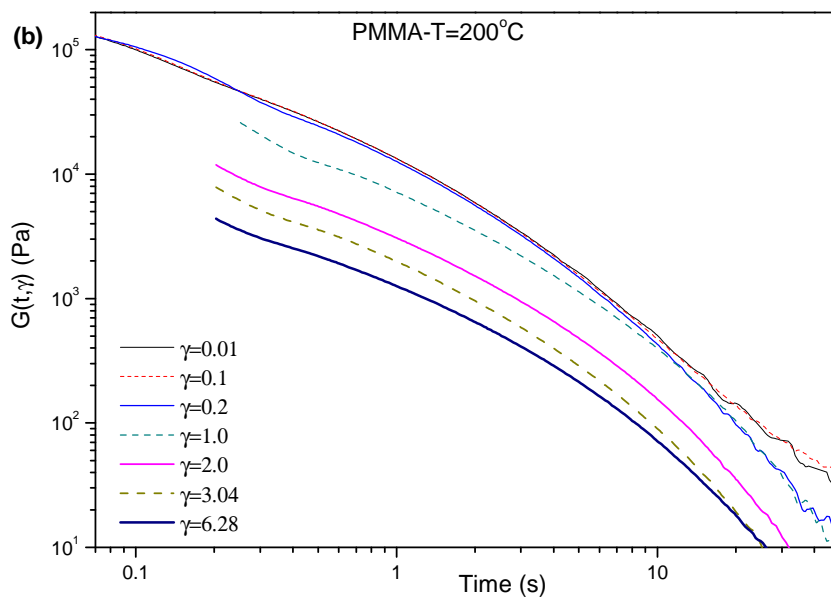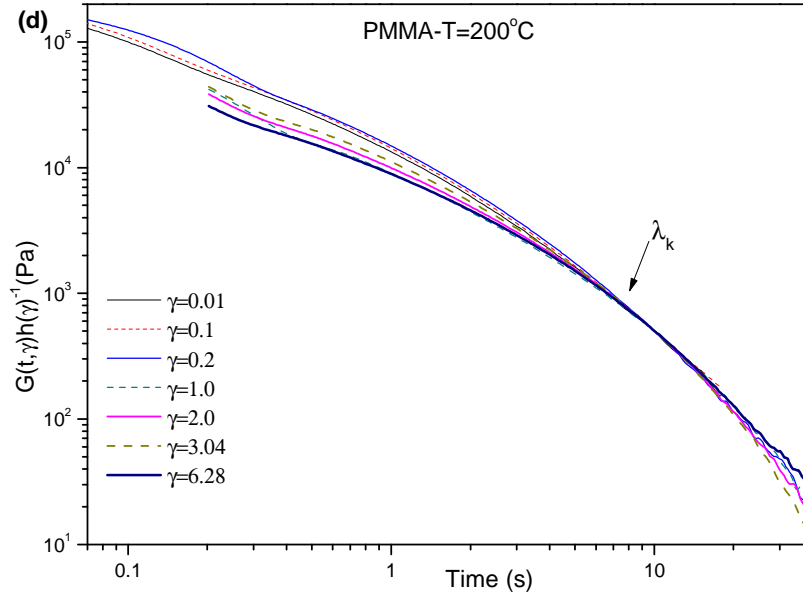
Figure IV-7. Time dependent nonlinear shear relaxation modulus G(t,γ) obtained at various shear strain magnitudes ranging from 0.01 to 6.28 at 200 °C for PVDF (a) and PMMA (b), respectively; (b) Shifted nonolinear shear relaxation moduli G(t,γ)h(γ)$^{-1}$ at 200 °C for PVDF (c) and PMMA (d). The arrow locates the time λ_k beyond which nonlinear moduli can be factorized (approximately) into separate strain- and time-dependent functions

From Figure IV-7(a) and (b), it is pronouncedly noticed that for both PVDF and PMMA, except at small strains lower than 1.0, the modulus curves drop to successively lower levels as the strain is increased. Stress damping (i.e., modulus decline) behavior is evident at large strain amplitudes for both polymers and it is clear that the PMMA behaves much stronger strain dependence than the PVDF. The critical γ, above which the relaxation modulus becomes dependent of the strain (i.e, "Strain softening") for PMMA is lower than that of PVDF, with a value above γ=1.0 for PVDF but below γ=1.0 for PMMA. The stress modulus versus time curves at long time period are able to be superposable by a vertical shift on log-log plot, implying that the nonlinear relaxation modulus can be separated into time-dependent,*G(t)*, and strain-dependent factors, *h(γ)*, as shown by following equation:

$$G(t, \gamma) = G(t)h(\gamma) \tag{IV-7}$$

where *h(γ)* is a factor depicted as a function of strain, called as damping function. The stress relaxation data sets at large strains are vertically shifted onto the linear relaxation curve, so as to verify the time-strain separability of PVDF and PMMA. Time-strain factorability is observed at long times and confirmed by the plot of *G(t, γ)h(γ)$^{-1}$*, as shown in Figure IV-7.(c) and (d). The separability time $\lambda_k \approx 0.34$ s ≈ 1.9 τ_{rep} for PVDF and $\lambda_k \approx 8.0$ s ≈ 8.3 τ_{rep} for PMMA. In particular, the damping function was calculated at the superimposable region (given t= 1 s for PVDF and t=10 for PMMA). Time-strain factorability occurs after the retraction process is completed. The λ_k is

expected to be approximated by the longest Rouse time τ_R of a hypothetical chain according to the Doi-Edwards (DE) prediction. That is, barrier-free retraction process of all chains on the Rouse time scale should give rise to a stress decline around τ_R during stress relaxation from a large step strain made at $W_{iR}>1$.

Theoretical interpretation for the stress relaxation behavior of test chain after a nonlinear step strain according to the DE scenario (Dealy and Larson 2006;Doi and Edwards 1986) is as follow, which is based on the chain stretching and orientation. When a sufficiently large and rapid "step" strain is applied to the entangled polymer chains that cannot relax within such short time, the chains are forced to deform affinely. This affine deformation gives rise the chain to stretch beyond its equilibrium tube contour length. After the large strain, the stretched chain segment begins to retract to its original equilibrium length, with a relaxation mechanism of retraction of the chain within its tube, i.e., contour length contour relaxation. This retraction is manifested with a fast relaxation process appearing in the relaxation modulus curve at early time. After this process is completed, the reminder of the relaxation process occurs as in the case of a linear response, via reptation, showing same shape as that of linear viscoelasticity (i.e. very small deformation) in the relaxation modulus curve.

In fact, most of the experiments suggested that the chain does not fully retract to the equilibrium length at $t\sim\tau_R$, instead, the time-strain separability becomes valid only at $t>\tau_{rep}$ ($>>\tau_R$). Mhetar and Archer (1999) attributed this delicate failure of time-strain separability occurring at $t\sim\tau_R$ to the lateral squeezing due to the tube, arguing that the squeezing effect vanishes and the chain recovers its equilibrium length only after the chain escapes the deformed tube and thus the time-strain separability happens at a time close to the terminal relaxation time. For this delicate failure, using the primitive chain network simulation, Watanabe and coworkers (Furuichi, et al. 2010) recently proposed a molecular origin regarding the local force balance between the subchains, the longitudinal Rouse relaxation, and the reptation. They argued that the retarded equilibration was related to the convective constrain release (CCR) activated decrease of the entanglement number per chain. They also correlated it to the corresponding softening of the subchain resulted from the monomer number decrease per chain, and most importantly to the reduction of the subchain tension at around the chain center compared to the DE prediction. Using particle-tracking velocimetric (PTV), Wang et al (2007, 2009) observed occurrence of macroscopic motion after step strain when it exceeds a critical value about unity for simple shear. The critical strain for strain softening at order of unity is consistent with our experiments of PMMA and PVDF melts. According to their scenario, such macroscopic motions produce strong strain softening. The substantial macroscopic motions increase as a larger step strain is imposed, thus leading to a greater decline in stress and a more serious damping phenomenon in relaxation modulus even probably producing a kink-like character. In their picture, nonlinear rheological phenomena are consequences of elastic yielding and chain disentanglement upon

force imbalance arising during or after external deformations. Upon a sudden external strain (affine deformation) given in a step shear experiment, an intrachain elastic retraction force, $f_{retract}$, is produced in each strand for a sake to return to the unperturbed state. When the $f_{retract}$ is sufficiently high above a large stepwise deformation to overcome the entropic barrier quantified by the cohesive entanglement force f_{ent} ($\sim k_B T / l_{ent}$), chain disentanglement and macroscopic yielding occur, leading to stress decay and modulus drop during relaxation.

One more explicit picture formulated for the stress relaxation behavior of polymer chains after nonlinear step strain is the microscopic theory of Sussman and Schweizer which postulated two competing parallel relaxation mechanisms under stress: strain dependent reptation and activated transverse barrier hopping(tube breaking). This scenario, though proposed based on rod polymer chains, is also very speculative for the dynamics of flexible chains. Like the work of Wang et al., they believed the entanglement force (tube confining barrier) is of finite. Upon applied deformation, substantial occurring events are stress-and orientation-driven tube dilation, transverse entropic barrier reduction, and ultimately tube destruction beyond a critical strain when the intrinsic entanglement force localizing the polymer in a tube is exceeded. More specifically, when the strain is very small, the transverse confinement is dynamically stable with the transverse barrier hopping relaxation staying at an inactive state, and the quiescent reptation dynamics remains essentially the same as the DE theory. When the strain is in an intermediate state when the strain barrier hopping relaxation emerges, the lateral hopping time becomes comparable to the terminal reptation time only when the barrier is relatively small. In this regime, the strain causes the entanglement network to collapse via transverse barrier hopping before reptative relaxaion is completed. When the strain is very large, beyond a critical value, complete destruction of transverse entropic barrier, that is, the tube constraints occurs, defining as a phenomenon of "absolute yielding". The tube destruction beyond a large step strain was supposed to be the reason of the ultrafast relaxation of stress on the short time scale as terminal relaxation time. After the initial fast relaxation, the entanglement constraints reemerge, resulting in the slower reptative relaxation process in long times as like quiescent relaxation.

In a word, a consensus of these different theoretical pictures seems to be that upon large external deformations, decrease of entanglement number per chain, or, chain disentanglement, i.e., tube breaking could happen, not matter according to which theoretical mechanisms, i.e., the lateral squeezing, the convective constrain release (CCR), the elastic yielding or the activated transverse barrier hopping. The damping function, $h(\gamma)$, was proposed by Doi-Edwards to describe such decrease of the number of the entanglement segment per chain. It could quantitatively describe the strain softening (or, stress damping) phenomenon and express the character of

the time-strain separability. Here, the $h(\gamma)$ is calculated as $h(\gamma) = G(\gamma, t) / G_e(t)$, with

$G_e(t)$ being the time-dependent modulus at linear region. It is worthwhile to mention

that Rolon-Garrido and Wagner (2009) published an interesting review article about the damping function in rheology in *Rheologica Acta*, in which many detailed theoretical backgrounds and physical interpretations have been addressed.
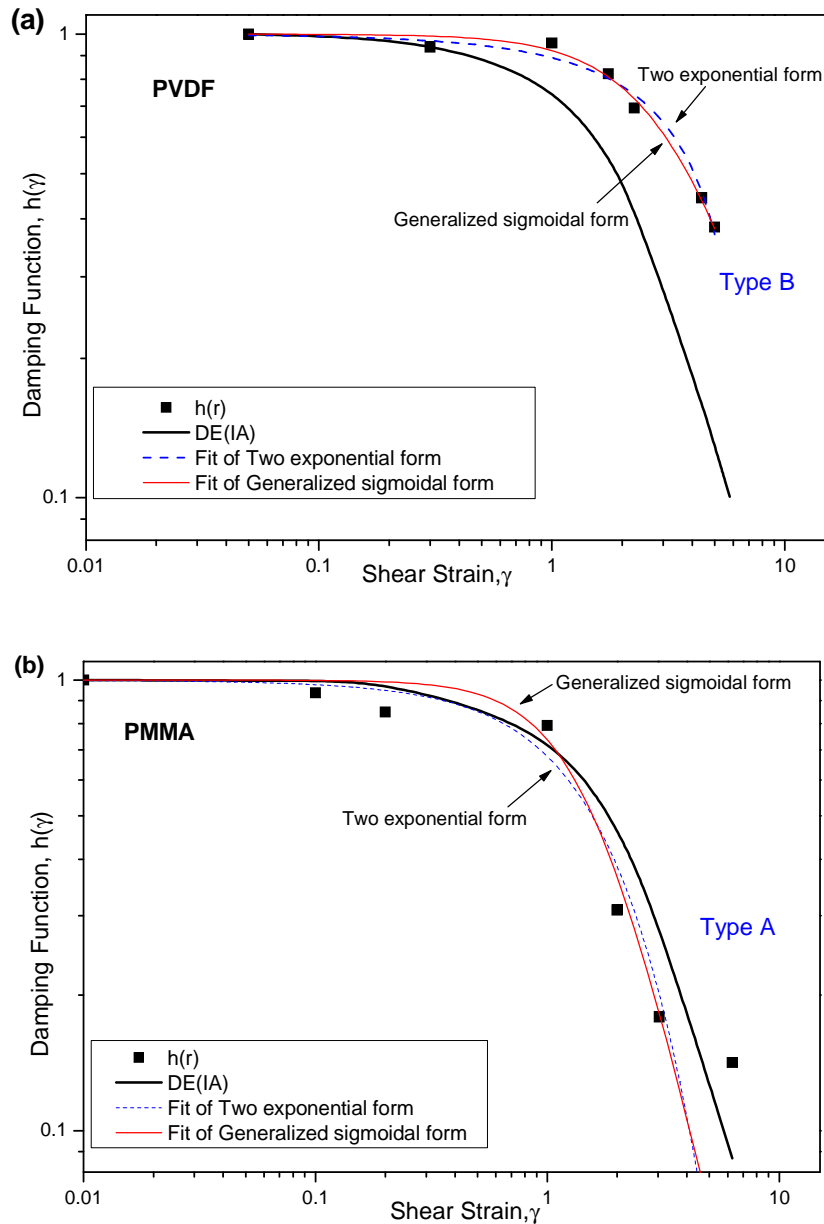
Figure IV-8. Instantaneous shear damping functions h(γ) for: (a) PVDF melt and (b) PMMA melt, respectively. Thick solid line (black) is the damping function predicted by the Doi-Edwards theory with the independent alignment approximation; Dash line (blue) and thin line (red) are fitting curve of two exponential form and fitting curve of generalized sigmoidal form, respectively.

Various empirical equations have been proposed to describe the damping functions, among which exponential forms and sigmoidal forms are two popular types. Laun (1978) used a two exponential functions as a representation of the damping function with an expression as follow:

$$h(\gamma) = f \exp(-n_1 \gamma) + (1 - f) \exp(-n_2 \gamma) \qquad \text{(IV-8)}$$

with *f*, n_1, n_2 being fiting paramters. As shown in Figure IV-8, the damping function of PVDF can be described by this expression with *f*= -28.2, n_1= -0.03 and n_2= -0.03; Likewise, it can be well fitted to that of PMMA with *f*= -0.67, n_1= 1.38 and n_2= 0.68. Another most widely used damping function for homopolymers is with sigmoidal form (Papanastasiou, et al. 1983) as $h(\gamma) = 1/(1 + a\gamma^2)$. Moreover, to get a better fit of their experimental data, Soskey and Winter (1984) proposed a generalized sigmoidal form

$$h(\gamma) = 1/(1 + \alpha\gamma^{\beta}) \qquad \text{(IV-9)}$$

with α and β as fitting parameters. As indicated in Figure IV-8, parameters α= 0.09, β= 1.84 and α= 0.36, β= 2.28 give the best fittings for the PVDF and PMMA melts, respectively. More meaningfully, a widely used Doi-Edwards theory (DE) predicted damping function that includes an independent alignment (IA) assumption has also been employed in this work. This DE (IA) damping function prediction is universal, which needs no adjustable parameters. It can be closely approximated by the type of generalized sigmoidal form (i.e, eq. (IV-9)) with α = 4/15 and β =2, that is:

$$\text{DE (IA) model:} \qquad h(\gamma) = 1/(1 + \frac{4}{15}\gamma^2) \qquad \text{(IV-10)}$$

According to the accordance of the *h(γ)-γ* dependence of polymers to the universal prediction of Doi-Edwards theory, Osaki (1993) classified the *h(γ)* behavior into three types, A ,B, and C. Type A corresponds to those with damping functions in essential agreement with the DE prediction. Type B materials behave with less damping than the DE prediction and in contrast, materials with more severe damping than the DE prediction are classified into Type C. Obviously, as shown in Figure IV-8, PVDF melt, with a weaker damping function than the DE (IA) prediction, belongs to the type-B behavior. It is widely accepted that melts with broad MWD or multiple branch points show somewhat this type of behavior. Nevertheless, the PMMA melts were found to exhibit normal type A behavior in agreement with the DE theory prediction. This is consistent with the results reported in earlier studies of PMMA solutions (Osaki 1993). It was argued that the DE prediction is the maximum degree of damping that can be predicted by any tube model. In some cases, the measured *h(γ)* can goes into type C regime (i.e., $h(\gamma) < h_{DF}(\gamma)$) when the step strain becomes sufficiently large, with an appearance of very sharp decrease in the relaxation modulus before a sudden return to superimposable region, which is sometimes called "kink" behavior in literatures. Now the type C behavior and the "kink" therein is thought to be resulted from the wall slip, i.e., adhesive failure between polymer melts and the metal surface (Dealy and Larson 2006; Rolon-Garrido and Wagner 2009). For instance, Nielsen and Hassager (2009) carried out step-strain

experiments of polyisoprene melt in AR-G2 rheometer within a strain range below a critical strain value. Because for strains larger than the critical one, it was observed that $h(\gamma) < h_{DE}(\gamma) < 1$, which was attributed to slip at the polymer-steel interface on the rheometer. However, within experimental errors, such type C behavior resulted from wall slip was not observed in this work for the neat polymers.

In short words, for the neat PVDF and PMMA melts, linear relaxation modulus G(t) was obtained for small step strain ($\gamma \ll 1.0$) while for large strain ($\gamma \geq 1.0$), nonlinear relaxation modulus G(t, γ) charactering strong stress damping behavior was obtained where the modulus becomes strain-dependent. G(t, γ) obeys time-strain separability at long time scales and the strain dependency can be described by a damping function. Such stress damping phenomenon at large deformation is attributable to the retraction of chain segments within the tube and the convective constraint release caused by flow-induced displacement of chains relative to each other and consequent loss of entanglements between chains according to the tube model (Doi-Edwards 1986; Marrucci 1996). Watanabe (2010) argues that the damping function $h(\gamma)$ deduced from the DE model represents a decrease of a number of the entanglement segment per chain (due to the chain contraction) and an increase of the monomer number per this segment(that reduces the tension along the chain backbone). This is conceptually equivalent to the disentanglement by deformation of a network strand of Wagner, the dynamic network picture of "elastic yielding" of Wang et al.(2007,2009), and the viewpoint of dynamical softening of the tube potential of Sussman and Schweizer(2011,2012), with a same final consequence of entanglement loss.

IV.4.3.2 Stress relaxation of bilayer structures with and without presence of interphase

Shear stress relaxation measurement of the multilayer polymers as well blend systems has been reported in the literature to be sensitive to the presence of the interface/interphase at neighboring layers (Silva, et al. 2012). Due to the different relaxation behavior of components and potential contribution of the interface/interphase, various models have been used to correlate the final relaxation behavior of the multiphase system to the component contributions. For example, Silva et al. (2012) suggested use of the reciprocal rule to predict the relaxation modulus of the bilayer structures with an assumption of zero interfacial thickness and no slippage in the condition of linear viscoelastic domain:

$$\frac{1}{G_{total}(t)} = \frac{\varphi_A}{G_A(t)} + \frac{\varphi_B}{G_B(t)} \tag{IV-11}$$

However, this model was proposed for the linear relaxation behavior of bilayer structure that is valid only for the linear domain where the effect of strain is excluded. A quantitative relation correlating the interphase to the relaxation modulus variation

of the multilayered structures in nonlinear regime (i.e., time-and-strain dependent) is far from being fully established. Hence, in this work, we attempt to give a clearer picture on predicting the stress relaxation behavior of multiphase systems in a wider regime including the nonlinear viscoelastic regime with large step shear strains. For this, step strain experiments have been carried out on multilayer structures with presence of an interphase (i.e. bilayer annealed for a certain time) and on those without interphase (i.e. unannealed bilayer) as reference.

In general, step strain experiment is given to a monolayer disk. Here, the samples used are multilayer structures consist of different viscoelastic melts, so the strain distribution for each layer should be different upon a nominal step strain being commanded for the total structure. Thus, we attempt to make an analysis on the rheological variation of the sandwich structures during the short period of the instant imposition of a step strain. During the transient ramp-up of the strain in the rise time

t_0, an apparent shear rate could be approximated as $\dot{\gamma}_0 = \gamma_0 / t_0$ with t_0 being the rise

time for the step strain (as shown in Figure IV-6a). Note that, the symbol γ_0 used here instead of γ for step strain is just for a specific purpose to emphasize the transient character of the initial period that the strain is imposed, corresponding to the initial value of the produced stress, σ_0, which becomes time-dependent thereafter. In fact, the meaning is the same with the γ used elsewhere for stress relaxation.

For a sandwich structure consists of layer A, layer B and interlayer (interphase), when a nominal step strain γ_0 is imposed (i.e., a constant stress σ_0 is produced thereafter), different individual layers are expected to have different relaxation responses due to their viscoelastic difference. That is, as shown in the scheme (Figure IV-9), though the nominal total step strain commanded to the multilayer structure is γ_0, the strains experienced by each layer may significantly differ from each other. They could be distinguished as $\gamma_{0,A}$, $\gamma_{0,B}$, $\gamma_{0,int}$, for layer A, B and interlayer, respectively. Meanwhile, the stress relaxes in different ways for each layer, denoted as $\sigma_A(t, \gamma_{0,A})$, $\sigma_B(t, \gamma_{0,B})$ and $\sigma_{int}(t, \gamma_{0,int})$, respectively, with an initial boundary condition being that $\sigma_A(t \rightarrow 0, \gamma_{0,A}) = \sigma_B(t \rightarrow 0, \gamma_{0,B}) = \sigma_{int}(t \rightarrow 0, \gamma_{0,int}) = \sigma_0$ at the very beginning. The stress is continuous across the interface upon the imposition of strain on the multilayered structures. Notice that the apparent stress of the total multilayer structure (σ_{total}) measured by the transducer at time *t* is the average of the real stresses of the layers, that is, $\sigma_{total} = \frac{1}{3}[\sigma_A(t, \gamma_{0,A}) + \sigma_B(t, \gamma_{0,B}) + \sigma_{int}(t, \gamma_{0,int})]$ if the structure is regarded as a

trilayer and $\sigma_{total} = \frac{1}{2}[\sigma_A(t, \gamma_{0,A}) + \sigma_B(t, \gamma_{0,B})]$ if it is regarded as a bilayer.
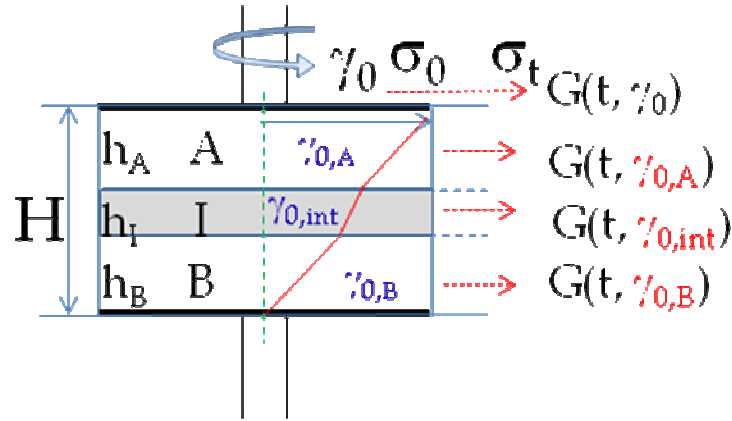
Figure IV-9. Schematic of a sandwiched multilayer polymer structure in response to a step strain γ_0. Different relaxation behaviors are expected in different layers.

Thus, the relaxation modulus experienced by the total sandwich structure could be expressed as:

$$
\begin{aligned}
G(t,\gamma_0) = \sigma_{total}(t,\gamma_0)/\gamma_0 &= \frac{1/3\big(\sigma_A(t,\gamma_{0,A}) + \sigma_B(t,\gamma_{0,B}) + \sigma_{int}(t,\gamma_{0,int})\big)}{\gamma_0} \\
&= \frac{1/3\big(G_A(t,\gamma_{0,A})\bullet\gamma_{0,A} + G_B(t,\gamma_{0,B})\bullet\gamma_{0,B} + G_{int}(t,\gamma_{0,int})\bullet\gamma_{0,int}\big)}{\gamma_0}
\end{aligned}
\tag{IV-12}
$$

Here, within the rise time t_0 of step strain, the strains experienced by layer A, $\gamma_{0,A;}$ layer B, $\gamma_{0,B}$ and interphase, $\gamma_{0,int}$ satisfy a relation as follow:

$$
\frac{\gamma_{0,i}}{\gamma_0} = \frac{\dot\gamma_{0,i}}{\dot\gamma_0} = \frac{\sigma_0/\eta_i}{\sigma_0/\eta_{total}} = \frac{\eta_{total}}{\eta_i}
\tag{IV-13}
$$

in which i represents component A,B and interphase, η_i and η_{total} are viscosity of component i and apparent viscosity of the total sandwich structure at the initial stress σ_0. Here, we assume that each layer has the same σ_0 during the instant ramp-up period, $t \leqslant t_0$. Their viscosities can be related via a reciprocal relation $\frac{1}{\eta_{total}} = \frac{\varphi_A}{\eta_A} + \frac{\varphi_B}{\eta_B} + \frac{\varphi_{int}}{\eta_{int}}$ as reported in the literature (Lin 1978, Bousmina 1999, Lamnawar 2008). Eq. (IV-13), i.e., $\gamma_{0,i} = (\eta_{total}/\eta_i)\gamma_0$ implies that the actual strain experienced by layer i can be determined from the nominal total step strain γ_0 imposed to the sandwich structure if its viscosity is known. In other words, the less viscous layer may experience a larger strain than γ_0, and the more viscous one a lower strain than γ_0. That means, it is possible that in some case of intermediate γ_0, the strain of less viscous component enters into the non-linear domain whereas the more viscous one with lower strain still lies in its linear domain.

After incorporation of eq. (IV-13) into eq. (IV-12) and rearrangement, one obtains

$$G(t, \gamma_0) = \frac{\eta_{total}}{3} \left[\frac{G_A(t, \gamma_{0,A})}{\eta_A} + \frac{G_B(t, \gamma_{0,B})}{\eta_B} + \frac{G_{int}(t, \gamma_{0,int})}{\eta_{int}} \right] \qquad \text{(IV-14)}$$

Since the relaxation modulus $G_i(t, \gamma_{0,i})$ of component i can be separated into a time dependent relaxation modulus $G_{i,e}(t)$ at linear region and a strain dependent factor $h_i(\gamma)$, eq. IV-14 could be rewritten as

$$G(t, \gamma_0) = \frac{\eta_{total}}{3} \left[\frac{G_{A,e}(t)h(\gamma_{0,A})}{\eta_A} + \frac{G_{B,e}(t)h(\gamma_{0,B})}{\eta_B} + \frac{G_{int}(t, \gamma_{0,int})}{\eta_{int}} \right] \qquad \text{(IV-15)}$$

If the system is assumed as a bilayer structure without interlayer, the eqs (IV-14, 15) reduce to be:

$$G(t, \gamma_0) = \frac{\eta_{total}}{2} \left[\frac{G_A(t, \gamma_{0,A})}{\eta_A} + \frac{G_B(t, \gamma_{0,B})}{\eta_B} \right] = \frac{\eta_{total}}{2} \left[\frac{G_{A,e}(t)h(\gamma_{0,A})}{\eta_A} + \frac{G_{B,e}(t)h(\gamma_{0,B})}{\eta_B} \right] \quad \text{IV-16)}$$

Hence, based on the equilibrium relaxation modulus $G_e(t)$ and the damping function $h(\gamma)$ of PMMA and PVDF melts as well as their viscosities at initial stress σ_0, the models can be used to make some predictions for relaxation modulus of the multilayer structures after a nominal step strain γ_0. As fitted before (see Figure IV-8), a damping function of $h(\gamma) = 1/(1 + 4/15\,\gamma^2)$ for PMMA and $h(\gamma) = 1/(1 + 0.09\,\gamma^{1.84})$ for PVDF can be used for predictions. Note that the apparent viscosities of these components at stress σ_0, calculated as $\eta_{app,i} = \sigma_0 / \dot{\gamma}_0 = \sigma_0 t_0 / \gamma_0$, were determined from a previously created curve of $\eta_{app,i} \sim \sigma_0$ obtained from different step strains of each component, i. As well, the relaxation modulus of the interphase after the step strain γ_0 is able to be estimated via eq. (IV-15).
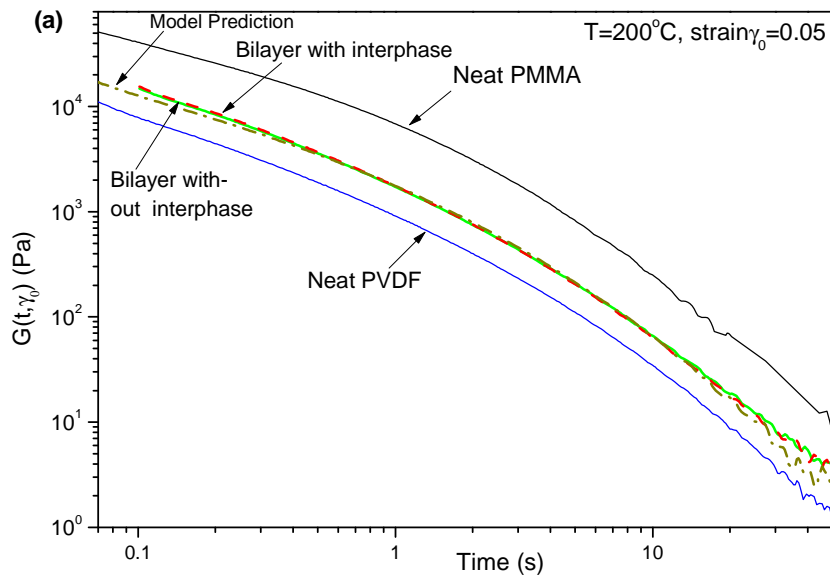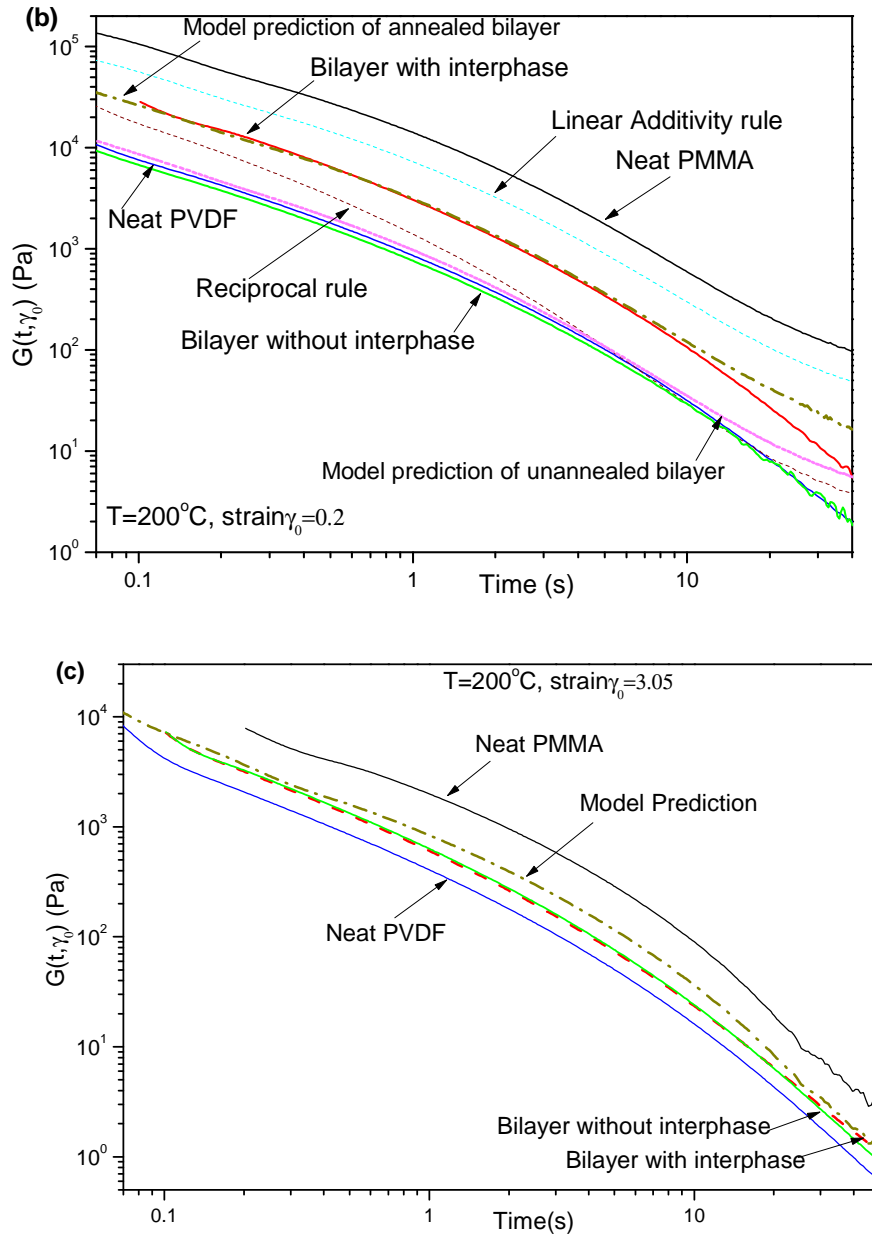
Figure IV-10 Time dependent nonlinear shear relaxation modulus $G(t, \gamma_0)$ for the annealed PMMA/PVDF sandwich structures and their neat components obtained after imposition of different strains:(a) $\gamma_0=0.05$; (b) $\gamma_0=0.2$; (c) $\gamma_0=3.05$. Predictions of the developed model, linear additivity rule as well as reciprocal rule are given in the figure.

Typical curves of stress relaxation moduli $G(t,\gamma)$ versus time for PMMA/PVDF bilayer structures with (annealed) and without (un-annealed) interphase as well as their monolayers achieved at a small deformation($\gamma_0=0.05$), an intermediate deformation($\gamma_0=0.2$) and a large deformation ($\gamma_0=3.05$) are shown in Figure IV-10. As indicated in Figure IV-10(a), at the linear viscoelastic region(small deformation), both the stress relaxation modulus $G(t,\gamma_0)$ of the bilayer with interphase (after annealing for 45mins) and the bilayer without interphase (without annealing) lie between those of their constituent components. It seems that there is no significant difference in the

$G(t,\gamma_0)$ between the bilayer with interphase and that without interphase. Prediction of the model (i.e., eq.(IV-16)) developed for the $G(t,\gamma_0)$ of bilayer structures is compared to the experimental result, where we can see that the model basically accords with the experiment.

At the region of intermediate deformation (Figure IV-10(b)), circumstance happens to be different from that of linear regime as the un-annealed bialyer greatly distinguishes himself from its counterpart of annealed one. When a nominal step strain of 0.2 was imposed, the annealed bilayer structure relaxed with a moderate relaxation modulus $G(t,\gamma_0)$ lying between those of pure components, whereas the un-annealed one falls far down from its counterpart to a level even lower than neat PVDF. For comparison sake, we also display in Figure IV-10(b) the predictions of linear additivity rule and reciprocal rule. It is pronounced that the predictions of these two rules deviate greatly from the experimental results of both bialyers with and without interphase. However, the present model (eq. IV-16) predictions in this study based on the initial stress σ_0 of annealed bilayer and un-annealed bilayer capture the basic tendency of experimental results in a more reasonable manner.

At the region of large shear deformation (Figure IV-10c)), the bialyer with interphase and that without interphase experienced similar stress relaxation behavior after the step strain like in the case of small deformation. Nevertheless, both the $G(t,\gamma_0)$ of them are lower than the theoretical prediction of the proposed model. In other words, the $G(t,\gamma_0)$ of the bilayer with interphase is reduced by the large deformation to be the same as that without interphase. A plausible mechanism for the damping of the $G(t,\gamma_0)$ of the bilayer without interphase under intermediate deformation and the damping of the bilayer with interphase under large deformation is the entanglement loss especially at the interface/interphase occurs after the large external deformations. This is similar with the stress damping (i.e., strain softening) behavior in the neat polymer melts. Note that a very severe stress damping behavior which may accompany with a kink-like appearance can be caused from experimental artifacts like slip (wall slip or stick-slip). For insurance purpose, same step strain experiments have also been carried out in ARES on both the bilayer strucutres with and without interphase. As shown in the Supporting information, similar experimental results have been obtained between ARES and DHR-2, implying that the $G(t,\gamma_0)$ damping in the case of bilayers is neither due to experimental artifacts nor the inertial effect of stress-controlled rheometer. It is supposed to be resulted from the first ultrafast relaxation process of chain retraction after readily occurred affine deformation and the final entanglement loss at the interface/interphase. Higher amount of entanglement in the interphase retards the damping behavior of the annealed bilayer to a larger deformation compared with its counterpart without interphase.
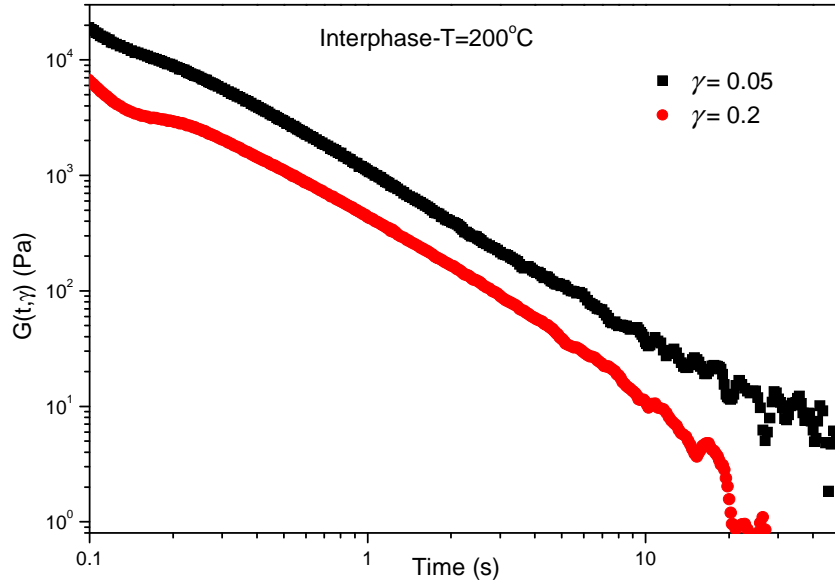
Figure IV-11 Time dependent nonlinear shear relaxation modulus G(t,γ_0) estimated for the interphase at the annealed bilayers (annealing for 45 mins at 200 ºC)

Here, the equation (IV-15) that regards the system as a trilayer structure, enables to estimate the relaxation behavior of the triggered interphase after imposition of a certain strain γ_0 if the η_{int} is known. Note that the η_{int} can be calculated via

$$\varphi_{int}/\eta_{int} = |1/\eta_{total} - \varphi_A/\eta_A - \varphi_B/\eta_B|,$$ where $\varphi_{int} = h_I/H$ with h_I being the interphase

thickness and H the total thickness of sandwich structure. This rule has been often used in the literature (Lamnawar and Maazouz 2008, Kim et al. 2003) as well as in our earlier work (Zhang et al. 2013). The thickness of the diffuse interphase, h_I, has been demonstrated to be around 85μm after annealing for 45mins at 200 ºC in rheometer under LVE condition. Figure IV-11 depicts the obtained stress relaxation behavior of the interphase versus time for different step strains. It can be seen that the *G(t,γ_0)* decline behavior, that is, the stress damping or so-called "strain softening" behavior is very significant for the interphase as the strain is increased. In particular, at γ_0 = 3.05, the *G(t,γ_0)* of the interphase is estimated to be negative in the shown time range (t > 0.1 s) as the modulus of the bilayer falls down from the model prediction (Figure IV-10c).

According to the tube model or other theoretical scenarios, such stress damping behavior is the consequence of entanglement loss resulted from "convective constraint release" during chain retraction or transverse relaxation of confinement barrier (tube breaking) or elastic yielding of entanglement network, etc. We assume the theoretical mechanism also holds for the interphase. Results in Figure IV-10 and Figure IV-11 imply that entanglement loss is more readily to happen in the interphase after large external deformations and even an interfacial failure may appear if the deformation is sufficiently large where the entanglement networks at the interphase are completely broken down. Such strong stress damping behaviors in

bilayer systems with and without interphase are due to the entanglement lack at the interface and the weak entanglement intensity at the interphase which is to be demonstrated also in the following section of startup shear and uni-axial extension measurements. The entanglement lack at the interface/ entanglement deficiency at the interphase makes the bilayer with (after annealing) and without (no annealing) interphase own different response to the small, intermediate and large external deformation. As the deformation is sufficiently small where chain motion is free from tube confining barrier and constraints, the un-annealed bilayer appears to have similar relaxation modulus $G(t,\gamma_0)$ as that of annealed bilayer, both of which essentially accord with theoretical predictions. When the deformation (in an intermediate range) is sufficient to break the interface of un-annealed bilayer but unable to destroy the interphase of annealed bilayer, the $G(t,\gamma_0)$of un-annealed bilayer is significantly lowered down from that of annealed bilayer. When the deformation is sufficiently large till enough to completely destroy the interphase of annealed bilayer, the $G(t,\gamma_0)$ of annealed bilayer also decreases in a same manner to that level of un-annealed one, showing negative deviations from the theoretical prediction.

From the words of Wang et al. (2007), the low cohesive entanglement force at the interfacial zone fails to against the elastic retraction force, $f_{retract}$, produced after affine deformation when the strain exceeds a critical value. Likewise, from the view of recent self-consistent microscopic theory of Sussman and Schweizer (2012), the tube transverse barrier potential in the interphase is easy to be reduced, i.e., tube breaking easily happens. In the case of very large deformation, perhaps the entanglements in the interphase are to be completely destroyed without re-emergence thereafter. After all, the experimental results obtained here is in accordance with the work of Zartman and Wang (2011) which focused on the mechanical failure at interphase in multicomponent polymer systems during shear and after shear cessation. At small and intermediate deformations, the interfaical failure is limited, the broken interface re-heals and can sustain the residual shear stress during the last stage of the relaxation whereas at very large deformation, the interphase fails to sustain the imposed stress like the interface at un-annealed bilayers.

IV.4.4. Transient rheological response during fast startup shear

IV.4.4.1 Startup shear of neat polymers

The stress growth experiment is predominately considered for nonlinear rheology of a viscoelastic material. Measurement of the shear stress growth and evolution of normal stress during startup of simple shear flow has been demonstrated to be sensitive to the main nonlinear viscoelastic features of entangled polymer liquids like solution, suspension and melts, etc.. Nonlinear viscoelastic features such as emergence of overshoot in transient shear flow and strain hardening in uniaxial extensional flow are of the least success in the fields to be described by the Doi-Edwards model (Hua, et al. 1999;Wang, et al. 2007). In order to explain the

nonlinear phenomena, Wang et al. (2007) proposed some new theoretical considerations, elastic breakdown of chain entanglement network for the overshoot and geometrical condensation for the strain hardening. Before revealing the transient rheological response of the bilayer systems, the nonlinear features of their constituent neat polymers during the startup continuous deformation are to be first focused.
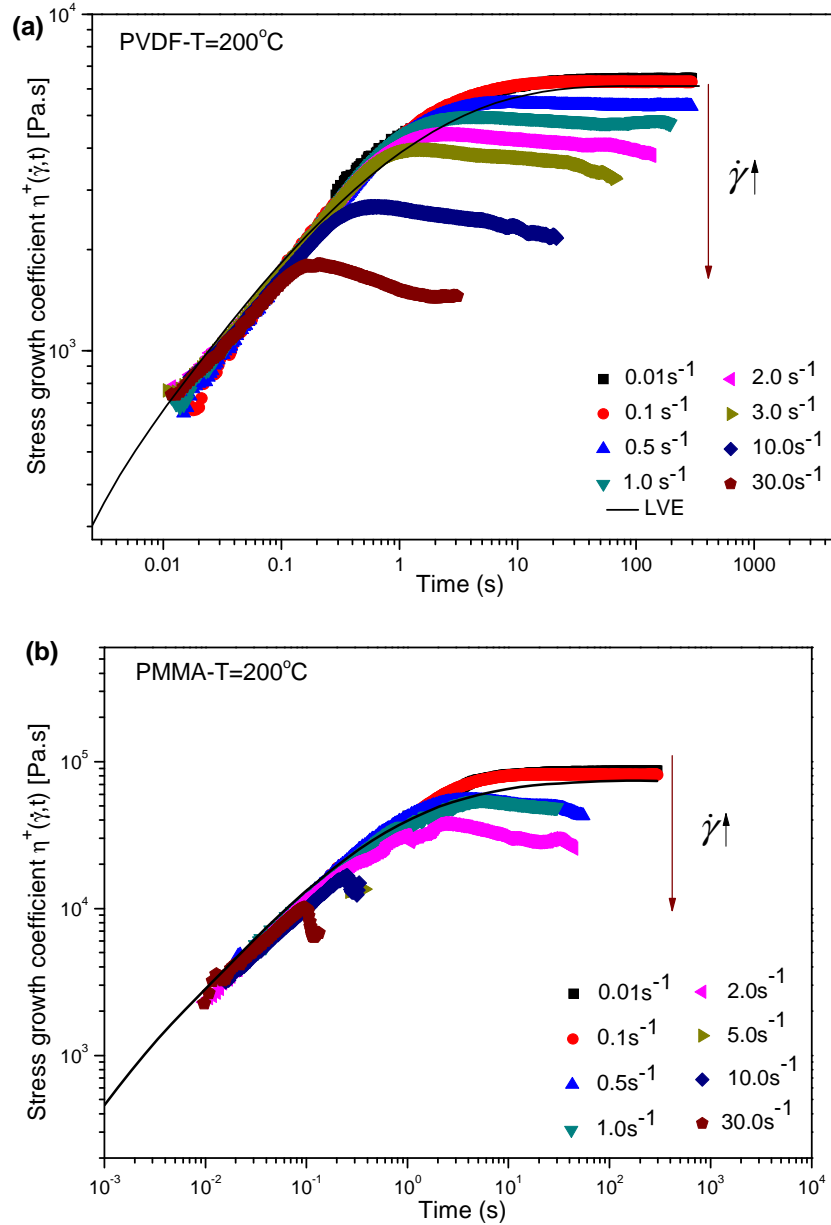
Figure IV- 12 Stress growth coefficient versus time for a startup shear measurement at 200 °C of PVDF (a) and PMMA (b). The solid line represents the linear viscoelasticity (LVE) determined from the relaxation spectra $\eta_0^+(t) = \int_0^t G(s)\,ds$.

Figure IV-12 displays the time-dependent shear stress growth coefficient (transient viscosity) of neat PVDF and PMMA components obtained in startup shear measurements at 200 °C. At a given shear rate, stress response or stress growth coefficient variation versus time can be divided into three regimes: Linear viscoelastic

regime at short times where the response is purely elastic and the stress growth coefficient increases monotonically regardless of the shear rates; steady-state regime at sufficiently long times where the transient viscosity remains invariable as a plateau, corresponding to the steady state behavior and transition regime at the intermediate times between the former two regimes, where an overshoot in material functions (i.e., a maximum in shear stress, transient viscosity and normal stress coefficient, etc.) may appear depending on the shear rate and the material structural characteristics. As shown in Figure IV-12, in the linear region at short times, the transient viscosity curves obtained at different shear rates superpose together, and the transient viscosity is independent of the shear rate. This accords with the results of linear viscoelasticity (LVE) determined from small amplitude oscillatory shear measurements (SAOS), which is denoted as a solid line in Figure IV-12. Therein for very small rates, the transient viscosity at the steady state corresponds to the zero shear viscosity. With the shear rate increased, the curves of $\eta^+(\dot{\gamma},t)$ becomes nonlinear, accompanying with emergence of an overshoot in contrast with the monotonic stress growth toward a steady state value for small rates. In general, in a startup shear, the overshoot emerges before reaching a steady state when the shear rate imposed to the entangled polymer satisfies with Weissenberg numbers $W_i = \tau_{rep}\dot{\gamma} > 1$. Meanwhile, as indicated in Figure IV-12, the higher the shear rate, at shorter time the transient viscosity curves fall below the LVE envelope curve as well the shear stress overshoot location *tos* drifts to progressively shorter times, which are consistent with previous observations reported in the literature (Sanchez-Reyes and Archer 2003). The nonlinear functions fall below the linear envelops at smaller and smaller strains as the shear rate increases, which is the so-called "strain softening" in transient shear flow during startup shear. It is necessary to mention that for PMMA melts, due to its high elastic modulus, a complete stress growth curve is not able to be reached at high shear rates since the stress is overloaded after certain high strains.
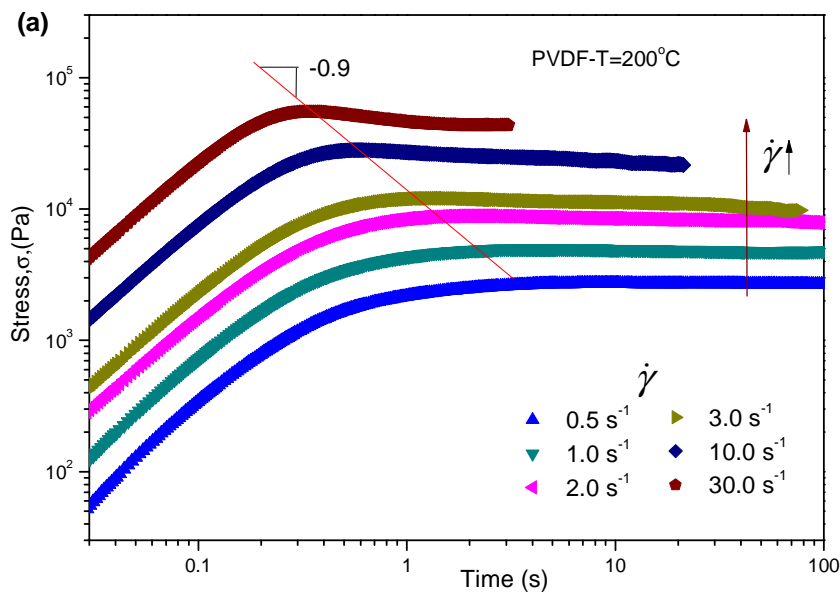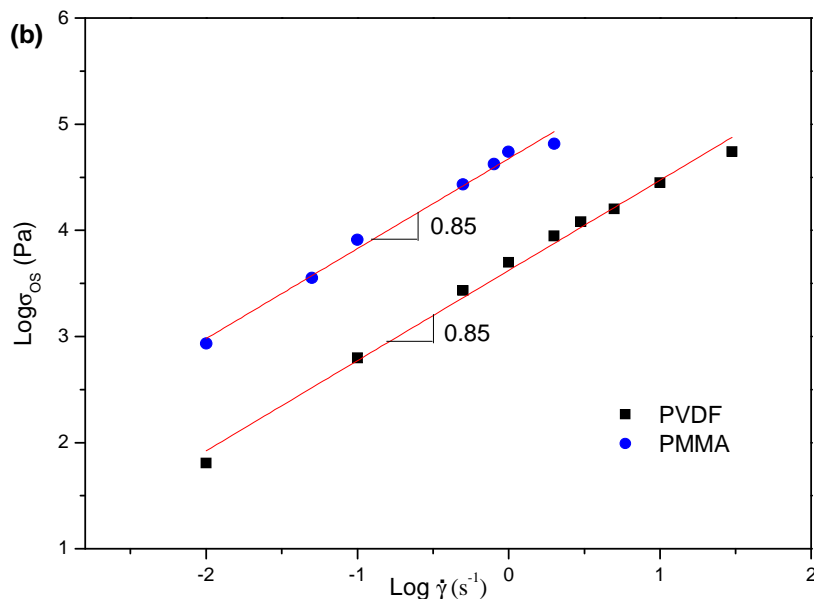
Figure IV- 13 (a) Stress versus time during startup shear measurement of PVDF;(b) Stress at overshoot σ_{OS} versus shear rate in logarithm scale for PVDF and PMMA melts, red continuous line denotes the linear fittings.

The "strain softening" and overshoot appeared in transient flow are two of most interesting nonlinear features. However, explanations for these nonlinear features are still far from maturity. These are argued to be associated to the chain stretching, retraction and constrain release according to the Doi-Edwards theory as well as its evolved versions incorporating convective constrain release (CCR) (Marrucci 1996) and to be associated to a yield point of polymer network according to the new theoretical consideration of Wang and coworkers (2007). Indeed, Convective Constraint Release (CCR) (Marrucci 1996) was developed to remedy the infinitely strong tube constraint assumption in the original DE model and hence revises the flaw feature of nonmonotonic steady-state flow curve in the prediction of original DE model.

For the stress overshoot appeared during startup shear in transient flow, the concept of Wang and coworkers (2007, 2009, 2012) assumes the stress maximum as a yield point, where the entanglement network ceases to undergo further molecular deformation due to a force imbalance between the intermolecular locking force that is causing the chain deformation and the intramolecular elastic retraction force. They argue that the stress overshoot is a consequence of molecular disentanglement in contrast to the tube model picture of the chain orientation. Though a very accurately quantitative theoretical description of the nonlinear features is yet available, they have attempted to sketch universal scaling behaviors to depict the intermolecular interactions during continuous deformation from aspects of forces development based on their experiments of a series of monodisperse styrene-butadiene rubber (SBR). Likewise, we also attempt to scale some relationships based on our experimental data, as shown in Figure IV-13.

During a startup continuous deformation with $W_i < 1$ (linear response zone), the state of chain entanglement is not altered by the external deformation, the measured stress rises monotonically obeying to the full elastic recovery upon letting go stress free. Upon a startup deformation with $W_i > 1$, linear response (elastic deformation) is only limited to strains below a critical level. Above the critical level, yielding behavior occurs with structural transformation from elastic to inelastic state, accompanying with emergence of so-called stress overshoot. It is believed that beyond the yield point, disentanglement occurs and the chain entanglement network has been irreversibly altered. During the continuing deformation at $W_i > 1$, the intermolecular gripping force, f_{img}, which is absent at quiescent state presents due to the chain uncrossability and declines as deformation continues since effectiveness of intermolecular interactions to grip the test chain decrease. It is stated that the yielding point appears when the rising intrachain retraction force, $f_{retract}$, (i.e. the measured stress) meets the declining f_{img}, equaling to the σ_{max} (or σ_{os}), deformation stops growing and chain disentanglement takes place with overshoot appearing. The f_{img} is postulated to be a function as:

$$f_{img} \sim f_{ent} (\dot{\gamma}\tau)^{\beta} (\gamma_0 + \gamma_{os})^{-\alpha} \tag{IV-17}$$

with α and β being exponents. In their work, Wang and Wang (2009) demonstrated a universal scaling law between the overshoot stress, σ_{os}, and overshoot time, t_{os}, as $\sigma_{os}(t,\dot{\gamma}) \sim (\tau/t_{os})^{\nu}$, with exponent $\nu=1/2$ for the elastic deformation regime ($\dot{\gamma} > \tau_R^{-1}$) and $\nu=1/4$ for the viscoelastic regime ($\tau_{rep}^{-1} < \dot{\gamma} < \tau_R^{-1}$). At the yield point, since $f_{img}=\sigma_{os}$ and γ_0 can be negligible compared to γ_{os}, thus

$$f_{ent} (\dot{\gamma}\tau)^{\beta} (\dot{\gamma} t_{os})^{-\alpha} \sim (\tau/t_{os})^{\nu} \tag{IV-18}$$

They obtained the parameter $\alpha=\beta=1/2$ for the elastic deformation regime in their work. As indicated in Figure IV-13(a), we observed that for the PVDF melt studied in this work in the viscoelastic regime, $W_i > 1$ and $W_{iR} < 1$, $\sigma_{os} \sim (t_{os})^{-0.9}$, and the σ_{os} of the studied PVDF and PMMA melts own a scaling relation with $\dot{\gamma}$ as $\sigma_{os} \sim (\dot{\gamma})^{0.85}$ as shown in Figure IV-13(b). Incorporation of these scaling laws into eq. (IV-18) gives $\alpha = \nu = 0.9$ and $\beta = 1.75$. Disagreement happens on the exact exponent values of the scaling laws between this work and that of Wang and Wang (2009). This could not be straightforwardly denied since in our opinion relation between the intermolecular gripping force, f_{img} ($\sim\sigma_{os}$), and time as well as shear rate cannot be exactly the same for different polymer melts. The intermolecular interaction could be related to a lot of topological effects such as monomeric friction of chains which could be significantly different for different polymers. Moreover, the scaling laws of Wang and Wang (2009) have been demonstrated only for the monodisperse polymers, however, the polymer investigated in this work are polydisperse. It is known that the short chains can have some tube dilation effects on the relaxation of of long chains.

IV.4.4.2 Startup shear of bilayer systems

In the present study, startup shear measurements at different shear rates have been carried out to the annealed bilayer (with interphase) and the un-annealed bialyer (without interphase) structures to probe the response of the interface/interphase. To our knowledge, few studies have been dedicated to this point despite of its significance in both fundamental and applied areas. Figure IV-14 depicts the evolution of stress growth coefficient η^+ versus time for the bilayer without interphase and the bilayer with interphase during continuous deformations at different nominal shear rates. The reciprocal rule prediction on LVE data, that is $1/\eta_{bi}^+ = \varphi_A/\eta_A^+ + \varphi_B/\eta_B^+$, is also plotted in the figure. The superposition and agreement with LVE envelop are also true for the transient viscosity curves at low shear rates (<1.0 s^{-1}) for both the un-annealed and annealed bilayers, whereas the curves turn into steady stage (or overshoot at high rates) earlier and the steady values are lower compared to the LVE reciprocal rule. That means the bilayer system is easier to reach the yield point of force imbalance. It is interesting to notice that for high shear rates above a critical value, the transient viscosity curves of bilayers begin to depart from the LVE envelop curve, even does the zone of linear rheological response. The deviation from LVE envelop begins at lower rates (no more than 5 s^{-1}) for un-annealed bilayer than its annealed couterpart due to its lack of cohesive strength at the interface. To give a more detailed and clear comparison between the bilayers without and with interphase, results in Figure IV-14 are re-plotted in Figure IV-15 at an individual window for each rate, where those of neat components as well their equivalent 50% blend are included.
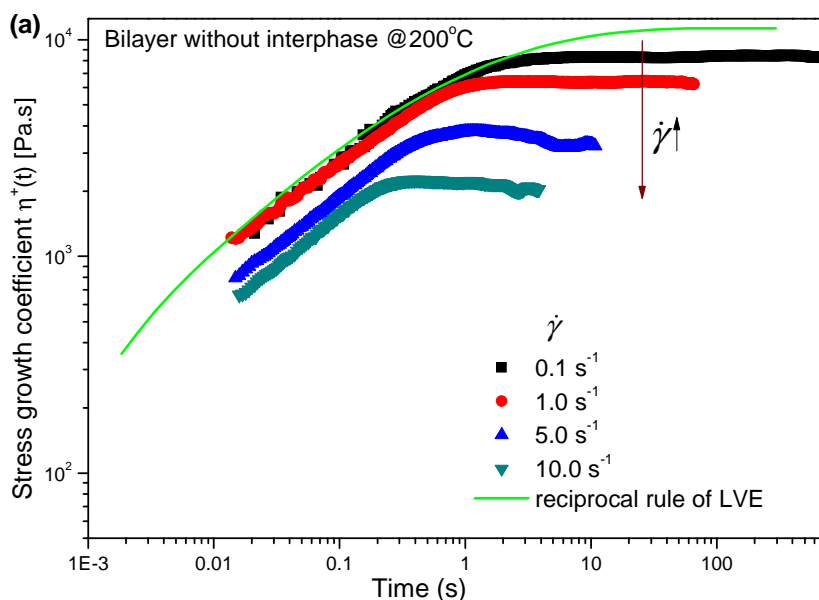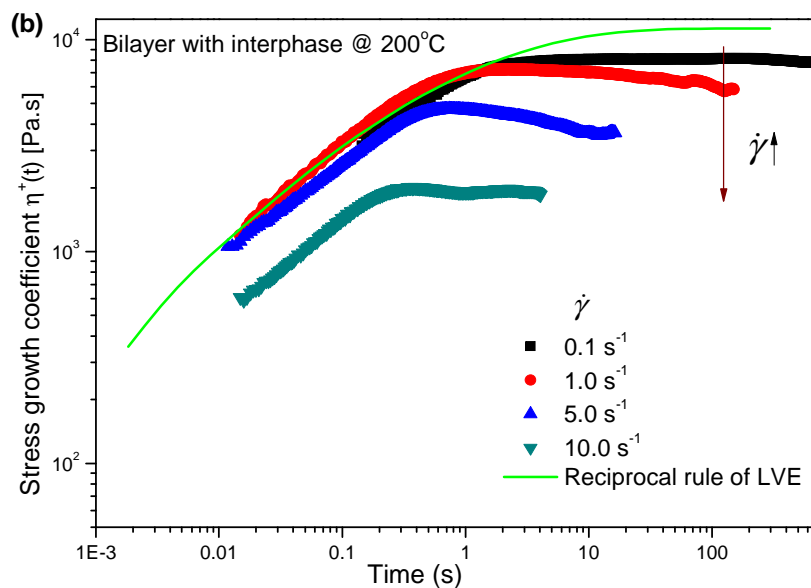
Figure IV-14 Startup stress growth coefficient as a function of time determined at different shear rates ranging from 0.1 s^{-1} to 10 s^{-1} for the bilayers without (a) and with interphase (b), respectively. Solid line is reciprocal rule obtained from LVE of neat components.

From Figure IV-15, we can emphasize that at low shear rates (c.a. $\dot{\gamma} \leqslant 1.0$ s^{-1}), both the bilayers with and without interphase have closely similar stress growth behavior in accord with reciprocal rule (Figure IV-15a,b), whereas great distinctions appear between these two at higher shear rates (Figure IV-15c,d). Like the stress relaxations in step strain experiments shown before, pronounced differences are noted for the bilayers in intermediate and large shear rates in comparison with neat materials under the same experimental conditions. Specifically, at the intermediate shear rates (e.g. 5 s^{-1}), the η^+ curve of bilayer without interphase is significantly deviated downward from its counterpart with interphase which accords with the reciprocal rule. At large rates (e.g. 10 s^{-1}), both the η^+ curves of bilayers with and without interphase fall down from the reciprocal rule prediction to a similar level that is even lower than neat PVDF. These observations are in good agreement with the work of Zartman and Wang (2009), in which the nature of possible mechanical failure at interphase in multicomponent polymer systems during shear and after shear cessation has been demonstrated based on styrene butadiene rubber (SBR)/polyisoprene (PI) weakly incompatible pair.
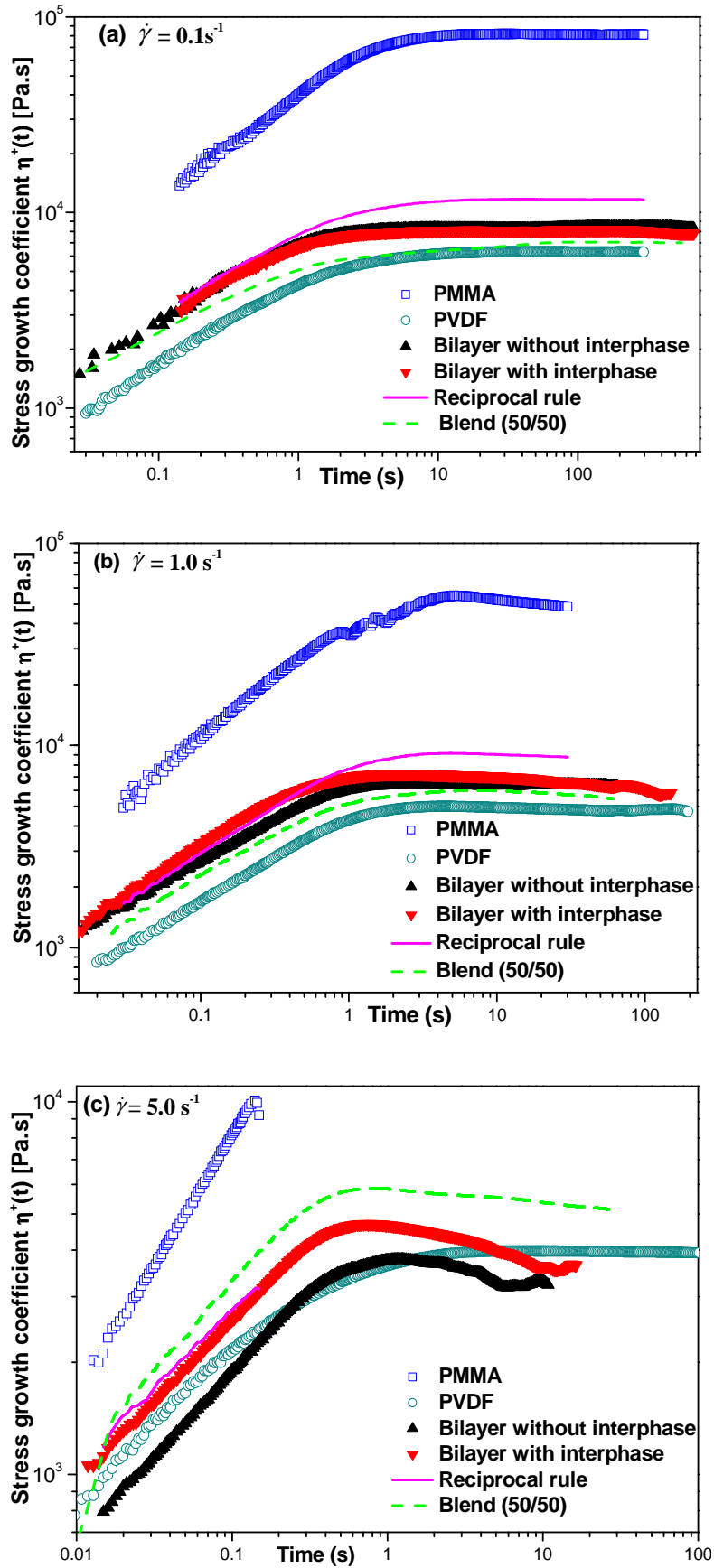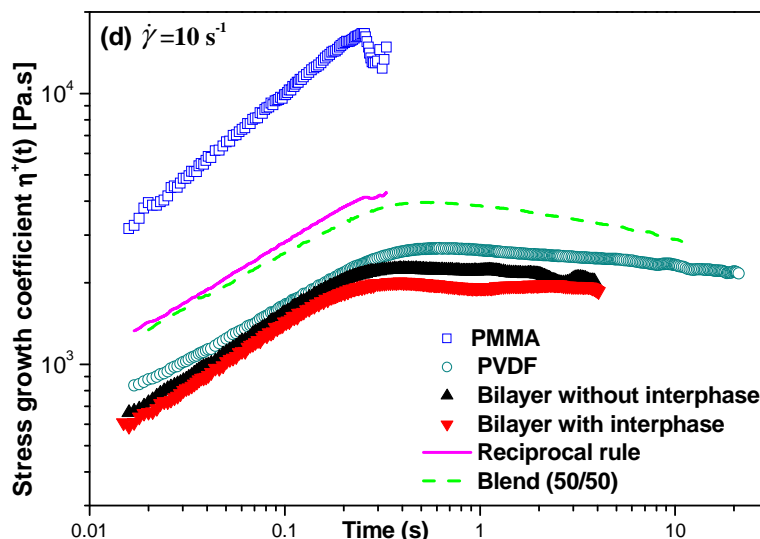
Figure IV-15 Plots of startup stress growth coefficient as a function of time for the bilayers with (annealed) and without interphase (un-annealed) at 200 °C with different nominal shear rates: (a) 0.1 s⁻¹; (b) 1.0 s⁻¹; (c) 5.0 s⁻¹; (d) 10.0 s⁻¹. Solid lines represent predictions of reciprocal rule and dashed lines are results of PMMA/PVDF-50/50 blend.

The significant transient viscosity reduction of the bilayer systems at high Weissenberg numbers, W_i, should be the macroscopic evidence of interfacial failure. Undoubtedly, it is attributed to the weak entanglement strength at the interfacial zone (interface or interphase). Indeed, this interfacial yielding could also cause so-called interfacial slippage, that is, bringing about a velocity difference across the interface. The startup shear measurement has been employed as a tool to probe the interfacial slippage for incompatible multilayered structures like polypropylene (PP)/polystyrene (PS) by Lee et al. (2009). This interfacial yielding at high shear conditions has also been well demonstrated in the step strain experiments after large deformations where significant damping behavior of the $G(t,\gamma_0)$ happens to the bilayer systems. Obviously, the triggered interphase at annealed bilayer plays a key role in delaying the interfacial yielding to a higher W_i and higher external deformations. Conversely, sharper interface at the un-annealed bilayer suffers from the interfacial yielding under a weaker shearing condition due to the lack of entanglements. Notice that even though the interphase would be full of entanglement arise from interdiffusion, it would still be weaker than each of the bulk polymers from the standpoint that the entanglement density in PMMA/PVDF blends is weaker than its bulks (Wu 1987).

From viewpoint of the DE model, the difference in the transient response of the stress component primarily originates from the intensity of the CCR mechanism on the orientation of the chains and the coupling to the chain orientation with the stretching dynamics in the flow(Schweizer, et al. 2004). Increasing the intensity of the CCR mechanism results in a reduction of the "effective" reptation time of the chains and the flow field becomes less effective in orienting the chains. Besides, the

maximum magnitude and the time when the maximum is reached reduce with increasing the intensity of the CCR mechanism. So one may suppose that the contribution of CCR mechanism in the interface/interphase at bilayer systems is more pronounced than in the bulks. Due to lack of chain interpenetration at the interface of un-annealed bilayer and entanglement deficiency in the interphase of annealed bilayer, one can imagine that at the interface/interphase the entanglement spacing, l_{ent}, can be longer than that of bulk polymers. Hence, from the force imbalance picture of Wang et al. (2007), lower cohesive entanglement force, f_{ent} ($\sim k_B T / l_{ent}$) at the interface/interphase are needed to be overcome for elastic yielding. In other words, the lower entanglement density at the interface/interphase in comparison with the constituent bulks gives rise the tube confining barrier (effective entanglement constraints) at the interfacial zone to be easier to be overcome to activate the transverse hopping relaxation (tube breaking). That means the entanglement networks at interface/interphase have priority to be destroyed during the fast startup external deformations, leading to interfacial yielding and possible interfacial slippage. Presence of the interphase can retard the interfacial yielding to happen at a severer shear condition. These are consistent with the results observed in the step strain experiments of multilayer polymers.

IV.4.5. Transient rheology in uni-axial extension

IV.4.5.1 Elongation rheology of neat polymers

Elongation rheology is one another method to measure the non-linear response of polymer melts. At a constant Hencky strain rate, simple extension is said to be a "strong flow" in the sense that it can generate a much higher degree of molecular orientation and stretching than flows in simple shear. Apart from its strong significance on providing experimental evidences for theoretical studies of non-linear responses like "strain-hardening", etc. for polymer melts, uniaxial extension has also been widely used for investigations of the interfacial effect in multiphase systems like blend and multilayer structures especially of incompatible and reactive ones. Uniaxial extension is believed to stretch the interfacial structure, thus increase the interfacial area per unit of volume and amplify the interfacial effect. Levitt et al. (1997) have demonstrated this technique to be a suitable tool to study the cross-linking reaction at the interface of multilayered structures.

Even though some similarities are existing in fast startup measurement, different transient responses of the melts to simple shear and uni-extension are still expected because of their kinematic difference in deformation of shear and extension. Startup deformation is underwent in an increasingly shrinking area in uni-axial extension instead of a constant area in simple shear. Like in the simple shear, for the condition $W_i \ll 1$, the extended samples also experience full elastic recovery deformation before arriving at a yielding point, with tensile stress growth (transient elongation viscosity) curves superposed with the Linear Viscoelastic Envelop (LVE), zero-rate extensional

viscosity, $\eta_{E0}^+(t)=3\eta_0^+(t)$. Essential differences appear for these two kinematicses under the conditions that the deformation rates are in excess of the dominant molecular relaxation rate ($W_i>1$). In that zone, the transient shear viscosity $\eta^+(t)$ in startup shear becomes always lower than the LVE, that is so-called "strain softening"; whereas the transient elongation viscosity $\eta_E^+(t)$ in startup extension is upward from the LVE (i.e., "strain hardening") for most polymers and is downward ("strain softening") for some other polymer melts like HDPE, depending on polymer chain architectures.
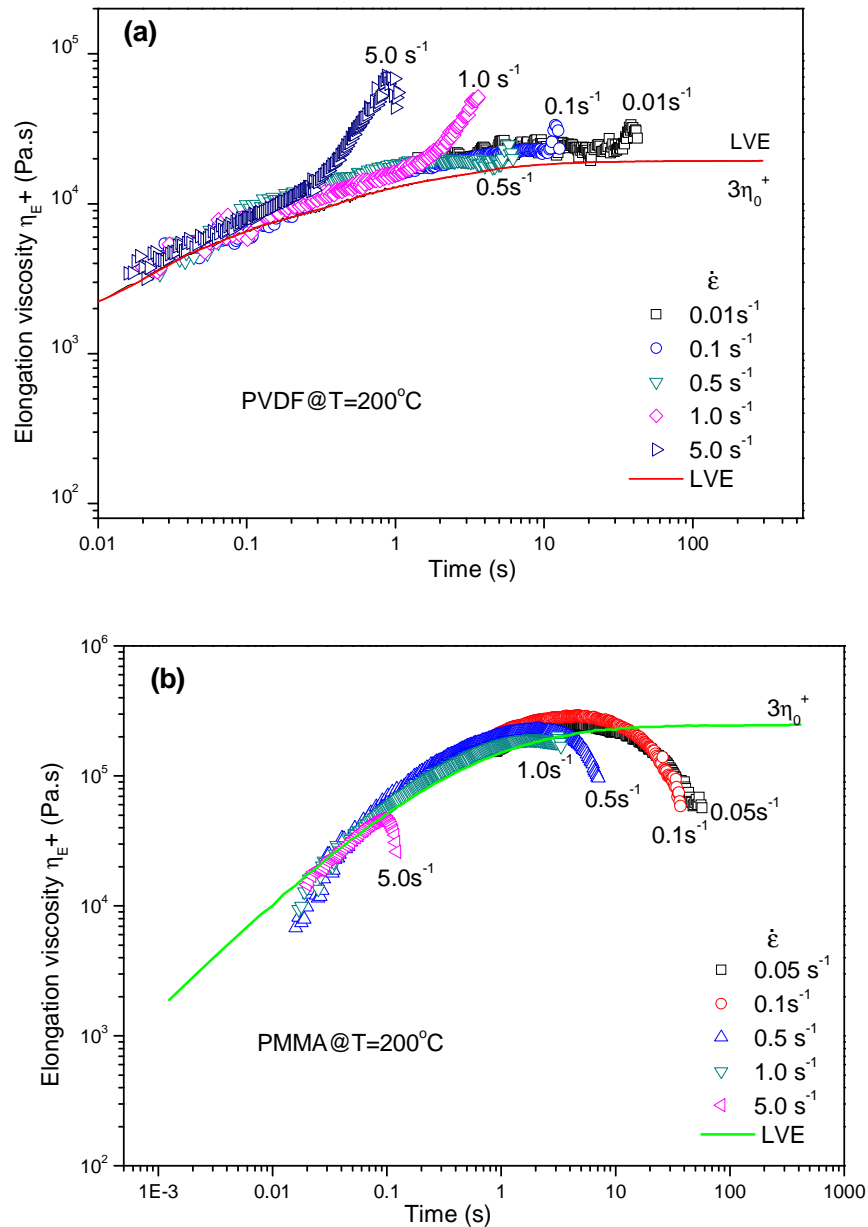
Figure IV-16 Elongation viscosity versus time in startup uni-axial extension with constant Hencky strain rates ranging from 0.01 to 5.0 s^{-1} at 200 ºC for PVDF (a) and PMMA (b). The solid line represents the linear viscoelasticity (LVE) (i.e., $3\eta_0^+(t)$) for each polymer determined from shear stress growth curves in startup shear.

Figure IV-16 depicts the transient elongation viscosity as a function of time

during startup uni-axial extension measurements at different constant Hencky strain rates, $\dot{\varepsilon}_H$, for PVDF and PMMA melts. Also presented in the figure are the zero-rate transient elongation viscosity limits ($3\eta_0^+(t)$), LVE curves, for each melts determined from their startup shear measurement. Good agreements with the LVE have been achieved for both the PVDF and PMMA melts at the full-elastic recovery region. The transient elongation viscosity $\eta_E^+(t)$ at this region is found to satisfy Trouton's ratio, that is, $\eta_E^+(t)=3\eta^+(t)$. Like most of well-entangled polymer melts, "strain hardening" behavior has also been clearly observed in the PVDF melt (Figure IV-16a) at finite constant Hencky rates (for $\dot{\varepsilon}_H$ higher than 1 s⁻¹) after critical strains and the upward deviation becomes more evident as the $\dot{\varepsilon}_H$ increases. Nevertheless, the PMMA melt (Figure IV-16b) studied in this work fails to display such "strain hardening", rather, "strain softening" is observed instead.

As mentioned before, the "strain softening" in startup shear could be attributed to the entanglement loss either resulted from the chain retraction, convective constrain release and entanglement number reduction according to tube model or resulted from the yielding of entanglement network when force imbalance is reached according to the theoretical picture of Wang et al.(2007). Liu et al. (2013) recently studied the kinematics difference between simple shear and uni-axial extension and proposed the origin of the "strain hardening" appearing in startup extension from a kinematics viewpoint. In simple shear, the shear stress σ12 is measured from the force imposed on a shear plane of constant area hence the σ12 grows linearly with time during continuous deformation. Nevertheless, in uni-axial extension especially at Wi>1, to maintain a constant Hencky rate, the cross-section area from where the Cauchy stress σc is evaluated shrinks exponentially with time during continuous deformation (eq.IV-2), hence the σc grows exponentially with time rather than in a linear relation. Only at vanishingly low rates, *Wi*<<1, the Cauchy stress σc could be approximately linear with time in startup uni-axial extension. Thus the true extensional stress could still increase much more strongly than linearly in time before entanglement yielding causes a sufficiently rapid decline of the tensile force.

The authors envisioned that the "strain hardening" in startup extension is caused from the difficult removal of chain entanglements within the increasingly shrinking area at high Hencky strain rates. In other words, if the reduction rate of the number of load-bearing entanglement strands in the cross-section cannot follow up with the exponential decrease of the cross-section area during an extension, entanglement density excess exist in the cross-section and hence "strain hardening" appears. For this, they (Liu, et al. 2013) suggested use of a damping function of stretching ratio λ, $h(\lambda)<1$, for the yielding of massive load-bearing entanglement ("strain softening") and introduced a factor of geometric condensation g(λ) associated with the definition of the Cauchy stress σc basing on the shrinking cross-section area during a startup extension. Then the $\eta_E^+(t)$ could be assessed from the linear transient elongation

viscosity, $\eta_{E0}^{+}(t)$, via $\eta_{E}^{+}(t) = \eta_{E0}^{+}(t)h(\lambda)g(\lambda)$. The g($\lambda$) factor, which was supposed to be the reason for the enhancement of the measured $\eta_{E}^{+}(t)$, was defined as $g(\lambda) = \lambda\left[(\lambda - 1/\lambda^2)/3\ln(\lambda)\right]$ with the stretching ratio λ being $\lambda = L(t)/L_0 = \exp(\dot{\varepsilon}_H t)$.

According to this theoretical scenario, whether the "strain hardening" occur or not depends on the competitions of the "strain softening" function *h(λ)* of massive entanglement yielding and the geometric condensation factor g(λ). For most of polymer melts, some obvious geometric condensation with a consequence of condensing the same number of load-bearing entanglement strands into a shrinking cross-sectional area is bound to occur before massive yielding of the entanglement strands takes place. In this case, *h(λ)*g(*λ*)>1, the "strain hardening" shows up, like the example of PVDF melt in this study. On the other hand, for some polymer melt like PMMA studied here, massive entanglement yielding happens earlier than the geometric condensation appears. In other words, the reduction rate of entanglement number in the cross-section can follow up with or even faster than the shrinking of the cross-section area during the startup extension, that is, no excess entanglement density is condensed into the shrinking area (i.e. *h(λ)*g(*λ*)<1), "strain softening" appears instead of the "strain hardening". This maybe is due to the extremely high stiffness of PMMA chains under the studied conditions and hence its high difficulty of stretching along with its readily yielding at a low degree of extension. The strong "strain softening" and readily yielding of PMMA melts has also been demonstrated in its startup shear and by its severe damping function in stress relaxation after large step strains (see Figure IV-7).

It is worthy of noting that in tube theories, the "strain hardening" in startup extension is thought to be resulted from chain stretch. Besides, long-chain branching (LCB) was also argued to be necessary for appearing strain hardening and a pom-pom model was developed by McLeish and Larson (1998) to offer a theoretical interpretation of the strain hardening. Despite of these, they are still not able to predict the strain hardening covering all the cases in an universal way. In addition, a slip-link model has also been proposed to predict the nonlinear rheological properties in shear and extension. Since this is out of the scope of the present study, we do not extend too much on this point here.

IV.4.5.2 Elongation rheology of multilayer systems

We remind here the starting point of this study is to give a picture on the nonlinear rheological response of the interphase generated at neighboring layers of multilayer structures. In a recent work where startup uni-axial extension was used to probe its sensitivity to the presence of the interphase in coextruded thermoplastic urethanes(TPUs) (Silva, et al. 2012). The authors failed to detect the presence of their interphase by this method because of the high viscosity ratio of their polymer pairs as well the relative low amount of interphase. In this work, with large amounts and

well quantitatively-characterized interphase generated at PMMA/PVDF alternating multilayers and using un-annealed multilayers (without interphase) as reference, we aim to probe the rheological response of the diffuse interphase to the fast startup extension. To this aim, both the multilayer structures with well-defined interphase prepared from compression molding and coextrusion were focused. In uni-axial extension, since the deformation happens via simultaneously stretching the multilayer specimen in a direction parallel to the interface, it is supposed to be more reliable to probe the contribution of interface/interphase and effect of the interfacial area can be highlighted.
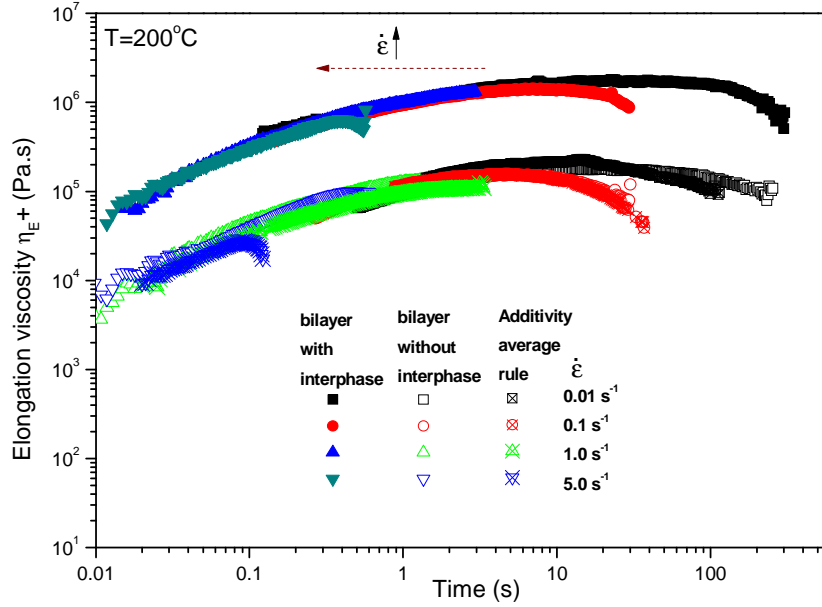
Figure IV-17 Curves of elongation viscosity versus time in uniaxial extensional startup measurement with constant Hencky strain rates ranging from 0.01 to 5.0 s⁻¹ at 200 °C for compressed PMMA/PVDF bilayers with interphase (annealed for 45mins)(solid symbols) and without interphase (unannealed)(open symbols).

When a mulitlayer structure is subjected to an uni-axial extension, the deformation rate for each layer is the same, i.e., Hencky strain rate, $\dot{\varepsilon}_H = 2\Omega R / L_0$. The total force measured is sum of contributions of each layer. Take an annealed bilayer structure with presence of an interphase as an example, the total force could be written as:

$$F_{total}(t) = \sigma_A(t)A_A(t) + \sigma_B(t)A_B(t) + \sigma_I(t)A_I(t) \qquad \text{(IV-19)}$$

in which $\sigma_i(t)$ is Cauchy stress of layer i, i denotes layer A,B and interphase.

The $A_i(t)$ is cross-sectional area of layer i with $A_i(t) = W_i(t)H_i(t)$ where $W_i(t)$ and $H_i(t)$ are time-dependent width and thickness of layer i, respectively. Hence, the transient extensional viscosity of the total sandwich structure can be described as:

$$\eta^+_{Etotal} = \frac{F_{total}(t)}{\dot{\varepsilon}_H A_{total}(t)} = \frac{\sigma_A(t)}{\dot{\varepsilon}_H}\varphi_A + \frac{\sigma_B(t)}{\dot{\varepsilon}_H}\varphi_B + \frac{\sigma_I(t)}{\dot{\varepsilon}_H}\varphi_I = \varphi_A\eta^+_{EA} + \varphi_B\eta^+_{EB} + \varphi_I\eta^+_{EI} \quad \text{(IV-20)}$$

where φ_i is composition of layer i with $\varphi_i = A_i(t)/A_{total}(t) = H_i(t)/H_{total}(t)$. When there is absence of interphase, eq. (IV-20) could be simplified to be a more simple additivity rule as

$$\eta^+_{Ebi} = \varphi_A\eta^+_{EA} + \varphi_B\eta^+_{EB} \qquad \text{(IV-21)}$$

Therefore, the $\eta^+_{Etotal}(t)$ of the total sandwich structure depends on the viscosity ratio of the constituent components and their compositions. As said by Silva et al. (2012), the $\eta^+_{Etotal}(t)$ can be dominated by the more viscous component if the compositions are similar. If the viscosity difference is not very significant, the $\eta^+_{Etotal}(t)$ may be greatly affected by the component composition to some extent. As displayed in Figure IV-17, the addivity rule of eq. (IV-21) well predicts the transient extensional viscosities of the un-annealed PMMA/PVDF bilayers at different constant Hencky rates. Furthermore, the compressed bilayers with interphase have been shown to have higher $\eta^+_E(t)$ than its counterpart of un-annealed bilayers as indicated in the figure. This should be the contribution of the high amount of triggered interphase (~85 μm) considering that the component viscosity ratio is not that high. Buildup of entanglements by mutual chain penetrations at the interfacial zone resulted from the interdiffusion process give rise to a higher tensile stress in startup extension in contrast to its un-annealed counterpart with lack of entanglement at the interface.
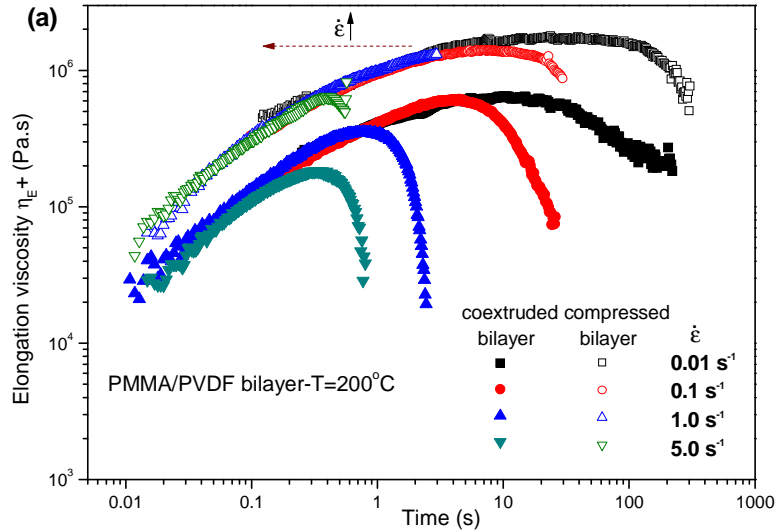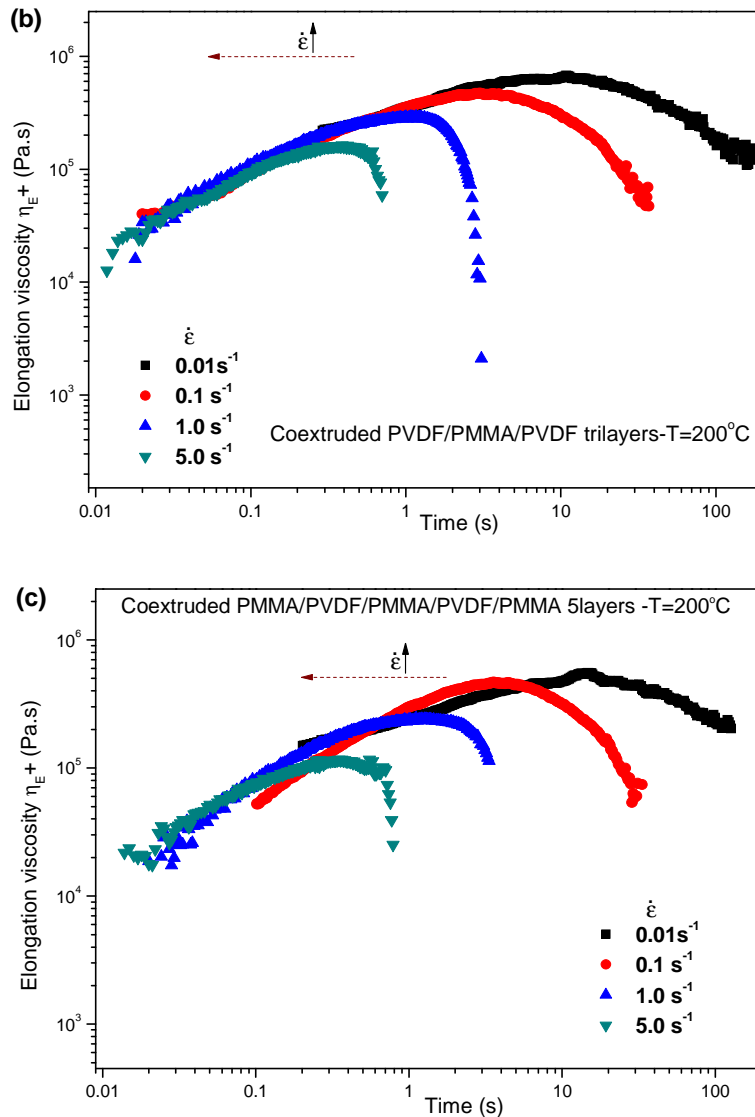
Figure IV- 18 Curves of elongation viscosity versus time in uniaxial extensional startup measurement with constant Hencky strain rates ranging from 0.01 to 5.0 s^{-1} at 200 °C for coextruded PMMA/PVDF multilayers with a given composition φ_{PMMA} = 50%: (a)PMMA/PVDF bilayers; (b)PVDF/PMMA/PVDF trilayers and (c) PMMA/PVDF/PMMA/PVDF/PMMA- 5layers .

Figure IV-18 depicts the elongation rheology of the coextruded multilayer structures of bilayer, trilayers and 5layers with a constant composition φ_{PMMA}=50% at different Hencky strain rates. It can be seen that as like neat polymers, the elongation viscosity of the multilayer structures follows the linear viscoelastic regime before deviating downwards from the linear envelope, indicating of "strain softening". Such "strain softening" as in the case of PMMA melts suggests that the $\eta_{E^+}(t)$ of multilayer structures with 50% composition is more dominated by the more viscous component of PMMA. In Figure IV-18a, results of compressed bilayers have also been displayed for comparison. At first glance, one may be astonished about the lower level of the $\eta_{E^+}(t)$ in coextruded bilayers compared to its compressed counterparts at same rates.

In fact, it is plausible and understandable if one takes a deep insight into the entanglement intensity of the interphase and its fraction taking account in the compressed sandwich structure and in that of the coextruded ones.
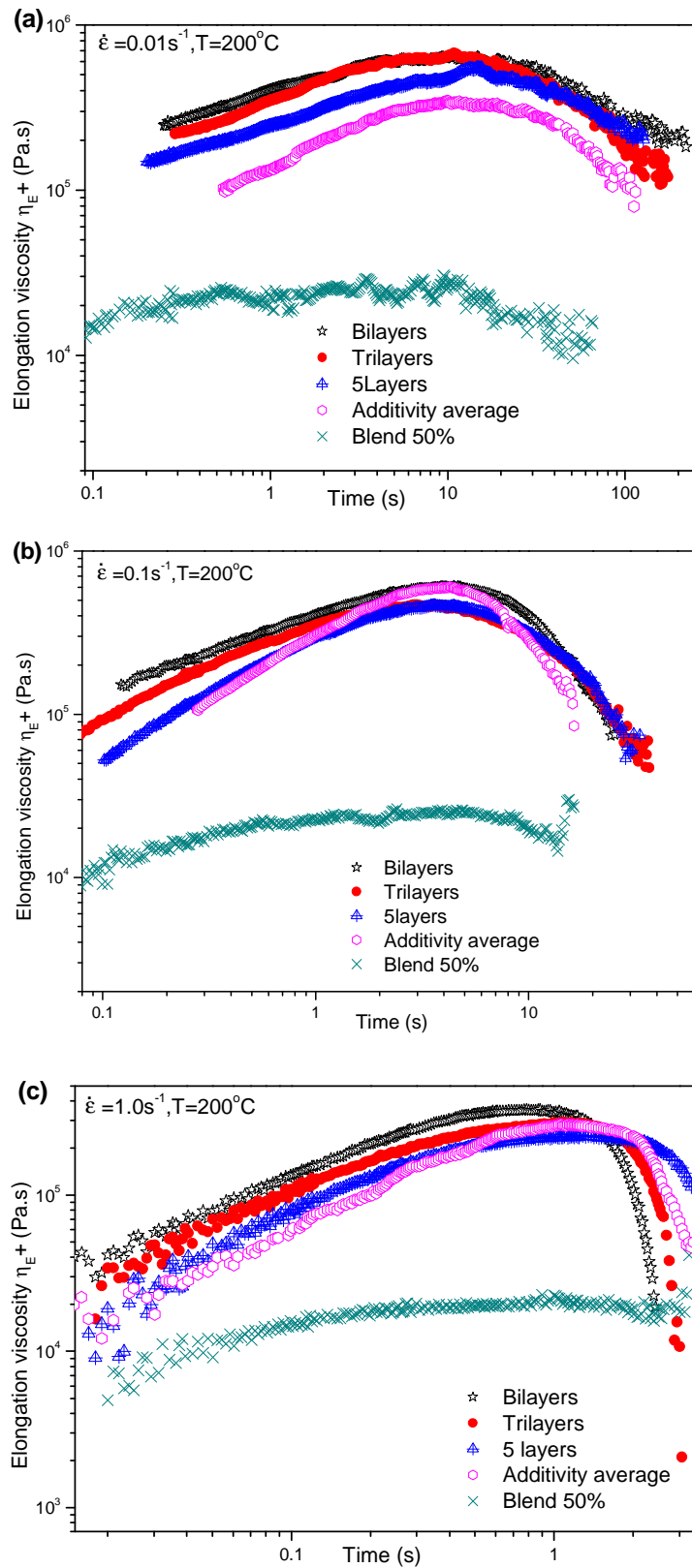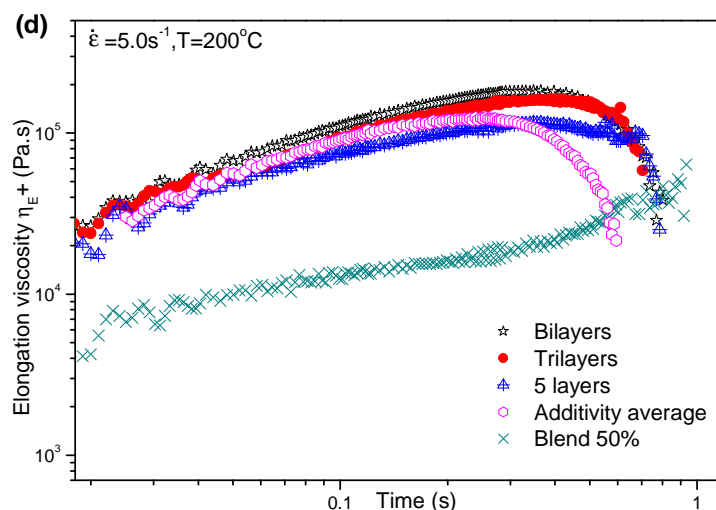
Figure IV-19 Comparisons of the transient elongation viscosity $\eta_E^+(t)$ of coextruded PMMA/PVDF mutilayer structures of different layer numbers versus time obtained at varying Hencky strain rates: (a) 0.01 s^{-1}; (b) 0.1 s^{-1}; (c) 1.0 s^{-1}; (d) 5.0 s^{-1}

It is sure that presence of certain amount of interphase is necessary to remove the entanglement gap at the sharp interface and thus to greatly increase the strength in the interfacial zone. So it requires either more torque for shear or more tensile force for stretching in extension, resulting in an increment of rheological functions in LVE and in startup uni-axial extension. In our earlier work (Zhang et al. 2012, 2013), we have already investigated in detail the kinetics of the interdiffusion process which gives rise to such strengthening at the interfacial zone. However, the strength of the sandwiched structure cannot grow infinitely with the amount of diffuse interphase. When the amount of the diffuse interphase reaches a level comparable to that of its constituent components, the situation could be a different picture. This is related to the entanglement intensity of the diffuse interphase. It is important to notice that the topological architecture of entanglement in the mixed state of different polymer chains like diffuse interphase should be very different from that of their constituent bulks, rather, it is more analogous to their blends. Even though the interphase is full of entanglement and the pair of melts is sufficiently compatible, one could not take for granted that it would own comparable entanglement strength as that of the bulk polymers. For the PMMA/PVDF mixtures, though they are full compatible, a weak thermorheological complexity still has been demonstrated as a consequence of the locally heterogeneous dynamics. The compatible dissimilar chains have been found to less likely entangle with each other than similar chains. The strong specific interchain interaction that is responsible for the compatibility tends to reduce the chain entanglement since it promotes local chain alignment, association as well reduces chain convolution and thus reduce entanglement probability between dissimilar chains (Wu 1987). This well illustrated a weaker entanglement density and intensity in the interphase composed of PMMA and PVDF melts in contrast to their bulk polymers.

To further address the problem of weak entanglement intensity of the diffuse interphase consists of PMMA and PVDF, results of PMMA/PVDF multilayer structures shown in Figure IV-18 are re-plotted in Figure IV-19 for each constant Hencky strain rate, where those of equivalent blend and additivity average rule are incorporated for comparison. Indeed, the $\eta_E^+(t)$ of blend (50%) is far below that of the linear additivity average prediction (i.e. negative deviation), which confirms the above analysis about the weaker entanglement intensity of PMMA/PVDF mixture than its bulks. At this point, the weaker entanglement intensity of the interphase dictates that after saturation of bridging the chain gap at the interface, when the interphase fraction reaches a comparable level to its bulks, the strength of the sandwiched structures in respond to a simple shear or an uni-axial extension may not continue to grow. Conversely, it may begin to slowly decrease as the interphase amount continues to increase. In the case shown in Figure IV-18a, the total thickness H_{total} of the coextruded bilayer is ~250 μm, whereas the H_{total} of the compressed bilayer is ~1.2 mm. Using the interphase thickness value of ~28 μm and ~85 μm determined (as presented in Figure IV-5) for the coextruded bilayer and compressed bilayer, respectively, the fraction of the interphase is calculated to be φ_I~11.2% in the coextruded sandwich structure and φ_I~7.1% in the compressed one. Obviously, the higher amount of the weakly-entangled interphase presented in the coextruded bilayer explains its lower transient extensional viscosity compared to its compressed counterpart. Certainly, both the $\eta_E^+(t)$ of these compressed and coextruded bilayers are greater than that of their un-annealed bilayers at same strain rates.

By increasing layer numbers in coextruded multilayer structures from bilayers to trilayers and 5layers, the amount of interphase was manually amplified by 2 folds and 4 folds, thus the contribution of the interphase could also be amplified. Within anticipations, the $\eta_E^+(t)$ is slightly reduced as the fraction of the interphase is amplified as indicated in Figure IV-19. That is, the higher the layer number used in multilayer structure, the lower the $\eta_E^+(t)$ is obtained, approaching toward that of 50%blend, which shows negative deviation from the additivity average rule. Besides, at $\dot{\varepsilon}_H$ = 5.0 s^{-1}, one can perceive that the "strain softening" behavior becomes weaker as layer number increases, close to the subtle "strain hardening" of the blend. This again significantly confirms the contribution of the diffuse interphase that embodies weak entanglement intensity. Upon discussing to a further step, the weak entanglement intensity of the diffuse interphase can be expressed in other sayings as weak tube confinement potential with highly dilated tube diameter or larger entanglement spacing, l_{ent}. Therefore, the diffuse interphase in this work is more readily to suffer from catastrophic interfacial yielding during continuous deformation in both simple shear and uni-axial extension. This may be somewhat responsible for the "strain softening" in the multilayered structures observed in startup uni-axial extension. Anyway, results of the elongation rheology corroborate those of step strains and startup shear as shown before.

IV.5. Conclusion

In this study, step strain experiments, fast startup experiments in shear and in uni-axial extensional flow have been implemented based on PMMA/PVDF alternating multilayer structures with absence (un-annealed) and presence (annealed) of a well-characterized diffuse interphase in comparison with their equivalent blends. Experimental results were analyzed and discussed under the tube model of DE theory as well as some recently developed conceptual frameworks such as dynamic network picture and microscopic dynamic theory of transverse tube confinement potential. It is unambiguous that nonlinear rheology is sensitive enough to the interface/interphase of multilayer structures as the interface/interphase is vulnerable to the fast large external deformation. In other words, "microscopic yielding" and "strain softening" prefer to happen to the interface/interphase zone in comparison to its bulks. Interfacial failure is significant for the un-annealed multilayers due to the lack of entanglements at the interface. The triggered interphase at the annealed multilayers is able to retard the interfacial failure to a larger deformation and higher deformation rates before being ultimately destroyed during or after fast and large enough deformations in simple shear and uni-axial extension. The ultimate breakdown of the interphase is supposed to be due to its weaker entanglement intensity compared to its constituent bulks, which renders it to be more readily overcome by the external deformation.

First of all, stress relaxation behaviors of neat polymer melts after a step strain were focused. The linear relaxation modulus G(t) was obtained for small step strain ($\gamma \leq$ ~1.0) while the nonlinear relaxation modulus $G(t,\gamma)$ charactering strong stress damping behavior was obtained for large strain ($\gamma \geq$ ~1.0). $G(t,\gamma)$ obeys time-strain separability at long time scales. PMMA melt was found to be more strain-dependent than PVDF melt. The strain-dependent behavior, i.e. "strain softening", was expressed by a damping function $h(\gamma)$, which represents reduction of load-bearing entanglement strands number. The $h(\gamma)$ of PVDF that behaves a type-B behavior and the PMMA melt that is a normal type-A could also be well fitted by a two exponential function and a generalized sigmoidal form. Theoretical controversy exists regarding the time-strain factorability and the stress damping phenomenon. The tube models attributed such nonlinear features to large orientation, chain retraction within tube and finally convective constraint release accompanying with loss of entanglements between chains. Some other theories argued that the "strain softening" has deal to do with the entanglement network yielding, breakdown of the tube confinement barrier, or in a new saying of transverse hopping relaxation (tube breaking). It seems that their common is that such nonlinear feature is a result of quick entanglement loss.

Stress relaxation of multilayers with and without interphase after a small, intermediate and large step deformation were probed, respectively. An original model was proposed to predict the nonlinear relaxation modulus $G(t,\gamma_0)$ of the

multiphase systems, which satisfactorily captured the experimental results. At very small deformation, no significant difference was observed between the bilayers with and without interphase, with the $G(t,\gamma_0)$ according with the model prediction. At intermediate deformation, the $G(t,\gamma_0)$ of the bilayer without interphase greatly fell down from its annealed counterpart. This may be the consequence of an interfacial failure at the interface of the un-annealed bilayer whereas such interfacial failure was hindered by the triggered interphase at the annealed bilayer. When the deformation was sufficiently large to induce the interfacial failure even at the annealed bilayer, its $G(t,\gamma_0)$ reduced to the same level as the bilayer without interphase, with both of them negatively deviated from the theoretical prediction. Such subsequent reduction of the $G(t,\gamma_0)$ of the bilayers without and with interphase is supposed to be resulted from the entanglement loss at the interface/interphase. Moreover, the proposed model enabled to estimate the stress relaxation behavior of the interphase, where strong damping behavior that perhaps due to the interfacial yielding was observed. In addition, the results of step strain experiments have been confirmed by the strain-controlled rheometer, ARES.

In fast startup shear, typical nonlinear features of stress overshoot and "strain softening" with transient viscosity, η^+, following below LVE envelop at Weissenberg number $W_i > 1$ have been clearly observed in the investigated polymer melts. The stress overshoot was interpreted as a yielding point of chain disentanglement under the theoretical picture of force imbalance between intrachain retraction force and intermolecular gripping force. The overshoot stress, σ_{os}, was found to scale with overshoot time, t_{os}, as $\sigma_{os} \sim (t_{os})^{-0.9}$, and scale with $\dot{\gamma}$ as $\sigma_{os} \sim (\dot{\gamma})^{0.85}$ for the melts in the viscoelastic regime. For multilayer structures with and without interphase, at small shear rates, the η^+ curves of both cases were found to follow up with the LVE prediction. At intermediate shear rates, like step strain experiments, the un-annealed bilayer evidently separated downward from the annealed one with interphase which was still attached to the LVE envelope. At high shear rates, both the η^+ curves of the bilayers with and without interphase fell far down from the theoretical prediction to a similar level. Such significant η^+ curve reduction of the un-annealed and annealed bilayers that subsequently occurred at intermediate rates and large rates again supportted the interfacial failure at the interface/interphase. The interphase at annealed bilayer plays a key role in delaying the interfacial failure to a higher deformation rate till its weak entanglements ultimately collapse.

In fast startup uni-axial extension, both the transient elongation viscosity of PVDF and PMMA melts in the full-elastic recovery region were found to satisfy with the LVE curve by Trouton ratio, i.e., $\eta_E^+(t)=3\eta^+(t)$. "Strain hardening" behavior was clearly observed in the PVDF melt at finite constant Hencky rates after critical strains and the upward deviation became more evident as the $\dot{\varepsilon}_H$ increased. Nevertheless, the PMMA melt of this work failed to display such "strain hardening", rather, "strain softening" was observed instead. Whether or not "strain hardening" in uni-axial

extension was argued to depend on competition between the massive entanglement yielding and the geometric condensation of excess entanglement strands into the shrinking area during stretching.

For startup uni-axial extension of the PMMA/PVDF alternating multilayer, fraction of the interphase and its entanglement intensity determine the level of the transient extensional viscosity. Presence of certain interphase that bridged the gap at the interface of neighboring layers greatly enhanced the $\eta_{E^+}(t)$ of the multilayer structures in comparison to those without interphase. Like its equivalent blends, the diffuse interphase consists of PMMA and PVDF mixtures owns weaker entanglement intensity than their constituent bulks. Therefore, after saturation of bridging the interface, as the amount of the interphase continued to increase to a comparable level with the bulks, the $\eta_{E^+}(t)$ of the multilayer structure began to decline, towards the behavior of the blend which showed a negative deviation. Such contribution of the interphase was greatly amplified by increasing layer numbers of the structure. The weak entanglement intensity may be associated to the weak tube confinement potential in the diffuse interphase, which can render it to be vulnerable to the external deformations.

On the whole, typical nonlinear rheological characteristics such as stress damping in nonlinear relaxation after large strains, stress overshoot and "strain softening" in fast startup shear and "strain hardening" behavior in fast startup uni-axial extension have been clearly observed in the neat polymer melts, which could be interpreted under the tube models and some recent conceptual frameworks. Absence and presence of an interphase between neighboring layers make the multilayer structures having different responses in these three nonlinear rheological measurements involve transient flow regime. Entanglement lacking at the interface and entanglement weak intensity at the diffuse interphase give rise to subsequently readily occurrence of interfacial yielding even interfacial failure of the multilayer structures during or after continuous large deformations in both simple shear and uni-axial extension. Hence, this work gives a real demonstration of the nonlinear rheology sensitivity to the rheological, geometrical and structural properties of the interphase.

Supporting Information IV: Comparisons between stress-controlled (DHR-2) and strain-controlled (ARES) rotational rheometers on nonlinear stress relaxation measurements (Critical technical part for accuracy analysis)

It is well known that the rheological measurements in linear viscoelastic regime are independent of measurement types: strain-controlled (separate motor transducer system) and stress-controlled (combined motor transducer system) rheometers. However, in nonlinear viscoelastic regime where the effect of strain becomes significant, it is of wonder whether differences exist between these two types of rheometers on nonlinear stress relaxation measurements. In a stress-controlled rheometer, as the controlled input signal is stress, an inertia effect is expected in a step strain experiment since a time lag is needed for the conversion from stress signal to strain signal. On the contrary, strain-controlled rheometer directly controls the deformation (or rate of deformation) as input signal and measure the stress signal using the separated torque transducer, which seems to be an obvious choice for step strain experiments.

Herein, we carried out same step strain experiments for PMMA/PVDF multilayers as well the neat polymers in a strain-controlled rheometer (ARES) to compare with those obtained in the stress-controlled rheometer (DHR-2) as reported in the main text. As mentioned before, one most important challenge in experimental technique for a step strain is to actuate a commanded strain within a rise time, t_0, as short as possible. The maximum prerequisite of the t_0 in a single step strain test for obtaining meaningful information about nonlinear relaxation behavior of a material is less than one tenth of the average relaxation time of the material. A "rule of thumb" in the literature is that only the results with $t>10t_0$ can represent the true behavior of the melt (Dealy and Larson 2006;Rolon-Garrido and Wagner 2009;Yu 2013).

As shown in Figure IV-S1a are time-dependent nonlinear shear relaxation modulus $G(t,\gamma)$ obtained by ARES for PVDF and PMMA melts, respectively. Comparing these results to those obtained via DHR-2 as shown in Figure IV-6a, one can see that the $G(t,\gamma)$ obtained by DHR-2 of PVDF melts are almost reproduced in ARES, with time-strain factorability happening at the order of 0.1s. Nevertheless, quite difference is perceived for PMMA melts between the DHR-2 (Figure IV-6b) and the ARES (Figure IV-S1b). Nearly neglect stress damping and strain-dependency (i.e., time-strain separability) especially for large step strains could be found in the $G(t,\gamma)$ of PMMA melts obtained in ARES(Figure IV-S1b), with them almost superposed together.
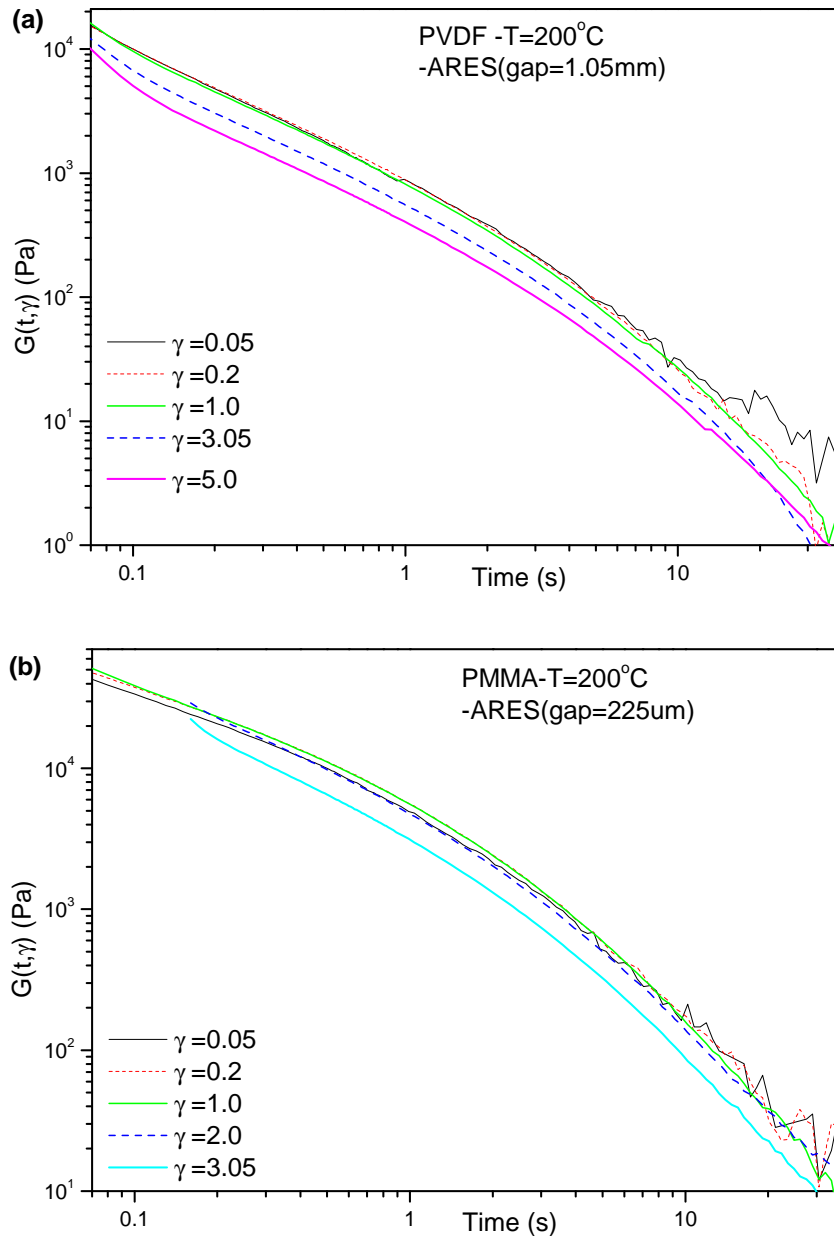
Figure IV-S1. Time dependent nonlinear shear relaxation modulus G(t,γ) obtained in ARES at various shear strain magnitudes at 200 °C for PVDF (a) and PMMA (b), respectively

When the actual strain evolution versus time during the finite rise time in ARES are examined as shown in Figure IV-S2, reasons behind the difference observed in PMMA melts between ARES and DHR-2 become clear. Evidently, for the PMMA melts, the motor in ARES failed to actuate the large commanded strain in a sufficiently short time, considering the t_0 is around 130 ms (i.e. 0.13 s), higher than the time (~0.1 s) stress damping behavior begins. It is deemed that the stress damping behavior that caused from chain retraction process happens only when there is no enough time for the chains to relax upon a large perfect "step" deformation whereby the chains are stretched affinely and a ultrafast relaxation of

chain retraction back to its equilibrium tube contour length occurs after the step deformation. That means the step strain should be given within a time at least lower than the relaxation time of polymer and if the time is much higher, the ultrafast relaxation of chain retraction (it is also called as contour length relaxation by Doi-Edwards) is not about to happen. For PMMA melts, even though the gap between parallel plates were adjusted to be a rather low value, i.e. 225 *μm*, for the step strain experiments, it was still difficult to get a perfect large "step" strain within a very short time. However, in DHR-2, as shown in Figure IV-6b, it is able to actuate a large "step" strain within a rather short rise time though a short period of stabilization exists due to the inertia effect.
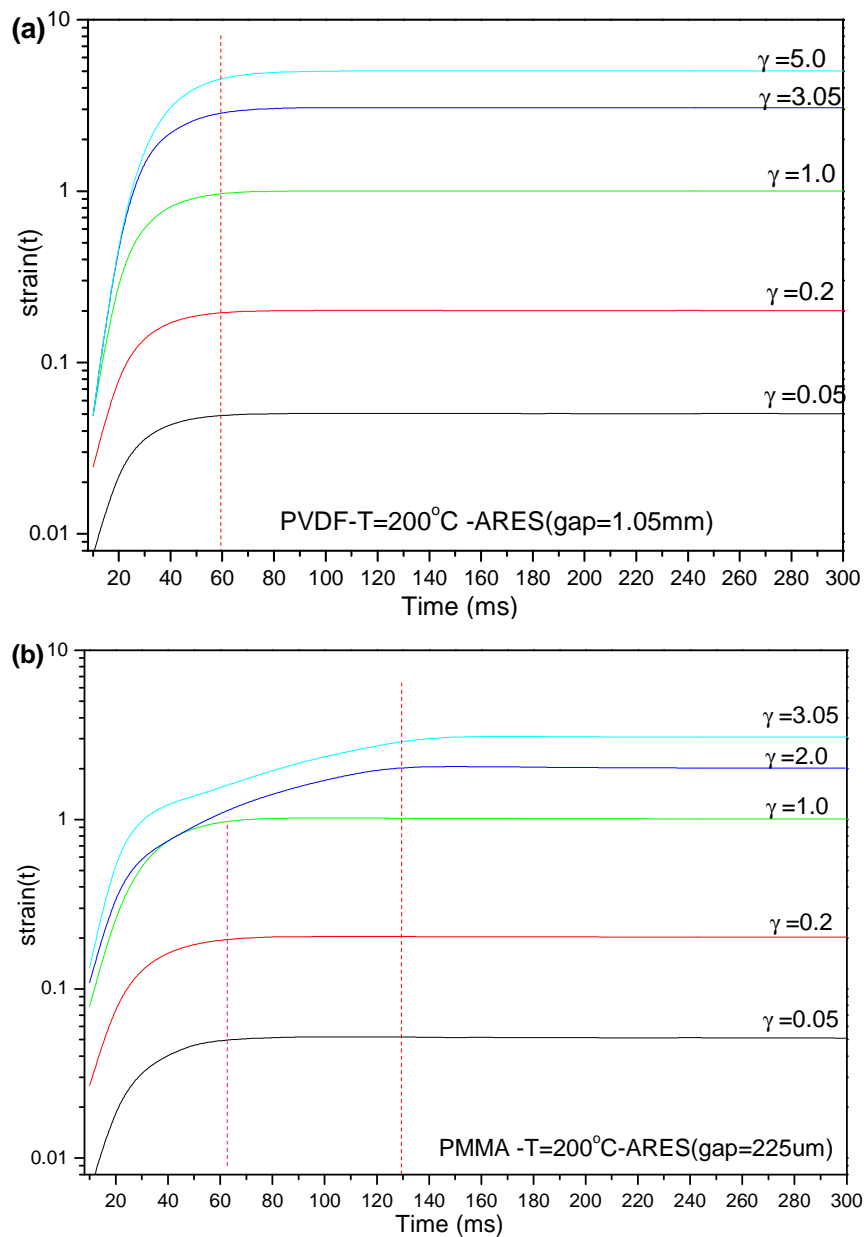
Figure IV-S2. Actual strain variation versus time upon an imposition of commanded strain obtained in ARES for PVDF (a) and PMMA (b) melts.

Besides, as also argued by Munstedt and coworkers (Stadler et al. 2008), some advantages of stress-controlled rheometer over strain-controlled rheometer on performing step strain experiments are:

i) The maximum strain obtainable in a stress-controlled rheometer is only limited by the material response and by the maximum force which can be applied. However, the maximum limitation of step strain that can be commanded by ARES is 599%, exceeding which is not accepted by the RSI Orchestrator software. This is due to the maximum angular displacement limited in strain-controlled rheometer with a rotation of 90°.

ii) Direct imposition of a high strain in a very short period of time would leads to high forces, which might damage the rheometer whereas in a stress-controlled rheometer, step strain is imposed by acting a maximum stress until the desired deformation is reached.

iii) ARES using separate transducers with each of which having short limited torque ranges, which easily cause noisy data when torque is lower than the minimums.

On basis of these standpoints, results obtained in DHR-2 are used for discussions in the present study.

Step strain experiments of multilayer structures in ARES

As shown in Figure IV-6b, it is lucky that the rise time t_0 in ARES for actuating a large nominal step strain for multilayer structures is short enough (<0.1s) for analysis. Same step strain experiments with similar strain amplitudes were carried out in ARES for the PMMA/PVDF bilayers with (annealed) and without (un-annealed) interphase. Some of important results are given in Figure IV-S3. Within experimental errors, the results of ARES are almost reproduced from those of DHR-2 as shown in Figure IV-10, which confirm the main conclusions obtained in DHR-2. In particular, at an intermediate deformation, γ=0.2, the G(t,γ) curve of bilayer without interphase is negatively separated from that of bilayer with interphase which accords with the model prediction. At large deformation, γ=3.05, both the G(t,γ) curves of bilayers with and without interphase significantly decrease in comparison to the model prediction.
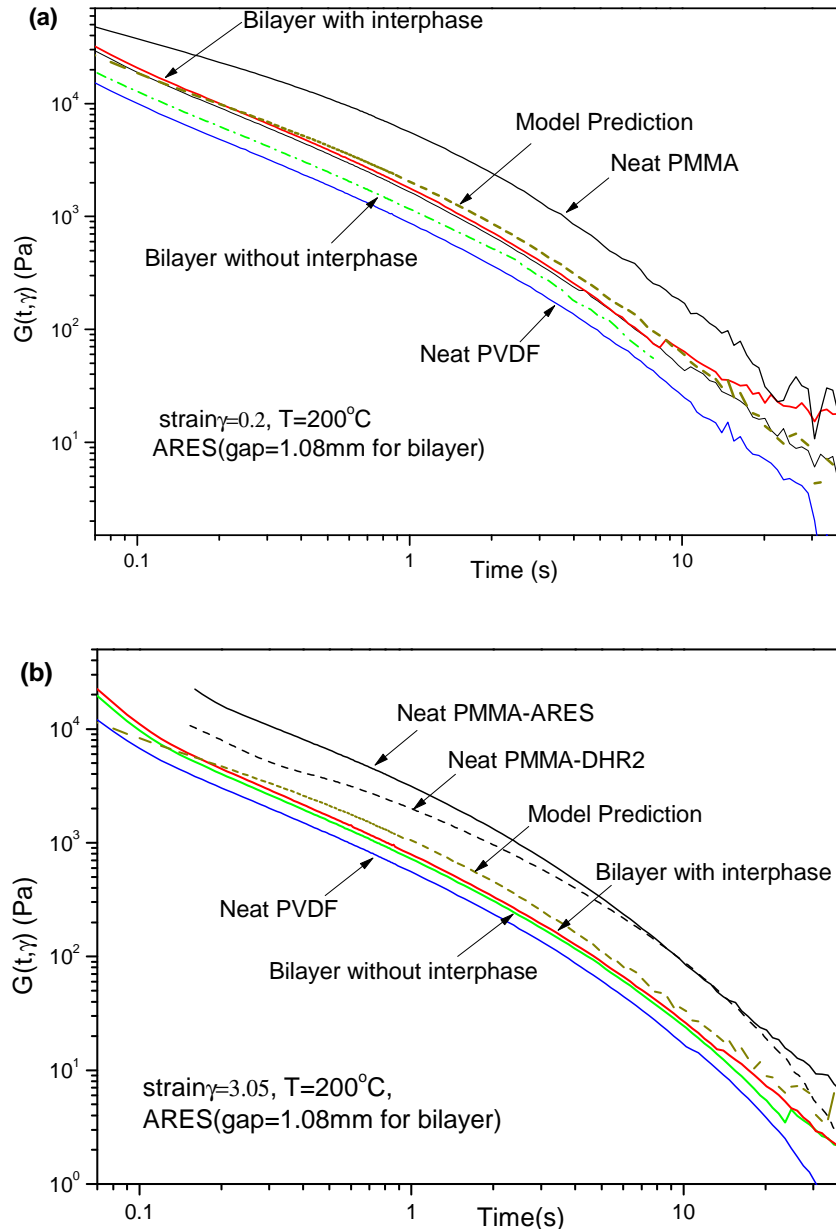
Figure IV-S 3. Time dependent nonlinear shear relaxation modulus G(t,γ) for the annealed PMMA/PVDF sandwich structures by ARES and their neat components obtained after imposition of different strains:(a) γ = 0.05; (b) γ = 0.2; (c) γ = 3.05. Predictions of the model developed in the main text are given in the figure.

Comparisons between ARES-G2 and DHR on transient rheology

Some other information about the latest generation of strain-controlled rheometer, namely, ARES-G2 (TA instruments), on measuring transient rheology in fast startup tests has been kindly provided from TA instruments. The measurement was based on a non-Newtonian fluid, polyisobutylene (PIB) solution (NIST Standard Reference Material 2490) and two types of rheometers, ARES-G2 and DHR-3 were compared at a wide range of shear rates. As shown in Figure IV-S4, DHR displays no worse in

compared to the strain-controlled rheometer of ARES-G2 in performing such step strain rate or step strain tests for the polymers. Moreover, the DHR rheometers have advantages over others in minimizing axial compliance which is also very critical for obtaining accurate information in transient measurements.
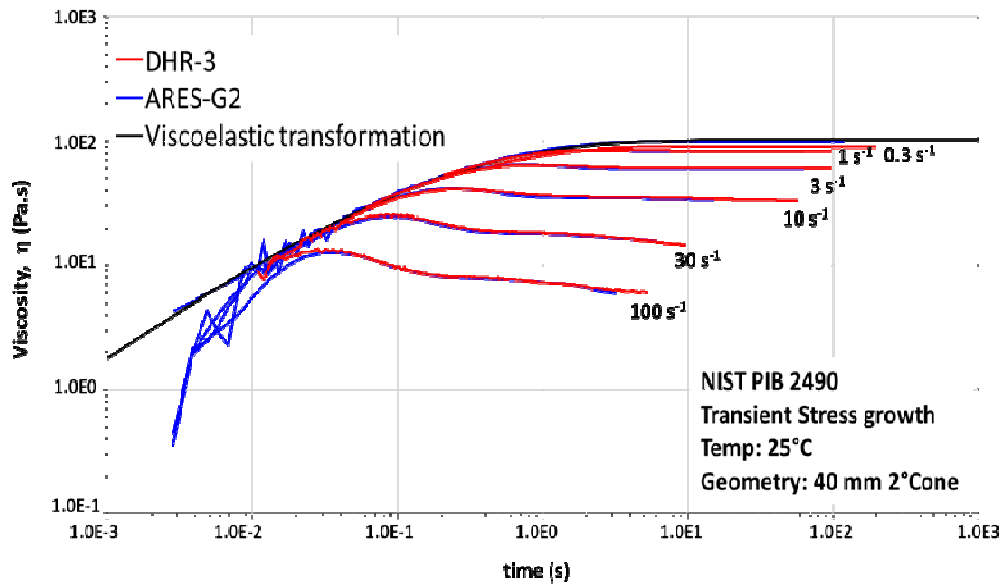
Figure IV-S4. Comparison between ARESG2 and DHR3 on fast startup shear measurements with different step shear rates provided from TA instrument.
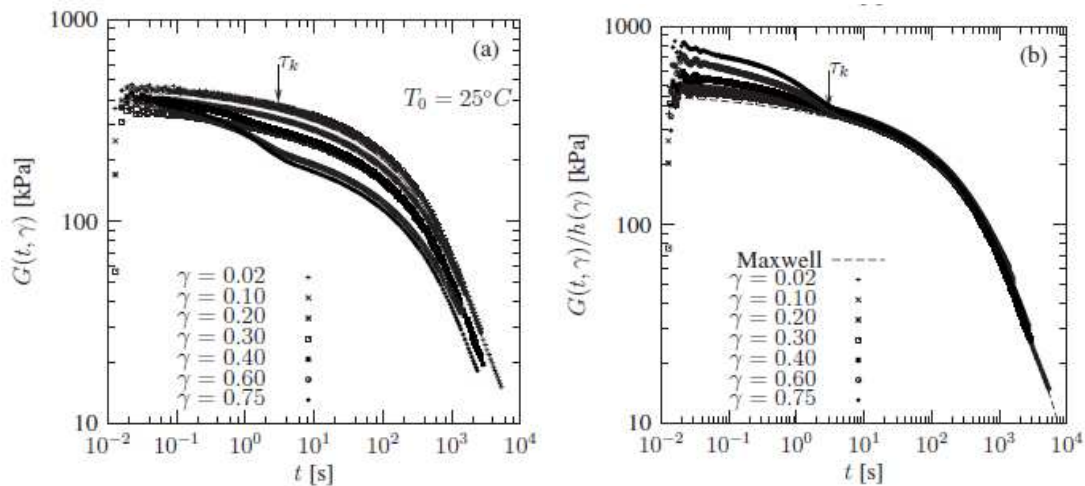
Figure IV-S5. (a) G(t,γ) and (b) G(t, γ)/h(t, γ), for discrete values of the applied strain from 0.02 to 0.75 showing from top to bottom measured in AR-G2. The dotted line is the predicted variation in G(t) from the Maxwell coefficients fitted to the SAOS measurements.(from Nielsen and Hassager 2009)

In addition, the strain-dependent stress damping behavior of neat polymer melts

has also been clearly reported by Nielsen and Hassager (2009) in step-strain experiments of polyisoprene (PI) performed in the ARES-G2 rheometer, as shown in Figure IV-S5. Their measured shear strain range was very limited. They reported that in their system, for strains higher than γ>0.75, slip at the polymer-steel interface in the rheometer can happen with the damping function $h(\gamma)$ entering into type-C region (i.e., $h(\gamma) < h_{DE}(\gamma) <1$). It was due to the weak adhesive strength between PI and steel surface. In the present study, note that the PMMA and PVDF melts were well attached to the aluminum plates and the damping function $h(\gamma) \geqslant h_{DE}(\gamma)$, lying in either type-A or type-B regions, indicating that the wall slip can be excluded.

Critical technical part for accuracy analysis

Note that in the main text, for analysis accuracy purpose, only the data of G(t,γ) obtained far above 0.1s were shown in the figures, especially for the large strain amplitudes in the cases of PMMA melt and bilayer systems. In fact, even for the worst case of PMMA melt with γ=6.28, the rise time, t_0, for strain step in stress-controlled rheometer, i.e. DHR-2, is less than 0.1s. Indeed, in the literature, in most cases of step strain experiments using stress-controlled rheometers, the t_0 is less than 0.1 s and many people showed and discussed their G(t,γ) data before 0.1s somewhere from 0.01s without any accuracy analysis (Juliani and Archer 2001; Ravindranath and Wang 2007; Ares et al. 2009). For instance, Juliani and Archer (2001) carried out their nonlinear step shear relaxation experiments on bidisperse 1,4-polybutadiene (PBD) blends using a stress-controlled rheometer, i.e., Paar Physica Modular Compact Rheometer (MCR 300), with data shown in Figure IV-S 6. As indicated in their work, the MCR 300 provided them a t_0 less than 0.1 s for their materials. Their material has a modulus close to ours and has a relaxation time in the same order as us. In their figures, they showed data for analysis and discussions starting from nearly 0.01 s which includes the period of strain imposition. This has also been done by many other researchers. With this period shown or not, especially for polymer melts, is still an open question in the literatures (Stadler et al. 2008; Ferri and Greco 2006; Juliani and Archer 2001).
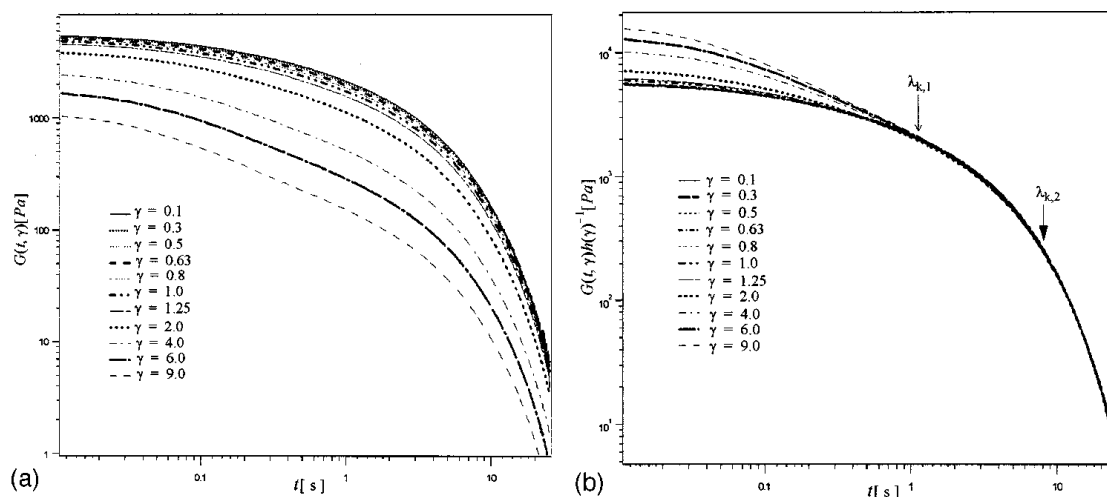
Figure IV-S6. (a) Time-dependent nonlinear shear relaxation moduli $G(t,\gamma)$ for bidisperse PBD blend(N/Ne = 13, $\tau_{rep} \sim$ 4.2s) at shear strain γ from 0.1 to 9.0. (b) Shifted nonlinear shear relaxation moduli $G(t,\gamma)h(\gamma)^{-1}$ for PBD. The arrows in the figure locate two possible assignments for the separability time (from Juliani and Archer 2001).

Although the data within such short period does not deserve enough confidence, as did in the previous studies, we also attempt to take the data in this period into account for bilayer system. Indeed, a fast and sharp drop of the $G(t, \gamma_0)$ curve of the bilayer systems occurs at short time in both DHR-2 and ARES. Here we re-plot Figure IV-11 with a wider time scale in Figure IV-S7 for the $G(t,\gamma_0)$ data of interphase which are estimated based on the models proposed in the main text. Evidently, a rapid decline of the relaxation modulus $G(t,\gamma_0)$ behavior at a short time (~0.08 s) can be observed for the interphase and becomes even more significant as the strain is increased. In particular, at γ_0= 3.05, the modulus straightforwardly dropped to zero before 0.1 s. Such a rapid decline of $G(t, \gamma_0)$ at short time was also observed for the neat polymer melts as confirmed by the ARES, consistent with the literature. According to the DE theory, it may be the evidence of the stress damping or so-called "strain softening" behavior arises from an ultrafast relaxation of the chain retraction after an affine deformation. By analogy to neat polymer, here for a first time we assume the rapid $G(t,\gamma_0)$ drop to be a result of interfacial yielding of entanglement network in the interphase upon external deformations. This has also been confirmed by the startup shear measurements. For clarity, more details about the accuracy analysis in such transient period of step strain imposition will be given in an individual technical paper.
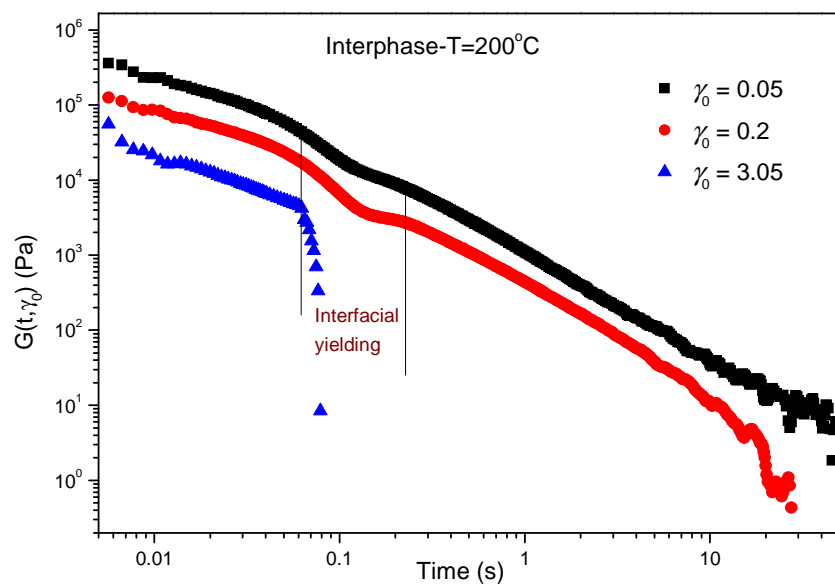
Figure IV-S7. Time dependent nonlinear shear relaxation modulus $G(t,\gamma_0)$ determined for the interphase at the annealed bilayers (annealing for 45 mins at 200 °C)

Chapter V: Fundamental Understanding and Modeling of the Diffuse Interphase Properties and Its Role in Interfacial Flow Stability of Multilayer Polymers

V.1. Abstract

This work aims to investigate the growth and structural evolution of a diffuse interphase generated in a flow field and to highlight its importance on controlling the final properties of compatible multilayer materials. The model polymers chosen for this work are based on poly(methyl methacrylate) (PMMA) and poly(vinylidene fluoride)(PVDF). Interdiffusion kinetics, geometrical and rheological properties of the interphase decoupled and coupled to flow have been probed and quantified. The diffuse interphase was firstly modelled under fundamental conditions of rheological measurements before being probed under real practical conditions of processing. In such compatible multilayer structures, interfacial slippage should be ruled out as examined by steady shear measurements, with only possibility to occur at a condition of rather short welding time under extremely high shear stress considering the probable chain disentanglements at the interphase therein. In the real experimental conditions of processing, competition between diffusion and flow has been assessed. On the one hand, polymer chain orientation in the shear flow field was demonstrated to decelerate the interdiffusion coefficient. On the other hand, intermixing (i.e. flow effect) at the vicinity of the interface triggered from excess interfacial shear stress favored development of the interphase. This was realized by inducing undulated structures with interfacial area increased and hence intermixing could significantly decrease the diffusion lengthscale and characteristic diffusion time by orders of magnitude under certain conditions. Indeed, this effect could be attenuated as temperature increases due to the reduction of the interfacial stress. The diffuse interphase generated in the flow field during processing has been well characterized via scanning electron microscopy coupled with energy dispersive X-ray analysis (SEM-EDX) and transmission electron microscopy (TEM). Results indicate that the interphase could own a geometrical property of tens microns depending on processing conditions and the interfacial zone was shown to be smooth with continuous transition between neighbouring layers without causing any interfacial disturbances. Moreover, amorphous-crystallization properties of the asymmetrical interphase has been highlighted and analyzed. Finally, concerning the

interfacial flow instability and encapsulation in coextrusion process, some key classical decisive parameters such as viscosity ratio, thickness ratio and elasticity ratio, etc. were studied based on stability charts. Differ from severe flow instability observed in incompatible multilayer systems, presence of the interphase at PMMA/PVDF multilayers plays a vital role in weakening (or even eliminating) the viscous instabilities and elastic instabilities and decaying the effect of classical factors despite of the very high rheological difference between PMMA and PVDF especially at low temperatures.

V.2. Introduction

In general, owning the advantage of combining separate features of different individual polymers together in a facile way, technology of coextrusion has been widely used to fabricate multilayered composite sheets or films for various applications ranging from food packaging products to optical reflective films(Lamnawar, et al. 2013). Its processing technique is realized by a combination of two or three extruders using a multimanifold die or a feedblock within which polymer melts are brought together and a specific multilayer assembling is created. However, in this kind of processing, the contrast in rheological and physico-chemical properties of polymers and the variations of experimental conditions (like coextrusion designs, flow rate and die geometry, etc.) may cause defects at the interface of neighbouring layers, which may bring severe detrimental defects on the optical, barrier and adhesion/mechanical properties of the final extrudate products (Han and Shetty 1976; 1978;Schrenk, et al. 1978). Two main defects that have been commonly observed are the interfacial instability (wave-type distortion or zig-zag defect) (Han and Shetty 1978;Schrenk, et al. 1978;Wilson and Khomami 1992) and the encapsulation phenomena that occur due to the tendency of the lower viscous polymer to encapsulate the higher viscous polymer(Hinch, et al. 1992;Wilson and Khomami 1992).

In the industrial production of multilayered structures, to get rid of bad adhesion between different incompatible polymers, normally a tie layer (usually block polymers) is introduced to link both the outer and inner layer through a physicochemical interaction (interdiffusion and/or reactive couplings) (Lamnawar, et al. 2013). So far, the interface/interphase (a non-zero thickness physicochemical zone) has aroused researchers' great interests regarding its effects on the physics and rheology of the multiphase systems of multilayer and/or blend (Lamnawar, et al. 2013;Silva, et al. 2010). Recently the interphase triggered between neighbouring layers as a result of the interdifusion and/or reactive compatibilization has been reported to affect the final properties of multilayered films like electrical property (Xu, et al. 2008), transport property(Carr, et al. 2013) and optical property of refractive index(Liu, et al. 2005), etc(Lamnawar, et al. 2013). The performance of the interphase is closely related to the interfacial microstructure, exactly speaking, local

entanglements that are gradually established via interchain penetration during the interdiffusion and/or reaction process. Due to its being experimentally unobtainable, detailed picture of such an interfacial structure has yet to be fully understood. Liu et al. (2005) made up an interphase material by decreasing the layer thickness of multilayer structure to a comparable size of the interphase through layer multiplying coextrusion, but with only mechanical strength being examined by T-peel test. Studies to understand the microstructure and properties of the interphase are still on the way, being far from enough. It should be of experimental and theoretical value to shed lights on such a physicochemical interaction as well as its role in controlling the interfacial defects of coextrusion.

Regarding the interfacial defects of coextrusion, a large number of literatures have come up reporting on the theoretical and experimental advances and the underlying origins from both mechanical and numerical approaches(Lamnawar, et al. 2013). Following the numerous studies published, a series of crucial parameters determining the interfacial defects have been pointed out and noted: layer depth ratio, viscosity ratio, elasticity ratio and die geometry, etc. Yih(1967) was the first who conducted a systematic numerical study on the stability of plane Poiseuille flow of two Newtonian fluids considered within a framework of linear stability theory and he pointed out that the viscosity difference can cause instability regardless of the Reynolds number. Recently, Wilson and Khomami (1992,1993a,b) have published a series of comprehensive works on the interfacial instabilities in multilayer flow of viscoelastic fluids. The authors investigated the linear stability of coextrusion processing from a mechanical viewpoint. Their facilities introduced temporally regular disturbances with controllable amplitudes and frequencies, by which they measured the growth rate of the disturbance amplitude along the downstream die position to examine the interfacial stability. They first investigated flows of immiscible fluids (PP/HDPE incompatible system) and found that theoretically predicted growth rates agreed with their experimental data. Subsequently, they considered a plane Poiseuille flow of a compatible polymer system (LLDPE/HDPE). In comparison to the high growth rate of the disturbance amplitude along the downstream die position in the cases of PP/HDPE incompatible system, the growth rate for the LLDPE/HDPE compatible system is significantly less despite the fact that the viscosity ratio for the LLDPE/HDPE system is higher.They pointed out that the linear stability in the compatible polymer systems was related to the interphase resulted from the diffusive and intermixing in the vicinity of the interface (Wilson and Khomami 1993b).

Despite of the interesting nature of this kind of research, it is of no help in understanding either the connection between the properties of the present interphase and the resulting final properties of multilayer polymers or the generation of interfacial flow instabilities. The direct correlation of interphase to the interfacial defects of coextrusion has not yet been reported. Even though improvement of the

interfacial defects have been aware of in the coextrusion of compatible polymer couples(Wilson and Khomami 1993b), no sufficient attention have been paid to the role of the interphase and much less the quantitative characterization of this interphase. Few studies have, with regard to fundamental and experimental aspects, been dedicated to the physical modeling of the present interphase and its effect on the flow stability. After presenting an upstream rheological study on the reaction/diffusion competition at neighboring layers based on a reactive mulitlayered system (RS) of polyamide (PA6)/polyethylene-grafted with glycidyl methacrylate (PE-GMA) and a non-reactive mulitlayered system (NRS) of PE/PA6, Lamnawar and Maazouz (2006,2008) demonstrated the importance of the generated interphase on alleviating the interfacial instabilities in coextrusion of this kind of reactive multilayered structures. However, the systems they used were very complex with regard to the high polydispersity and reactivity. To have a better understanding, it would be preferable to work firstly with model polymers in order to probe the effects of the diffuse interphase in the flow stability during coextrusion. The complexities in analysing the role of interphase in coextrusion of two incompatible, reactive polymers are considerably reduced by using a compatible pair. This is because in the incompatible, reactive polymer system, the amount of the triggered interphase is limited during the short contact time of the two melt streams in the coextrusion while in the compatible ones, the interphase are more considerable as interdiffusion can occur in a more rapid rate(Lamnawar, et al. 2013).

In our previous work(Zhang, et al. 2012; 2013), rheology has been demonstrated to be a reliable method for monitoring the diffusion process at a polymer/polymer interface based on both symmetrical and asymmetrical bilayer structures consist of PVDF and PMMA model polymers. Modelling has been realized to describe the kinetics of the interdiffusion (self-diffusion, mutual diffusion) and to express the developments (thickness, rheology) of the interphase triggered between the neighbouring layers. These upstream studies render us to understand the interphase at polymer/polymer interface generated in compatible and/or reactive systems from an fundamental aspect. But the direct correlations of the understandings on the interphase to the real processing is still lacking, especially the study of the interphase in flow field. The main objective of this paper is to probe the interdiffusion as well as the growth and structural evolution of the interphase triggered in the approx real experimental conditions of processing before disclosing its role on weakening the interfacial flow instability of coextrusion. To attain this objective, a brief view of the diffuse interphase at fundamental conditions will be given before the interfacial rheology of multilayered structures, microphysics of the interphase at practical condition of coextrusion and processing of multilayer compatible systems being investigated and discussed.

V.3. Experimental Section

V.3.1 Materials

The polymers used in this study were supplied by ARKEMA. Poly (methyl methacrylate)(PMMA)/poly(vinylidene fluoride) (PVDF) were used as a compatible system and PMMA/ polyethylene(PE) were also employed as an incompatible system for comparison purpose. Two poly (methyl methacrylate) (PMMA)s of different molar mass, namely PMMA-1, PMMA-2 were included to allow us to vary the viscosity and elasticity ratios. The main characteristics of the materials are listed in Table V-1. For clarity purpose and easy reading of this paper, more characterization information of the studied polymers which have been provided in ref. (Lamnawar and Maazouz 2009;Zhang, et al. 2012; 2013), are not addressed here

Table V-1 Characteristics of the investigated polymers

Samples	Trademark/Supplier	$T_c(^oC)^a$	$T_g(^oC)^a$	$T_m(°C)^a$	M_w^b(g/mol)	M_w/M_n^b	Ea(KJ/mol)^c
PVDF	Kynar 720/ARKEMA	136.40	-42	170	210,000	2.0	59
PMMA-1	V825T/ ARKEMA	——	112	——	100,000	1.9	160
PMMA-2	V046/ ARKEMA	——	102	——	137,000	2.0	157
PE	Lacqtene/ARKEMA			114	207,000	9.9	53

^{a} measured in our laboratory by a TA Instruments Q20 DSC at a heating and cooling rate of 10 ºC/min under N2.
^{b} determined in our laboratory by size exclusion chromatography (SEC) with tetrahydrofuran (THF) as the eluent for PMMA, dimethyl formamide(DMF) for PVDF and trichlorobenzene (TCB) for PE at 135 ºC. ^{c}energy of activation of the viscous flow (Ea) obtained from a master curve at a reference temperature of 220 ºC, PE obtained at 240 ºC.

V.3.2 Rheological measurements

V.3.2.1 Rheology of monolayers

All the polymer granules were dried at 80 ºC under vacuum to remove any moisture before use. Samples for the measurements in rotational rheometer were prepared by compression molding at 180 ºC with a pressure of 200 bars between two Teflon films to obtain a smooth surface. Then the samples were cut into round disks with a diameter of 25 mm and the disks were annealed at 80 ºC under vacuum for at least 24 h before measurements to eliminate the possible effect of surface orientation brought about by the compression molding.

Dynamic rheological measurements of neat polymers were carried out using a strain-controlled rotational rheometer, ARES (Advanced Rheometrics Expansion System) and a stress-controlled rotational rheometer, DHR-2 (Discovery Hybrid Rheomter, TA instrument) with a parallel-plate geometry (Φ = 25 mm) at varying temperatures from 180 °C to 260 °C under nitrogen atmosphere. All dynamic frequency sweep tests were carried out in a linear viscoelastic (LVE) region. Dynamic strain sweep tests were conducted beforehand to determine the linear viscoelastic

domain. Steady shear measurements of the neat polymers were carried out in the same rotational rheometer (parallel-plate geometry, Φ=25 mm) for low nominal shear rates. For high shear rates, a pressure-controlled CEAST Capillary rheometer using a die with a 180º entry angle and various L/D ratios for Bagley correction (L/D=30, 20, 5) was employed.

V.3.2.2 Rheology of multilayer structures

The interdiffusion process and interphase development occurred at asymmetric polymer/polymer interfaces of multilayer assemblies were monitored by small amplitude oscillatory shear (SAOS) measurements (parallel-plate, Φ = 25 mm, gap = 1.2 mm). The multilayer assemblies (total thickness = 1.2 mm, same geometry of each layer) were prepared by bringing round disks of PMMA (upper layer) on top of PVDF (lower layer) alternately into intimate contact at room temperature before loading them between the plates and annealing them in the oven at a given temperature. Steady shear measurements were also carried out to investigate whether the interfacial slippage may occur in such compatible multilayered structures. Nitrogen purging was maintained throughout all the measurements to avoid potential degradation and oxidation of the polymers.

V.3.2.3 Effect of pre-shear

To take into account and simulate factors like high steady shear, intermixing, etc. that may be encountered in the practical and complex conditions of coextrusion processing, a pre-shear mode was introduced to the multilayer strucutres before carrying out the dynamic time sweep test to examine its effect on the interdiffusion kinetics. Meanwhile, cross-section morphology of the specimens which were immediately quenched upon being subjected to the pre-shear were observed under scanning electron microscopy (Enviromental SEM Hitachi S-3500N). Also observed under SEM were those specimens that experienced annealing process for a given time with and without pre-shear.

V.3.3 SEM-EDX analysis and TEM observation of the interphase generated in flow field

For a purpose to characterize the interphase triggered between PMMA and PVDF neighbouring layers in flow field during coextrusion process in a quantitative manner, a technique combining SEM and energy dispersive x-ray analyzer (EDX) was employed to determine the concentration profile across the interphase upon the bilayer extrudates. This technique makes use of the characteristic x-ray fluorescence of characteristic atoms present in the sample (that is, fluorine (F) for PVDF and oxygen (O) for PMMA). It has been demonstrated to be more than adequate for measuring the interdiffusion of compatible polymer systems (Raghava and Smith 1989;Zhang, et al. 2013). The quenched coextruded bilayer specimens were microtomed normal to the interfacial plane using an ultramicrotome before being

exposed in a Hitachi S800 FEG Scanning electron microscopy (SEM) with an EDX microanalysis system. The EDX analyzer collected the x-ray data across a path (20 analysis points) of a line scan of electron beam that conducted from one bulk (e.g. PVDF) to the other (e.g. PMMA) in a desired field. At each point the number of x-ray events of given energy generated within a fixed time period was recorded as a function of x-ray energy and at the same time the position of the path was photographically recorded. As the number of x-ray counts is directly proportional to the number of atoms (and hence the amount of characteristic element of the polymer) from which they originate, a concentration profile can be developed for the characteristic element, and the involved polymer across the interphase in the annealed specimen. Moreover, the cross section morphology of the quenched coextruded bilayer specimens were examined in a Philips CM 120 transmission electron microscopy (TEM) operating at an accelerating voltage of 80 kV.

V. 3.4 Coextrusion process and interfacial stability

V. 3.4.1 Apparatus
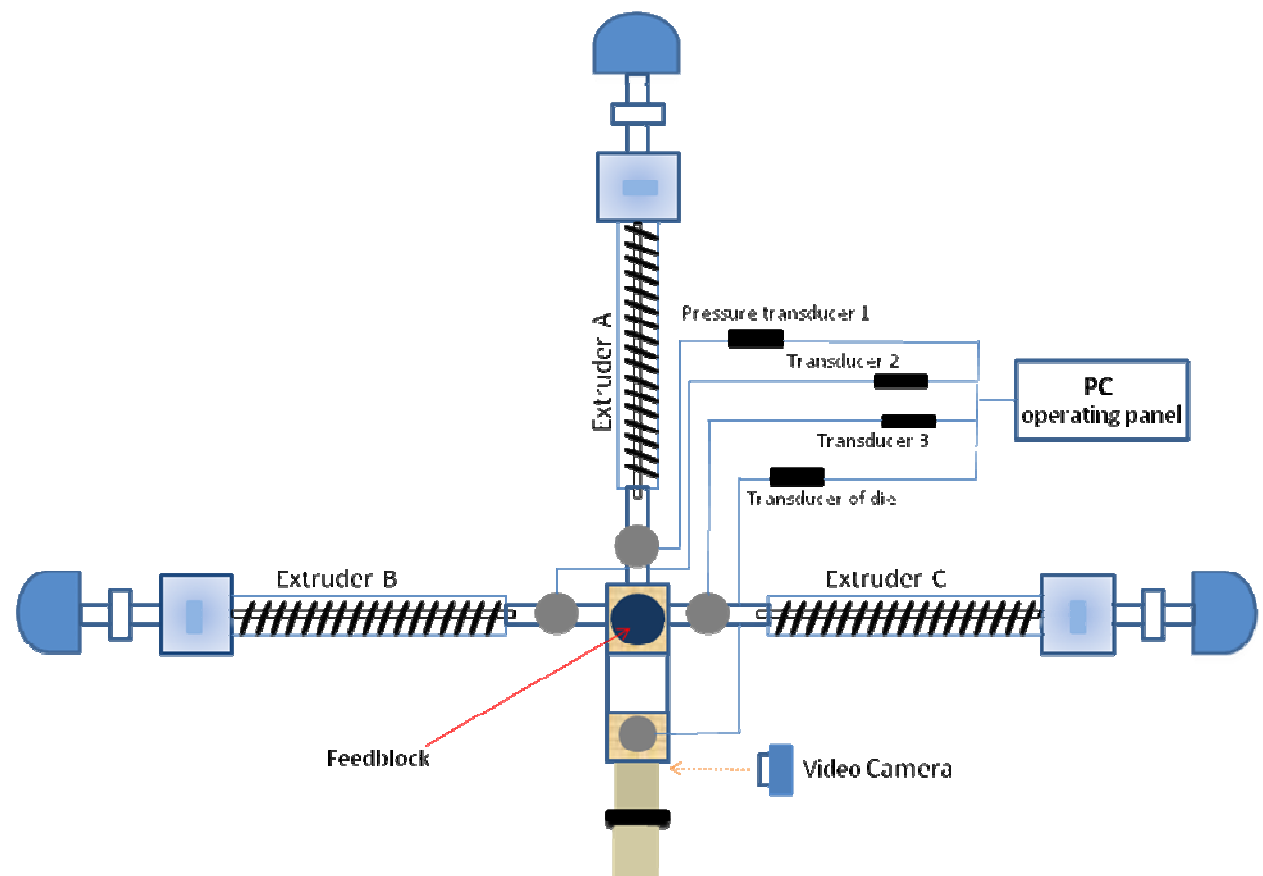
Figure V-1. Schematic of experiment apparatus: laboratory device of coextruder with a feedblock/multimanifold system

In contrast to the work of Lamnawar et al.(2009) in which an industrial machine was used, a laboratory instrumental setup of coextruder especially designed in a home

mode, which was equipped with a feedblock/ multimanifold hybrid system connecting three extruders and a hanger die, was employed to elaborate the multilayer sheets in this study. The manipulations of the extruders (temperature, rotating rate, pressure drop,…) were accomplished in an independent automatic operating panel. Details concerning this specific laboratory setup are presented in TableV-2. A schematic of the instrumental coextrusion device composed of three extruders is given in Figure V-1. The video camera was used to observe and capture the flow stability and possible generated defects of the coextruded melts upon the exit of the die.

Table V-2 Characteristics of extruders

Extruder/details	A(central)	B(binder)	C(external)
Screw diameter (mm)	18	12	15
L/d	25	25	25
N max (rpm)	69.9	69.9	69.9
Flow rate (g/min)	0-69	0-69	0-69

V. 3.4.2 Experimental procedures

In the coextruder setup, extruder A (Φs=18mm, L/d=25) was used for PMMA and extruder C (Φs=15mm, L/d=25) for PVDF in order to elaborate mono and bilayer structures. The temperature profile in the extruder was set to 210, 220 and 220 °C from the feeding to the metering zone, respectively. The polymers were brought together in the multimanifold system before going to the hanger die that arranged them into more than two alternating layers. Two typical configurations, CBABC 5layers and CA bilayers, are shown in FigureV-2a,b. To make easy reading of this paper, only the CA bilayer structure results are to be presented and discussed here. The geometry and dimension of the fluid channels in the feedblock, multimanifold and the connecting hanger die are also given in FigureV-2c,d. The thickness ratio of the layers was changed by varying the flow rate of each polymer melt. A calibration curve of flow rate versus screw rate for each polymer was created beforehand by adjusting the screw rate of extruder from 5 to 65 rpm/min. After exiting the die, the bilayer films were passed over a water-cooled double chill roll and quenched to room temperature. Both the extrudates at the die exit and the quenched ones were visualized to examine the interfacial defects (flow stability, encapsulation, etc.) at the fluid interface.
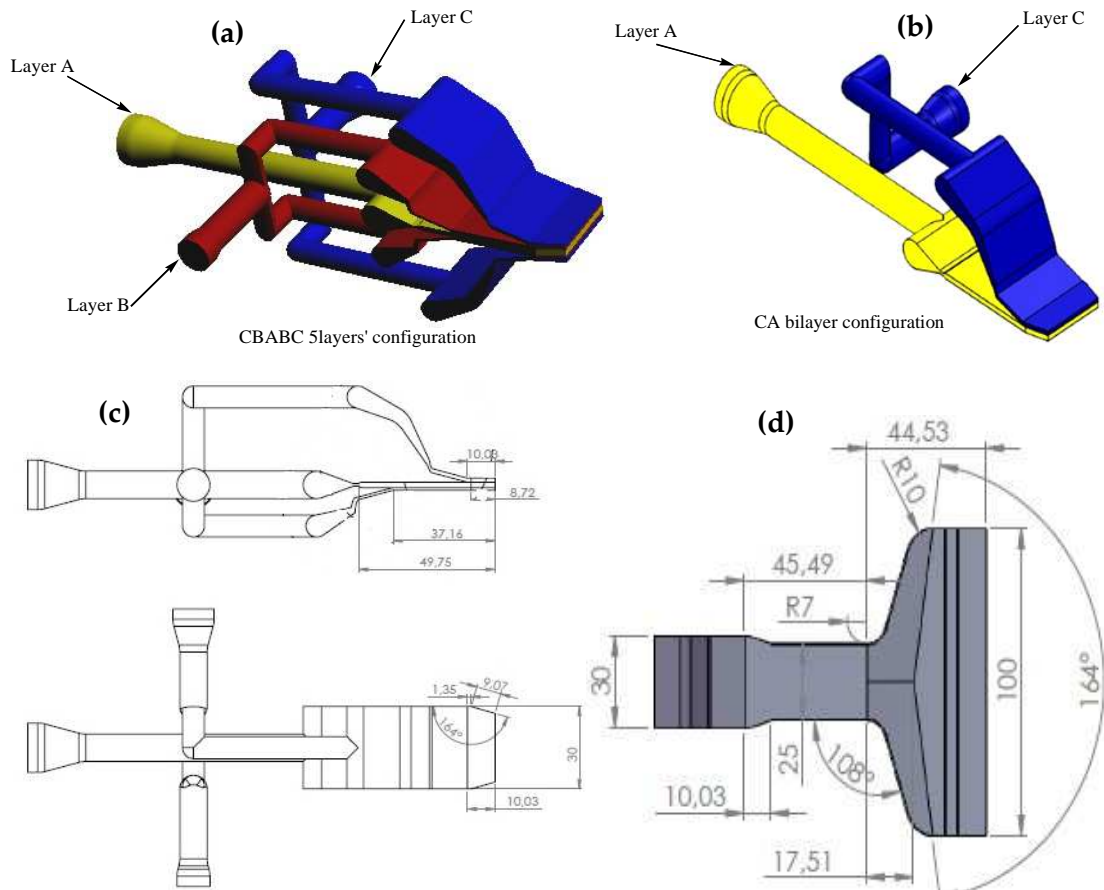
Figure V-2. Schematic of multilayer configurations in the feedblock/multimanifold of coextruder: (a) CBABC 5layers' configuration and (b) CA bilayer configuration; Plans of (c) fluid channels of CBA layers and (d) geometry of the hanger die.

Estimation of the contact time in coextrusion process

To quantitatively characterize the interdiffusion process and the interphase development during the coextrusion process, mathematical calculations of some parameters like contact time are needed. The contact time is the time that the polymer streams resided in the confluent region in the multimanifold system and the die. That is, the time between the moment that the separate polymer fluent merged into a combine when they flow into the die land to the moment that the confluent flows out at the die exit and being quenched. It could be estimated by an expression as follow:

$$t_{contact} = \frac{V_{conf}}{Q_{mass}} \rho$$

(V-1)

where V_{conf}, ρ, Q_{mass} represent the volume of the confluent region in the manifold of feed block and die, the apparent density of the confluent melts and the mass flow rate, respectively. According to the dimensions of the fluid channels and die given in

FigureV-2 c,d, V_{conf} has been estimated to be 1.7×10^{-5} m^3.

V.4. Results and Discussion

V.4.1 Viscoelastic properties of neat polymers

Rheological properties like storage modulus (G'), loss modulus (G") and dynamic viscosity (η^*), etc. of the investigated polymers in the molten state have been measured as a function of angular frequency at given temperatures ranging from 180 °C to 260 °C. Master curves of the polymers have been obtained at a reference temperature of 220°C, from which the activation energies of viscous flow were calculated, as listed in Table V-1. More molecular characteristics of the polymers have been given in our earlier publications (Zhang, et al. 2012; 2013), and those concerning PE involved in this paper have been reported in previous series (Lamnawar and Maazouz 2006; 2008). Here, only typical curves of η^* versus angular frequency of PMMA-1 and PVDF are shown in Figure V-3a, where one can observe a shear-thinning behavior at higher frequencies and a Newtonian behavior at lower frequencies for the two neat polymers. PVDF exhibited a more moderate shear-thinning behavior than PMMA at any given temperature. Indeed, as the temperature increases, the Newtonian behaviour is more pronounced for both polymers. The corresponding viscosity ratios of PMMA to PVDF at different temperatures are plotted versus angular frequency in Figure V-3b. It is worthy of mentioning that PMMA is more viscous than PVDF at the same temperature, but as the temperature is raised, their viscosities approach each other and become nearly equivalent at 260 ºC.
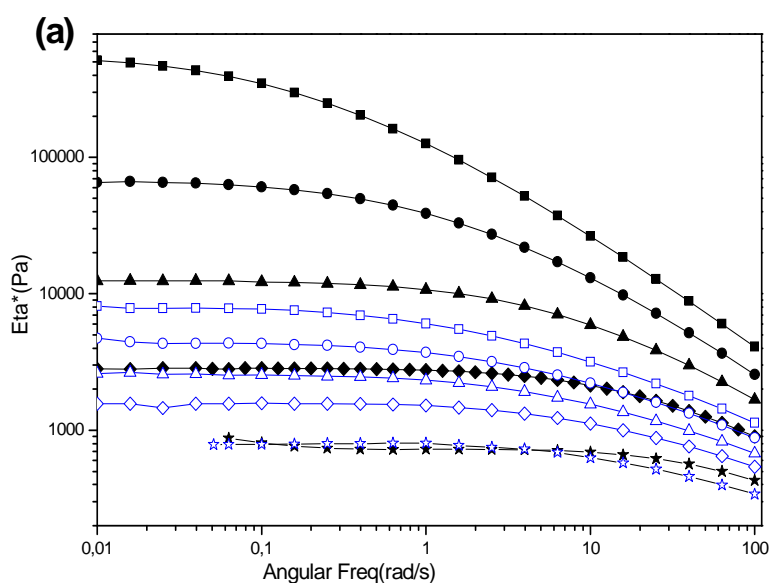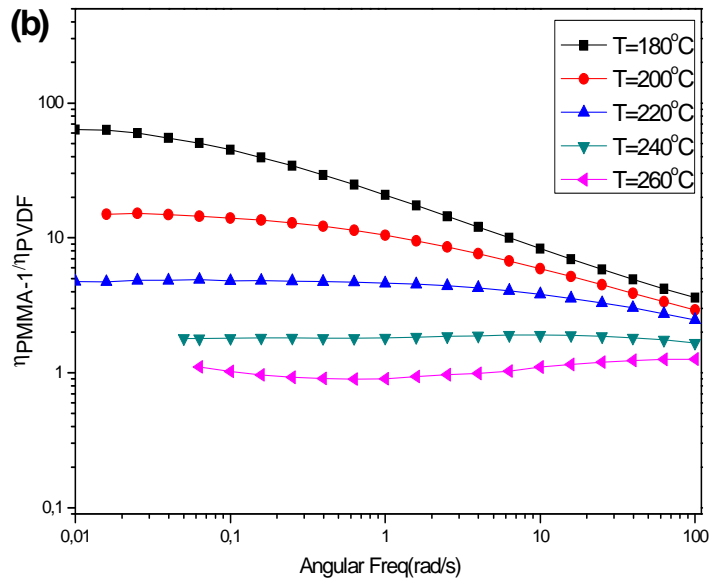
Figure V-3. (a). Plots of η* versus angular frequency for the neat polymers PMMA-1 (filled symbols) and PVDF (open symbols) at different temperatures: (■, □) 180 °C; (●, ○) 200 °C; (▲, △) 220 °C; (◆, ◇) 240 °C; (★, ☆) 260 °C; (b) Viscosity ratio of PMMA/PVDF versus temperature; (c) Zero shear viscosity ratio and Average relaxation time ratio versus temperature (viscosity ratio=30.86@190 °C)
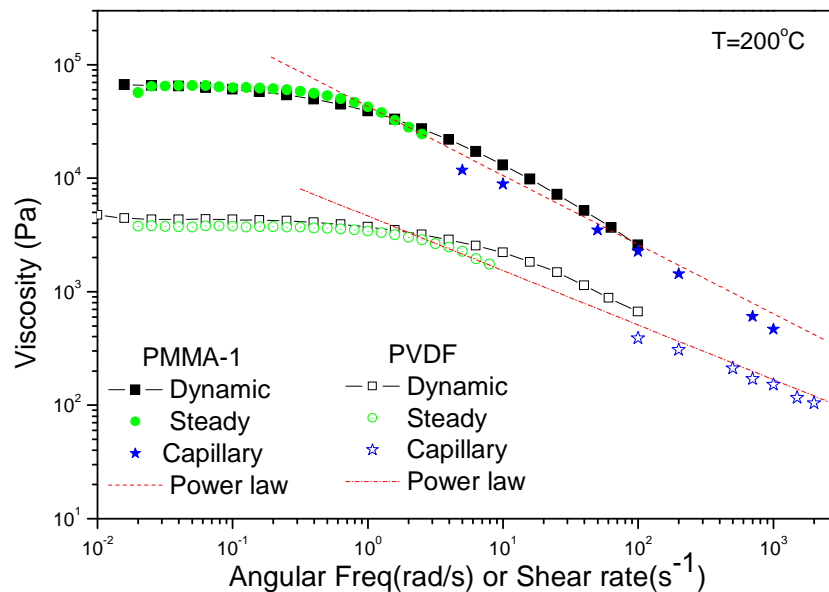
Figure V-4. Viscosity of pure PMMA-1 (filled symbols) and pure PVDF (open symbols) via different methods: dynamic shear mode (square); steady shear mode in rotational rheometer (circle); steady shear mode in capillary rheometer (asterisk)

Moreover, typical experimental results of PMMA and PVDF obtained in steady shear measurements that conducted by rotational rheometer for low shear rate and by capillary rheometer for high shear rate are given in Figure V-4. As shown in this figure, it is obvious that dynamic shear viscosity and steady shear viscosity well

satisfy the Cox-Merz relationship. The dashed lines are fitting lines of power law to the experimental data for the non-Newtonian region, from where the power-law constant *n* are obtained: 0.39 for PMMA and 0.52 for PVDF, respectively.

V.4.2 Modeling of the diffuse interphase triggered at fundamental conditions

In order to understand the diffuse interphase generated at neighbouring layers under practical coextrusion condition, it is of necessity to first give a brief view of the interdiffusion kinetics and its interphase development at a fundamental and static condition. For this, comprehensive studies on the interdiffusion occurrs at a symmetrical and an asymmetrical polymer/polymer interface have been carried out by annealing bilayer structures in the oven of rotational rheometer (Zhang, et al. 2012; 2013). Measurements were performed at a given temperature and a given angular frequency in LVE by online tracking variation of the rheological functions (like complex modulus G*) of the assembly versus annealing time. During the healing process, chains on both sides began to invade the interface, with a motion pattern generally considered to be governed by repation kinetics that put forward by de Gennes (1971) and developed by Doi-Edwards (1986). As chains on both sides uninterruptedly penetrate into the other side and entanglements in the interfacial region continuously become established, the sharp interface decays as the time elapses. It is replaced by a broadening interphase, which can be considered as a macroscopic blend composed of PMMA and PVDF chains. As more and more chains cross the interface, the entanglement density at the interfacial zone increases, thus the interphase becomes strengthened and more robust. Therefore more torque is required for shear and hence the higher the complex modulus of the system becomes. The increment of the complex modulus is only attributed to the strengthening brought about by the interdiffusion process since no variation of the G* has been found for the neat polymers due to their thermal stability at the experimental conditions. This is the physics of monitoring the interdiffusion kinetics by following the evolution of the viscoelastic properties of bilayer assembly versus healing time.

Indeed, quantification of the diffusion coefficient, especially in polymer melts, is quite a tremendous task since a great number of parameters are needed upon modelling. For the aysmmetrical bilayer system, a rheological model correlating the D_m to the measured rheological properties has been developed in our earlier work(Zhang, et al. 2013) based on a primitive model of Qiu-Bousmina (2000). The new model takes into account rheology of the interphase (complex modulus of interphase $G_I^*(t)$) rather than using rheolgy of the total sandwich structure ($G_{s,t}^*$) for the D_m determination. The model is derived within the framework of reptation theory of Doi-Edwards (1986) and fast-mode theory of Kramer (1984). Here, for clarity purpose, only the final mathematical term of the modified model is shown as follow:

$$D_m = \left[\frac{(2/3)^{1/3}\, p}{\left(9q + \sqrt{3}\sqrt{-4p^3 + 27q^2}\right)^{1/3}} + \frac{\left(9q + \sqrt{3}\sqrt{-4p^3 + 27q^2}\right)^{1/3}}{2^{1/3}3^{2/3}} \right]^2 \tag{V-2}$$

with mathematical functions p and q as

$$p = \frac{8\beta\omega G_N^0}{\pi^2}\left(\frac{\varphi_A}{G_{A,0}^*} + \frac{\varphi_B}{G_{B,0}^*} \right) \tag{V-3}$$

$$q = \frac{8\beta\omega G_N^0}{\pi^2}\frac{H}{2t^{1/2}}\left(\frac{1}{G_{s,t}^*} - \frac{1}{G_{s,0}^*} \right) \tag{V-4}$$

where β is a shorten form of

$$\beta = \frac{N_b^e N_b^3 b_b^4}{\pi^2 e_b^2}\left(\frac{\varphi_B}{N_A} + \frac{\varphi_A}{N_B} \right)\left(\frac{\varphi_B}{N_A} + \frac{\varphi_A}{N_B} - 2\chi\varphi_A\varphi_B \right) \tag{V-5}$$

In the equations, φ_i, N_i denote volume fraction and repeat unit number of composition i, i=A or B and χ is the Flory-Huggins interaction parameter; N_b^e, N_b, b_b, e_b and G_N^0 are the average number of repeat units between entanglements, the repeat unit number, the effective bond length, the step length of the virtual tube and the plateau modulus of the interphase (or equivalent blend), which is also a function of the composition. $G_{i,t}^*$ represents the complex modulus of layer i at a diffusion time t>0 with an initial complex modulus of layer i as $G_{i,0}^*$ at t=0; and H is the total thickness of the sandwich (1.2 mm for the PMMA/PVDF assembly used in this work). Details on the deduction of the model and the information of the modifications are available for readers in Ref. (Zhang, et al. 2013). Indeed, the original modification of the model consists on the calculation and modelling of the monomeric friction coefficients of each polymer in the multiphase systems and correlates it to the diffusion quantifications. The rheology method, Lodge-McLeish model, and test of the time-temperature superposition (tTS) principle were employed to probe the thermorheological complexity of this polymer couple. The monomeric friction coefficient of each species in the blend has been examined to vary with composition and temperature and to be close in the present experimental conditions, and the failure of the tTS principle was demonstrated to be subtle.
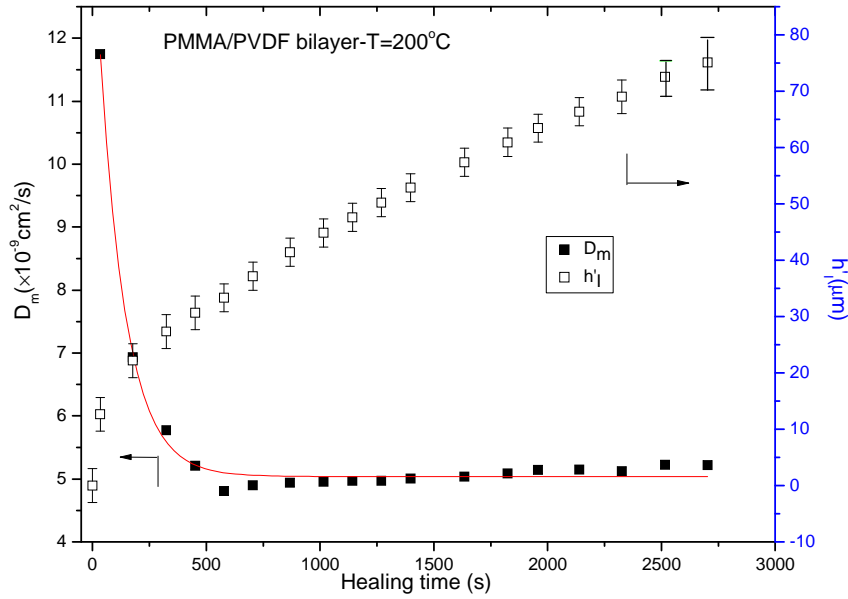
Figure V- 5. Evolution of mutual diffusion coefficient (D_m) and interphase thickness (h'_I) versus time for PMMA-1/PVDF bilayer at 200 ºC, 0.1 rad/s

According to the model of the mutual diffusion coefficient proposed above based on the concept of the interphase (eq.V-2), we can also gain some insights into the feature of the interphase. In particular, thickness of the interphase could be determined from the mutual diffusion coefficient via an equation as follow:

$$h_I^{'} = 2\left(D_m t\right)^{1/2} \tag{V-6}$$

Figure V-5 portrays a typical plot of the evolution of apparent mutual diffusion coefficient (D_m) and the corresponding thickness of the generated interphase with time for a PMMA-1/PVDF asymmetrical bilayer at T = 200 ºC, ω = 0.1 rad/s. The apparent D_m decreases gradually with time before reducing to a constant in the longer time limit. At the first beginning, the dynamics is dominated by short chains or segmental motions in a Rouse behavior with a higher diffusion coefficient. After more and more long chains participate into the diffusion, the D_m decreases to a plateau stage, which is a sum of contributions from species of different chain lengths according to Doi-Edwards theory (1986). Likewise, the interphase grows gradually versus time, reaching a thickness of several dozens' microns after diffusion for 45 mins (e.g. ~77 *μm* at 200 ºC), a similar order as that reported by other methods and techniques. Moreover, as the time elapsed, G* of the interphase asymptotically approached the corresponding value of its equivalent blend as shown in our earlier work (Zhang, et al. 2013). This implies that a short-time interdiffusion along with the establishment of entanglements by interchains within the interphase give rise to greatly enhanced properties of the interphase. Anyway, it is clear that the interphase can reach an order of microns in a time scale of several minutes to tens minutes even in a fundamental condition of small-amplitude oscillatory shear measurements. One can imagine that in the practical condition of coextrusion processing, where shear

flow is involved, the interdiffusion situation can be more complicated and the kinetics can be more rapid. This is the dedication of following sections to quantify the interphase properties in the practical condition of coextrusion processing.

V.4.3 Rheology at compatible alternating multilayer structures with various number of layers

V.4.3.1 Rheological measurements of PMMA/PVDF multilayer structures

With a knowledge that the rheological response of bilayer is sensitive to the interdiffusion process and generation of the interphase occurs at the interface, it is also of great interest to examine the rheology of such miscible multilayer structures by varying layer number. The complex viscosity, η^* is reported versus the angular frequency (ω), for all PMMA-1/PVDF multilayers of different layer numbers (2, 4, 6, 8) in Figure V-6. For comparison, complex viscosities of the pure polymers as well as blends of identical compositions and the theoretical predictions of log-additivity rule, $\lg \eta_{mul} = \varphi_A \lg \eta_A + \varphi_B \lg \eta_B$ (plotted in broken curve) and reciprocal rule, $\eta_{mul} = \varphi_A / \eta_A + \varphi_B / \eta_B$ (plotted in dotted curve), are also incorporated into the figure. As one can see, the complex viscosities of multilayer structures lie between those of their constitute components, independent of the total number of layers, with values closer to the predictions of reciprocal rule, except for the terminal region (at low angular frequencies) where slight increases are observed and the higher the number of layers, the greater the increase. These increases can be attributed to the pronounced consequences of interdiffusion occurred between neighbouring layers at low angular frequencies since longer times were allowed at these regions for diffusion than at high angular frequencies. Moreover, it is noted that PMMA-1/PVDF blend has a similar complex viscosity with multilayer systems as well as that predicted by reciprocal rule through the frequency ranges measured.
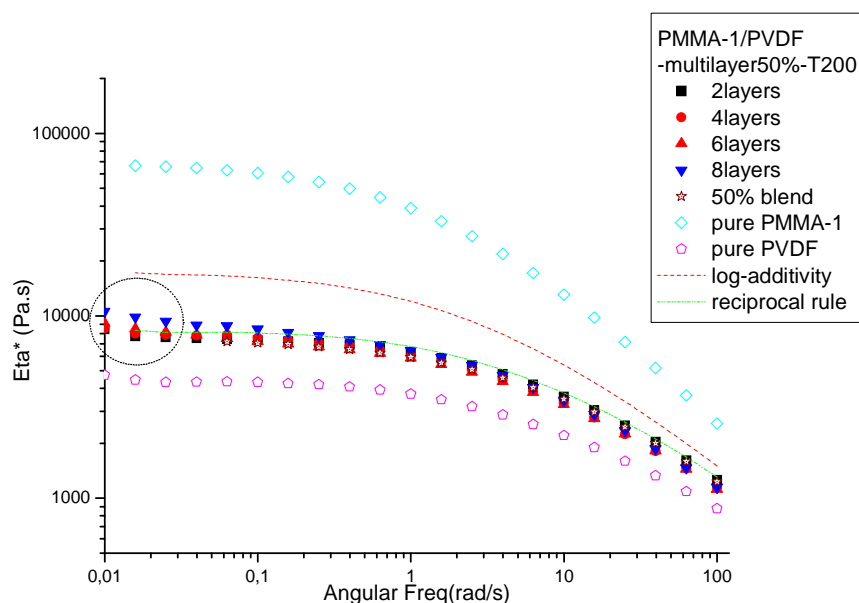
Figure V-6. Complex viscosity (Eta*) versus angular frequency (ω) of PMMA-1/PVDF multilayer structures for different layer numbers at 200 °C

It seems that the effect of layer number is not very apparent. Note that in this section the fundamental study was carried out in LVE regime in which the diffusion is decoupled from flow. Now, one more interesting objective of this study is to perform some experiments in which the flow is coupled to the diffusion. Hence, an open question is addressed here, can slip occur at the polymer/polymer interface of a compatible alternating multilayer structure?

V.4.3.2 Steady shear flow of compatible alternating multilayer structures

Slip occurs at polymer-polymer interface was firstly proposed to interpret the macroscopic observations of anomalously low viscosities in blends of immiscible polymers by Lin(1979) in a phenomenological model. The mechanism of slip can be attributed, from polymer chain dynamics viewpoint, to the lack of chain entanglements at the interface of immiscible polymers. Typically, formation of chain entanglements in the interfacial region is believed to be the origin of enhanced adhesive strength at the interface. For an immiscible polymer pair, commonly the

interfacial width $h_I(\sim b/\sqrt{6\chi})$ is less than the radius of gyration $R_g(\sim b/\sqrt{6/N})$, that means

the number of chain entanglements in the interfacial region is less than the entanglement density in the bulk phase and the interfacial friction is dominated by Rouse dynamics. Thus with low entanglement density and weak interactions, the interfacial region cannot sustain high stress transferred from one component to the others when they are subjected to shear and hence slip occurs(Zhao and Macosko 2002).

Zhao and Macosko (2002) unambiguously evidenced the interfacial slip with polystyrene (PS)/polypropylene (PP) multilayer system by pressure drop

measurements in an in-line slit rheometer and apparent steady shear viscosity measurements in parallel-plate rheometer. They observed that significant slip occurs at high shear stress and slip velocity can be scaled versus shear stress. At the same time, Lam et al.(2003, 2004) also simplified the morphology of a polymer blend into a multilayer structure, and quantified the interfacial slip based on this structure. They used a confocal microscopy to visualize the interfacial slippage directly and also proposed an energy model to quantify the interfacial slip velocity from dynamic shear measurements of multilayer structures. Later, Zhang et al (2006b) demonstrated an idea that the rapid shear flow experienced by a multilayer melt during coextrusion can destroy interfacial entanglements, disentanglements of polymer chains at interfaces induced by high shear stress promote interfacial slip, and further reduce the adhesion of interface.

Now one might have an idea in mind that interfacial slip is dependent upon entanglement density of the interfacial region, hence any factors that affect the entanglement density (like diffusion. disentanglement. etc.) may have an impact on the occurrence of interfacial slip. For immiscible polymers, interfacial slip has been widely accepted to happen under certain conditions due to the fact of low entanglement density at the interface. Nevertheless, for miscible and/or compatibilized immiscible polymers, since the spontaneous interdiffusion and/or reaction process progressively evokes the establishment of entanglements at the interface, slip phenomenon has not been focused. In fact, at the very short welding time of miscible polymers, the entanglement density at the interface is also very low. So it is of interest to check whether slip can occur in miscible polymer pairs at short welding time, especially under high shear condition.

Despite the maximum shear stress to which multilayers were subjected in this study was around 3700~4000 Pa at 100rad/s, it was still not enough to induce slip, as no significant deviation from reciprocal rule is observed in FigureV-6. This accords with the preceding experimental results of Zhao and Macosko (2002) and Lam et al. (2003) etc. though their polymer systems are immiscible and ours are miscible. According to Zhao and Macosko (2002), interfacial slip that unlikely to be observed under small amplitude dynamic shear is due to the fact that the shear stress in linear viscoelastic region, where material structure remains undisrupted, is too small to cause interfacial slip. Steady shear measurement in parallel plate rheometer has been demonstrated to be able to detect the slip(Lam, et al. 2003;Zhao and Macosko 2002). For the purpose to probe the possible slip in short diffusion period, we performed steady shear measurements on the PMMA/PVDF multilayer structures at 200 °C. For immiscible polymer pairs like PMMA/PE, we have demonstrated that slippage can appear at a relatively lower shear rate (<1.0 s^{-1}). Likewise, we firstly implemented steady shear tests on PMMA-1/PVDF multilayer structures within lower shear rate (<1.0 s^{-1}). However, the apparent viscosities show no any deviations from reciprocal rule, indicating no slip, as shown in Figure V-7-a (open symbols). When steady shear

measurements were conducted over higher shear rate which began from 1.0 s^{-1} (filled symbols in Figure V-7-a), negative deviations of apparent viscosities from $\eta_{av,no-slip}$ of neat PMMA-1 and PVDF appear when $\dot{\gamma} \geq 10$ s^{-1}. One may argue that these negative deviations must be due to the effect of edge failure at high shear rate. Indeed, edge failure can be determined by monitoring the first normal stress difference ($\sigma_{11}-\sigma_{22}$) versus shear rate. Failure to reach steady state and a continuous decrease in the magnitude of ($\sigma_{11}-\sigma_{22}$) at a given shear rate was used as a sensitive indication of the onset of edge failure(Padmanabhan and Macosko 1997). In Figure V-7-b, it can be seen that edge failure did not appear above $\dot{\gamma} = 10$s^{-1} until $\dot{\gamma} \geq 15.8$ s^{-1}. Therefore the deviations of viscosities over the range 10s$^{-1} \leq \dot{\gamma} \leq 15.8$ s^{-1} may be attributed to possible slip induced by high shear stress ($\tau \sim 25$ kPa when $\dot{\gamma} = 10$ s^{-1}). The slip velocity displayed in Figure V-7-b was determined from the apparent viscosity of multilayer structure via a relation given by eq. (V-7) (Zhao and Macosko 2002).

$$V_{slip} = \frac{H\dot{\gamma}}{n-1}\left(1 - \frac{\eta_n}{\eta_{av,no-slip}}\right) \tag{V-7}$$

in which

$$\eta_{av,no-slip} = \frac{\eta_A \eta_B}{\varphi_A \eta_A + \varphi_B \eta_B} \tag{V-8}$$

Here, H is total thickness of multilayer structure and n is layer number; η_n, η_A and η_B are apparent visocity of multilayer structure, component A and component B at nominal shear rate $\dot{\gamma}$, respectively. Note that the slip velocities at $\dot{\gamma} \geq 15.8$ s^{-1} displayed in the figure in fact are questionable due to the significant effect of edge failure in this zone. They are shown here just for guides to eyes.

Despite the experimental data are limited, a clear tendency of slip for miscible multilayer structures at short welding time still can be arrived: at low shear condition, slip can absolutely be negligible as it is inhibited by the rapid diffusion and low shear stress, while above a high critical shear rate (or shear stress), subtle slip can be detectable before the edge failures of sample happen. That is because the weakly entangled polymer chains at the interface within the short welding time may be disentangled by the high shear stress. Theoretically, after diffusion along one dimension direction for a time scale of reptation time (τ_{rep}), interfacial thickness reaches a distance of one entanglement mesh size, strong adhesive bond strength at the interface is supposed to achieve. Nevertheless, in practice, chains diffuse towards tri-dimensional space and it takes a longer time than τ_{rep} for the chains to form entanglements at the interface with a density similar to the bulk. Thus due to lack of entanglement density at the short welding time, the Rouse-like region at the interface is vulnerable to high shear conditions. Indeed, experimental results here greatly corroborate those of step strain and startup shear experiments in Chapter IV.
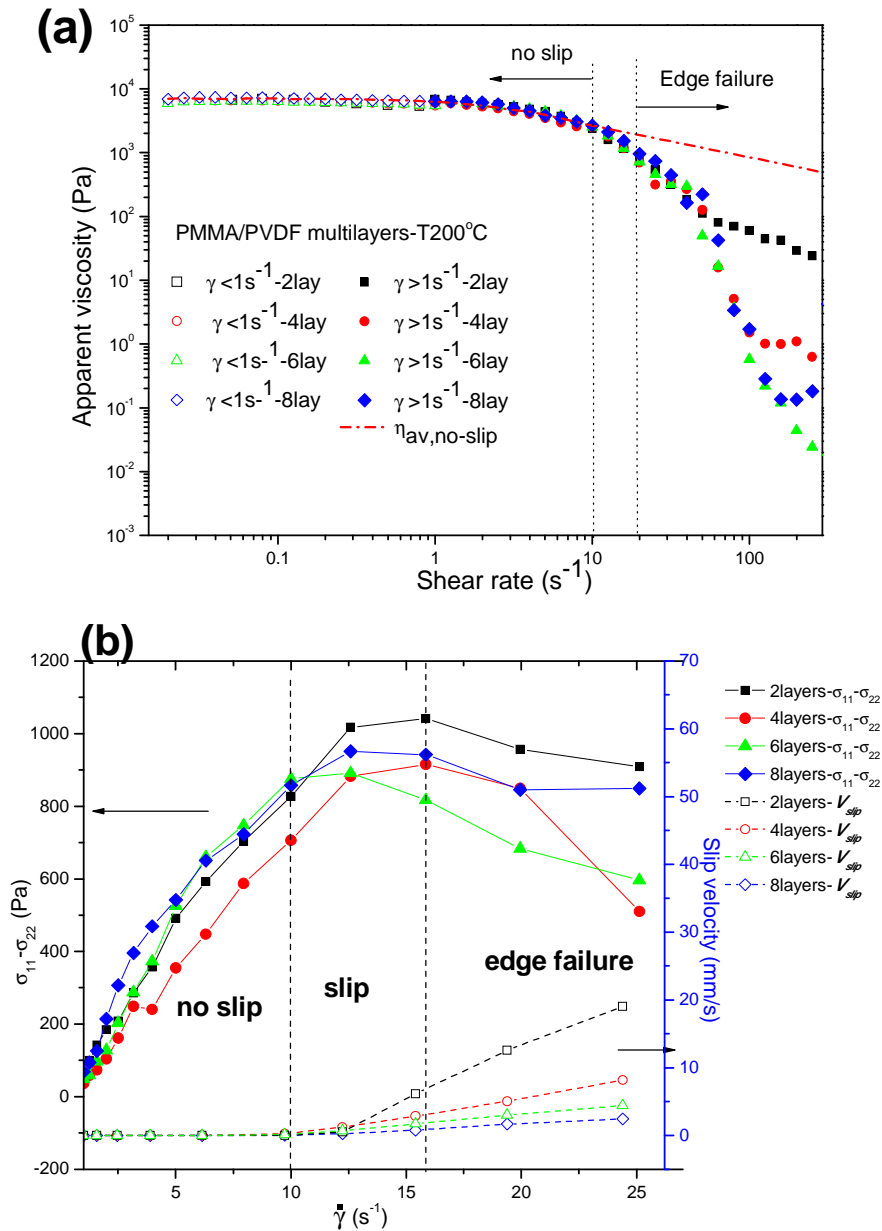
Figure V-7. (a) Apparent viscosity of PMMA-1/PVDF multilayers versus nominal shear rate measured under steady shear mode in parallel plates rheometer at low shear rate (open symbols) and high shear rate (filled symbols). (b) First normal stress difference (σ_{11}-σ_{22}) and slip velocity (determined from eq. (V-7)) versus shear rate ($\dot{\gamma}$) for PMMA-1/PVDF multilayer structures

V.4.4 Interdiffusion quantification in experimental conditions of coextrusion process

V.4.4.1 Orientation effect

In the previous sections, some achievements have been obtained on the interdiffusion process in a fundamental bilayer system by rheology regarding the diffusion coefficient and the interphase thickness. In the practical conditions of a coextrusion system, the situation is more complicated considering that the orientation of polymer

chains in shear flow field may pronouncedly influence the rate of interdiffusion (Kim and Han 1991). According to this work, it is necessary to take into account the effect of the orientation by introducing an orientation factor, α, into the calculation of the diffusion coefficient. Our new contribution in this field is to gain a rheological modelling of the diffusion coefficient as developed in our previous work (Zhang, et al. 2012; 2013). It is supposed that when there is no flow, the polymer chains have an average orientation angle of 45 degrees whereas the average orientation angles in the respective phases will be greater than 45 degrees when they are under a shear field, as schemed in Figure V-8. In fact, aside from the chain orientation, there are some intermixing at interface vicinity happening in shear flow field in the practical processing of coextrusion, the effect of which will be discussed in next section. In a shear field, the orientation factor can be described by an expression as follow:

$$\alpha_i = \frac{\cos\left\{(\pi/4) + \left[\tan^{-1}\left(3\sigma_{int}(\overline{M}_{wi}/\overline{M}_{ni})^3/G_{Ni}^0\right)\right]/2\right\}}{\cos(\pi/4)} \qquad \text{(V-9)}$$

where σ_{int} is the interfacial stress at the interface. To determine the σ_{int}, firstly we assume that the velocity distribution for the multilayer flow of incompatible non-Newtonian fluids is also valid for the case of PMMA/PVDF in this study.
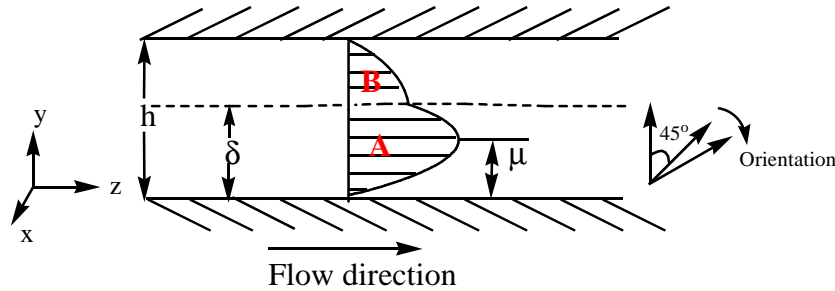
Figure V- 8. Schematic of a velocity profile in a two-component coextrusion

Thus, σ_{int} can be calculated by solving the equation of motion in rectangular coordinates (x,y,z):

$$-\partial P/\partial z + \partial\sigma_{yz}/\partial y = 0 \qquad \text{(V-10)}$$

for phases A and B, respectively, with boundary conditions being that $(\sigma_{yz})_A = (\sigma_{yz})_B = \sigma_{int}$ at $y=\delta$, where δ is the position of interface; $(v_z)_A = 0$ at $y=0$ and $(v_z)_B = 0$ at $y=h$. The parameter σ_{yz} is the shear stress, and $(v_z)_A$, $(v_z)_B$ are the velocities for phases A and B, respectively. Moreover, a power law

$$(\sigma_{yz})_i = m_i\dot{\gamma}^{n_i} \qquad \text{(V-11)}$$

is used for phase *i*, where *i* is A or B and m_i, n_i are the power law constants for phase *i*. and $\dot{\gamma}$ is the velocity gradient defined as

$$\dot{\gamma} = \left| \frac{dv_{z,A}}{dy} \right| \quad 0 \le y \le \delta \tag{V-12}$$

for phase *A* and

$$\dot{\gamma} = \left| \frac{dv_{z,B}}{dy} \right| \quad \delta \le y \le h \tag{V-13}$$

for phase *B*. On the basis of the above equations, the σ_{int} can be determined as follow:

$$\sigma_{int} = -\kappa(\delta - \mu) \tag{V-14}$$

in which κ is the pressure gradient defined by $\kappa = -\partial P_A / \partial_z = -\partial P_B / \partial_z = const.$; δ is the position of interface and μ is the position at which the maximum in velocity (and hence, the minimum in shear stress) occurs. These two parameters can be determined from the velocity profile based on the following equation group (eq.V-15, 16):

$$\left(\frac{\kappa}{m_A} \right)^{S_A} \left(\frac{1}{S_A + 1} \right) \left(\mu^{S_A+1} - |\mu - \delta|^{S_A+1} \right) = \left(\frac{\kappa}{m_B} \right)^{S_B} \left(\frac{1}{S_B + 1} \right) \left| (h - \mu)^{S_B+1} - (\delta - \mu)^{S_B+1} \right| \tag{V-15}$$

$$\frac{Q_A}{Q_B} = \frac{(\kappa/m_A)^{S_A}}{(\kappa/m_B)^{S_B}} \left(\frac{S_B + 1}{S_A + 1} \right) \left\{ \frac{\mu^{S_A+1}\delta - \left[\mu^{S_A+2}/(S_A+2) \right] - \left[(\delta-\mu)^{S_A+2}/(S_A+2) \right]}{(h-\mu)^{S_B+1}(h-\delta) - \left[(h-\mu)^{S_B+2}/(S_B+2) \right] + \left[(\delta-\mu)^{S_B+2}/(S_A+2) \right]} \right\} \tag{V-16}$$

where $S_i = 1/n_i$, Q_A/Q_B is the volumetric flow ratio.

With the pressure gradient detected by the transducers and the rheological behaviours of polymers being known, δ and μ are able to be calculated via the above equations for a given volumetric flow ratio in experiments. For example, in the case of PMMA-1/PVDF bilayer coextruded at 200 ℃, the interfacial position δ, the position of maximum velocity μ, the interfacial stress σ_{int} and the interfacial shear rates obtained in the runs of different flow rate ratios are listed in Table V-3. In fact, for a compatible system, the thin interface can be replaced with a thick interphase after a certain time.

We can note that the flow is not symmetrical and the interfacial position δ/h decreases when the flow rate is increased. Among the different flow rate ratios (Q_{PVDF}/Q_{PMMA}) ranging from 0.3 to 2.6, one can see that when $Q_{PVDF}/Q_{PMMA}=0.6$, the δ/h is closest to the μ, with the interfacial stress and the interfacial shear rate being the smallest. It should be important to note that the interfacial shear stress (or interfacial shear rate) as shown in Table V-3, is too small to generate the interfacial slippage since the shear stress required for slippage is above 25 kPa, as demonstrated in the above section.

Table V-3 Interfacial shear stress and interfacial shear rate calculated for the PMMA-1/PVDF bilayer at 200 °C

Flow Rate(kg/h)		$t_{contact}$ (s)	pressure gradient $\kappa(\times10^4$Pa/mm$)$	Interfacial position[a]	position of v_{max}, μ	Interfacial stress $\sigma_{int}(\times10^4$Pa$)$	$\dot\gamma_{int}^{PMMA}$ $(\times10^{-2}$s$^{-1})$	$\dot\gamma_{int}^{PVDF}$ (s^{-1})
Q_{PMMA}	Q_{PVDF}							
0.6	0.18	93	4.86	0.81	0.76	0.49	0.38	1.10
0.6	0.36	79	4.73	0.73	0.78	0.47	0.35	1.04
0.6	0.6	65	5.57	0.66	0.76	1.17	3.58	3.91
0.6	0.96	52	5.83	0.58	0.75	1.92	12.83	8.38
0.6	1.56	39	6.46	0.51	0.72	2.65	29.12	9.30

[a] the interfacial position is expressed as δ/h; total thickness h=2mm in the studied die.
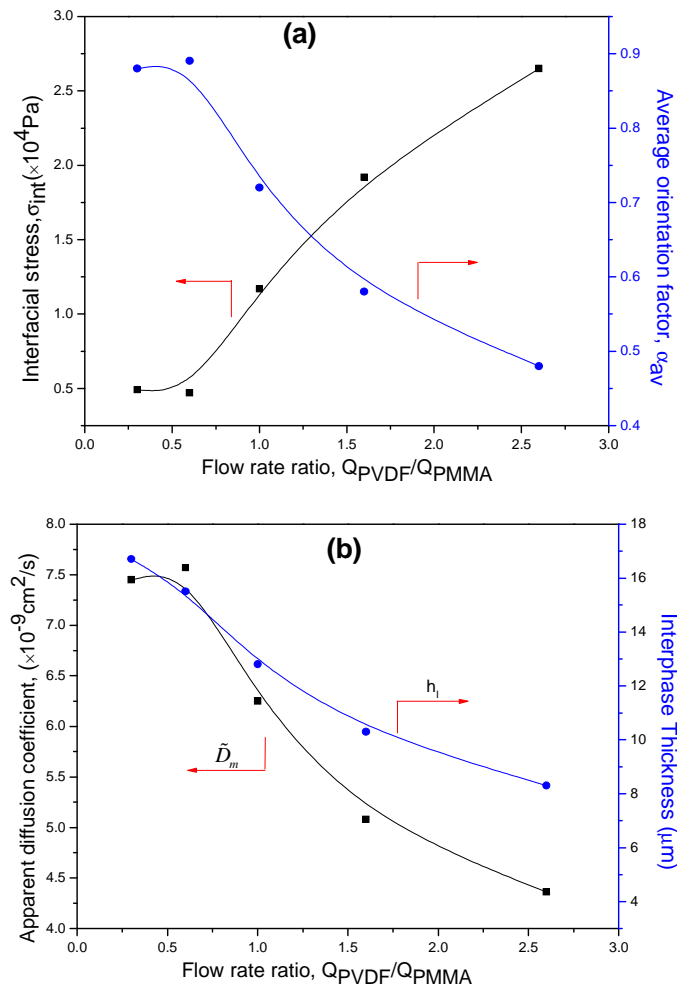
Figure V-9. (a) The average chain orientation factor, α_{av}, and interfacial stress, σ_{int} as a function of flow rate ratio Q_{PVDF}/Q_{PMMA} in shear flow field for PMMA-1/PVDF bilayer coextruded at 200 °C; (b) Apparent diffusion coefficient, $\tilde{D}_m$ and corresponding predicted interphase thickness h_I as a function of flow rate ratio Q_{PVDF}/Q_{PMMA}

On the basis of these important parameters as shown in Table V-3, orientation factor,α, of each polymer chain can be determined. Then the average chain orientation factor, α_{av}, as displayed in Figure V-9(a), was determined as arithmetic average of the orientation factor of PMMA chains and that of PVDF chains.

- 234 -

According to the orientation factors and the mutual diffusion coefficient D_m evolving with time obtained at the fundamental conditions of rheological measurements in LVE, the apparent mutual diffusion coefficient in the shear flow field of coextrusion conditions can be estimated as follow:

$$\tilde{D}_m = \alpha_{av} D_m \qquad\qquad (V\text{-}17)$$

The results of $\tilde{D}_m$ are given in Figure V-9(b) and the corresponding interphase thickness calculated based on the $\tilde{D}_m$ are also given in the figure. Obviously, the orientation factors are below 1, which results in lower diffusion coefficient during coextrusion process than that in the static condition. This means that the polymer chain orientation in the shear flow field during coextrusion has a decelerating effect on the interdiffusion process between neighbouring layers. Moreover, when Q_{PVDF}/Q_{PMMA}=0.6, where the δ/h is closest to the μ and the interfacial stress and the interfacial shear rate is the smallest, the orientation factor is close to 1. The larger deviation of the Q_{PVDF}/Q_{PMMA} from 0.6, the higher the value of the interfacial shear stress and the greater the orientation effect. The variation of Q_{PVDF}/Q_{PMMA} was realized by fixing Q_{PMMA}=0.6 kg/h and varying the Q_{PVDF}, thus the total flow volume was changed. So as the Q_{PVDF}/Q_{PMMA} increased, the contact time of polymers inside the die was decreased and so as the thickness of the interphase.

V.4.4.2 Intermixing induced from shear flow: probed by performing a pre-shear in rheological measurement of multilayer structures

Although an interesting work has been dedicated to the effect of orientation on the interdiffusion in coextrusion of compatible polymers, a very important point, i.e. intermixing induced from the high shear flow in the processing conditions was neglected in the study of Kim and Han (1991). Indeed, effect of the shear flow could be very significant, especially in the early stage of processing. It has been reported that the flow in heterogeneous melt blending can result in a rate constant over 1000 times higher than that in the quiescent bilayer condition for an interfacial reaction between amine and anhydride terminal functions(Macosko, et al. 2005). A shear flow is able to induce a local pressure drop at the interface between two fluids and thus gives rise to undulated structure and hence convective mixing(Patlazhan, et al. 2006).

Due to the high complexity of probing this problem in the real shear flow field of processing conditions in coextrusion, it is of interest to simulate this problem by introducing a certain amount of pre-steady shear before the rheological measurements of interdiffusion process at PMMA/PVDF multilayer structures in linear viscoelastic regime. Implement of a pre-steady shear to the multilayer structures may give us some ideas on the practical mixing process, especially in the early stages of polymer processings. This would be a good option to simulate

intermixing in the practical situation of coextrusion and to see its effects on the interdiffusion process in a more closely manner. A given amount of steady shear flow $\gamma(t) = \dot{\gamma} * t$ was introduced to the multilayer assembly, by rotating the plate of the parallel-plate rheometer before beginning a time sweep test in LVE. Figure V-10 shows the G*(t) versus healing time for PMMA-1/PVDF-6 alternating layer structures at T = 200 °C, ω = 0.1rad/s without and with a given pre-shear $\gamma(t) = 4\,s^{-1} \times 60\,s$, respectively. We can see that the effect of pre-shear is pronounced, that is, the G*(t) of multilayer assemblies subjected to pre-shear experiences an increase with a higher slope before reaching a steady stage in comparison to those without pre-shear. The characteristic diffusion time needed to reach the steady stage is significantly reduced and the steady value was lowered down a bit.
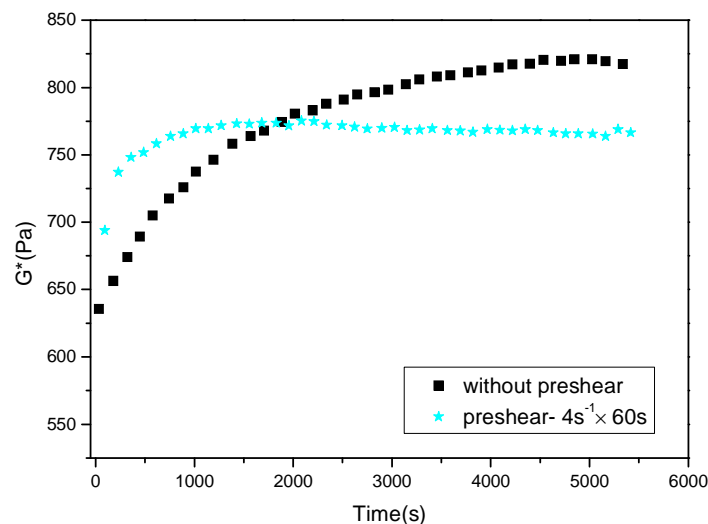
Figure V- 10. G*(t) versus healing time for PMMA/PVDF -6 alternating layers subjected to no preshear and preshear(2s⁻¹×60s) before being annealed at 200 °C. 0.1rad/s

Different underlying physics behind the effect of such pre-shear on diffusion process are to be addressed here. On the one hand, as stated in literatures (Bousmina, et al. 1998;Lamnawar and Maazouz 2006; 2008), the applied pre-shear to the multilayer assembly may perturb the chains configuration at the interface, extract some chains from the bulk to the interface and consequently influence the segmental motions. This may result in a situation of excess chain ends at the interfacial region, which is in favour of interdiffusion kinetics according to the theory of "Minor chain reptation model" proposed by Wool (1995). On the other hand, the steady shear flow imposed to the multilayer assemblies would be presumed to deform or change the interfacial structure. To examine this potential variation of the interfacial structure, once the pre-steady shear was accomplished, we removed the specimens out of the rheometer and quenched them immediately in liquid nitrogen before observing their

cross-section morphology under SEM.
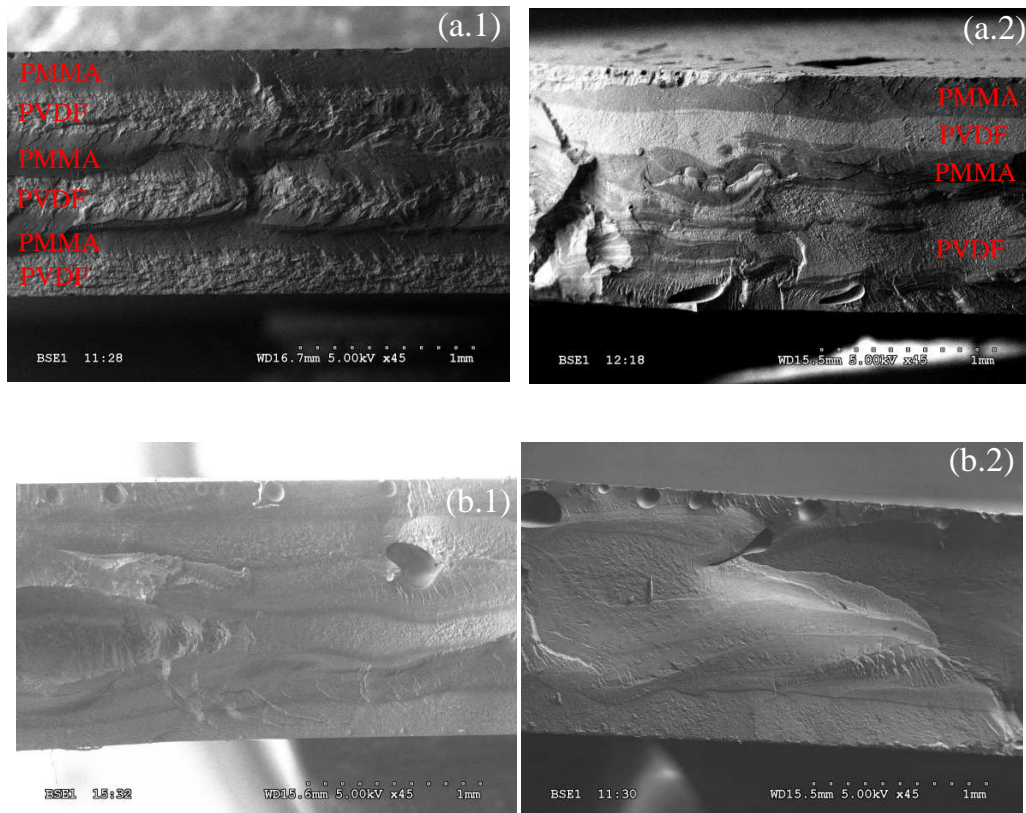
Figure V-11. Micrographs of PMMA/PVDF multilayers: (a) specimens immediately quenched when the pre-shear mode was accomplished. Due to the different index of refraction, PMMA and PVDF phases are clearly distinguished with PMMA layers being darker and PVDF layers being whiter: (a.1)-6layers, no pre-shear; (a.2)-6layers, $\gamma = 4$ s^{-1} × 60 s; (b) specimens quenched after the healing process for 1.5 h at 200 °C. 0.1 rad/s: (b.1)-6layers, no pre-shear; (b.2)-6layers, $\gamma = 4$ s^{-1} × 60 s.

Evidenced from Figure V-11, the cross-section morphologies of specimens subjected to pre-shear are significantly distinguished from those without pre-shear. In great contrast to the evident uniform 6-layers assembly structure observed in the specimens without pre-shear (Figure V-11-a.1), fractal undulated structure can be clearly visible in the specimens being subjected to the high amounts of pre-shear (4 s^{-1} × 60 s) as shown in Figure V-11-a.2. This indicates certain amount of steady shear enables structural deformations at the vicinity of the interface at neighbouring layers. Furthermore, after the whole healing process for 1.5 h, the multilayer assembly specimens have also been quenched rapidly and observed under SEM. Apparently, different from the visible light boundary of two phases observed in that being subjected to no pre-shear (Figure V-11-b.1), the specimens being subjected to pre-shear owns a homogenous morphology without any visible boundaries as shown in Figure V-11-b.2. These experimental observations manifest the acceleration of the interdiffusion and homogenization process caused from certain amount of pre-shear.

An attributable origin to the fractal undulated structure may be related to a local pressure gradient developed at a vicinity of the interface due to the viscosity imbalance between upper and lower polymer layers in the presence of a steady shear flow field. A considerable pressure gradient may result in an invasion of a less viscous fluid to a more viscous one (i.e. more viscous fluid is extended to the less viscous one) and hence leads to the formation of undulated structure (as schemed in Figure V-12). The greater the viscosity ratio, the more serious the evolution of the interface disturbance behaves. The purposed mechanism is in accordance with those of Patlazhan et al.(2006). Indeed, this origin for the interfacial perturbation is to some extent identical with the so-called "viscous encapsulation" that resulted from the viscosity contrast at the interface. However, such interfacial indulated structures and the viscosity imbalance vanish rapidly in the compatible systems thanks to the fast interdiffusion at micro-level and thereby the intermixing is greatly acclerated.
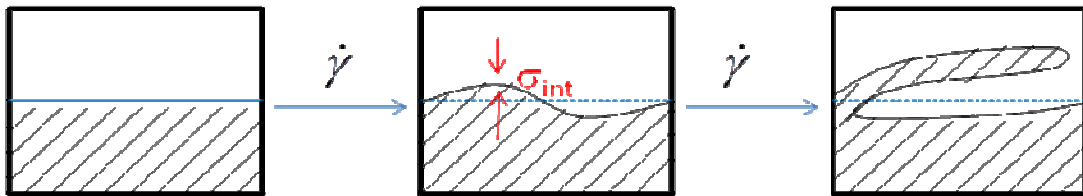
Figure V-12. Schematic of interfacial morphology evolution upon being subjected to certain amount of steady shear

Recently, basing on incompatible functional polymers, Song et al.(2011, 2013) demonstrated that the extensional and compressive flow in coextrusion overcomes the diffusion barriers by decreasing the diffusion length scale, thus enhances diffusive flux of local reactive functions and eventually contributes to the accelerated reaction rate during coextrusion. Change of the diffusion lengthscale or diffusion layer after being subjected to the external flow could be appraised from a theoretical viewpoint. In principle, when a steady shear flow $\gamma(t) = \dot{\gamma}*t$ is imposed to the multilayer structure, effect of the appearing fractal undulated structures on the diffusion kinetics can be laterally described by the reduction of the initial striation thickness (i.e. a lengthscale for interdiffusion), r_0, varying with time in a term of (Tadmor 2006):

$$r(t) = r_0 \,/\, (1 + \dot{\gamma}*t) \tag{V-18}$$

Here, the striation thickness, $r(t)$, is defined in as total volume divided by one-half of the total interfacial area. A foremost contribution of the flow in shear field given to a mixture is to initiate the interfacial surface to increase resulted from the continuous deformation or shear strain whereby separates the components. Thus, the striation thickness is reduced from the total shear strain to a lower level for interdiffusion process in order to arrive at the vanish of the composition nonuniformity. Reduction of the corresponding characteristic diffusion time for such

striation thickness could be expressed in a term of

$$t_D = r^2(t) / D_m \qquad \text{(V-19)}$$

This theoretical prediction well accords the experimental observations in this study in a qualitative aspect. We can hereby conclude that certain amount of pre-steady shear could promote the kinetics of interdiffusion process, more exactly, homogenizing process, by introducing excess chain ends at the interface and more importantly inducing fractal undulated structures at the vicinity of the interface from flow. The latter strikingly increases the interfacial area and hence reduces the striation thickness whereby shortens the characteristic time for interdiffusion and homogenization process in a pronounced way. These investigations give us a clear idea that even though the orientation/extension of polymer chains in the shear flow field of processing may slow down the D_m, the intervention of the intermixing arise from the shear flow could shorten the striation thickness to a level that the interdiffusion process can readily occur, thus effectively accelerate the homogenization rate of the liquid-liquid phase. We can take the case of Q_{PVDF}/Q_{PMMA}=1.0 at 200 °C given in Table V-3 as an example, assuming an interfacial shear rate $\dot{\gamma}_{int}$ being averaged from $\dot{\gamma}_{PMMA}$ and $\dot{\gamma}_{PVDF}$ to be 1.973 s^{-1}, with a contact time of 65 s, one can obtain $r(t)=r_0/129$ from eq.(V-18). Thus even though the diffusion coefficient is 0.72 times lower as a result of chain orientation in this case (i.e., $\tilde{D}_m$ =0.72 D_m as given by eq.(V-17)), the characteristic diffusion time t_D can be a factor of 8.3×10^{-5} lower than that in static condition according to eq.(V-19). Obviously, in the practical condition of coextrusion, the intermixing in the shear flow field acts a more significant role in reducing the diffusion length scale than the deceleration of diffusion coefficient arised from chain orientation. The interfacial stress resulted from the rheological contrast of the two components at the vicinity of the interface gives rise to intermixing (a more great flow effect). Dominant contribution of such flow effect is augmenting interfacial area through generating undulated structures therefore increasing the diffusive flux between two phases. The eventual combination effect of orientation and intermixing is to impel the homogenizing process and undoubtedly favour the broadening of the interfacial zone (development of the interphase). Broadening of such interphase developed during the coextrusion process was well characterized in this study via SEM-EDX analysis and TEM observation on the quenched coextruded bilayer as shown in next section. Results show that the real interphase triggered in practical condition of coextrusion is indeed broadened in comparison to its theoretical prediction of orientation effect in absence of intermixing. Theoretically predicted values of the interphase thickness in a processing condition incorporating the effect of chain orientation but without considering the effect of intermixing as shown in Figure V-9b indicated a thickness of ~12 μm for coextrusion at 200°C with a flow rate ratio equalling to 1. Experimental

result from SEM-EDX analysis for the bilayer coextrude at similar condition demonstrated the real interphase thickness to be 28 μm as shown in Figure V-13b. That means the intermixing broadens the interfacial zone at least by 2 folds.

V.4.5 Characterization of the diffuse interphase generated in coextrusion by SEM-EDX and TEM

As demonstrated before, in the practical processing conditions of coextrusion, the coupling between interdiffusion process and intermixing (i.e., flow effect) resulted from the interfacial stress significantly favours development of the interphase and homogenization process at the interface. We remain that few work has been dedicated to the physicochemical affinity (i.e., interphase) between the neighbouring layers of coextruded multilayer structures and its impact on the interfacial defects. In the present work, to quantitatively characterize the interphase generated in coextrusion process, scanning electron microscopy combining with energy dispersive X-ray (SEM-EDX) analysis has been employed to determine the concentration profile of composition and hence the geometrical properties of the interphase on the quenched coextruded PMMA/PVDF bilayer. The physics of this spectroscopic technique on determining the interphase has been detailed in our earlier work (Zhang, et al. 2013), which makes use of the X-ray fluorescence of the characteristic fluorine (F) atom in PVDF and the characteristic oxygen (O) atom in PMMA to monitor the composition changes versus the interfacial region. As shown in Figure V-13 (a) is a micrograph superimposed with a trace of the line scan including 20 points collected within a distance of 134.9 μm perpendicular to the interphase in the case of PMMA-1/PVDF bilayer specimen coextruded at 200 ℃ with Q_{PMMA}/Q_{PVDF} = 1.0. In this case, the interphase is theoretically predicted to reach 12.8 μm under the steady condition with orientation effect but in absence of flow effect (as shown in Figure V-9b). The corresponding experimentally measured concentration profile of F and O element (quantified in portion of peak area, A%) obtained on this bilayer specimen is displayed in Figure V-13 (b), from which an approximate 28 μm thick interphase could be seen. This implies that under the real practical condition of coextrusion process, the interphase could be exactly greater than that theoretically predicted in conditions of no flow effect. In other words, the intermixing in processing conditions actually expands the amount of the interphase. We have also confirmed that the interphase is asymmetrical rather than absolutely symmetrical. In effect, the intermixing is attenuated when temperature is increased as the interfacial shear stress is reduced when the rheology of the components is approaching each other at higher temperatures. Properties of the interphase are related to a lot of parameters like contact time, processing temperature, interfacial shear stress and compatibility of the polymers, etc.
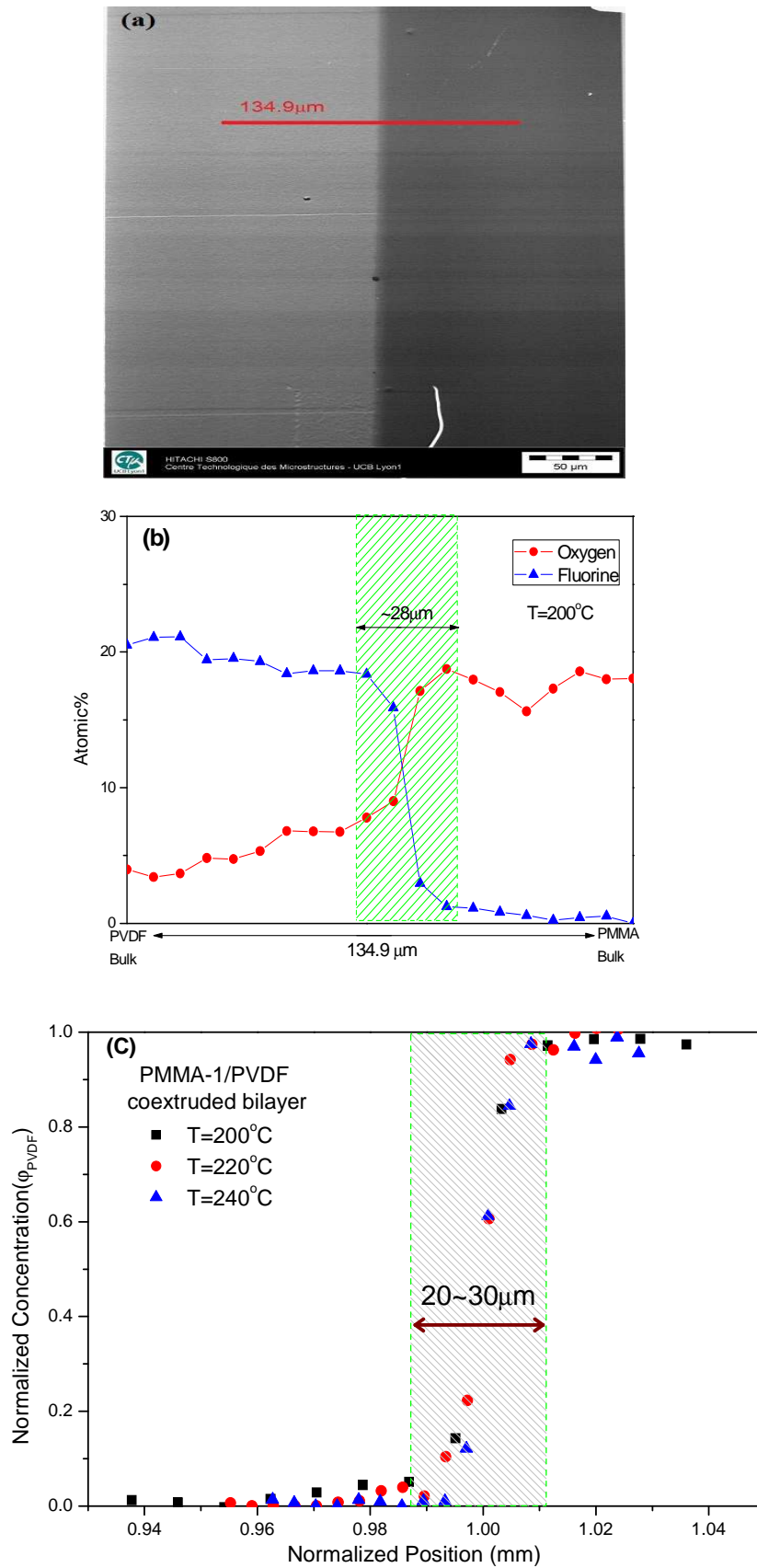
Figure V-13. (a) SEM micrograph on the interfacial region for PMMA-1/PVDF bilayer films coextruded at 200 ᵒC with Q ratio = 1.0 and (b) corresponding EDX experimentally

measured concentration profiles of F and O (in atomic fraction) vs. measured distance (134.9μm) as indicated in (a); (c) Normalized PVDF concentration profile vs. normalized position for the PMMA-1/PVDF bilayer coextruded at different temperatures (Q ratio = 1.0):(■)200 ℃;(●)220 ℃;(▲)240 ℃. The shadow zone designates the interphase zone.

We had a first mind that the generated interphase should be undoubtedly greater at higher temperatures during the coextrusion process since the D_m is higher at higher temperatures(Zhang, et al. 2013). However, beyond our expectation, as displayed in Figure V-13 (c), at higher temperatures the bilayer were coextruded, that is, at 220 ℃ and 240 ℃, the created interphase owns a thickness with only similar order of magnitude (20~30 μm) like lower temperatures. Note that normalized position is made using interface position (1.0 mm, total thickness *h*=2 mm, PVDF is upper layer) as reference. As a matter of fact, this is not extraordinary if we take into consideration of the impact of intermixing on the interphase development in coextrusion process. As indicated in our earlier work (Zhang, et al. 2013), the effect of temperature on the D_m between PMMA and PVDF is not in a very large scale, nevertheless, the intermixing resulted from interfacial stress could reduce the characteristic diffusion time by several orders as explained in the former section of this study. In effect, as temperature increased, the interfacial stress could be significantly decreased and also reduced was the intermixing. As displayed in Table 4, the interfacial stress could be reduced by c.a. 2 orders of magnitude from 200 ℃ to 240 ℃, which greatly explains the existence of weaker intermixing at higher temperatures. Moreover, it can be assumed that the interfacial stress and intermixing is overestimated, especially at high temperatures, as an assumption of sharp interface is taken for all the calculations but in fact an interphase appears rapidly for the compatible system, so the intermixing can be even weaker than expected. Obviously, attenuation of the intermixing is more predominant than the increase of the D_m when the temperature is increased. This explains the result of similar interphase obtained at higher temperatures. Additionally, the reduction of contact time in the die at higher temperatures allows a shorter time for interdiffusion process and interphase development.

Table V-4 Interfacial shear stress and interfacial shear rate calculated for the PMMA-1/PVDF bilayer at different temperatures with Q_{ratio} = 1.0

Temperature (℃)	pressure gradient κ(×10⁴Pa/mm)	Interfacial position[a]	position of $\upsilon_{max,}$ μ	Interfacial stress σ_{int}(Pa)	$\dot{\gamma}_{int}^{PMMA}$ (s⁻¹)	$\dot{\gamma}_{int}^{PVDF}$ (s⁻¹)
200	5.57	0.66	0.76	1.2×10⁴	3.6×10⁻²	3.9
220	3.48	0.60	0.66	4.2×10³	2.6×10⁻³	0.8
240	1.71	0.58	0.56	7.8×10²	3.5×10⁻⁵	3.3×10⁻²
260	0.66	0.55	0.50	7.2×10²	2.8×10⁻⁵	2.8×10⁻²

[a] the interfacial position is expressed as δ/h; total thickness h=2mm in the studied die.
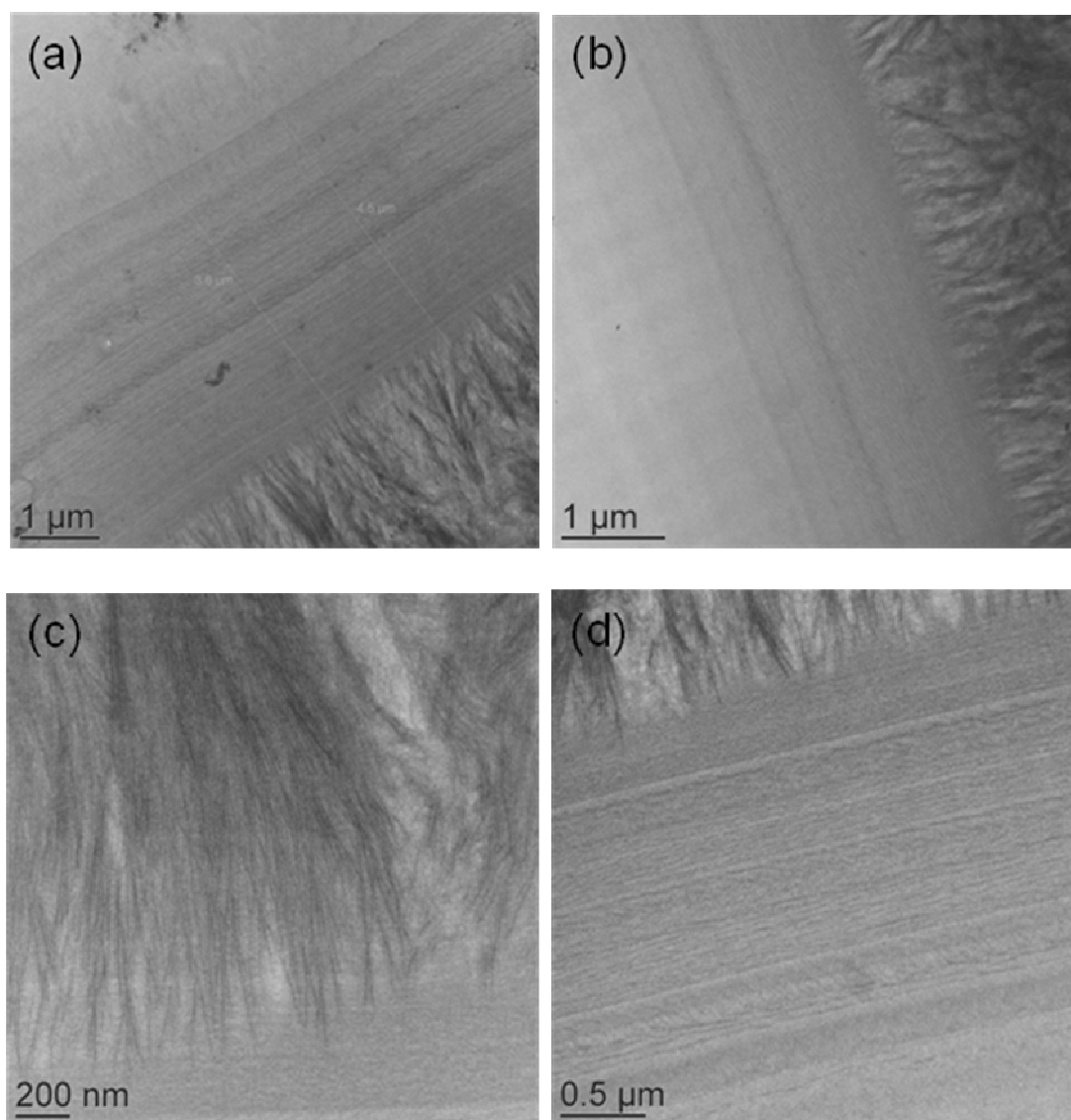
Figure V-14. TEM micrographs of the interfacial zone for the quenched coextruded PMMA-1/PVDF bilayer films (Q ratio =1) at:(a) 220 °C; (b) 240 °C; (c) magnification of image (a) on the PVDF crystal zone; (d) magnification of image (a) on the interphase

Furthermore, TEM was used for morphological observations of the interfacial zone on the PMMA-1/PVDF bialyers after the coextrusion process. As presented in Figure V-14, no matter in the bilayer coextruded at 220 °C (Figure V-14-a) or at 240 °C (Figure V-14-b), crystalline morphology in PVDF-riched side and amorphous morphology in PMMA-riched side are clearly distinguished. It should be noted that besides these two morphologies, it seems that an intermediate morphological region lies between these two phases could be observed in the TEM images. It has been well known that in PMMA/PVDF blends, crystallization can take place when the content of PVDF are more than 60% by weight (Wu, et al. 1986). The interfacial zone generated from the interdiffusion process can be assumed to be equivalent blends with varying compositions, where perfect PVDF crystals were well produced at the PVDF-riched side as shown in Figure V-14-c. It was argued that the transition from

the perfect order in the crystal to the isotropy in the amorphous phase cannot occur abruptly, rather is replaced by a crystal-amorphous interphase (Mijovic, et al. 1997). The existence of such crystal-amorphous interphase in polymer blends has been claimed by previous researchers. It was explained based on the theoretical consideration of chain packing at the surface of lamellar crystals and the different morphological components lead to distinct relaxation dynamics. The intermediate morphological region here (Figure V-14-d) is characterized with a weaker crystallization and different crystal structures scaling with ~4 *μm* thickness. We do not extend much on this point as it is not the objective of this study, but it will be an interesting focus in our further work. One another point interests us is that both the TEM images and SEM-EDX analysis indicate that the interfacial zone experiences a smooth and stable transition between neighbouring layers even after coextrusion process as like that observed in static conditions, with no any interfacial instability being found. This absolutely proves that creation of the interphase at the interface exactly removes the interfacial defects without causing any waviness or rugged shape.

V.4.6 Highlighting role of the diffuse interphase in the processing properties of coextrusion

After having a basic understanding of the interdiffusion kinetics and the triggered interphase in both fundamental conditions of rheological measurements and practical processing conditions of coextrusion, a set of experiments concerning optimizing the coextrusion process have been carried out by listing some important parameters that govern the interfacial flow stability. Bilayer systems composed of PMMA/PVDF was firstly studied as a compatible polymer pair and PMMA/PE was considered as an incompatible one for comparison. In this work, the films were visualized from the flow direction when they were flowing out at the die exit to examine its flow stability. Upon the observations, special attentions were paid to the wavelike shape (highly irregular or sometimes regular waviness) appearing at the flow and the encapsulation that emerges with an appearance of a greater thickness at the edge of the bilayer films.

In the experiments, following variables were considered: viscosity ratio of polymer pairs varied by changing the processing temperature; thickness ratio varied by changing the flow rate ratio of the two polymer melt streams; elasticity ratio (average relaxation time ratio or first normal stress difference ratio) by using PMMAs of different molecular weight. It is noted that other factors such as interfacial tension and density difference which had been reported to have minor effects were not considered in this work(Lamnawar, et al. 2013). Indeed, for the compatible systems, the interfacial tension is close to zero. More importantly, greater interests were given to the effect of the presence or absence of the interphase at polymer-polymer interface. Role of the interphase was highlighted by comparing the situations of flow stability of the compatible pair to that of the incompatible ones at similar conditions.

The experiments were carried out at different conditions, with temperatures varying from 190 °C to 260 °C, and with flow rate ratio of PVDF or PE versus PMMA varying from 0.3 to 2.6. To observe more clearly the flow instability and the edge caused from encapsulation, traces of coloured PVDF pigments were mixed into the PVDF layer with a presumption of no effect on their rheological properties.

V.4.6.1 Coextrusion of different polymer systems and investigation of interfacial flow stability
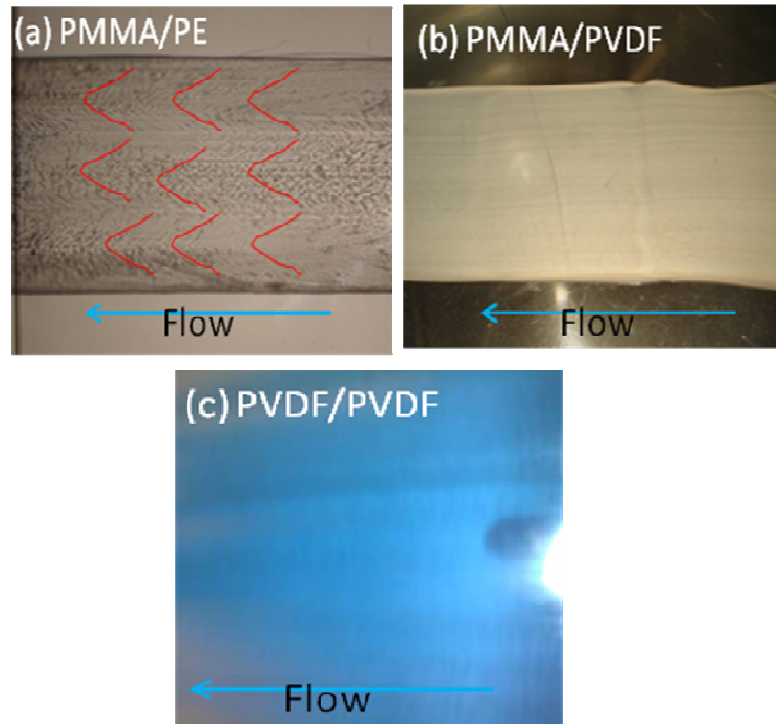
Figure V-15. A typical image of interfacial instability (wave pattern) observed in the case of PMMA-PE couple (T=220 °C. Q_{PE}/Q_{PMMA} = 1.0) (a) and typical images of stable interface of PMMA/PVDF couple (T=220 °C. Q_{PVDF}/Q_{PMMA} = 1.0) (b) and PVDF/PVDF couple (c).

Indeed, whether or not the compatibility or incompatibility of polymer pair being coextruded plays a role in bringing about the onset of interfacial instability was considered by Han (Han 1981), whereas the role of the interphase was not highlighted and no further focus was given in their work. In our recent review article (Lamnawar, et al. 2013), we have focused on the fundamental studies of the interfacial phenomena (i.e., interdiffusion/interfacial slippage/interfacial reaction) and addressed the importance of the physicochemical affinity (i.e., interphase, a result of the interfacial phenomena) at neighboring layers related to the interfacial defects of the coextrusion process based on the advances reported in literatures. Despite this, the experimental studies dedicated to the role of the interphase in coextrusion are still rare. In this study, with such an aim to disclose the role of the interphase in controlling the flow instability, compatible polymer pairs of PVDF/PMMA1 or PMMA2; symmetrical bilayers of same polymers and incompatible polymer pair composed of PMMA/PE were taken into considerations and their

interfacial flow situations were compared. Typical samples obtained at an interfacial stability theoretically favorable condition of Q ratio=1 are illustrated in Figure V-15, where a severe wave-like distortion at the interface with rugged shape can be obviously observed in the case of PMMA/PE incompatible bilayer co-extrudates (Figure V-15a). This is in quite a good agreement with those reported in literatures regarding the unstable appearance. Nevertheless, the coextrusion of PMMA/PVDF (Figure V-15b) and PVDF/PVDF (Figure V-15c) compatible bilayers exhibit a stable interfacial flow at the exit of the die under this condition, with smooth surface and stable flow observed. Indeed, for the PMMA/PE pair, in addition to the wavelike form at the interface, the solid co-extruded bilayer could be easily delaminated by hand since there is no adhesion between neighboring layers. On the contrary, no sharp interface can be found and good adhesion is formed for the cases of PMMA/PVDF and PVDF/PVDF or PMMA/PMMA pairs.

In the analysis, to compare the interfacial flow stability between different experimental conditions, we construct a stability chart by listing the situation of the flow stability obtained at different conditions in a same figure, as shown in Figure V-16. Here, the x-axis indicates the varying flow rate ratio employed in the experiments from 0.3 to 2.6, the varying flow rate ratio indicates varying thickness ratio. The y-axis indicates the zero-shear viscosity ratio of the investigated polymer pairs at 200 °C. In this stability chart, two types of interfacial defects, flow instability (wavy shape, etc.) and encapsulation, are considered, the empty and wavy small rectangle in the left part of the symbol indicates stable and unstable (or wavy interface) of the bilayer systems, respectively; and the light colored empty and hachured small rectangle in the right part of the symbol represents the state of no encapsulation and that of high encapsulation, respectively.

Figure V-16. Chart of stability/instability and encapsulation/un-encapsulation observed experimentally for different couples of coextruded bilayers versus flow rate ratio:

PMMA-2/PE; PMMA-1/PVDF; PMMA-2/PVDF. m_0 in y axis denotes the zero viscosity ratio of PMMA/PE or PMMA/PVDF.

In particular, the zero shear viscosity ratio and elasticity ratio of PMMA versus PVDF at different temperatures are plotted in Figure V-17. It should be noted that here the elasticity ratio is expressed by the average relaxation time ratio of PMMA versus PVDF. The relaxation times were determined from the Cole-Cole curves (η'' vs. η') in their rheological characterizations. In general, the first normal stress difference of polymers, $N_1 = \sigma_{11} - \sigma_{22}$, is used more often to describe their difference in elasticity (Lamnawar and Maazouz 2009;Su and Khomami 1992;Wilson and Khomami 1993a). According to the relation $N_{1,i} = 2\eta_{0,i}\lambda_i\dot{\gamma}^2$ where $\eta_{0,i}$, λ_i are zero shear viscosity and relaxation time of component i, respectively, the first normal stress difference ratio (indication of elasticity), $N_{1,A}/N_{1,B} = (\eta_{0,A}/\eta_{0,B})(\lambda_A/\lambda_B)$, is directly related to the relaxation time ratio $M_\lambda = \lambda_A/\lambda_B$ at a given shear rate $\dot{\gamma}$. When the viscosity ratio is known at certain conditions, their relaxation time ratio, M_λ, can be enough to express the elasticity ratio at a given shear rate $\dot{\gamma}$. Indeed, the Weissenberg number, $W_i \equiv \dot{\gamma}\lambda$, which governs the degree to which the normal stress differences differ from zero, can also be used as an elasticity expression. thus $M_\lambda = \lambda_A/\lambda_B = \dot{\gamma}\lambda_A/\dot{\gamma}\lambda_B = W_{i,A}/W_{i,B}$ is sufficient to indicate the elasticity ratio.
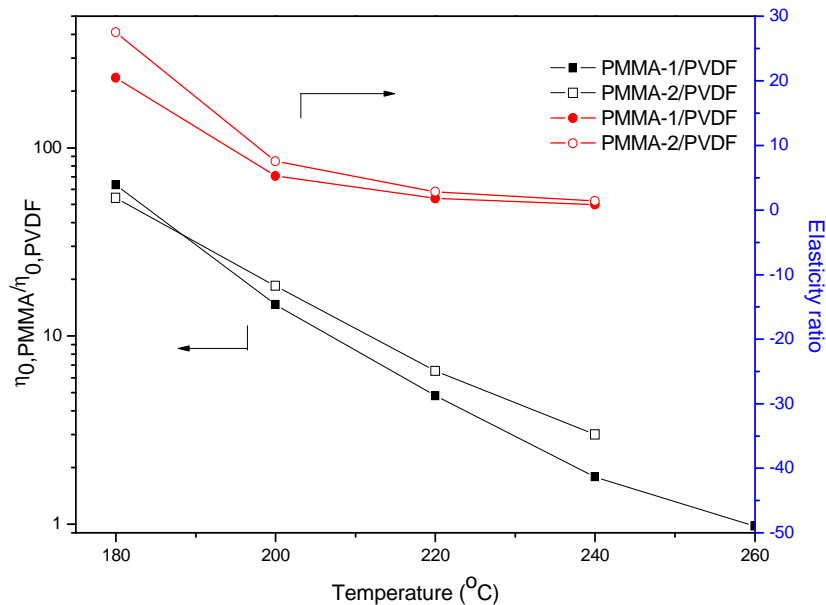
Figure V-17. Zero shear viscosity ratio of PMMA to PVDF and elasticity ratio of PMMA to PVDF as a function of temperature (viscosity ratio = 30.86 @ 190 ºC)

Hence, based on this analysis guide-line and the experimental results obtained

for the various bilayer systems as summarized in this stability chart (Figure V-16), we can see at the first sight that the interfacial flow situation including the instability and encapsulation of the incompatible PMMA/PE bilayer system is pronouncedly distinguished from those of compatible counterparts. Despite of the change of flow rate ratio from 0.3 to 2.6, severe flow instability was always observed for the PMMA/PE bialyer system. Such flow instability is only a bit alleviated at Q_{PE}/Q_{PMMA}=0.3. Contrast to the severe flow instability, only few encapsulation is found in this bilayer system within the range of the measured flow rate ratios. Completely different from the incompatible PMMA/PE bilayer, at the similar conditions the interfacial flow in the compatible PMMA/PVDF bilayer and those symmetrical bilayers of same polymers appear to be stable without apparent interfacial distortion or rugged interface observed. Only some subtle encapsulation (reflected by a thicker edge) could be noted for the PMMA/PVDF bilayers at higher value of Q_{PVDF}/Q_{PMMA}. In fact, from the y-axis it is clearly shown that the PMMA/PVDF pairs have higher viscosity ratios than that of PMMA/PE pair. It has been widely reported that the higher the viscosity stratification is, the more severe the interfacial instability appears given that the thickness ratio deviates from 1 and the less viscous fluid is not the thinner layer(Lamnawar, et al. 2013). Evidently, it is not the case in this study. Having greater viscosity ratio than PMMA-2/PE pair, the PMMA-1or PMMA-2/PVDF pairs experience stable interfacial flow rather than the severe flow instability of its counterpart at given thickness ratio and temperature. This implies that there are some other underlying mechanisms behind here. Exactly speaking, the flow instability in coextrusion encountered by the incompatible polymer systems under certain conditions could be removed in the compatible systems. As demonstrated in the above sections, in the compatible systems like PMMA/PVDF, especially under the practical conditions of coextrusion, certain mount of interphase is able to be generated at polymer-polymer interface from the interdiffusion process and be favoured from the intermixing. The presence of mounts of the interphase seems to be the sole reason for the removal of the flow instability in the case of the compatible systems .

V.4.6.2 Flow stability of PMMA/PVDF bilayer coextruded at different temperatures

Different temperatures were used to vary the viscosity ratio of PMMA vs. PVDF to examine its effect on the flow stability in such compatible systems. For this, a new stability chart was established as shown in Figure V-18 by listing together the situation of flow stability obtained at different temperatures varying from 190 °C to 260 °C and different flow rate ratio Q_{PVDF}/Q_{PMMA} ranging from 0.3 to 2.6. In the figure, the y axis is the zero shear viscosity ratio of PMMA-1 versus PVDF (i.e. η_{PMMA}/η_{PVDF}). Besides, the elasticity ratio expressed by the average relaxation time ratio

$M_{\lambda} = \lambda_{PMMA} / \lambda_{PVDF}$ is also listed in the chart. We can see that even at the condition of

high viscosity ratio and elasticity ratio at low temperatures, eg. η_{PMMA}/η_{PVDF} = 30.8 and $M_\oplus$ = 12.89 at 190 °C, the interfacial flow was still stable, with few interfacial waviness observed during the flow exiting the die. This is quite distinct from the viscous instability reported in the literature for incompatible polymer pair which says that high viscosity ratio of the fluids may destabilize the interface. In fact, this universal tendency of severer interface instability at higher viscosity ratio is also valid in the present system considering that the interfacial flow stability situation is worse at lower temperature as shown in Figure V-18. But the extent of the instability is rather limited, which is probably attributed to the appearance of the interphase at the present pair. On the other hand, different from the few interfacial waviness observed at the low temperatures, a great thickness was found at the edge of the bilayer films, that is so-called encapsulation. Photographs of the encapsulation experimentally observed are shown in Figure V-19. It is noted that colored pigments were used for PVDF layers for clear observations. As pointed out by Wilson and Khomami (1992), encapsulation phenomena occur irrespective of the stability/instability of the interface. In the case of this study, the less viscous polymer, here PVDF, tends to immigrate to the region of high shear rate (i.e. the wall), thereby producing encapsulation, that is, the less viscous fluid encapsulating the more viscous components, and resulting in a great thickness nonuniformity in coextrusion flow which gives rise to a thick edge of the sheet. The encapsulation becomes even more serious as flow rate ratio increases, as shown in Figure V-18.
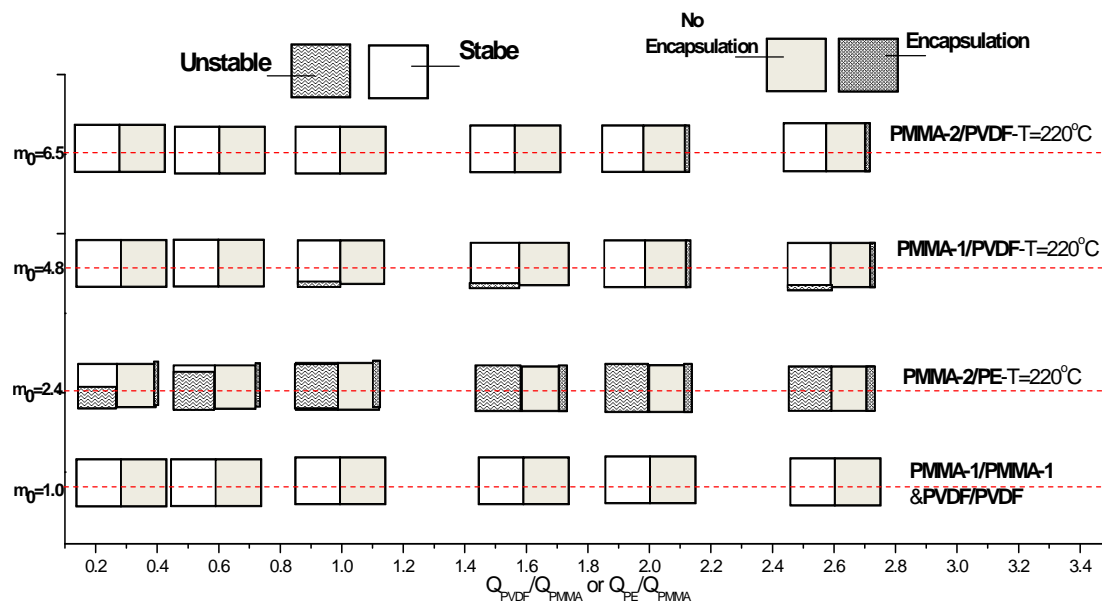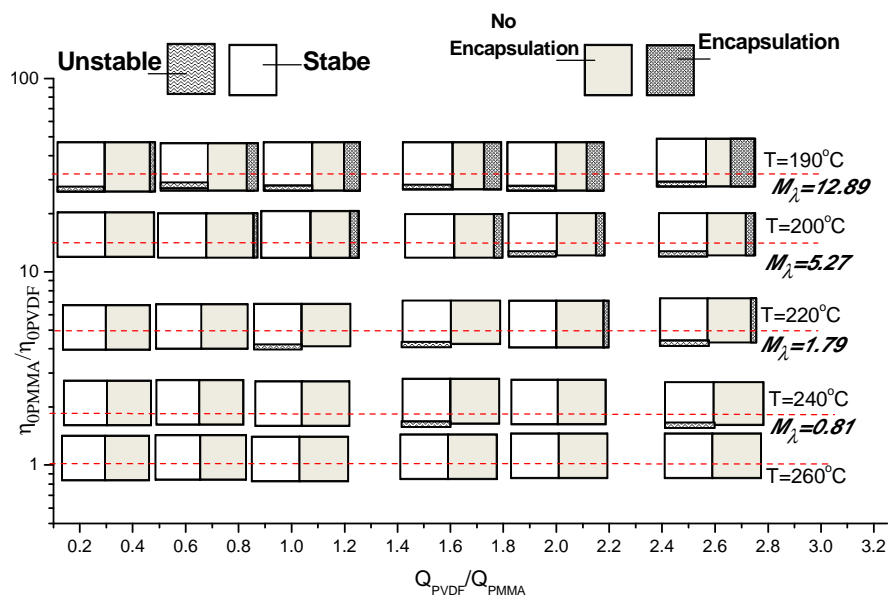

Figure V-18. Chart of stability/instability and encapsulation/no-encapsulation observed experimentally for PMMA-1/PVDF coextruded bilayers (evolution of viscosity ratio vs. flow rate ratio). M_λ denotes the elasticity ratio expressed by $\lambda_{PMMA}/\lambda_{PVDF}$.
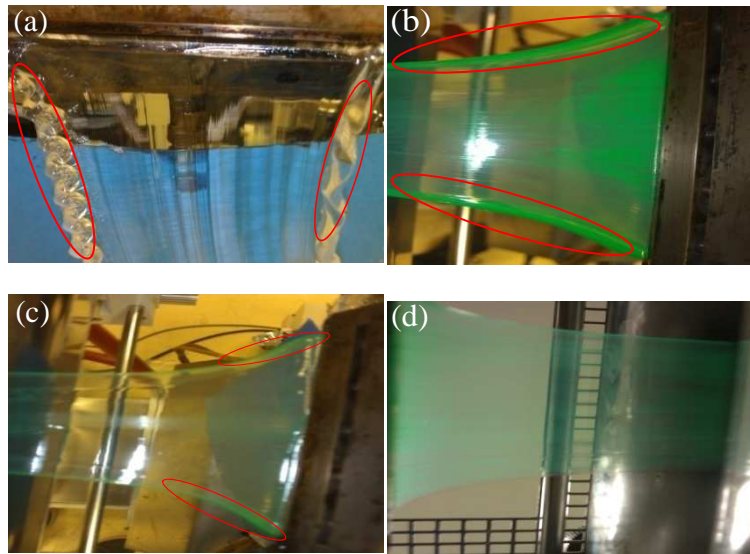
Figure V-19. Photographs of flow stability situations of PMMA-1/PVDF bilayer with $Q_{PVDF}/Q_{PMMA}= 2.0$ obtained at different temperatures: (a) T=190 °C; (b) T=200 °C; (c) T=220 °C; (d) T=260 °C. (traces of PVDF green pigments were added to the PVDF layer)

Furthermore, both Figure V-18 and Figure V-19 show that at a given flow rate ratio, as the temperature increase, the interfacial flow of the PMMA/PVDF bilayer becomes more stable and the encapsulation is also reduced. In particular, at T=260 °C, the flow is always stable irrespective of the flow rate ratio (layer thickness ratio) and no encapsulation is found. On the one hand, this could be attributed to the decrement of the rheological difference between PMMA melt and PVDF melt as temperature increase, especially the η_{PMMA}/η_{PVDF} and $\lambda_{PMMA}/\lambda_{PVDF}$ approach 1.0 when T= 260 °C, as indicated in Figure V-17. On the other hand, as the temperature increase, the interdiffusion process between the melts and the development of the interphase are evidently mounting up, hence greatly improve the flow stability and the encapsulation situation. Apparently, this is in accordance with the results obtained in our earlier studies(Lamnawar, et al. 2012) that the encapsulation appeared to be hindered by the interdiffusion process occurred in the case of compatible pair system and the formation of a certain amount of interphase.

In addition, it has been reported in the literature that for non-Newtonian fluids, the variation of the elasticity ratio could have an independent effect as viscosity ratio on the interfacial flow stability of coextrusion processing(Su and Khomami 1992;Valette, et al. 2004). To examine this effect of elasticity ratio, a condition with constant viscosity ratio but different elasticity ratio is necessary to be selected. PMMA-1/PVDF and PMMA-2/PVDF pairs satisfy this requirement at 190 °C since they have similar viscosity ratio while PMMA-2/PVDF has a higher relaxation time ratio than PMMA-1/PVDF in this condition as shown in Figure V-17. Coextrusion experiments performed on PMMA-2/PVDF and PMMA-1/PVDF with same processing conditions were compared at 190 °C. Unexpectedly, no significant difference was observed between these two polymer pairs with regard to their

interfacial waviness and encapsulation situation despite of the change of thickness ratio. This implies that the elastic instability is also weakened in such compatible pairs.

With regard to the interfacial flow instability of coextrusion, it has been reported that the interfacial flow instability is related to the interfacial shear stress, σ_{int}. That is, there exists a critical value, $(\sigma_{int})_{crit}$ for a given polymer system above which the interfacial instability sets in and may appear to be independent of layer thickness ratio (Han and Shetty 1978;Schrenk, et al. 1978). Actually, results in this study also give some hints that higher σ_{int} brings about severer interfacial flow instability. More importantly, as demonstrated in former section, the high σ_{int} in low temperature, especially at early stage (as the σ_{int} may diminish when interdiffusion occurs) contributes to bringing about some intermixing that promotes formation of thick interphase, which ultimately guarantees good interfacial flow stability.

Hitherto, a clear idea comes into mind is that for compatible polymer systems like PMMA/PVDF, existence of certain interphase at the interface may greatly alleviate the viscous instability as well as the elastic instability. The plausible mechanisms for such weak sensitivity of compatible polymer systems embodying mounts of interphase to the interfacial disturbance may be two folds. On the one hand, the effective viscosity and elasticity differences between the two components at the vicinity of the interface are greatly reduced by the interdiffusion process since the interphase appears as a continuous transition zone with characteristic gradually varying from one component to the other, which has been well demonstrated by SEM-EDX and TEM tools (see the above section). On the other hand, the interdiffusion process and intermixing consume the great portion of the energy from the shear stress and normal stress imbalance at the interface which at first should allow the interfacial waviness to be produced in the incompatible polymer systems. It is worthy of noting that despite here only a qualitative relation between the interfacial defects of coextrusion and the amount of the generated interphase have been highlighted, it is believed that a sufficient amount of interphase is required for stable flow stability. That is because the interphase alleviates the rheological difference at the vicinity of the interface and has an energy dissipation effect.

V.5. Conclusions

This study is dedicated to understandings of the diffuse interphase generated both under the fundamental condition of rheological measurement and under the practical processing condition of coextrusion before highlighting its role in controlling the interfacial flow instability of multilayer coextrusion. For this, measurements were carried out based on a PMMA and PVDF compatible bilayer system.

Under fundamental conditions, interdiffusion kinetics, rheological and

geometrical properties of the generated interphase were estimated via a modified rheological model. Moreover, rheology of PMMA/PVDF laminated multilayer structures was examined by varying the layer number and interfacial slippage was also focused by steady shear measurements. The interfacial slippage can be excluded in such compatible systems since the small shear stress is not enough to fight against the entanglement formation brought about from the interdiffusion, with potential to occur only at short welding time under an extremely high shear stress.

During the coextrusion process, orientation of polymer chains in shear flow field was demonstrated to hinder the diffusion coefficient. Nevertheless, intermixing that occurs at the vicinity of the interface due to the interfacial stress could significantly reduce the characteristic diffusion time and hence favour the development of the interphase. This was investigated by performing a pre-shear mode on the PMMA/PVDF multilayer structures before tracking the interdiffusion process in LVE. The flow effect contributes to increasing the interfacial area through generating undulated structures as demonstrated by SEM, therefore reducing diffusion lengthscale (striation thickness) thus increasing the diffusive flux between two phases. It may reduce the characteristic diffusion time to several orders of magnitude lower at certain conditions. Effect of intermixing predominates that of chain orientation. The eventual combination effect of orientation and intermixing is to widen the interphase and significantly accelerate the homogenization rate in the interfacial region, thus improve the interfacial flow stability of coextrusion. Indeed, effect of intermixing can be attenuated when temperature is increased since the interfacial shear stress diminishes as the rheological difference is narrowing at higher temperatures. This may also affect the development of the interphase. Geometrical and morphological properties of the interphase generated in the real conditions of coextrusion process have been well determined via SEM-EDX and TEM tools. Within the short time of processing, thickness of the interphase can reach more than 20 *μm*. Moreover, the measured real interphase supports the favourable effect of the intermixing and its attenuation as temperature increase. TEM morphological observations show that the morphology in the interfacial zone consists of a crystalline PVDF-riched phase, an amorphous PMMA-riched phase and an intermediate morphological region involves crystal-amorphous interphae. More interestingly, TEM observations indicate that stable interfacial zone with smooth and continuous transition from one layer to its neighbour is obtained after coextrusion processing without causing any interfacial disturbances.

With respective to the flow stability and encapsulation of multilayer coextrusion, classical parameters such as thickness ratio, viscosity ratio and elasticity ratio, etc. have been evaluated by elaborating stability charts based on PMMA/PVDF asymmetrical and PMMA/PMMA (or PVDF/PVDF) symmetrical compatible bilayer systems as well as PMMA/PE incompatible bialyer system. Thickness ratio, viscosity ratio and elasticity ratio were changed by varying flow rate ratio, temperature and

using different PMMAs (i.e. PMMA-1 and PMMA-2), respectively. Results indicated that differ from the severe flow instability observed in the PMMA/PE incompatible bilayers, coextrusion of the compatible bilayers appeared to be smooth and stable with no apparent interfacial defects observed at the similar conditions. Despite of their decisive role in the incompatible system, these key factors seem not that important in a compatible system. The interfacial flow instability of coextrusion is reduced (or even eliminated) despite of the very high viscosity ratio of PMMA versus PVDF as well as the variation of elasticity ratio, especially at low temperature. This would be attributed to the appearance of certain amounts of interphase generated from interdiffusion at neighbouring layers and favoured from intermixing. In other words, presence of the interphase weakens the viscous instability and elastic instability in compatible multilayer systems as it alleviates the rheological difference at the vicinity of the interface and has an energy dissipation effect. Overall, this study will be of some value on showing guide-lines for stable coextrusion of multilayer polymers since it presents us an idea that it is imperative to enrich the classical mechanical approach by taking into account of the role of the interphase during the optimization of the coextrusion processing conditions.

General Conclusions and Perspectives

General Conclusions:

To meet the goals of understanding the interfacial phenomena at polymer/polymer interface and exploring the interfacial rheology as well as its relations to the processing, this study was carried out based on two model compatible polymers composed of poly(vinylidene fluoride)(PVDF) and poly(methyl methacrylate) (PMMA) with varying molar masses. In the context of this manuscript, interdiffusion kinetics and the diffuse interphase triggered thereafter between neighboring layers as well as their role in coextrusion processing have been focused from the aspects of linear and nonlinear rheology.

An overview of bibliography was stated in Chapter I with regard to the interfacial phenomena and the multilayer structures coextrusion as well as their interplays. The interfacial phenomena include interdiffusion, interfacial slippage and interfacial reaction, etc. From a theoretical viewpoint, dynamics of the interdiffusion process, that is, self diffusion between same polymer chains and mutual diffusion between dissimilar polymer chains are mostly described under the tube model of Doi-Edwards (DE) reptation theory. Note that since different monomeric friction coefficients, mobilities as well miscibility exist between dissimilar chains, two divergent theories, that is, fast-mode theory and slow-mode theory, have emerged for the mutual diffusion kinetics. In experiments, various techniques ranging from sophisticated spectroscopic tools like neutron reflectivity to commonly used tools like rheometer have been employed. Their advantages and shortcomings on following the interdiffusion kinetics have been compared in this review work. Moreover, in a multiphase system especially for an incompatible one, interfacial slippage may occur under severe shear conditions. Direct methods like optical visualization and indirect methods of rheology have been developed in literatures to quantify the interfacial slippage by a slip velocity. Chemical reaction is a common means used to introduce compatibilization effects and suppress the interfacial slippage. Numerous theoretical and experimental studies have emerged on the interfacial reaction kinetics (reaction controlled or diffusion controlled) and the interfacial morphology development in the past decades. Besides, nonlinear rheology on multilayer polymer systems especially the interface/interphase in literatures are still very scarce. Some brief introductions on the nonlinear rheological measurements in transient regime such as step shear strain, startup in simple shear and uni-axial extension have been given in the chapter especially regarding the multilayer polymer systems. On the other hand, theoretical and experimental advances achieved on the multilayer polymer coextrusion regarding the interfacial defects, i.e., interfacial flow instabilities and encapsulations have been reviewed in the chapter. So far, most of these studies are restricted to numerical and mechanical approaches such as linear

stability analysis, and neutral stability analysis, etc.. Despite this kind of interesting researches, few works have been devoted to the correlations of the interfacial defects to the physicochemical affinity at the neighboring layers especially the interfacial rheology. Based on such state of the art, this study has dealt with:

In the first step (Chapter II), the interdiffusion process at a molten polymer/polymer interface based on PMMA/PMMA and PVDF/PVDF symmetrical bilayers was investigated via a small-amplitude oscillatory shear measurement (SAOS). The interdiffusion kinetics was analyzed under the framework of the Doi-Edwards theory, and the self diffusion coefficients (D_s) of polymers were determined via quantitative rheological models. Meanwhile, effects of healing time, angular frequency (ω), temperature and molecular weight on the interdiffusion kinetics have been examined. Main conclusions consist of : i) transition from non-Fickian to normal Fickian region could be clearly identified at a critical time, t_c, greater than reptation time; ii) the obtained D_s are consistent with the literatures using spectroscopical tools; iii) diffusions of different motion units could be mirrored from results obtained at different frequencies, with all chains included in the terminal zone; iv) temperature dependence of the D_s can be described by Arrhenius law and the obtained D_s is found to be inversely proportional to the average chain length, consistent with recent studies using Time-Resolved Neutron Reflectivity; etc. Moreover, properties of the symmetrical diffuse interphase triggered between the neighboring layers were examined.

Thereafter (Chapter III), studies were carried out on the asymmetrical molten polymer/polymer interface of PMMA/PVDF bilayer to investigate the mutual diffusion kinetics and to probe and model the asymmetrical diffuse interphase via SAOS measurements. Before setting out this work, the thermorheological complexity of this compatible polymer couple was studied via Rheology method, Lodge-McLeish model and test of the time-temperature superpositon (tTS) principle. The monomeric friction coefficient of each species in mixed state have been examined to vary with composition and temperature and to be close in the present experimental conditions. These were attributed to the presence of strong enthalpic interaction between PMMA and PVDF chains that couples the component dynamics. Based on this physics, rheological modeling of the mutual diffusion kinetics was performed from a viewpoint of the generated interphase by connecting the mobility at the interfacial region to the viscoelasticity of the interphase using a presumably apparent friction resistance factor. The model that was modified from a primitive Qiu-Bousmina model by taking into account the effect of the interfacial rheology appears to produce a greater D_m and to be more sensitive to the segmental motions. The effects of annealing factors as well as structural properties such as molar mass and Flory-Huggins parameter on the interdiffusion kinetics have been discussed. More importantly, viscoelastic properties and geometrical properties of the diffuse interphase are able to be quantified based on the modified model. The interphase has

similar performance with its equivalent blend and owns a thickness in an order of 70-80 μm in the conditions of this work. Scanning electron microscopy coupled with energy dispersive X-ray analysis (SEM-EDX) and transmission electron microscopy (TEM) were also carried out to examine the interfacial structure and to validate the rheological results in terms of concentration profile. In a word, after a full understanding of the weak thermorheological complexity in such compatible polymer system, rheological modeling seems to be a suitable tool to quantify the interdiffusion kinetics and to probe the diffuse interphase properties.

Furthermore (Chapter IV), nonlinear rheological measurements like step shear strain, fast startup in simple shear and in uni-axial extension were performed to the PMMA/PVDF alternating multilayer structures in both cases with and without well-characterized diffuse interphase. It aimed to see whether or not the nonlinear rheology is sensitive to the presence of the generated diffuse interphase and thus effect of large deformation in shear and extension has been assessed. For neat polymer melts, typical nonlinear rheological features have been clearly observed, that is, stress damping of relaxation modulus $G(t,\gamma)$ in step strain experiments, stress overshoot as well as "strain softening" in fast startup shear and typical "strain hardening" behavior in fast startup uni-axial extension. The nonlinear features were interpreted in terms of DE theory and some other recent theoretical scenarios in the literatures. For multilayer polymer systems, an original model was proposed to fit the stress relaxation behavior and to estimate the relaxation modulus $G(t,\gamma)$ of the interphase. In both the step strain and startup shear measurements, interfacial failure begins at intermediate deformations for the multilayers without interphase while the interphase triggered at the annealed multilayers greatly delays the interfacial failure to a large deformation. Entanglement lacking at the interface and entanglement weak intensity at the diffuse interphase render them to be subsequently readily destroyed during or after continuous large deformations. Step strain results were confirmed via different types of rheometers. Furthermore, transient viscosity in startup uni-axial extension depends on the interphase fraction in the mulatilayer structure and its entanglement intensity. The triggered diffuse interphase bridged the entanglement gap at the interface and enhanced the transient extensional viscosity of the final multilayer system. However, the weaker entanglement intensity of the diffuse interphase compared to its constituent bulks makes the elongation viscosity of the total structure subtly decline as the interphase is in a large fraction, approaching that of equivalent blend which shows a negative deviation. Besides, the "strain softening" behavior is also sensitive to the interphase as interfacial area increases. In brief, nonlinear rheology of multilayer structure is sensitive to the presence of interface/interphase.

After full understandings of a diffuse interphase decoupled to flow, in last step (Chapter V), this study dealt with the development of the diffuse interphase coupled to flow as in practical processing conditions and its importance on controlling the

final properties of compatible PMMA/PVDF multilayer materials. In this part, competition between diffusion and flow has been assessed. On the one hand, polymer chain orientation in the shear flow field was demonstrated to decelerate the interdiffusion coefficient. On the other hand, due to the excess interfacial shear stress, intermixing occurs at the vicinity of the interface, which could significantly favor the development of the interphase. Pre-shear mode in rheology coupled with SEM observation was used to probe such intermixing effect between neighboring layers in a multilayer structure. Intermixing appeared as undulated structures were induced with interfacial area increased and hence the diffusion lengthscale and characteristic diffusion time significantly decreased by orders of magnitude under certain conditions. The final result of these two effects gave rise to a significant broadening of the diffuse interphase. Such interphase formed during processing has been well characterized once again via SEM-EDX and TEM. Results indicated that the geometrical property of the interphase could reach ten to several tens microns depending on processing conditions. One other interesting result deals with the smooth interfacial structure with continuous transition from a PVDF-rich crystal phase to a PMMA-rich amorphous phase with an intermediate crystal-amorphous interphase. Finally, concerning the interfacial flow instability and encapsulation in coextrusion process, some key classical decisive parameters such as viscosity ratio, thickness ratio and elasticity ratio, etc. were studied based on a stability chart. Differ from severe flow instability observed in incompatible multilayer systems, presence of the interphase at PMMA/PVDF multilayers plays a vital role in weakening (or even eliminating) the viscous instabilities and elastic instabilities and decaying the effect of classical factors despite of the very high rheological difference between the studied PMMA and PVDF especially at low temperatures.

Overall, this thesis is dedicated to the junction between polymer physics, interfacial rheology and processing in a systematic and thorough manner.

Work in progress & Perspectives:

Even though a number of studies have come up on the subject of the interfacial phenomena with interfacial slippage/interdiffusion/interfacial reaction involved, it is still far from completely understood with respective to the underlying physics. In the present study, complex problem of the interfacial phenomena is simplified firstly by focusing on an interphase triggered only from interdiffusion process, with the interfacial reaction left aside. Indeed, we think that the interphase generated from interfacial reaction (we call it reacted interphase) should be very different from those generated upon interdiffusion, as the reacted interphase mainly consists of graft or block copolymers rather than blends in the diffuse interphase. The dedications of our next step will be two-folds: rheological response (in both linear and nonlinear domains) of the interfacial reaction and the reacted interphase based on reactive and

incompatible polymer systems composed of model end-functional polymers; the other one is on a reactive and compatible polymer system with the reaction/interdiffusion competition involved.

Specifically, for the reactive incompatible polymer systems, our interests cover:

-- kinetics competition between different reactive couples, i.e., groups with fast and slow reaction kinetics. In an interfacial coupling, the reaction could be determined by both the local reactivity of functions and the diffusion of reactive groups from bulk to the interface. With different reactivity couples, kinetics difference may exist as reaction-controlled or diffusion-controlled. For this case, model polymers with different functionalities and reaction kinetics will be used.

-- to the best of our knowledge, few studies have been dedicated to the nonlinear rheology of a reactive multilayer polymer system. One of our ideas is to disclose the nonlinear rheological response such as stress relaxation behavior of the reacted interphase which is supposed to be different from the diffuse interphase.

-- elongation rheology has been demonstrated to be a sensitive tool for presence of the diffuse interphase in this study. What will it behave in the case of reactive system and how about its effect on interfacial reaction? It is one of our motivations in this subject.

-- our further work also can focus on rheological modeling of the interfacial rheology at reactive multilayer system as it is still lacking.

The above-listed interests also holds for the reactive compatible polymer systems, where the situation can be even more complicated and interesting as the occurrence of both diffusion and reaction can be simultaneous. For this topic, modified PVDF and functional PMMA model polymers will be employed. It must be an interesting thing to compare the cases of independent interdiffusion, independent interfacial reaction and diffusion/reaction couplings together in similar conditions. Undoubtedly, the interfacial structures and morphological properties in all the involved systems will be characterized through various microscopic tools like AFM, SEM, TEM and XRD, etc. One more idea inspired from the present study is to examine the thermorheological complexity, i.e., component dynamics of PMMA/PVDF blends, via dielectric and nonlinear rheology measurements including elongation.

Besides, the interests on this subject of interfacial phenomena could be extended to an even further step. For instance, what will the interphase behave at a nano-scale level, in an order close to its chain gyration radius and how the rheological models go at such level for the properties of interphase are some open questions. Our longer term work aims to probe the interphase at a nano-scale level based on nanolayers fabricated via coextrusion processing using layer-multiplication technique.

Publications & Communications

This work has produced:

A- One Book Chapter

1. Khalid Lamnawar, **Huagui Zhang**, Abderrahim Maazouz. one chapter " Coextrusion of Multilayer Structures, Interfacial Phenomena" in **Encyclopedia of Polymer Science and Technology** (4th edition, John Wiley & Sons Inc, **2013**), DOI: 10.1002/0471440264.pst584

B- Articles in Peer-Reviewed Journals

2. **Huagui Zhang**, Khalid Lamnawar, Abderrahim Maazouz. Rheological modeling of the mutual diffusion and the interphase development for an asymmetrical bilayer based on PMMA and PVDF model compatible polymers. *Macromolecules,* 46, **2013**, 276-299.   Doi: 10.1021/ma301620a

3. **Huagui Zhang**, Khalid Lamnawar, Abderrahim Maazouz. Rheological investigation of diffusion process and the interphase of symmetrical bilayers based on PVDF and PMMA with varying molecular weight. *Rheologica Acta***, 51, **2012**: 691-711**.**

4. **Huagui Zhang,** Khalid Lamnawar, Abderrahim Maazouz. Role of the interphase in the interfacial flow stability in coextrusion of compatible multilayered polymers. *Key Engineering Materials,* Vols. 554-557 (**2013**) pp 1738-1750. doi:10.4028/www.scientific.net/KEM.554-557.1738

C- Articles to Be Submitted

1. Huagui Zhang, Khalid Lamnawar, Abderrahim Maazouz. Role of the interphase in the interfacial flow stability of multilayer coextrusion based on PMMA and PVDF compatible polymers. to be submitted to *Polymer Engineering and Science* .

2. Huagui Zhang, Khalid Lamnawar, Abderrahim Maazouz. Nonlinear Rheology of Interphase: Relaxation after Step Strain, Startup Shear and Uniaxial Extension of PMMA/PVDF Compatible Multilayers. to be submitted to *Journal of Rheology.*

3. Huagui Zhang, Khalid Lamnawar, Abderrahim Maazouz. Reaction kinetics comparison between different reactive couples and nonlinear rheological response of the reacted interphase. to be submitted to *Macromolecules* (under preparation)

4. Huagui Zhang, Khalid Lamnawar, Abderrahim Maazouz. Fundamental understanding on structural evolution of diffuse interphase in flow field. to be submitted to *European Polymer Journal* (under preparation)

D- Conferences and Reviewed Proceedings

1. <u>**Huagui Zhang**</u>, Khalid Lamnawar, Abderrahim Maazouz. Rheological modeling of the interdiffusion and the interphase development at a symmetrical and an asymmetrical bilayer based on PMMA and PVDF model polymers, *Le Groupe Français d'Études et d'Applications des Polymères, (JEPO40), 30 Sep. to 5 Oct.2012*, Anduze (Gard) : France (2012), <u>*Oral Presentation*</u>.

2. <u>**Huagui Zhang**</u>, Khalid Lamnawar, Abderrahim Maazouz. Rheological modeling of the diffusion process and the interphase of symmetrical bilayers based on PVDF and PMMA with varying molecular weights, *47ème Colloque national du Groupe Français de Rhéologie, 29-31 Oct. 2012*, Pau, France (2012), <u>*Oral Presentation.*</u>

3**. Huagui Zhang,** Khalid Lamnawar, Abderrahim Maazouz. Modeling of the interdiffusion and the interphase development by rheology of a symmetrical and an asymmetrical bilayer based on PMMA and PVDF model polymers, *The 28th International Conference of The Polymer Processing Society (PPS-28), 11-15 Dec.2012*, Pattaya, Thailand (2012)*, Oral Presentation.*

4. Huagui Zhang**, Khalid Lamnawar**, Abderrahim Maazouz. Role of the interphase in the interfacial flow stability of multilayer coextrusion of compatible polymers. *ESAFORM conference on Material Forming*, 22-24 April, 2013, Aveiro (Portugal), *Oral Presentation.*

5. Huagui Zhang*, **Khalid Lamnawar,** Abderrahim Maazouz. Coextrusion of compatible multilayered polymers: fundamental understanding and modeling of the role of the diffuse interpahse in the interfacial flow stability. *The 29th International Conference of The Polymer Processing Society (PPS-29), July 15-19, 2013,* Nuremberg, Germany*, **Keynote Presentation**.*

6. **Huagui Zhang,** Khalid Lamnawar, Abderrahim Maazouz. Interfacial Flow Stability in Coextrusion of Compatible Multilayered Polymers. *Conference EUROTECH 2013- The Society of Plastics Engineers (SPE),* 4-5July, 2013, Lyon, France(2013), *Oral Presentation*.

Appendix I:

Bibliographic work on interfacial flow instabilities of coextrusion processing

Here we add some more details of bibliographic work regarding the interfacial flow instabilities of coextrusion process from theoretical and experimental aspects. As already mentioned, the formation of interfacial waves can occur during the manufacture of multilayer products. As shown in Figure A-I-1, at low flow rates (a), the interface is smooth whereas interfacial instability appears for moderate flow (b). For high flow rates (c), the distortion becomes more severe.
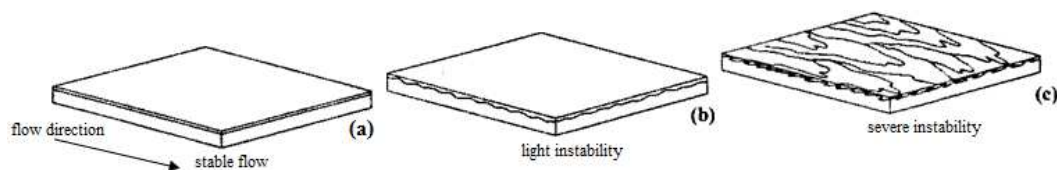
Figure A-I-1 Schematics of interfacial instabilities for different flow rates (Schrenk, et al. 1978)

A-I.1 Theoretical studies

1) Capillary instabilities

It is noted that there are at least three forces that can destabilize an interface: the capillary force, viscous force and elastic force(Lamnawar, et al. 2013). The obtained results pointed out that the capillary instability had faint effects on the flow stability of polymers. The articles dedicated to the role of the interfacial tension on the flow stability for the incompatible systems are few in number. Joseph and Renardy (1992) noted that, for a long wave, the capillary instability may preferentially develop when the interfacial tension is great and the flow is slow; in other words, at low Reynolds numbers, the capillary instability cannot be eliminated by the shear. When the flow is rapid, one should rather have an idea in mind that instabilities may be caused by the difference in viscosity or elasticity.

2) Viscous instabilities

A great number of theoretical studies have been conducted with an aim to determine whether an interface will remain stable. They were carried out on the interfacial stability of stratified flow, by means of a linear stability theory proposed by Yih (1967). This method, also called the asymptotic method in some cases, has been widely discussed in the literature but we would still like to remind the readers of its principle.

For a specific fluid couple, these studies assume a fixed stratified flow, providing boundary conditions at the wall and at the interface (velocity continuity and strain at the interface…), and make a hypothesis that the flow is exteriorly subjected to a two-dimensional infinitesimally sinusoidal disturbance, affecting the velocity, the strain, the pressure and the place of the interface. This perturbation may induce a wave at the interface which can propagate the length of the flow:

$$X(x, y, t) = X_0(y) \exp[i\alpha(x - ct)] \quad \text{(A-I-1)}$$

where X is the subjected perturbation variable, and the terms α, x, c and t designate respectively the wave number of the disturbance, the flow direction, the complex wave speed and the time. All the parameters are dimensionless. Following Yih (1967), all other authors introduced the two-dimensional infinitesimal disturbances into the equation of motion and continuity. The linear stability is governed by the sign of the imaginary part of the complex wave speed c. If it is positive, the amplitude of the disturbance increases with time and the flow is unstable; if negative, the flow is stable; and if zero, the flow is marginally stable. The problem is either solved asymptotically (for very short and very long waves) or numerically (for all wave lengths).

* Newtonian fluids

Yih (1967) considered both plane Couette and Poiseuille flows of two superposed layers of Newtonian fluids of different viscosities submitted to very long waves. By using a linear stability theory, he was able to demonstrate that viscosity stratification could lead to instabilities, even for materials with low Reynolds numbers. He demonstrated that in a case with the same thickness and same density, the plane Poiseuille flow was always unstable regardless of the Reynolds number. In other words, the instability was not the consequence of the transition from the laminar regime to the turbulence regime of any one of the two fluids. Moreover, since Yih assumed that there was no interfacial tension between the two fluids, it cannot be related to the capillary instability. His calculation is valid for very long waves at any Reynolds number but no physical explanation of the phenomenon is given.
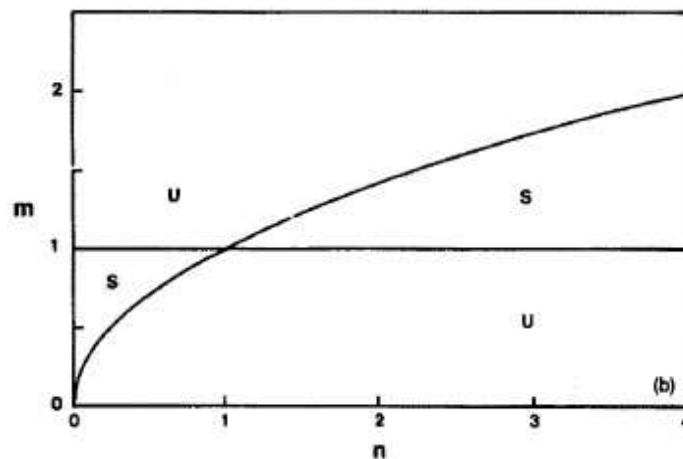
Figure A-I-2 Stability chart of the Poiseuille flow fortwo layers at long waves (Yantsios and Higgins 1988). The viscosity ratio and thickness ratio are designated by m and n, respectively. The stable and unstable zones are represented by S and U.

Hooper and Boyd(1983) argued that capillary forces present a strong stabilizing effect on the viscous instability in the case of short waves. Yiantsios and Higgins(1988) added that the longer the waves are, the weaker is this stabilizing effect. Their studies extended Yih's analysis to the linear stability of a plane Poiseuille flow of two superposed fluids of different viscosities for small to large wavenumbers, taking into account also the geometric and physical parameters of flow systems, like

the viscosity ratio and thickness ratio, etc. (Figure A-I-2). For some regions in the parameter plane, the flow for long waves is stable if the less viscous fluid flows in the thinner layer. Moreover, various authors(Lamnawar, et al. 2013) also observed that a thin layer of the less viscous fluid next to the wall is linearly stable in the case of long waves. This phenomenon is known as the thin layer effect.

   * *Non-Newtonian fluids*

For a non-Newtonian fluid, some new parameters should be introduced into the theoretical model for the Newtonian one. By suggesting an elastic component to the non-Newtonian fluid based on the linear stability theory, Li(1969) argued that, for an Oldroyd model and for long waves, normal stress differences are not the cause of the instability but merely accentuate it due to viscous stratification. Because of a false equation, Li(1969) did not predict that an instability can be caused by solely a difference in elasticity. Waters and Keeley (1987) showed for an Oldroyd-B model and for long waves that shear-thinning also influences the stability of the interface. Later, Chen and Zhang (1993) pointed out an error in the shear stress condition at the interface used in these previous studies. Moreover, he has shown that for a Couette flow, the jump of the normal stress leads to the interfacial instability.

   Pinarbasi and Liakopoulos (1995) have computed the stability of a two-layer Poiseuille flow of Carreau-Yasuda and Bingham-like fluids at moderate wavenumbers. Their results indicate that increasing the stress growth exponents or apparent yield stresses of the viscoplastic fluids has a stabilizing effect on the interface. For shear-thinning fluids, increasing the zero-shear-rate viscosity ratio or shear thinning of the fluids destabilizes the interface. The effect of other parameters can be stabilizing or destabilizing depending on the flow configuration and wavelength. Numerous studies have also been carried out on fluids of non-Newtonian behavior with different constitutive laws, such as the Oldroyd B model, the Ellis model, the White-Metzner model and the modified Leonov model, etc. (Lamnawar, et al. 2013).

   Su and Khomami (1992) performed both asymptotical and numerical calculations for Oldroyd-B fluids and gave the most complete results on the interfacial instability for these fluids with constant and shear rate-dependent viscosities. The influence of the die geometry was also considered. It has been shown that the elasticity and viscosity ratio as well as inertial forces play a crucial role in determining the stability of the interface at all disturbance wavelengths. The variation of the viscosity ratio does not greatly alter the stabilizing or destabilizing effects of the elasticity (particularly at intermediate and short waves) on the interfacial stability. Unlike a flow of superposed Newtonian fluids, for a flow of Oldroyd-B liquids with constant viscosity, an increase in Reynolds number is always destabilizing, particularly at depth ratios greater than a critical value. However, for Oldroyd-B fluids with a shear-thinning viscosity, an increase in Reynolds number could stabilize the interface at low depth ratios (i.e., when shear thinning is more pronounced in the more viscous layer).

   In their studies of the flow stability of a Poiseuille plane at two layers, Laure *et al.*(1997) evidenced the additive characterization of the elasticity and Newtonian contributions by an asymptotic study at long waves. For this purpose, the authors have traced a stability chart, particularly in a model of the elastic part (at a Reynolds number of zero and by slightly

varying the ratio of elastic contributions denoted by $M_\lambda = \dfrac{\alpha_2 \lambda_2}{\alpha_1 \lambda_1}$ where $\alpha_k = \dfrac{\eta_{p,k}}{\eta_k}$ and λ_k designate the ratio of viscous contributions and the relaxation time of the layer k, respectively).The stability chart represented in Figure A-I-3 displays two more stable domains than the case of purely Newtonian fluids. These authors have also numerically studied the flow stability at moderate wavelengths, and extended their work to the case of symmetrical flow at three layers. Wilson and Rallison (1997) have extended the study to short wavelengths in the case of a plane Poiseuille flow with three layers of two fluids. It was demonstrated that in most configurations, the short wavelength mode presented a greater amplification rate than its long wavelength counterpart. The study was generalized by Scotto and Laure (1999) for the case of a non-symmetrical flow.
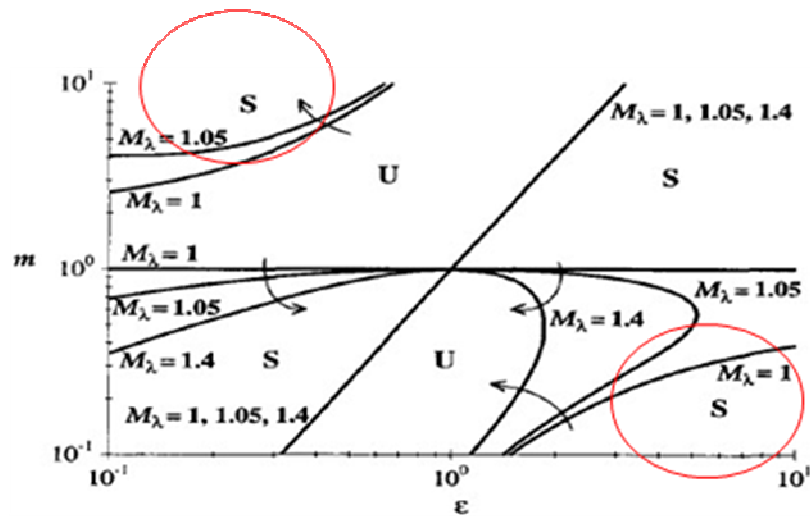
Figure A-I-3 Stability chart of the Poiseuille flow of two fluids Oldroyd-B (Re=0) (Laure, et al. 1997).The stability is expressed as a function of the viscosity ratio m and thickness ratio ε for different values of elasticity ratio M_λ. S and U denote stable and unstable zones, respectively. The arrows indicate the shift of the curves with the elasticity ratio.

3) Elastic instabilities in coextrusion

Numerous studies have been carried out in which different elastic and viscoelastic rheological models are submitted to the linear stability theory. Hinch et al.(1992) proposed a physical mechanism to explain how a jump in primary normal stress difference can cause instability whenever there is an absence of a jump in viscosity across the interface. If the central fluid is the most elastic, the first normal stress difference at the interface is negative. The interface is then deformed by the normal force. The principle of mass conservation imposes a return flow that occurs in the thickest layer. Figure A-I-4a presents a case where the central fluid occupies the thickest layer. In this case, the return flow is in the opposite direction of the normal force, which results in a reduction of the interfacial wavelength. Figure A-I-4b presents a case where the central layer is the thinnest. Here, the applied force at the interface and the perturbation flow are in the same direction and the interface becomes unstable. Hinch et al.(1992) has also pointed out that the interfacial stability is almost not at all affected by the second normal stress difference in the case of polymer materials. Su and Khomami (1992) studied the pure

elastic instability and the viscous instability by comparing the growth rate of waves that formed in a die of finite geometry. In these two cases, the maximum growth rates were obtained for a dimensionless wave number α close to 1 and were of the same order of magnitude. Furthermore, when the less elastic fluid occupied more than half of the channel, the difference in elasticity destabilized the interface at all disturbance wavelengths.
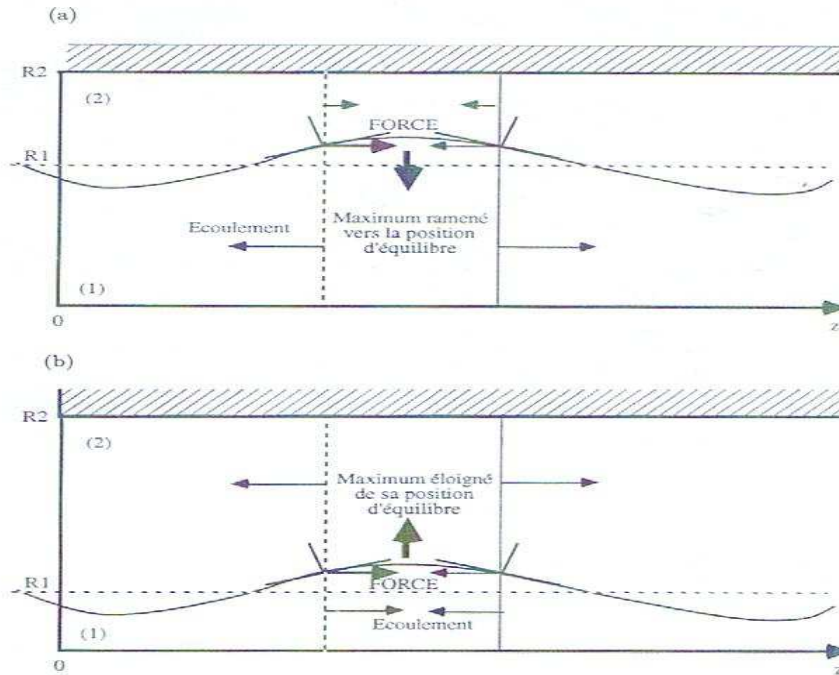
Figure A-I- 4 Illustration of the mechanism proposed by Hinch et al.(1992): the most elastic fluid lies at the heart of the flow, the central layer is the (a) thickest (b) thinest.

4) Other causes of instability

Besides the causes discussed above, it has also been shown that instability can occur in flows when there is a difference in density across the interface, with other parameters remaining unchanged. However, it was argued that coextrusion flows of molten polymers are not affected by this factor of density difference, at least not significant if it cannot be neglected as viscous or elastic forces are involved(Lamnawar, et al. 2013).

In short summary, a flow is preferentially stable when the less viscous fluid is the minor component in the flow; a very strong stabilization occurs when the less viscous fluid is a skin layer (skin layer effect); For shear thinning fluids, the zero-shear-rate viscosity ratio, the shear-thinning behavior, the elasticity difference as well the first normal stress difference, etc. can have either a stabilizing or destabilizing influence on the flow stability, depending on the flow configuration (layer depth ratio) and wavelength.

A-I.2 Experimental studies

1) Industrial studies on coextrusion

On the one hand, these results do not need any extrapolation to industrial conditions but on the other hand, only few parameters have been measured as the machines are equipped with very few sensors. Schrenk et al.(1978) studied the symmetrical flow of three fluids in a plane die based on an acrylonitrile butadiene styrene copolymer and polystyrene by examining several variables: temperature, layer thickness ratio, total extrusion rate and die gap. They noted that the wave grows along the die and the passage from a stable regime to an unstable one may be caused by changing any of the examined variables. They formulated a hypothesis that instabilities appear if a critical interfacial shear stress is exceeded.

Han and Shetty (1976) carried out their experiments with polystyrene(PS) and low-density polyethylene (LDPE) with configurations of three and five layers. In a configuration of LDPE/PS/LDPE, they observed no evidence of interfacial instabilities even at total flow rates greater than that at which the PS/LDPE/PS configuration gave rise to the instability. This indicated the importance of the skin layer. They argued that the critical wall shear stress is an important parameter for the onset of interfacial instability, which separates the stable region from the unstable region, and the value varies with the ratio of layer thickness (Figure A-I-5a). They agreed with Schrenk et al. (1978) when it came to the concept of the interfacial shear stress (Figure A-I-5b), i.e., that there exists a critical value of interfacial shear stress for a given polymer system at which interfacial instability sets in, which may appear to be independent of the layer thickness ratio.
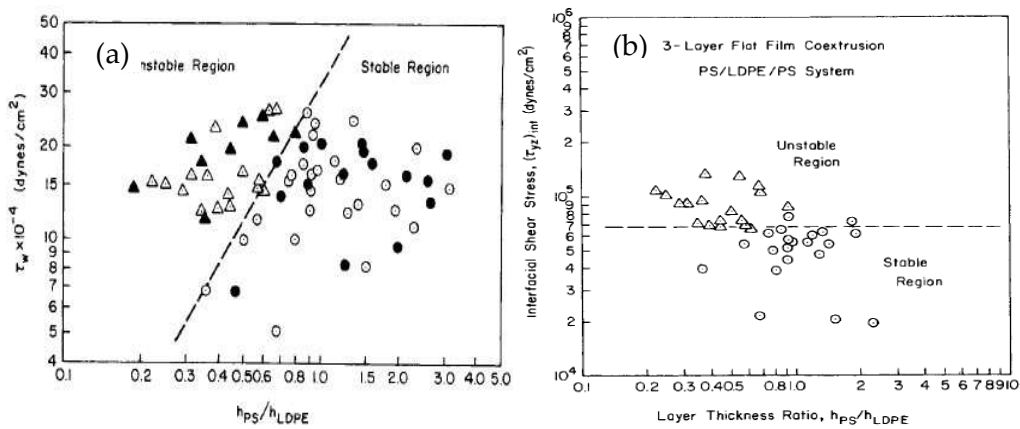
Figure A-I-5 (a)Wall shear stress vs layer thickness ratio, open and closed symbols for the PS/LDPE/PS 3-layer system and the PS/LDPE/PS/LDPE/PS 5-layer system, respectively; circles and triangles for a stable interface and unstable interface, respectively. (b) Interfacial shear stress vs layer thickness ratio for the PS/LDPE/PS 3-layer system (from Han and Shetty 1978)

After having gained an understanding of the conditions for the onset of the interfacial instability, they constructed stability maps using the viscosity ratio and elasticity ratio versus the layer thickness ratio (Figure A-I-6). Figure A-I-6a indicates that under certain conditions (e.g., for a viscosity ratio of less than 4), the flow stability can be independent of the thickness ratio. Likewise, Figure A-I-6b says that if the ratio of the first normal stress difference of PS to LDPE is less than 0.5 or more than 1, the interface remains stable regardless of the layer thickness ratio.
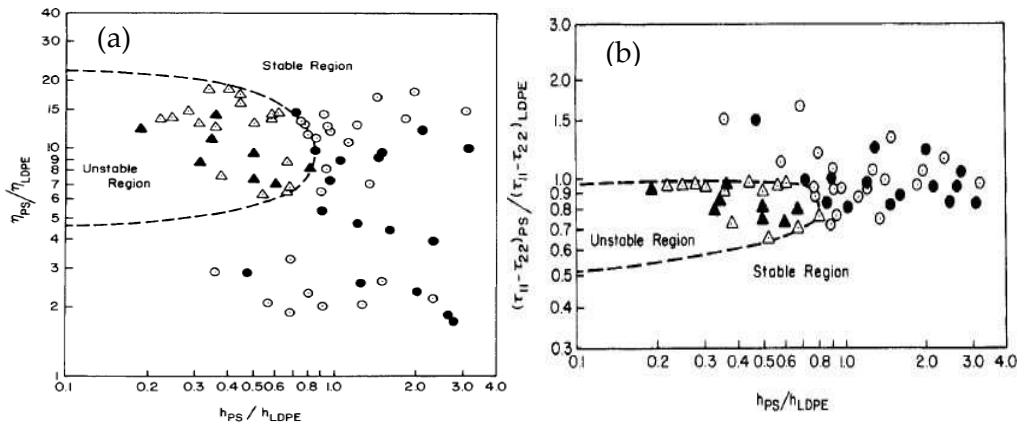
Figure A-I-6 (a) Stability map plotted as the viscosity ratio of PS to LDPE vs the layer thickness ratio; (b) Stability map plotted as the normal stress difference ratio of PS to LDPE vs the layer thickness ratio (from Han and Shetty 1978)

2) Studies with imposing controlled perturbations (linear stability theory)

In these types of studies concerning the observations of the development of interfacial instabilities, one usually introduces a periodic oscillation with a controllable amplitude and frequency to the flow in order to produce temporally regular disturbances. The only comprehensive work using controlled perturbations includes the studies of Wilson and Khomami(1992; 1993a;1993b). The authors worked on a plane geometry using either two incompatible (i.e., PP/HDPE) or two compatible (i.e., HDPE/LDPE) fluids. They modified their extruders to generate a regular disturbance by forcing the extruder screw forward a predetermined amount and installed a bleed valve which allows the extruder's die inlet pressure to be maintained at its original value while the rate of screw rotation is increased. This results in a temporally regular pressure pulse of the form *P=Asin(wt)* where the amplitude A is determined by the amount of screw displacement and the frequency w is identical to the screw rotation frequency. To follow the evolution of the pressure disturbances, four optical viewing windows were installed at fixed positions along the flow channel in the section of the coextrusion die. This optical method was used to analyze the taken images, rendering it possible to restore the evolution of the moving interfacial wave including the amplitude and the frequency.

Based on this experimental approach, the authors carried out stability experiments regarding materials and geometrical parameters (e.g., layer thickness ratio, wavenumber, etc.) by examining the growth rate or decay rate of the disturbance and compared the experimental results to those predicted by the linear stability theory. This allowed the authors to determine the conditions of stabilities by creating stability contours of the dimensionless wavenumber α vs the layer-depth ratio (Figure A-I-7a) as well as curves of the growth rate of disturbance vs the dimensionless wavenumber (Figure A-I-7b). For the incompatible polymer systems of PP/HDPE, they observed that the interface could become unstable when the layer-depth ratio and disturbance wavenumber were in a certain region and the maximum growth rate of the disturbances was in the vicinity of a dimensionless wavenumber of one. Their observations agreed qualitatively with results from the literature and supported the theoretical predictions.
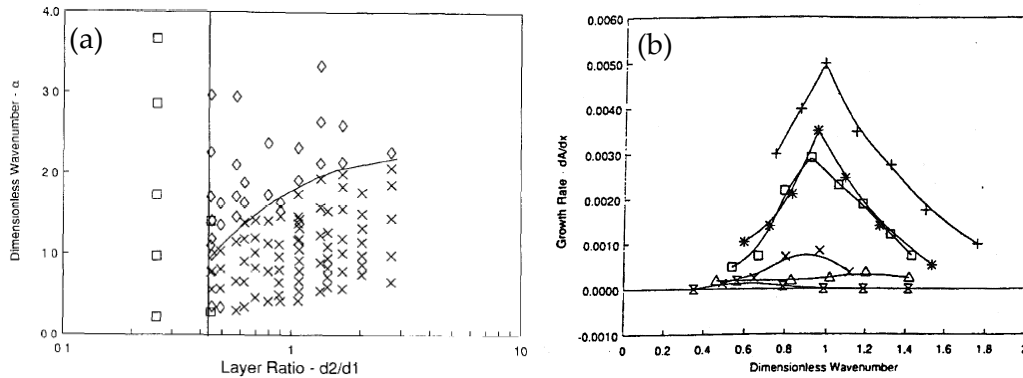
Figure A-I- 7 (a) Experimental stability contour for a PP/HDPE system, (□), stable; (Δ), unstable; (×), indeterminate; (b) Experimental disturbance growth rate plotted versus the dimensionless wavenumber for different values of the layer thickness ratio dHDPE/dPP :(+) 2.04, (*) 1.45, (□) 1.09, (×) 0.88, (Δ) 0.69, (✖) 0.45. (from Wilson and Khomami 1992)

In their second experimental study(Wilson and Khomami 1993a) regarding the effect of elastic difference, the authors attempted to vary the layer-depth ratio and the first normal stress difference ratio with the viscosity ratio held constant and compared their results to the theoretical predictions of linear stability analysis. Using the same experimental approach, they observed that the jump in the first normal stress difference (elasticity effect) at the interface was directly related to the growth or decay rate of the interfacial wave and hence the overall stability of the interface, which is in agreement with theoretical predictions(Karagiannis, et al. 1990).

Valette et al.(2004) carried out theoretical and experimental investigations on the convective linear instability of the coextrusion flow of a polyethylene and polystyrene bilayer in a slit geometry. Under prototype industrial conditions (coextrusion machine shown in Figure A-I-8) comprising a Kaufmann extruder (PE) and a Haake-Rheocord extruder (PS)), the authors found a stable/unstable transition which led to the occurrence of stable/unstable sheets at the die exit. The motor of the Kaufmann extruder was piloted by a tension generator rendering it possible to introduce a controlled perturbation in the flow when the tension varied with time. The die was equipped with a lateral wall made of glass, through which the flow could be observed. Due to the small size of the gap, the authors used a CCD camera with a macroscopic object.

Experimentally, two methodologies were utilized: i) The extrudates were examined at the exit of the die and the instabilities were analyzed; ii) with the transparent die, the development of instabilities inside the die was observed. Upon analysis of the obtained results after varying many key parameters of the process, it was pointed out that the transition was controlled by the temperature and the flow rate ratio. The agreement observed between experimental results and theory was found to be imperfect. The authors pointed out that the instabilities were of convective nature, i.e., they developed progressively from the point of convergence of the polymers. For the transition, a transparent die was used to measure the amplification of different controlled perturbations at the entry of the die and to evidence the convective nature

of this instability since it presented a dominant mode (in fact, at the converging point of the flow, the perturbation developed along the length of the flow with a variable ratio of amplification. This implies that the visualization of the defects in the samples obtained at the exit of the die was not necessarily indicative of the stability or instability of the flow).
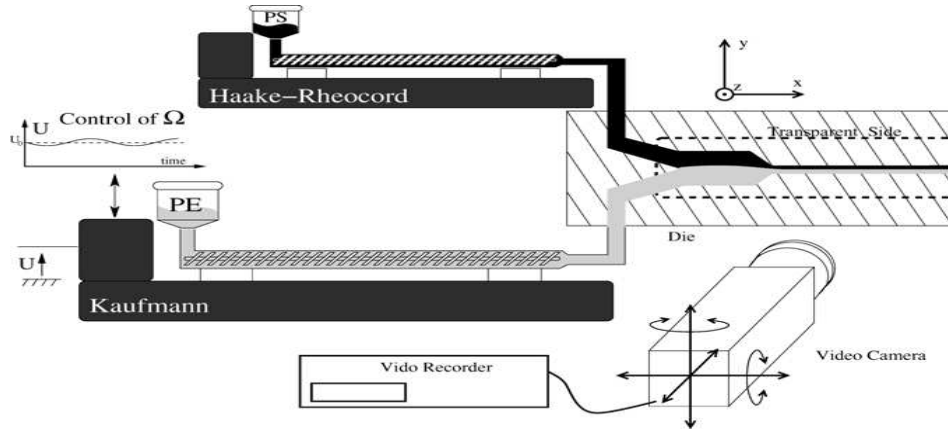
Figure A-I- 8 A schematic of the experimental apparatus utilized (Valette, et al. 2004)

Subsequently, the authors developed two numerical tools to predict the instabilities. The first used a direct modeling based on a law of Maxwell behavior to evidence the convective nature of the instabilities. Particular attention should be paid to the case where the perturbation has a large period ($\alpha \rightarrow 0$), a case commonly called "asymptotic stability". The authors demonstrated that the calculation of the asymptotic stabilities could explain certain observations. However, other observations were not in accordance with the numerical results since some stable flows were observed in the zones that were numerically predicted to be unstable. Indeed, a stable asymptotic flow should correspond to a product without defects, at least in the large wavelength domain, whereas an unstable asymptotic flow can correspond to a correct sample if the amplification ratio of the defect is sufficiently weak or/and if the length of the die is small. This motivated the development of a method enabling to quantify the deterioration of the interface in the case of an unstable flow. The authors (Valette, et al. 2004) then proposed a study of the spatial linear stability for the law of White-Metzner. Meanwhile, they improved the analysis of stability in order to predict the spatial growth of the defects by calculating the spatial amplification rate for a perturbation.

In sum, fruitful literatures on experiments include investigations using a processing approach and/or pure mechanics in the framework of linear stability. Some studies aim to manifest the industrial situation, and some others dedicate to investigations with introduction of controlled perturbations and examination of their propagations via transparent die or equipped with observation windows. The objectives are to isolate physical criteria for the interfacial instabilities and enable comparisons between experiments and theory predictions.

References

1. Aho, J.; Rolon-Garrido, V. H.; Syrjala, S.; Wagner, M. H. *Rheologica Acta* **2010,** 49, (4), 359-370.

2. Ajji, A.; Utracki, L. A. *Polymer Engineering and Science* **1996,** 36, (12), 1574-1585.

3. Andrade, R. J.; Maia, J. M. *Journal of Rheology* **2011,** 55, (5), 925-937.

4. Ansari, M.; Hatzikiriakos, S. G.; Sukhadia, A. M.; Rohlfing, D. C. *Rheologica Acta* **2011,** 50, (1), 17-27.

5. Appel, M.; Fleischer, G.; Karger, J.; Fujara, F.; Chang, I. *Macromolecules* **1994,** 27, (15), 4274-4277.

6. Arendt, B. H.; Krishnamoorti, R.; Kornfield, J. A.; Smith, S. D. *Macromolecules* **1997,** 30, (4), 1127-1137.

7. Ares, A.; Silva, J.; Maia, J. M.; Barral, L.; Abad, M. J. *Rheologica Acta* **2009,** 48, (9), 993-1004.

8. Barroso, V. C.; Covas, J. A.; Maia, J. M. *Rheologica Acta* **2002,** 41, (1-2), 154-161.

9. Bella, R.; Cassagnau, P.; Fenouillot, F.; Falk, L.; Lacoste, C. *Polymer* **2006,** 47, (14), 5080-5089.

10. Berezkin, A. V.; Kudryavtsev, Y. V. *Macromolecules* **2011,** 44, (1), 112-121.

11. Berezkin, A. V.; Kudryavtsev, Y. V. *Macromolecules* **2013,** 46, (12), 5080-5089.

12. Bernstein, R. E.; Cruz, C. A.; Paul, D. R.; Barlow, J. W. *Macromolecules* **1977,** 10, (3), 681-686.

13. Berret, J. F. *Langmuir* **1997,** 13, (8), 2227-2234.

14. Bousmina, M.; Palierne, J. F.; Utracki, L. A. *Polymer Engineering and Science* **1999,** 39, (6), 1049-1059.

15. Bousmina, M.; Qiu, H.; Grmela, M.; Klemberg-Sapieha, J. E. *Macromolecules* **1998,** 31, (23), 8273-8280.

16. Brochard-Wyart, F.; de Gennes, P.-G. *C.R.Acad.Sci.,Ser.II:Mech.,Phys.,Chim.,Sci.Terre U.* **1993,** 317, 13-17.

17. Brochard, F.; Jouffroy, J.; Levinson, P. *Macromolecules* **1983,** 16, (10), 1638-1641.

18. Canalda, J. C.; Hoffmann, T.; Martinezsalazar, J. *Polymer* **1995,** 36, (5), 981-985.

19. Carini, G.; D'Angelo, G.; Tripodo, G.; Bartolotta, A.; Di Marco, G.; Lanza, M.; Privalko, V. P.; Gorodilov, B. Y.; Rekhteta, N. A.; Privalko, E. G. *Journal of Chemical Physics* **2002,** 116, (16), 7316-7322.

20. Carr, J. M.; Mackey, M.; Flandin, L.; Hiltner, A.; Baer, E. *Polymer* **2013,** 54, (6), 1679-1690.

21. Chen, K. P.; Zhang, Y. *Journal of Fluid Mechanics* **1993,** 247, 489-502.

22. Chen, Q.; Matsumiya, Y.; Masubuchi, Y.; Watanabe, H.; Inoue, T. *Macromolecules* **2008,** 41, (22), 8694-8711.

23. Chopra, D.; Vlassopoulos, D.; Hatzikiriakos, S. G. *Journal of Rheology* **2000,** 44, (1), 27-45.

24. Chung, G. C.; Kornfield, J. A.; Smith, S. D. *Macromolecules* **1994,** 27, (4), 964-973.

25. Colby, R. H. *Polymer* **1989,** 30, (7), 1275-1278.

26. Composto, R. J.; Kramer, E. J.; White, D. M. *Macromolecules* **1988,** 21, (8), 2580-2588.

27. Composto, R. J.; Kramer, E. J.; White, D. M. *Polymer* **1990,** 31, (12), 2320-2328.

28. Crank, J., *The mathematics of diffusion*. Clarendon: Oxford, 1975.

29. Crist, B.; Green, P. F.; Jones, R. A. L.; Kramer, E. J. *Macromolecules* **1989,** 22, (6), 2857-2858.

30. de Gennes, P. G. *J. Chem. Phys.* **1971,** 55, (2), 572.

31. Dealy, J. M.; Larson, R. G., *Structure and rheology of molten polymers: from structure to flow behavior and back again.* Hanser: Munich, 2006.

32. Dipaolabaranyi, G.; Fletcher, S. J.; Degre, P. *Macromolecules* **1982,** 15, (3), 885-889.

33. Doi, M.; Edwards, S. F., *The Theory of Polymer Dynamics*. Clarendon Press: Oxford, UK, 1986.

34. Doi, M.; Ohta, T. *Journal of Chemical Physics* **1991,** 95, (2), 1242-1248.

35. Dooley, J. Technische Universiteit Eindhoven, Eindhoven, the Netherlands, 2002a.

36. Dooley, J. *coextrusion.* Encyclopedia of Polymer Science and Technology ed.; John Wiley & Sons, Inc.: New York, 2002b.

37. Es-Haghi, S. S.; Yousefi, A. A.; Oromiehie, A. *Journal of Polymer Science Part B-Polymer Physics* **2007,** 45,

(20), 2860-2870.

38. Feng, J. Y.; Li, L.; Chan, C. M.; Weng, L. T. *Surface and Interface Analysis* **2002,** 33, (5), 455-458.

39. Ferri, D.; Greco, F. *Macromolecules* **2006,** 39, (17), 5931-5938.

40. Ferry, J., *Viscoelastic properties of polymers.* Wiley: New York, 1980.

41. Fetters, L. J.; Lohse, D. J.; Richter, D.; Witten, T. A.; Zirkel, A. *Macromolecules* **1994,** 27, (17), 4639-4647.

42. Fox, T. *Bulletin of the American Physical Society* **1956,** 1, 123.

43. Fredrickson, G. H. *Physical Review Letters* **1996,** 76, (18), 3440-3443.

44. Fredrickson, G. H.; Leibler, L. *Macromolecules* **1996,** 29, (7), 2674-2685.

45. Fredrickson, G. H.; Milner, S. T. *Macromolecules* **1996,** 29, (23), 7386-7390.

46. Fuchs, K.; Friedrich, C.; Weese, J. *Macromolecules* **1996,** 29, (18), 5893-5901.

47. Furuichi, K.; Nonomura, C.; Masubuchi, Y.; Watanabe, H. *Journal of Chemical Physics* **2010,** 133, (17).

48. Furukawa, H. *Physical Review A* **1989,** 40, (11), 6403-6406.

49. Gaikwad, A. N.; Choperena, A.; Painter, P. C.; Lodge, T. P. *Macromolecules* **2010,** 43, (10), 4814-4821.

50. Gaikwad, A. N.; Wood, E. R.; Ngai, T.; Lodge, T. P. *Macromolecules* **2008,** 41, (7), 2502-2508.

51. Garbella, R. W.; Wendorff, J. H. *Makromolekulare Chemie-Macromolecular Chemistry and Physics* **1988,** 189, (10), 2459-2473.

52. Gevgilili, H.; Kalyon, D. M. *Journal of Rheology* **2001,** 45, (2), 467-475.

53. Gilmore, P. T.; Falabella, R.; Laurence, R. L. *Macromolecules* **1980,** 13, (4), 880-883.

54. Graessley, W. W. *Journal of Polymer Science Part B-Polymer Physics* **1980,** 18, (1), 27-34.

55. Graessley, W. W.; Edwards, S. F. *Polymer* **1981,** 22, (10), 1329-1334.

56. Green, P. F.; Doyle, B. L. *Macromolecules* **1987,** 20, (10), 2471-2474.

57. Green, P. F.; Russell, T. P.; Jerome, R.; Granville, M. *Macromolecules* **1988,** 21, (11), 3266-3273.

58. Guegan, P.; Macosko, C. W.; Ishizone, T.; Hirao, A.; Nakahama, S. *Macromolecules* **1994,** 27, (18), 4993-4997.

59. Gupta, M.; Lin, Y. J.; Deans, T.; Baer, E.; Hiltner, A.; Schiraldi, D. A. *Macromolecules* **2010,** 43, (9), 4230-4239.

60. Hahn, B.; Wendorff, J.; Yoon, D. Y. *Macromolecules* **1985,** 18, (4), 718-721.

61. Haley, J. C.; Lodge, T. P.; He, Y. Y.; Ediger, M. D.; von Meerwall, E. D.; Mijovic, J. *Macromolecules* **2003,** 36, (16), 6142-6151.

62. Haley, J. C.; Lodge, T. R. *Journal of Rheology* **2005,** 49, (6), 1277-1302.

63. Han, C. D., *Multiphase Flow in Polymer Processing.* Academic Press: New York, 1981.

64. Han, C. D.; Kim, J. K. *Macromolecules* **1989a,** 22, (4), 1914-1921.

65. Han, C. D.; Kim, J. K. *Macromolecules* **1989b,** 22, (11), 4292-4302.

66. Han, C. D.; Shetty, R. *Polymer Engineering and Science* **1976,** 16, (10), 697-705.

67. Han, C. D.; Shetty, R. *Polymer Engineering and Science* **1978,** 18, (3), 180-186.

68. Hannachi, A.; Mitsoulis, E. *Advances in Polymer Technology* **1993,** 12, (3), 217-231.

69. Harton, S. E.; Stevie, F. A.; Ade, H. *Macromolecules* **2005,** 38, (9), 3543-3546.

70. Hassanabadi, H. M.; Rodrigue, D. *Rheologica Acta* **2012,** 51, (11-12), 991-1005.

71. Hatzikiriakos, S. G. *Progress in Polymer Science* **2012,** 37, (4), 624-643.

72. He, Y. Y.; Lutz, T. R.; Ediger, M. D. *Journal of Chemical Physics* **2003,** 119, (18), 9956-9965.

73. Hellmann, E. H.; Hellmann, G. P.; Rennie, A. R. *Macromolecules* **1991,** 24, (13), 3821-3827.

74. High, M. S.; Painter, P. C.; Coleman, M. M. *Macromolecules* **1992,** 25, (2), 797-801.

75. Hinch, E. J.; Harris, O. J.; Rallison, J. M. *Journal of Non-Newtonian Fluid Mechanics* **1992,** 43, (2-3), 311-324.

76. Honerkamp, J.; Weese, J. *Rheologica Acta* **1993,** 32, (1), 65-73.

77. Hong, J. S.; Kim, Y. K.; Ahn, K. H.; Lee, S. J.; Kim, C. *Rheologica Acta* **2007,** 46, (4), 469-478.

78. Hooper, A. P.; Boyd, W. G. C. *Journal of Fluid Mechanics* **1983,** 128, (Mar), 507-528.

79. Hu, G. H.; Lamba, M.; Laurienzo, P.; Malinconico, M.; Pota, F. *Journal of Polymer Materials* **1998,** 15, (1), 81-89.

80. Hua, C. C.; Schieber, J. D.; Venerus, D. C. *Journal of Rheology* **1999,** 43, (3), 701-717.

81. Iza, M.; Bousmina, M. *Journal of Rheology* **2000,** 44, (6), 1363-1384.

82. Jabbari, E.; Peppas, N. A. *Polymer* **1995,** 36, (3), 575-586.

83. Jeon, H. K.; Kim, J. K. *Macromolecules* **2000,** 33, (22), 8200-8210.

84. Jiang, G. J.; Wu, H.; Yan, B. W.; Guo, S. Y.; Huang, J. *Journal of Polymer Science Part B-Polymer Physics* **2009,** 47, (11), 1112-1124.

85. Jiao, J. B.; Kramer, E. J.; de Vos, S.; Moller, M.; Koning, C. *Macromolecules* **1999,** 32, (19), 6261-6269.

86. Jonas, A.; De Luca, A. C.; Pesce, G.; Rusciano, G.; Sasso, A.; Caserta, S.; Guido, S.; Marrucci, G. *Langmuir* **2010,** 26, (17), 14223-14230.

87. Jones, R. A. L.; Klein, J.; Donald, A. M. *Nature* **1986,** 321, (6066), 161-162.

88. Joseph, D. D., Renardy, Y.Y., *Fundamental of Two-Fluid Dynamics. I. Mathematical Theory and Applications*. Springer-Verlag: New York, 1992.

89. Joubert, C.; Cassagnau, P.; Choplin, L.; Michel, A. *Journal of Rheology* **2002,** 46, (3), 629-650.

90. Jud, K.; Kausch, H. H.; Williams, J. G. *Journal of Materials Science* **1981,** 16, (1), 204-210.

91. Juliani ; Archer L.A. *Journal of Rheology* **2001,** 45, (3), 691-708.

92. Kanetakis, J.; Fytas, G. *Macromolecules* **1989,** 22, (8), 3452-3458.

93. Karagiannis, A.; Hrymak, A. N.; Vlachopoulos, J. *Rheologica Acta* **1990,** 29, (1), 71-87.

94. Karim, A.; Mansour, A.; Felcher, G. P.; Russell, T. P. *Physical Review B* **1990,** 42, (10), 6846-6849.

95. Kawaguchi, D.; Masuoka, K.; Takano, A.; Tanaka, K.; Nagamura, T.; Torikai, N.; Dalgliesh, R. M.; Langridge, S.; Matsushita, Y. *Macromolecules* **2006,** 39, (16), 5180-5182.

96. Kawaguchi, D.; Nelson, A.; Masubuchi, Y.; Majewski, J. P.; Torikai, N.; Yamada, N. L.; Sarah, A. R. S.; Takano, A.; Matsushita, Y. *Macromolecules* **2011,** 44, (23), 9424-9433.

97. Kazatchkov, I. B.; Hatzikiriakos, S. G. *Rheologica Acta* **2010,** 49, (3), 267-274.

98. Khomami, B. *Journal of Non-Newtonian Fluid Mechanics* **1990,** 37, (1), 19-36.

99. Kim, B. J.; Kang, H. M.; Char, K.; Katsov, K.; Fredrickson, G. H.; Kramer, E. J. *Macromolecules* **2005a,** 38, (14), 6106-6114.

100. Kim, E.; Kramer, E. J.; Osby, J. O. *Macromolecules* **1995a,** 28, (6), 1979-1989.

101. Kim, H. Y.; Jeong, U.; Kim, J. K. *Macromolecules* **2003,** 36, (5), 1594-1602.

102. Kim, H. Y.; Ryu, D. Y.; Jeong, U.; Kho, D. H.; Kim, J. K. *Macromolecular Rapid Communications* **2005b,** 26, (17), 1428-1433.

103. Kim, J. K.; Han, C. D. *Polymer Engineering and Science* **1991,** 31, (4), 258-269.

104. Kim, K. J.; Cho, Y. J.; Kim, Y. H. *Vibrational Spectroscopy* **1995b,** 9, (2), 147-159.

105. Klein, J. *Nature* **1978,** 271, (5641), 143-145.

106. Klein, J. *Science* **1990,** 250, (4981), 640-646.

107. Klein, J.; Briscoe, B. J. *Proceedings of the Royal Society of London Series a-Mathematical Physical and Engineering Sciences* **1979,** 365, (1720), 53-73.

108. Kramer, E. J.; Green, P.; Palmstrom, C. J. *Polymer* **1984,** 25, (4), 473-480.

109. Kumagai, Y.; Watanabe, H.; Miyasaka, K.; Hata, T. *Journal of Chemical Engineering of Japan* **1979,** 12, (1), 1-4.

110. Kumar, S. K.; Colby, R. H.; Anastasiadis, S. H.; Fytas, G. *Journal of Chemical Physics* **1996,** 105, (9), 3777-3788.

111. Kunz, K.; Stamm, M. *Macromolecules* **1996,** 29, (7), 2548-2554.

112. Kwei, T. K. W., T.T., *In Polymer Blends*. Academic Press: New York, 1978; Vol. 1, p 141-185.

113. Lai, C. Y.; Ponting, M. T.; Baer, E. *Polymer* **2012,** 53, (6), 1393-1403.

114. Lam, Y. C.; Jang, L.; Li, L.; Yue, C. Y.; Tam, K. C.; Hu, X. *Journal of Polymer Science Part B-Polymer Physics* **2004,** 42, (2), 302-315.

115. Lam, Y. C.; Jiang, L.; Yue, C. Y.; Tam, K. C.; Li, L. *Journal of Rheology* **2003,** 47, (3), 795-807.

116. Lamnawar, K.; Baudouin, A.; Maazouz, A. *European Polymer Journal* **2010a,** 46, (7), 1604-1622.

117. Lamnawar, K.; Bousmina, M.; Maazouz, A. *Macromolecules* **2012,** 45, (1), 441-454.

118. Lamnawar, K.; Maazouz, A. *Rheologica Acta* **2006,** 45, (4), 411-424.

119. Lamnawar, K.; Maazouz, A. *Rheologica Acta* **2008,** 47, (4), 383-397.

120. Lamnawar, K.; Maazouz, A. *Polymer Engineering and Science* **2009,** 49, (4), 727-739.

121. Lamnawar, K.; Vion-Loisel, F.; Maazouz, A. *Journal of Applied Polymer Science* **2010b,** 116, (4), 2015-2022.

122. Lamnawar, K.; Zhang, H.; Maazouz, A., *Coextrusion of multilayer structures, interfacial phenomena.* Encyclopedia of Polymer Science and Technology ed.; John Wiley & Sons, Inc.: New York, 2013; DOI: 10.1002/0471440264.pst584.

123. Larson, R. G. *Journal of Polymer Science Part B-Polymer Physics* **2007,** 45, (24), 3240-3248.

124. Laun, H. M. *Rheologica Acta* **1978,** 17, (1), 1-15.

125. Laure, P.; LeMeur, H.; Demay, Y.; Saut, J. C.; Scotto, S. *Journal of Non-Newtonian Fluid Mechanics* **1997,** 71, (1-2), 1-23.

126. Lee, B. L., White, J. L. *Trans. Soc. Rheol.* **1974,** 18, (3), 467.

127. Lee, H. M.; Park, O. O. *Journal of Rheology* **1994,** 38, (5), 1405-1425.

128. Lee, P. C.; Park, H. E.; Morse, D. C.; Macosko, C. W. *Journal of Rheology* **2009,** 53, (4), 893-915.

129. Leonard, C.; Halary, J. L.; Monnerie, L. *Polymer* **1985,** 26, (10), 1507-1513.

130. Levitt, L.; Macosko, C. W.; Schweizer, T.; Meissner, J. *Journal of Rheology* **1997,** 41, (3), 671-685.

131. Li, C. H. *Physics of Fluids* **1969,** 12, (3), 531-538.

132. Li, J. Q.; Ma, G. Q.; Sheng, J. *Journal of Macromolecular Science Part B-Physics* **2011,** 50, (4), 741-761.

133. Liao, Y.; Nakagawa, A.; Horiuchi, S.; Ougizawa, T. *Macromolecules* **2007,** 40, (22), 7966-7972.

134. Likhtman, A. E. *Journal of Non-Newtonian Fluid Mechanics* **2009,** 157, (3), 158-161.

135. Lin, C. C. *Polymer Journal (Tokyo)* **1979,** 11, 185.

136. Liu, G. X.; Sun, H.; Rangou, S.; Ntetsikas, K.; Avgeropoulos, A.; Wang, S. Q. *Journal of Rheology* **2013,** 57, (1), 89-104.

137. Liu, R. Y. F.; Bernal-Lara, T. E.; Hiltner, A.; Baer, E. *Macromolecules* **2004,** 37, (18), 6972-6979.

138. Liu, R. Y. F.; Bernal-Lara, T. E.; Hiltner, A.; Baer, E. *Macromolecules* **2005,** 38, (11), 4819-4827.

139. Liu, R. Y. F.; Jin, Y.; Hiltner, A.; Baer, E. *Macromolecular Rapid Communications* **2003,** 24, (16), 943-948.

140. Liu, Y.; Reiter, G.; Kunz, K.; Stamm, M. *Macromolecules* **1993,** 26, (8), 2134-2136.

141. Lodge, A. S., *Elastic Liquids*. Academic Press: London, 1964.

142. Lodge, A. S. *Industrial & Engineering Chemistry Research* **1995,** 34, (10), 3355-3358.

143. Lodge, T. P.; McLeish, T. C. B. *Macromolecules* **2000,** 33, (14), 5278-5284.

144. Lodge, T. P.; Wood, E. R.; Haley, J. C. *Journal of Polymer Science Part B-Polymer Physics* **2006,** 44, (4), 756-763.

145. Lv, Y. D.; Huang, Y. J.; Kong, M. Q.; Zhu, H.; Yang, Q.; Li, G. X. *Rheologica Acta* **2013,** 52, (4), 355-367.

146. Lyu, S. P.; Cernohous, J. J.; Bates, F. S.; Macosko, C. W. *Macromolecules* **1999,** 32, (1), 106-110.

147. Macosko, C. W.; Jeon, H. K.; Hoye, T. R. *Progress in Polymer Science* **2005,** 30, (8-9), 939-947.

148. Maia, J. M.; Andrade, R. J.; Covas, J. A.; Laeuger, J. *Xvth International Congress on Rheology - the Society of Rheology 80Th Annual Meeting, Pts 1 and 2* **2008,** 1027, 1111-1113.

149. Maia, J. M.; Binding, D. *Rheologica Acta* **1999,** 38, (2), 160-171.

150. Maia, J. S., Jorge; Patrick, Harris. Layer multiplying die for generating interfacial surfaces. 2012,US Patent 0235319 A1.

151. Marrucci, G. *Journal of Non-Newtonian Fluid Mechanics* **1996,** 62, (2-3), 279-289.

152. McLeish, T. C. B. *Advances in Physics* **2002,** 51, (6), 1379-1527.

153. Mead, D. W. *Journal of Rheology* **1994,** 38, (6), 1769-1795.

154. Mechbal, N.; Bousmina, M. *Macromolecules* **2007,** 40, (4), 967-975.

155. Meissner, J. *Chemical Engineering Communications* **1985,** 33, (1-4), 159-180.

156. Mhetar, V.; Archer, L. A. *Macromolecules* **1998,** 31, (24), 8607-8616.

157. Mhetar, V.; Archer, L. A. *Journal of Non-Newtonian Fluid Mechanics* **1999,** 81, (1-2), 71-81.

158. Mijovic, J.; Sy, J. W.; Kwei, T. K. *Macromolecules* **1997,** 30, (10), 3042-3050.

159. Mitsoulis, E. *Journal of Polymer Engineering* **2005,** 25, (5), 393-410.

160. Mitsoulis, E.; Wagner, R.; Heng, F. L. *Polymer Engineering and Science* **1988,** 28, (5), 291-310.

161. Mooney, M. *Journal of Rheology* **1931,** 2, 210-222.

162. Morrison, F. A.; Larson, R. G. *Journal of Polymer Science Part B-Polymer Physics* **1992,** 30, (9), 943-950.

163. Msakni, A.; Chaumont, P.; Cassagnau, P. *Rheologica Acta* **2007,** 46, (7), 933-943.

164. Mueller, C. D.; Nazarenko, S.; Ebeling, T.; Schuman, T. L.; Hiltner, A.; Baer, E. *Polymer Engineering and Science* **1997,** 37, (2), 355-362.

165. Muller, M. *Macromolecules* **1997,** 30, (20), 6353-6357.

166. Nielsen, J. K.; Hassager, O. R., H.K.; McKinley, G.H. *Journal of Rheology* **2009,** 53, 1327.

167. Nishi, T.; Wang, T. T. *Macromolecules* **1975,** 8, (6), 909-915.

168. O'Shaughnessy, B.; Vavylonis, D. *Macromolecules* **1999,** 32, (6), 1785-1796.

169. Orr, C. A.; Cernohous, J. J.; Guegan, P.; Hirao, A.; Jeon, H. K.; Macosko, C. W. *Polymer* **2001,** 42, (19), 8171-8178.

170. Osaki, K. *Rheologica Acta* **1993,** 32, (5), 429-437.

171. OShaughnessy, B.; Sawhney, U. *Physical Review Letters* **1996,** 76, (18), 3444-3447.

172. Oyama, H. T.; Inoue, T. *Macromolecules* **2001,** 34, (10), 3331-3338.

173. Padmanabhan, M.; Macosko, C. W. *Rheologica Acta* **1997,** 36, (2), 144-151.

174. Pahl, S.; Fleischer, G.; Fujara, F.; Geil, B. *Macromolecules* **1997,** 30, (5), 1414-1418.

175. Palierne, J. F. *Rheologica Acta* **1990,** 29, (3), 204-214.

176. Papanastasiou, A. C.; Scriven, L. E.; Macosko, C. W. *Journal of Rheology* **1983,** 27, (4), 387-410.

177. Park, H. E.; Lee, P. C.; Macosko, C. W. *Journal of Rheology* **2010,** 54, (6), 1207-1218.

178. Patashinski, A. Z.; Orlik, R.; Paclawski, K.; Ratner, M. A.; Grzybowski, B. A. *Soft Matter* **2012,** 8, (5), 1601-1608.

179. Pathak, J. A.; Colby, R. H.; Kamath, S. Y.; Kumar, S. K.; Stadler, R. *Macromolecules* **1998,** 31, (25), 8988-8997.

180. Pathak, J. A.; Kumar, S. K.; Colby, R. H. *Macromolecules* **2004,** 37, (18), 6994-7000.

181. Patlazhan, S.; Schlatter, G.; Serra, C.; Bouquey, M.; Muller, R. *Polymer* **2006,** 47, (17), 6099-6106.

182. Patrick J. Harris, J. P., Benjamin A. Huntington, Roger T. Bonnecaze, Donald Meltzer; Maia, J. *Polymer Engineering and Science* **2013**, (in press, DOI: 10.1002/pen.23597).

183. Paul, D. R.; Barlow, J. W. *Journal of Macromolecular Science-Reviews in Macromolecular Chemistry and*

Physics **1980,** C18, (1), 109-168.

184. Pinarbasi, A.; Liakopoulos, A. *Journal of Non-Newtonian Fluid Mechanics* **1995,** 57, (2-3), 227-241.

185. Plazek, D. J. *Journal of Polymer Science Part B-Polymer Physics* **1982,** 20, (4), 729-742.

186. Puissant, S.; Vergnes, B.; Agassant, J. F.; Demay, Y.; Labaig, J. J. *Polymer Engineering and Science* **1996,** 36, (7), 936-942.

187. Qiu, H.; Bousmina, M. *Journal of Rheology* **1999,** 43, (3), 551-568.

188. Qiu, H.; Bousmina, M. *Macromolecules* **2000,** 33, (17), 6588-6594.

189. Qiu, H.; Bousmina, M. *Canadian Journal of Chemical Engineering* **2002,** 80, (6), 1206-1213.

190. Qiu, H.; Bousmina, M.; Dealy, J. M. *Rheologica Acta* **2002,** 41, (1-2), 87-92.

191. Raghava, R. S.; Smith, R. W. *Journal of Polymer Science Part B-Polymer Physics* **1989,** 27, (12), 2525-2551.

192. Rahim, M. A.; Choi, W. S.; Lee, H. J.; Park, J. B.; Jeon, I. C. *Polymer* **2011,** 52, (14), 3112-3117.

193. Ravindranath, S.; Wang, S. Q. *Macromolecules* **2007,** 40, (22), 8031-8039.

194. Reiter, G.; Steiner, U. *Journal De Physique Ii* **1991,** 1, (6), 659-671.

195. Riedl, B.; Prudhomme, R. E. *Polymer Engineering and Science* **1984,** 24, (17), 1291-1299.

196. Roland, C. M.; McGrath, K. J.; Casalini, R. *Macromolecules* **2006,** 39, (10), 3581-3587.

197. Rolon-Garrido, V. H.; Wagner, M. H. *Rheologica Acta* **2009,** 48, (3), 245-284.

198. Saito, T.; Macosko, C. W. *Polymer Engineering and Science* **2002,** 42, (1), 1-9.

199. Sanchez-Reyes, J.; Archer, L. A. *Macromolecules* **2002,** 35, (13), 5194-5202.

200. Sanchez-Reyes, J.; Archer, L. A. *Journal of Rheology* **2003,** 47, (2), 469-482.

201. Sasaki, H.; Bala, P. K.; Yoshida, H.; Ito, E. *Polymer* **1995,** 36, (25), 4805-4810.

202. Schmidt, J. M. US Patent 3459 834. 1969.

203. Schnell, R.; Stamm, M.; Creton, C. *Macromolecules* **1998,** 31, (7), 2284-2292.

204. Schrenk, W. J.; Bradley, N. L.; Alfrey, T.; Maack, H. *Polymer Engineering and Science* **1978,** 18, (8), 620-623.

205. Schulze, J. S.; Cernohous, J. J.; Hirao, A.; Lodge, T. P.; Macosko, C. W. *Macromolecules* **2000,** 33, (4), 1191-1198.

206. Schulze, J. S.; Moon, B.; Lodge, T. P.; Macosko, C. W. *Macromolecules* **2001,** 34, (2), 200-205.

207. Schweizer, T.; van Meerveld, J.; Ottinger, H. C. *Journal of Rheology* **2004,** 48, (6), 1345-1363.

208. Scott, C.; Macosko, C. *Journal of Polymer Science Part B-Polymer Physics* **1994,** 32, (2), 205-213.

209. Scotto, S.; Laure, P. *Journal of Non-Newtonian Fluid Mechanics* **1999,** 83, (1-2), 71-92.

210. Sentmanat, M. L. *Rheologica Acta* **2004,** 43, (6), 657-669.

211. Shearmur, T. E.; Clough, A. S.; Drew, D. W.; van der Grinten, M. G. D.; Jones, R. A. L. *Polymer* **1998,** 39, (11), 2155-2159.

212. Silva, J.; Machado, A. V.; Maia, J. *Rheologica Acta* **2007,** 46, (8), 1091-1097.

213. Silva, J.; Machado, A. V.; Moldenaers, P.; Maia, J. *Journal of Rheology* **2010,** 54, (4), 797-813.

214. Silva, J.; Maia, J. M.; Huang, R. Z.; Meltzer, D.; Cox, M.; Andrade, R. *Rheologica Acta* **2012,** 51, (11-12), 947-957.

215. Snijkers, F.; Ratkanthwar, K.; Vlassopoulos, D.; Hadjichristidis, N. *Macromolecules* **2013,** 46, (14), 5702-5713.

216. Song, J.; Baker, A. M.; Macosko, C. W.; Ewoldt, R. H. *AIChE Journal* **2013,** 59, (9), 3391-3402.

217. Song, J.; Ewoldt, R. H.; Hu, W. L.; Silvis, H. C.; Macosko, C. W. *AIChE Journal* **2011,** 57, (12), 3496-3506.

218. Soskey, P. R.; Winter, H. H. *Journal of Rheology* **1984,** 28, (5), 625-645.

219. Stadler, F.J.; Auhl D.; Munstedt H. Macromolecules 2008, 41,(10), 3720-3726.

220. Stary, Z.; Pemsel, T.; Baldrian, J.; Munstedt, H. *Polymer* **2012,** 53, (9), 1881-1889.

221. Struglinski, M. J.; Graessley, W. W. *Macromolecules* **1985,** 18, (12), 2630-2643.

222. Su, Y. Y.; Khomami, B. *Journal of Rheology* **1992,** 36, (2), 357-387.

223. Sun, Y. J.; Hu, G. H.; Lambla, M.; Kotlar, H. K. *Polymer* **1996,** 37, (18), 4119-4127.

224. Sussman, D. M.; Schweizer, K. S. *Journal of Chemical Physics* **2011a,** 135, (13).

225. Sussman, D. M.; Schweizer, K. S. *Physical Review Letters* **2011b,** 107, (7).

226. Sussman, D. M.; Schweizer, K. S. *Physical Review Letters* **2012a,** 109, (16).

227. Sussman, D. M.; Schweizer, K. S. *Macromolecules* **2012b,** 45, (7), 3270-3284.

228. Sussman, D. M.; Schweizer, K. S. *Macromolecules* **2013,** 46, (14), 5684-5693.

229. Tadmor, Z. G., C.G., *Principles of polymer processing*. A John Wiley&Sons,Inc.,Publication: Hoboken, New Jersey, 2006.

230. Takahashi, M. *Nihon Reoroji Gakkaishi* **2007,** 35, (5), 235-244.

231. Takahashi, M. H., J.;Shimono,S.;Matsuda,H. *Netsu Sokutei* **1995,** 22, 2.

232. Takahashi, T.; Takimoto, J. I.; Koyama, K. *Journal of Applied Polymer Science* **1999,** 72, (7), 961-969.

233. Tapadia, P.; Wang, S. Q. *Physical Review Letters* **2006,** 96, (1).

234. Tsenoglou, C. *Macromolecules* **1991,** 24, (8), 1762-1767.

235. Utracki, L. A. *Polymer Engineering and Science* **1995,** 35, (1), 2-17.

236. Valette, R.; Laure, P.; Demay, Y.; Agassant, J. F. *Journal of Non-Newtonian Fluid Mechanics* **2004,** 121, (1), 41-53.

237. Van Gurp, M.; Palmen, J. *Rheology Bulletin* **1998,** 67, 5-8.

238. Van Puyvelde, P.; Oommen, Z.; Koets, P.; Groeninckx, G.; Moldenaers, P. *Polymer Engineering and Science* **2003,** 43, (1), 71-77.

239. Vanalsten, J. G.; Lustig, S. R. *Macromolecules* **1992,** 25, (19), 5069-5073.

240. Vaudreuil, S.; Qiu, H.; Kaliaguine, S.; Grmela, M.; Bousmina, M. *Macromolecular Symposia* **2000,** 158, 155-168.

241. Venerus, D. C.; Nair, R. *Journal of Rheology* **2006,** 50, (1), 59-75.

242. Vinckier, I.; Mewis, J.; Moldenaers, P. *Rheologica Acta* **1997,** 36, (5), 513-523.

243. Wagner, M. H. *Journal of Rheology* **1994,** 38, (3), 655-679.

244. Wagner, M. H.; Kheirandish, S.; Yamaguchi, M. *Rheologica Acta* **2004,** 44, (2), 198-218.

245. Wagner, M. H.; Meissner, J. *Makromolekulare Chemie-Macromolecular Chemistry and Physics* **1980,** 181, (7), 1533-1550.

246. Wagner, M. H.; Rolon-Garrido, V. H. *Journal of Rheology* **2012,** 56, (5), 1279-1297.

247. Wang, H. P.; Keum, J. K.; Hiltner, A.; Baer, E.; Freeman, B.; Rozanski, A.; Galeski, A. *Science* **2009,** 323, (5915), 757-760.

248. Wang, S. Q.; Ravindranath, S.; Boukany, P. E. *Macromolecules* **2011,** 44, (2), 183-190.

249. Wang, S. Q.; Ravindranath, S.; Wang, Y. Y.; Boukany, P. Y. *Journal of Chemical Physics* **2007,** 127, (6).

250. Wang, S. Q.; Wang, Y. Y.; Cheng, S. W.; Li, X.; Zhu, X. Y.; Sun, H. *Macromolecules* **2013,** 46, (8), 3147-3159.

251. Wang, Y. Y.; Wang, S. Q. *Journal of Rheology* **2009,** 53, (6), 1389-1401.

252. Watanabe, H.; Chen, Q. A.; Kawasaki, Y.; Matsumiya, Y.; Inoue, T.; Urakawa, O. *Macromolecules* **2011,** 44, (6), 1570-1584.

253. Watanabe, H.; Matsumiya, Y.; Takada, J.; Sasaki, H.; Matsushima, Y.; Kuriyama, A.; Inoue, T.; Ahn, K. H.; Yu, W.; Krishnamoorti, R. *Macromolecules* **2007,** 40, (15), 5389-5399.

254. Watanabe, H.; Yao, M. L.; Osaki, K.; Shikata, T.; Niwa, H.; Morishima, Y. *Rheologica Acta* **1999,** 38, (1), 2-13.

255. Waters, N. D.; Keeley, A. M. *Journal of Non-Newtonian Fluid Mechanics* **1987,** 24, (2), 161-181.

256. Welch, G. *Polymer* **1974,** 15, 429.

257. Wendorff, J. H. *Journal of Polymer Science Part C-Polymer Letters* **1980,** 18, (6), 439-445.

258. Wilson, G. M.; Khomami, B. *Journal of Non-Newtonian Fluid Mechanics* **1992,** 45, (3), 355-384.

259. Wilson, G. M.; Khomami, B. *Journal of Rheology* **1993a,** 37, (2), 315-339.

260. Wilson, G. M.; Khomami, B. *Journal of Rheology* **1993b,** 37, (2), 341-354.

261. Wilson, H. J.; Rallison, J. M. *Journal of Non-Newtonian Fluid Mechanics* **1997,** 72, (2-3), 237-251.

262. Wool, R. P., *Polymer Interface: Structure and Strength*. Hanser Gardner Publication: New York, 1995.

263. Wool, R. P.; Oconnor, K. M. *Journal of Applied Physics* **1981,** 52, (10), 5953-5963.

264. Wu, D. Y.; Meure, S.; Solomon, D. *Progress in Polymer Science* **2008,** 33, (5), 479-522.

265. Wu, S., *Polymer Interface and Adhesion*. Marcel Dekker: New York, 1982.

266. Wu, S. *Journal of Polymer Science Part B-Polymer Physics* **1987,** 25, 2511-2529.

267. Wu, S. *Journal of Polymer Science Part B-Polymer Physics* **1989,** 27, (4), 723-741.

268. Wu, S.; Chuang, H. K.; Chang, D. H. *Journal of Polymer Science Part B-Polymer Physics* **1986,** 24, (1), 143-159.

269. Xu, S. X.; Wen, M.; Li, J.; Guo, S. Y.; Wang, M.; Du, Q.; Shen, J. B.; Zhang, Y. Q.; Jiang, S. L. *Polymer* **2008,** 49, (22), 4861-4870.

270. Yang, L. A.; Suo, T. C.; Niu, Y. H.; Wang, Z. G.; Yan, D.; Wang, H. *Polymer* **2010,** 51, (22), 5276-5281.

271. Yang, X. P.; Halasa, A.; Hsu, W. L.; Wang, S. Q. *Macromolecules* **2001,** 34, (24), 8532-8540.

272. Yang, Z.; Han, C. D. *Macromolecules* **2008,** 41, (6), 2104-2118.

273. Yiantsios, S. G.; Higgins, B. G. *Physics of Fluids* **1988,** 31, (11), 3225-3238.

274. Yih, C.-S. *J. Fluid Mech.* **1967,** 27, 337-352.

275. Yokoyama, H.; Kramer, E. J. *Macromolecules* **2000,** 33, (5), 1871-1877.

276. Yu, W., *Rheological Measurements*. Encyclopedia of Polymer Science and Technology ed.; John Wiley & Sons, Inc.: New York, 2013.

277. Yu, W.; Bousmina, M.; Grmela, M.; Palierne, J. F.; Zhou, C. X. *Journal of Rheology* **2002,** 46, (6), 1381-1399.

278. Yu, W.; Li, R. M.; Zhou, C. X. *Polymer* **2011,** 52, (12), 2693-2700.

279. Yukioka, S.; Nagato, K.; Inoue, T. *Polymer* **1992,** 33, (6), 1171-1176.

280. Zartman, G. D.; Wang, S. Q. *Macromolecules* **2011,** 44, (24), 9814-9820.

281. Zeroni, I.; Ozair, S.; Lodge, T. P. *Macromolecules* **2008,** 41, (13), 5033-5041.

282. Zhang, C. L.; Feng, L. F.; Gu, X. P.; Hoppe, S.; Hu, G. H. *Polymer* **2007,** 48, (20), 5940-5949.

283. Zhang, H. G.; Lamnawar, K.; Maazouz, A. *Rheologica Acta* **2012,** 51, (8), 691-711.

284. Zhang, H. G.; Lamnawar, K.; Maazouz, A. *Macromolecules* **2013,** 46, (1), 276-299.

285. Zhang, J. B.; Cole, P. J.; Nagpal, U.; Macosko, C. W.; Lodge, T. P. *Journal of Adhesion* **2006a,** 82, (9), 887-902.

286. Zhang, J. B.; Ji, S. X.; Song, J.; Lodge, T. P.; Macosko, C. W. *Macromolecules* **2010,** 43, (18), 7617-7624.

287. Zhang, J. B.; Lodge, T. P.; Macosko, C. W. *Journal of Rheology* **2006b,** 50, (1), 41-57.

288. Zhao, R.; Macosko, C. W. *Journal of Rheology* **2002,** 46, (1), 145-167.

289. Zhao, R.; Macosko, C. W. *AIChE Journal* **2007,** 53, (4), 978-985.

SIGLE	ECOLE DOCTORALE	NOM ET COORDONNEES DU RESPONSABLE
CHIMIE	**CHIMIE DE LYON** http://www.edchimie-lyon.fr M. Jean Marc LANCELIN Insa : R. GOURDON	M. Jean Marc LANCELIN Université Claude Bernard Lyon 1 Bât CPE 43 bd du 11 novembre 1918 69622 VILLEURBANNE Cedex Tél : 04.72.43 13 95 Fax : lancelin@hikari.cpe.fr
E.E.A.	**ELECTRONIQUE, ELECTROTECHNIQUE, AUTOMATIQUE** http://edeea.ec-lyon.fr Secrétariat : M.C. HAVGOUDOUKIAN eea@ec-lyon.fr	M. Gérard SCORLETTI Ecole Centrale de Lyon 36 avenue Guy de Collongue 69134 ECULLY Tél : 04.72.18 60 97 Fax : 04 78 43 37 17 Gerard.scorletti@ec-lyon.fr
E2M2	**EVOLUTION, ECOSYSTEME, MICROBIOLOGIE, MODELISATION** http://e2m2.universite-lyon.fr Insa : H. CHARLES	Mme Gudrun BORNETTE CNRS UMR 5023 LEHNA Université Claude Bernard Lyon 1 Bât Forel 43 bd du 11 novembre 1918 69622 VILLEURBANNE Cédex Tél : 04.72.43.12.94 e2m2@biomserv.univ-lyon1.fr
EDISS	**INTERDISCIPLINAIRE SCIENCES-SANTE** Sec : Safia Boudjema M. Didier REVEL Insa : M. LAGARDE	M. Didier REVEL Hôpital Cardiologique de Lyon Bâtiment Central 28 Avenue Doyen Lépine 69500 BRON Tél : 04.72.68 49 09 Fax :04 72 35 49 16 Didier.revel@creatis.uni-lyon1.fr
INFOMATHS	**INFORMATIQUE ET MATHEMATIQUES** http://infomaths.univ-lyon1.fr	M. Johannes KELLENDONK Université Claude Bernard Lyon 1 INFOMATHS Bâtiment Braconnier 43 bd du 11 novembre 1918 69622 VILLEURBANNE Cedex Tél : 04.72. 44.82.94 Fax 04 72 43 16 87 infomaths@univ-lyon1.fr
Matériaux	**MATERIAUX DE LYON** Secrétariat : M. LABOUNE PM : 71.70 –Fax : 87.12 Bat. Saint Exupéry Ed.materiaux@insa-lyon.fr	M. Jean Yves BUFFIERE INSA de Lyon MATEIS Bâtiment Saint Exupéry 7 avenue Jean Capelle 69621 VILLEURBANNE Cédex Tél : 04.72.43 83 18 Fax 04 72 43 85 28 Jean-yves.buffiere@insa-lyon.fr
MEGA	**MECANIQUE, ENERGETIQUE, GENIE CIVIL, ACOUSTIQUE** M. Philippe Boisse Secrétariat : M. LABOUNE PM : 71.70 –Fax : 87.12	M. Philippe Boisse INSA de Lyon Laboratoire LaMCoS Bâtiment Jacquard 25 bis avenue Jean Capelle 69621 VILLEURBANNE Cedex Tél :04.72.18.71.70 Fax : 04 72 43 72 37 mega@lamcos.insa-lyon.fr
ScSo	**ScSo*** M. OBADIA Lionel Insa : J.Y. TOUSSAINT	M. OBADIA Lionel Université Lyon 2 86 rue Pasteur 69365 LYON Cedex 07 Tél : 04.78.69.72.76 Fax : 04.37.28.04.48 Lionel.Obadia@univ-lyon2.fr

*ScSo : Histoire, Geographie, Aménagement, Urbanisme, Archéologie, Science politique, Sociologie, Anthropologie

NOM : ZHANG   DATE de SOUTENANCE : **Jeudi 19 Décembre 2013**

Prénom : **Huagui**

TITRE: **Fundamental Studies of Interfacial Rheology at Multilayered Model Polymers for Coextrusion Process**

NATURE : **Doctorat**   Numéro d'ordre : 2013-ISALXXXX

Ecole doctorale : **Matériaux de Lyon**   Spécialité : **Matériaux Polymères et composites**

RESUME : Fundamental studies have been devoted in this work to probe and modelize the interfacial phenomena at multilayered polymer systems based on two model compatible polymers of poly(vinylidene fluoride)(PVDF) and poly(methyl methacrylate)(PMMA) with varying molar masses. Linear and nonlinear rheology have been demonstrated to be sensitive to the presence of diffuse interphase triggered from interdiffusion at polymer/polymer interface. Firstly, the interdiffusion kinetics as well as the development of the interphase decoupled to flow as generated at a symmetrical (self diffusion) and an asymmetrical (mutual diffusion) bilayer have been investigated using small-amplitude oscillatory shear measurements. Results were analyzed according to Doi-Edwards theory (tube model) and the effects of annealing factors as well as structural properties on the diffusion kinetics have been studied. The PMMA/PVDF mixtures have been examined to be a couple of weak thermorheological complexity, owning close monomeric friction coefficients of each species in the present experimental conditions. Based on this physics, a new rheological model was developed to quantify the interdiffusion coefficients by taking into account the component dynamics in mixed state and the concept of interfacial rheology. Rheological and geometrical properties of the interphase have been able to be quantified through this model, as validated by scanning electron microscopy coupled with energy dispersive X-ray analysis (SEM-EDX) and transmission electron microscopy (TEM).

Secondly, experiments of step strains, startup in simple shear and in uni-axial extension have been carried out on the PMMA/PVDF multilayer structures to investigate the sensitivity of nonlinear rheology to the well-defined diffuse interphase. An original model was proposed to fit the stress relaxation behavior of multilayer structures and to determine the relaxation behavior of the interphase. Lack of entanglement at the interface and weak entanglement intensity at the diffuse interphase make them to be subsequently readily to suffer from interfacial yielding even interfacial failure during and after continuous large deformations in simple shear and un-axial extension. Presence of interphase delays the interfacial yielding to a larger external deformation or a higher deformation rate. Besides, elongational properties of the multilayer structures have been shown to be a function of composition as controlled by layer number(interfacial area) and interphase properties (rheology related to entanglement intensity). Finally, the diffuse interphase development coupled to flow in practical coextrusion process has been considered. The compromising result between negative effect of chain orientation and favorable effect of flow on diffusion kinetics gives rise to a broadening interphase after coextrusion. An experimental strategy was formulated to optimize the coextrusion processing by considering the classical factors based on a flow stability chart. Presence of the diffuse interphase was demonstrated to significantly weaken (or even eliminate) the viscous and elastic instabilities despite of the high rheological contrast between PMMA and PVDF melts especially at low temperatures. Hence, this work gives guidelines on the key role of the interphase plays in structure-property-processing relationships.

Keywords: *Linear and Nonlinear Rheology; Shear and Elongation; Multilayer; Interphase;*

Laboratoire (s) de recherche : Ingenierie des Matériaux Polymères (IMP) CNRS UMR 5223 INSA de Lyon.

Composition du jury : Prof. MAIA, João M (Reviewer); Prof. HU Guo-Hua (Reviewer); Prof. CASSAGNAU Philippe examiner); Prof. BOUSMINA Mosto (Examiner); Prof. MAAZOUZ abderrahim (Supervisor) ; Dr. LAMNAWAR khalid (Co-Supervisor).